frontiers | Research Topics

Host-parasite interactions at the cellular, tissue, and organism level

Edited by
Xuexian Yang, William Harold Witola, Hongzhi Chen, Hua Cong and Xiang Wu

Published in
Frontiers in Immunology

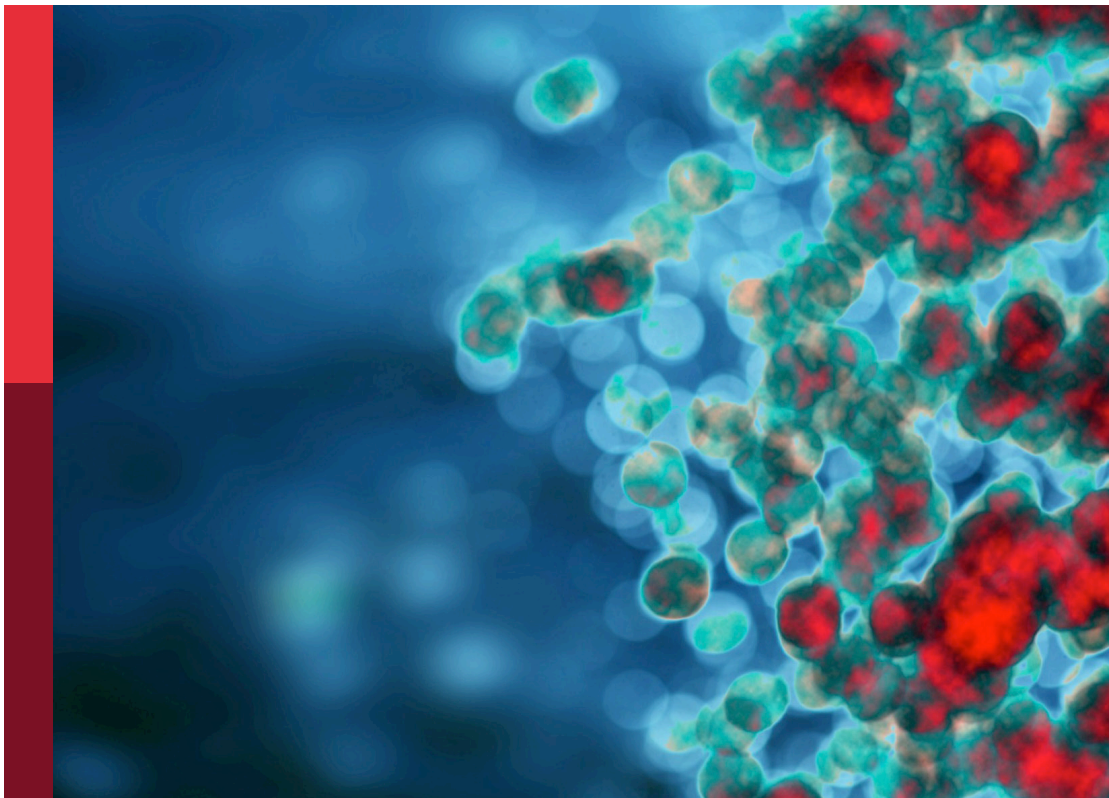

ISSN 1664-8714
ISBN 978-2-8325-4973-5
DOI 10.3389/978-2-8325-4973-5

About Frontiers

Frontiers is more than just an open access publisher of scholarly articles: it is a pioneering approach to the world of academia, radically improving the way scholarly research is managed. The grand vision of Frontiers is a world where all people have an equal opportunity to seek, share and generate knowledge. Frontiers provides immediate and permanent online open access to all its publications, but this alone is not enough to realize our grand goals.

Frontiers journal series

The Frontiers journal series is a multi-tier and interdisciplinary set of open-access, online journals, promising a paradigm shift from the current review, selection and dissemination processes in academic publishing. All Frontiers journals are driven by researchers for researchers; therefore, they constitute a service to the scholarly community. At the same time, the *Frontiers journal series* operates on a revolutionary invention, the tiered publishing system, initially addressing specific communities of scholars, and gradually climbing up to broader public understanding, thus serving the interests of the lay society, too.

Dedication to quality

Each Frontiers article is a landmark of the highest quality, thanks to genuinely collaborative interactions between authors and review editors, who include some of the world's best academicians. Research must be certified by peers before entering a stream of knowledge that may eventually reach the public - and shape society; therefore, Frontiers only applies the most rigorous and unbiased reviews. Frontiers revolutionizes research publishing by freely delivering the most outstanding research, evaluated with no bias from both the academic and social point of view. By applying the most advanced information technologies, Frontiers is catapulting scholarly publishing into a new generation.

What are Frontiers Research Topics?

Frontiers Research Topics are very popular trademarks of the *Frontiers journals series*: they are collections of at least ten articles, all centered on a particular subject. With their unique mix of varied contributions from Original Research to Review Articles, Frontiers Research Topics unify the most influential researchers, the latest key findings and historical advances in a hot research area.

Find out more on how to host your own Frontiers Research Topic or contribute to one as an author by contacting the Frontiers editorial office: frontiersin.org/about/contact

Host-parasite interactions at the cellular, tissue, and organism level

Topic editors

Xuexian Yang — University of New Mexico, United States
William Harold Witola — University of Illinois at Urbana–Champaign, United States
Hongzhi Chen — Central South University, China
Hua Cong — Shandong University, China
Xiang Wu — Central South university, China

Citation

Yang, X., Witola, W. H., Chen, H., Cong, H., Wu, X., eds. (2024). *Host-parasite interactions at the cellular, tissue, and organism level*. Lausanne: Frontiers Media SA. doi: 10.3389/978-2-8325-4973-5

Table of contents

frontiers | Frontiers in Immunology

TYPE Original Research
PUBLISHED 25 July 2023
DOI 10.3389/fimmu.2023.1201455

OPEN ACCESS

EDITED BY
Xiang Wu,
Central South University, China

REVIEWED BY
Maria Elizbeth Alvarez Sanchez,
Universidad Autónoma de la Ciudad de México, Mexico
Shuaiqin Huang,
Central South University, China

*CORRESPONDENCE
Xuenong Luo
luoxuenong@caas.cn

†These authors have contributed equally to this work

RECEIVED 06 April 2023
ACCEPTED 26 June 2023
PUBLISHED 25 July 2023

CITATION
Chen G, Pu G, Wang L, Li Y, Liu T, Li H, Zhang S, Wang X, Liu X and Luo X (2023) *Cysticercus pisiformis*-derived novel-miR1 targets TLR2 to inhibit the immune response in rabbits.
Front. Immunol. 14:1201455.
doi: 10.3389/fimmu.2023.1201455

Cysticercus pisiformis-derived novel-miR1 targets TLR2 to inhibit the immune response in rabbits

Guoliang Chen[1†], Guiting Pu[1†], Liqun Wang[1], Yanping Li[1], Tingli Liu[1], Hong Li[1], Shaohua Zhang[1], Xuelin Wang[2], Xiaolei Liu[2] and Xuenong Luo[1,3*]

[1]State Key Laboratory for Animal Disease Control and Prevention, Key Laboratory of Veterinary Parasitology of Gansu Province, Lanzhou Veterinary Research Institute, Chinese Academy of Agricultural Sciences, Lanzhou, Gansu, China, [2]Key Laboratory for Zoonosis Research of the Ministry of Education, Institute of Zoonosis, and College of Veterinary Medicine, Jilin University, Changchun, China, [3]Jiangsu Co-Innovation Center for the Prevention and Control of Important Animal Infectious Disease and Zoonoses, Yangzhou University, Yangzhou, China

Cysticercosis pisiformis, a highly prevalent parasitic disease worldwide, causes significant economic losses in the rabbit breeding industry. Previous investigations have identified a novel microRNA, designated as novel-miR1, within the serum of rabbit infected with *Cysticercus pisiformis*. In the present study, we found that *C. pisiformis*-derived novel-miR1 was released into the rabbit serum via exosomes. Through computational analysis using TargetScan, miRanda, and PITA, a total of 634 target genes of novel-miR1 were predicted. To elucidate the functional role of novel-miR1, a dual-luciferase reporter assay was utilized and demonstrated that novel-miR1 targets rabbit Toll-like receptor 2 (TLR2). Rabbit peripheral blood lymphocytes (PBLCs) were transfected with novel-miR1 mimic and mimic NC, and the *in vitro* experiments confirmed that novel-miR1 suppressed the expression of pro-inflammatory cytokines such as TNF-α, IL-1β, and IL-6 through the nuclear factor kappa B (NF-κB) pathway. *In vivo* experiments demonstrated that novel-miR1 was significantly upregulated during the 1–3 months following infection with *C. pisiformis in* rabbits. Notably, this upregulation coincided with a downregulation of TLR2, P65, pP65, TNF-α, IL-1β, and IL-6 in PBLCs. Collectively, these results indicate that the novel-miR1 derived from *C. pisiformis* inhibited the rabbits' immune response by suppressing the NF-κB-mediated immune response. This immune modulation facilitates parasite invasion, survival, and establishment of a persistent infection.

KEYWORDS

rabbit, Cysticercosis pisiformis, novel-miR1, TLR2, NFκB

1 Introduction

Cysticercus pisiformis is a widely prevalent larval form of tapeworm that primarily parasitizes the liver, omentum, and mesenteries of lagomorphs and rodents, leading to the development of cysticercosis pisiformis (1, 2). Among these hosts, rabbits are the most frequently affected and suffer significant consequences from cysticercosis pisiformis. This parasitic infection adversely affects rabbit reproductive rates and poses a serious threat to endangered rabbit species such as the teporingo (*Romerolagus diazi*) (3, 4). Moreover, it leads to decreased body weight and cholesterol levels, even leading to death (5). Importantly, *C. pisiformis* infection in rabbits impairs their immune responses, rendering them susceptible to secondary infections by other pathogens (6), which has substantial economic impacts in the rabbit breeding industry and impacts animal welfare.

Exosomes, extracellular vesicles ranging in size from 40 to 160 nm, are released by various cells, including both prokaryotes and eukaryotes (7). Numerous studies have reported that exosomes are mediators of vesicle transport, playing a pivotal role in parasite–host interactions (8–11). *Trichinella spiralis* excretory/secretory products have been shown to modulate programmed death 1-mediated M2 macrophage polarization (12). Exosomes derived from *T. spiralis* impact the nuclear factor kappa B (NF-κB) and mitogen-activated protein kinase (MAPK) signaling pathways, thereby inhibiting M1 macrophage polarization (13). Similarly, *Taenia asiatica* exosomes inhibit LoVo cell proliferation and autophagy via the Adenosine 5'-monophosphate (AMP)-activated protein kinase (AMPK) pathway (14). Notably, miRNAs are essential cargo within exosomes and are the key functional units (15, 16). *Echinococcus multilocularis* exosomes containing emu-miR-4989 induces UBE2N suppression (17). *Fasciola hepatica* releases fhe-miR-125b through exosomes to target the mammalian Argonaut protein (Ago-2) within macrophages during infection to downregulate the production of inflammatory cytokines (18). miR-1-3p and let-7-5p expressed by *T. spiralis* larvae-derived extracellular vesicles promote the polarization of bone marrow macrophages toward the M2b type while inhibiting fibroblast activation (19).

MicroRNAs (miRNAs) are small noncoding RNAs that play important roles in posttranscriptional gene silencing (20). They are capable of binding to the 3′-untranslated region (UTR), coding region, or 5′-UTR of the target mRNA to inhibit translation or facilitate mRNA degradation in a wide variety of physiological and pathological processes, including growth, proliferation, differentiation, development, metabolism, infection, immunity, and cell death (21, 22). Data from numerous studies have shown that miRNA expression profiles are altered during parasite infection and suggest that differentially expressed miRNAs play important roles in host immune responses (18, 23–25).

Toll-like receptors (TLRs) are pattern recognition receptors (PRRs) that play a crucial role in recognizing pathogen-associated molecular patterns (PAMPs) and activate intracellular signaling pathways, leading to the induction of inflammatory cytokine genes such as TNF-α, IL-6, IL-1β, and IL-12 (26, 27). Among the TLRs, TLR2 is involved in the recognition of various PAMPs derived from bacteria, fungi, parasites, and viruses (28). Upon recognition of PAMPs, including proteins, lipoproteins, lipids, nucleic acids, and endogenous ligands, TLR2 induces interferon (TIRF), leading to the activation of MAPKs through the MyD88 pathway or the Toll/IL-1R-related adaptor protein, resulting in the translocation of NF-κB and subsequent transcription and synthesis of pro-inflammatory cytokines (29).

Helminths, a class of pathogens, also elicit immune responses through TLR2. For instance, *Clonorchis sinensis* heat shock cognate B (CsHscB) activates TLR2 to induce the expression of IL-10, exerting immune regulatory activities (30). During *T. spiralis* infection, TLR2 is upregulated in the mouse small intestine, suggesting its crucial role in host defense mechanisms against this parasite (31). TLR2 is also important for the development of a Th1-dominant immune response in the mouse model of *Taenia crassiceps* cysticercosis (32). Cystic echinococcosis-derived antigens, including hydatid cyst fluid (HCF), germinal layer antigens (GL), somatic and excretory/secretory (ES) products of protoscoleces (PSC), have been shown to downregulate the expression of TLR2 in ovine peripheral blood leukocytes, potentially contributing to the establishment of chronic infection by suppressing host immunity (33).

Therefore, TLR2 plays important roles in the induction of innate immune responses. Despite the knowledge on the important roles played by parasite-derived miRNAs during infection, little is known about the role of TLR2 as a pattern recognition receptor in the context of *C. pisiformis* infection in rabbits. In our experiments, we observed a significant upregulation of novel-miR1, derived from *C. pisiformis*, in the serum of infected rabbits. Furthermore, TLR2 was predicted and verified as a target of novel-miR1. This study aims to investigate the mechanism underlying the interaction between novel-miR1 and TLR2 in rabbits infected with *C. pisiformis*. The findings will contribute valuable insights into the mechanism of *C. pisiformis* infection, thereby benefiting the diagnosis and treatment of cysticercosis pisiformis and providing strategies for the prevention and control of helminth infections.

2 Methods

2.1 Rabbit and *C. pisiformis* collection

Fifty-day-old New Zealand White rabbits weighing 1.5~2 kg were obtained from the Laboratory Animal Center of Lanzhou Veterinary Research (Lanzhou, China). The rabbits were allowed to adaptively acclimate for 1 week prior to the experiment. A total of six rabbits were orally infected with 1 ml of infective *Taenia pisiformis* eggs (1,000 eggs/ml), establishing the *C. pisiformis* infection group (CPi). As a negative control group (NC), three rabbits were administered 1 ml of phosphate-buffered saline (PBS) via oral gavage. All rabbits were reared with the same forage and clean water. Following the collection of required blood samples, necropsy was performed on the six rabbits to confirm *C. pisiformis* infection. The examination results are shown in Supplementary Table S1.

All rabbit experiments conducted in this study were approved by the Animal Ethics Committee of Lanzhou Veterinary Research Institute, Chinese Academy of Agricultural Sciences (Permit No. LVRIAEC-2016-006), and the protocols used were strictly in accordance with the guidelines of animal welfare. Every effort was made to minimize any potential harm to the experimental rabbits in accordance with the study protocols.

2.2 Cells and media

Rabbit peripheral blood lymphocytes (PBLCs) were isolated from 5-ml fresh rabbit blood samples collected in tubes containing EDTA and separated using rabbit peripheral blood lymphocytes isolation kit based on Ficoll density gradient centrifugation (TBD Science, China, LTS10965). Cell viability was tested by trypan blue staining (TBD Science, China, TBD20180079) following the manufacturer's instructions. The isolated PBLCs were cultured in RPMI 1640 medium (Gibco, Grand Island, NY, USA) supplemented with 10% fetal bovine serum (FBS) (Gibco), penicillin (100 unit/ml) (Gibco), and streptomycin (100 μg/ml) (Gibco).

HEK293T cells were cultured in DMEM (Gibco) containing 10% FBS, penicillin (100 unit/ml), and streptomycin (100 μg/ml). All cells were cultured at 37°C in a 5% CO_2 cell culture incubator.

2.3 Exosome isolation and identification

T. pisiformis larvae were harvested from the peritoneal cavities of CPi rabbits and cultured in 10 ml RPMI 1640 medium (Gibco, Grand Island, NY, USA) supplemented with 10% exosome-depleted FBS and antibiotics (100 U/ml penicillin, 100 μg/ml streptomycin) at 37°C in 5% CO_2 cell culture incubator. After 12 h, the culture media were collected and replaced with fresh medium. The collected media were centrifuged at 2,000×g at 4°C for 10 min to remove cell debris, and the exosomes were isolated using the Minute™ Hi-Efficiency Exosome Isolation Reagent (Cat. No. EI-027; Invent Biotechnologies, Inc., Plymouth, MN, USA) following the manufacturer's protocol. The exosome precipitate was resuspended in 500 μl phosphate-buffered saline (PBS) filtered through a 0.2-μM pore filter. The concentration of exosomes was determined using a Pierce BCA Protein Assay Kit (Thermo Fisher Scientific, Waltham, MA, USA). The particle size of the exosomes was analyzed using a NanoSight LM10 instrument (Nanosight, Wiltshire, UK). The exosome size and morphology were observed through transmission electron microscopy (TEM, Hitachi Ltd., Tokyo, Japan). Briefly, exosomes were adsorbed onto a 200-mesh formvar-coated copper grid (Agar Scientific Ltd., Stansted, UK) and incubated for 10 min at room temperature. After staining with 2% tungstophosphoric acid solution for 1 min, the exosomes were examined under an electron microscope (34).

2.4 Exosome labeling and confocal laser scanning microscope analysis

To visualize exosomal uptake by rabbit PBLCs, we labeled exosomes with DiD dye (ab275319, Abcam, Cambridge, MA, USA). A total of 6 μg of exosomes were mixed with 2 μl DiD dye (0.2%) and diluted to 1 ml PBS (35). As a negative control, only DiD dye mixed with PBS was used. The mixture was then incubated at 37°C for 30 min to allow for labeling of the exosomes. The labeled exosomes were subsequently washed with PBS and centrifuged at 120,000×g and 4°C for 1 h. The resulting precipitate was resuspended in 180 μl of PBS.

Subsequently, the labeled exosomes were added to three wells of a 12-well plate containing rabbit PBLCs and incubated for 12 h in a 5% CO_2 incubator at 37°C. Following incubation, the cells were stained with 10 μg/ml of 4,6 diamidino-2-phenylindole (DAPI) (Beyotime, Shanghai, China) for 5 min. The stained PBLCs were added to a glass slide and covered with a coverslip for imaging under a confocal laser scanning microscope (Nikon, Tokyo, Japan) (36).

2.5 Novel-miR1/siRNA transfection and exosome treatment

PBLCs were isolated from fresh peripheral blood from healthy rabbits. The isolated cells were diluted to 2~10 × 10^6 cells/ml in RPMI 1640 medium supplemented with 10% FBS, penicillin (100 unit/ml), and streptomycin (100 μg/ml). Subsequently, 1 ml of the PBLC suspension was added to each well of a 12-well plate and cultured in a 37°C incubator with 5% CO_2. For transfection experiments, 10 pmol/L of novel-miR1 mimic, mimic NC, inhibitor, inhibitor NC, siTLR2, and siRNA NC (RiboBio, Guangzhou, China) were transfected into the PBLCs using 2 μl of Lipofectamine RNAiMAX transfection reagent (Thermo Fisher Scientific, USA) for a duration of 24 h. In exosome treatment experiments, 20 μg of total exosome protein or an equivalent volume of PBS was added per well and coincubated for 24 h.

2.6 Extraction of miRNAs and RNA

The miRNAs were separated from fresh blood samples or *C. pisiformis*-derived exosomes using an EasyPure miRNA Kit (TransGen, China) according to the manufacturer's instructions. Total RNA was isolated from the PBLCs and *C. pisiformis* using TRIzol reagent (Thermo Fisher Scientific) following the manufacturer's protocol.

2.7 Real-time qPCR analysis

The expression of novel-miR1 and TLR2 in serum miRNAs or PBLC RNA in CPi and NC groups was analyzed using real-time quantitative PCR (qPCR). The miRNAs were reverse-transcribed into cDNA using the Mir-XTM miRNA First-Strand Synthesis Kit (Clontech, Mountain View, CA, USA). The cDNA first-strand synthesis of PBLC total RNA was performed using the HiScript® III 1st Strand cDNA Synthesis Kit (Vazyme, China). All cDNAs were used for real-time fluorescence qPCR detection using an ABI 7500 quantitative PCR instrument (Thermo Fisher Scientific).

qPCR was performed in a 20-μl reaction volume, including 10 μl SYBR Advantage Premix (2×) (Takara, Japan), 2 μl cDNA, 0.4 μl ROX Dye (50×), 0.8 μl specific forward primer, 0.8 μl specific reversed primer, and 6 μl RNase-free water. qPCR was performed with the following: 95°C for 10 min and 40 cycles of 95°C for 15 s and 60°C for 34 s. The relative expressions were normalized to U6 small nuclear RNA (snRNA) or GAPDH. All primers were designed and produced by Sangon Biotech (Sangon Biotech, China) (Table 1). The relative expression of novel-miR1 was calculated using the $2^{-\Delta\Delta Ct}$ method (37).

To demonstrate the source of novel-miR1 in rabbit serum, an absolute quantification qPCR was performed. Total RNA (1 μg) from all samples, including rabbit serum (CPi and NC), *C. pisiformis*, and *C. pisiformis* exosomes, was reverse-transcribed into cDNA using the Mir-XTM miRNA First-Strand Synthesis Kit. qPCR was conducted on an ABI 7500 using a TransStart Tip Green qPCR SuperMix Kit (TransGen Co., Beijing, China) with the following protocol: initial denaturation at 95°C for 30 s, followed by 40 cycles of 95°C for 15 s and 60°C for 34 s. The copy number of novel-miR1 in the samples was determined using a standard curve established with 10-fold serial dilutions (1×10^7 to 1×10^2 copies/μl) of the standard novel-miR1.

TABLE 1 Primer sequences used in quantitative PCR.

Primer name	Primer sequence (5′–3′)
Novel-miR1	TATACGCAGGTGCGAAAGCAGG
IL-17RB-F	ACGAGACGACAGTCCAAGTG
IL-17RB-R	GTGGAAAACCCAATCACGGC
CEBPA-F	TTCAGGAGTAACCGTGTGCC
CEBPA-R	CGGCAGAAACCCTCCAAGTA
CASP9-F	CTGTTTCCGAGCGAGGGATT
CASP9-R	CCTGGCCCCGCTAAGTTTTA
TLR2-F	CGCTGAAAAACCTGACCGAC
TLR2-R	TGTGTATCCGTGTGCTGGAC
MAPK12-F	CCTACTTCGAGTCCCTGCAC
MAPK12-R	AAGTGACACGCTTCCACTCG
GSAP-F	GACCTCATGTGCCGCATACT
GSAP-R	ACTGCCACGCCTATTGAAGT
IL10RA-F	TCCCCGCTTGCAATTCTCAT
IL10RA-R	TGTGAGCTGACCACACACTG
IRF8-F	AGGCTCGCGGGTTTATGATT
IRF8-R	CTTCGCCGTCGCACATTAAG
TNF-α-F	GACGGGCTGTACCTCATCTAC
TNF-α-R	GACCTTGTTCGGGTAGGAGAC
IL-1β-F	GGCAGGTCTTGTCAGTCGTT
IL-1β-R	AGTTCTCAGGCCGTCATCCT
IL-6-F	AGAACCATCGAGAGCATCCG
IL-6-R	GCCTTGGAAGGTGCAGATTG
IL-10-F	GTCACCGATTTCTCCCCTGT
IL-10-R	GATGTCAAACTCACTCATGGCT
GAPDH-F	TTGAAGGGCGGAGCCAAAA
GAPDH-R	CAGGATGCGTTGCTGACAATC

2.8 Function prediction of novel-miR1

To investigate the potential functional roles of novel-miR1, we employed bioinformatics tools to predict its target genes. The software TargetScan (http://www.targetscan.org/), miRanda (http://www.microrna.org/), and PITA (http://www.pita.org.fj/) were utilized, and the analysis was conducted on the *Oryctolagus cuniculus* genome (https://www.ncbi.nlm.nih.gov/genome/316?genome_assembly_id=1549366). The predicted miRNA target genes were determined by selecting the intersection set of results obtained from the three software programs. The functions of the identified target genes were analyzed by Gene Ontology (GO) functional annotation clustering analysis and Kyoto Encyclopedia of Genes and Genomes (KEGG) pathway analysis. These analyses were performed using the online DAVID bioinformatics database functional annotation tool (https://david.ncifcrf.gov/).

2.9 Luciferase reporter assay

HEK293T cell lines were employed for the co-transfection experiments. The novel-miR1 mimic or mimic NC was cotransfected with dual-luciferase reporter plasmids (pmir-GLO-TLR2, pmir-GLO-TLR2-WT, or pmir-GLO-TLR2-Mut). The luciferase reporter assay was performed using the Dual-Luciferase Reporter Assay System (Promega, Madison, WI, USA). For accurate comparisons, firefly luciferase activity was normalized to the Renilla luciferase activity. The effect of a novel-miR1 on the luciferase reporter constructs containing the TLR2 3′-UTR or the corresponding mutant was determined by comparing the reporter activity with the control. Each luciferase reporter assay was conducted in triplicate.

PBLCs proteins were extracted using RIPA lysis buffer supplemented with 1% protease inhibitor. Here, 30 μg total proteins were incubated at 100°C for 10 min. The protein samples were separated on a 10% SDS-PAGE gel alongside prestained protein markers. The separated proteins were transferred to a PVDF membrane and blocked with 5% skimmed milk at room temperature for 3 h. Rabbit anti-TLR2 monoclonal antibody (1:1,000; Abcam; cat. no. Ab209217), phospho-NF-κB p65 (Ser536) rabbit monoclonal antibody (1:1,000; Abcam; cat. no. ab239882), NF-κB p65 rabbit polyclonal antibody (1:1,000; Abcam; cat. no. Ab16502), rabbit anti-IL-6 polyclonal antibody (1:1,000; Bioss, Woburn, MA, USA; cat. no. bs-0782R), rabbit anti-TNF-α polyclonal antibody (1:1,000; Bioss; cat. no. bs-2081R), mouse anti-IL-1β monoclonal antibody (1:500; Santa Cruz Biotechnology, Dallas, TX, USA; cat. no. sc52012), and mouse anti-β-actin monoclonal antibody (1:2,000 dilution, Beyotime

Biotechnology, China) were used as the primary antibodies in this study. The secondary antibodies used were goat anti-mouse IgG/HRP antibody (1:4,000 dilution, Beyotime Biotechnology) or goat anti-rabbit IgG/HRP antibody (1:4,000 dilution, Beyotime Biotechnology), as per the manufacturer's instructions. The membrane was reacted with ultrasensitive ECL luminescence reagent (Beyotime Biotechnology) for color detection.

2.10 Cytokine analysis

Enzyme-linked immunosorbent assay (ELISA) was performed to quantify the levels of IL-6 (ml027844), TNF-α (ml028087), and IL-1β (ml027165). ELISA kits were obtained from Shanghai Enzyme-linked Biotechnology Co. Ltd. (Shanghai, China). PBLCs were isolated from the blood of CPi and NC rabbits and the cell culture supernatants were collected to measure the cytokine levels following the manufacturers' instructions.

2.11 Statistical analysis

The Student's t-test method was used to analyze the significance of the miRNA expression, ImageJ was used for Western blot grayscale analysis, and GraphPad 9 was used to create the relative expression diagram. $p < 0.05$ was considered statistically significant.

3 Results

3.1 Novel-miR1 derived from *C. pisiformis* exosomes was identified in infected rabbit serum

Exosomes derived from *C. pisiformis* were successfully isolated, and their measured size was about 100 nm (Figures 1A, B). To better understand the origin of the novel-miR1 in rabbit serum, absolute qPCR was used to detect the levels of miRNA in samples obtained from rabbit blood (CPi, NC), *C. pisiformis*, and *C. pisiformis* exosomes. The results revealed a significant enrichment of novel-miR1 within the *C. pisiformis* exosomes (Figure 1C). These findings indicate that novel-miR1 in infected rabbit serum is released into the bloodstream through *C. pisiformis* exosomes.

3.2 TLR2 is targeted by novel-miR1

A total of 634 target genes were predicted for novel-miR1 using TargetScan, miRNADA, and PITA (Figure 2A, Supplementary Table S2). GO functional annotation clustering analysis (Supplementary Table S3) revealed enrichment of novel-miR1 target genes in various biological processes (BPs), such as positive regulation of GTPase activity, intracellular signal transduction, protein autophosphorylation, protein stabilization, and ion transport. Molecular function (MF) analysis highlighted ATP binding, protein homodimerization activity, guanyl-nucleotide exchange factor activity, and transcription factor binding as enriched functions. Cellular component (CC) analysis showed localization to cytoplasm, nucleoplasm, integral component of plasma membrane, and lysosomal membrane (Supplementary Table S3). The top 10 terms for BP, MF, and CC are presented in Figure 2B. KEGG pathway analysis revealed the involvement of novel-miR1 target genes in 60 signaling pathways. Notably, these pathways included crucial signaling cascades such as Ras, MAPK, mTOR, Wnt, and ErbB. Moreover, the target genes were found to cluster in pathways related to pathogenic infection and immune responses, such as pathways in cancer, human immunodeficiency virus 1 infection, tuberculosis, *Salmonella* infection, human cytomegalovirus infection, hepatitis B, Kaposi sarcoma-associated herpesvirus infection, Influenza A, and T-cell receptor (Supplementary Table S4). Figure 2C illustrates the top 30 signaling pathways represented by the novel-miR1 target genes, highlighting the significant role of novel-miR1 in pathogenic infection.

To further investigate the immunoregulatory function of novel-miR1 in rabbit serum, rabbit PBLCs were transfected with novel-miR1 mimic to achieve overexpression of novel-miR1 (850-fold change, Figure 2D). Eight immune-related target genes (*IL17RB, CEBPA, CASP9, MAPK12, GSAP, TLR2, IL10RA,* and *IRF8*) were selected

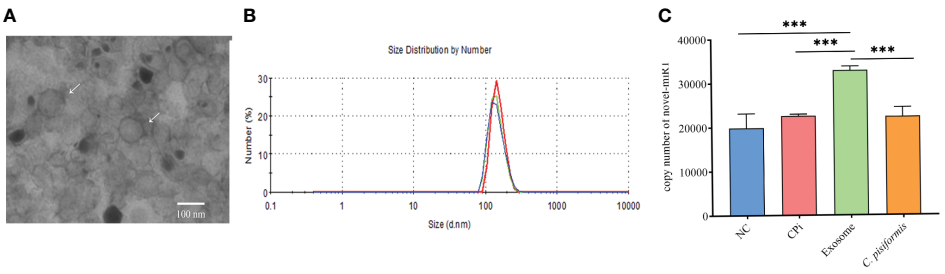

FIGURE 1
Identification and analysis of novel-miR1 source and target genes. **(A)** Morphological characterization of *C. pisiformis* exosomes through transmission electron microscope (TEM). **(B)** Size distribution of exosome of *C. pisiformis* by nanoparticle tracking analysis (NTA). **(C)** Quantification of novel-miR1 copy numbers in different samples. NC represents the negative control rabbit serum miRNA, CPi represents the *C. pisiformis*-infected rabbit serum total miRNA, exosomes are the *C. pisiformis* exosome total miRNA, and *C. pisiformis* represents the *C. pisiformis* total miRNA. Novel-miR1 copy numbers were determined by absolute quantitative PCR using 20 ng total miRNAs. *** indicates a significance level of $p \leq 0.001$.

for validation by qPCR analysis. Compared to the control group, novel-miR1 overexpression significantly inhibited the expression of *MAPK12*, *TLR2*, and *IRF8* ($p < 0.05$), while *IL17RB*, *CEBPA*, and *GSAP* exhibited a tendency toward downregulation (Figure 2E).

Next, we verified the relationship between novel-miR1 and TLR2 and found that the seed sequence of novel-miR1 can bind to the 3′ UTR of *TLR2* (Gene ID: 100009578) using TargetScan software (Figure 2F). To verify the targeting relationship between novel-miR1 and TLR2, we conducted a dual luciferase reporter experiment by cotransfecting the vectors pmirGLO-TLR2-WT, pmirGLO-TLR2-Mut, and pmirGLO with novel-miR1 mimic/mimic NC into HEK293T cells. The results showed a decrease in firefly luciferase activity when pmirGLO-TLR2-WT was cotransfected with novel-miR1 mimics. However, differences were not found in the cells cotransfected with novel-miR1 mimics and pmirGLO-TLR2-Mut or novel-miR1 mimics and pmirGLO (Figure 2G). Additionally, Western blot analysis indicated that novel-miR1 inhibited the protein expression of TLR2 in PBLCs (Figures 2H, I).

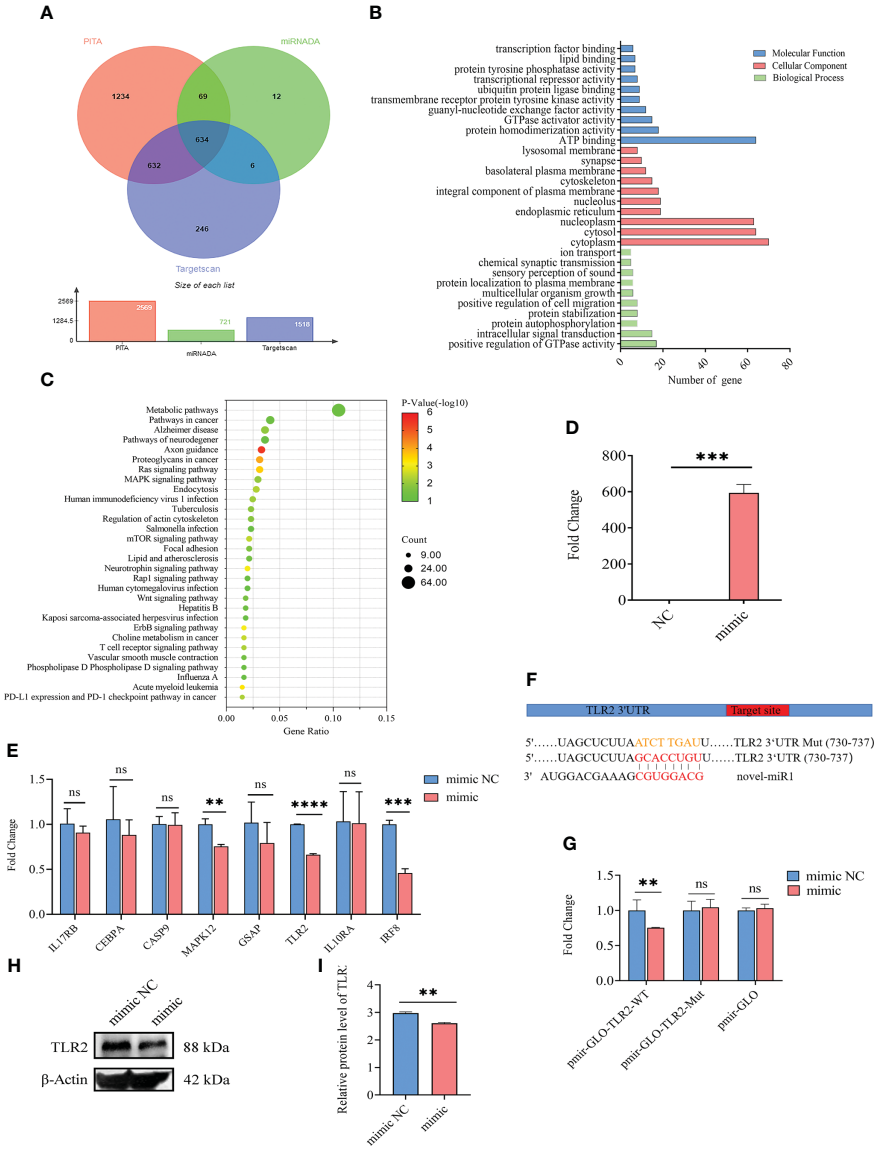

FIGURE 2
Targeting of *TLR2* 3′-UTR by novel-miR1. **(A)** Venn diagram showing the intersection of predicted target genes from different software programs, namely, PITA, miRanda, and TargetScan. **(B)** Gene Ontology (GO) molecular function annotations of the target genes of novel-miR1. The top 10 GO terms for biological processes, cellular component, and molecular function are shown based on their respective p-values. **(C)** Kyoto Encyclopedia of Genes and Genomes (KEGG) pathway analysis of the predicted target genes of novel-miR1. The size of dots indicates the number of genes associated with each pathway. **(D)** Overexpression of novel-miR1 in rabbit PBLCs. **(E)** Relative expression of novel-miR1 target genes in rabbit PBLCs after novel-miR1 treatment. **(F)** novel-miR1 binding *TLR2* 3′-UTR site and the sequences of luciferase reporter plasmids (pmir-GLO-TLR2-WT and pmir-GLO-TLR2-Mut). **(G)** Luciferase reporter assay results indicating the downregulation of *TLR2* through binding to its target 3′-UTR. **(H)** Western blot assay results showing the downregulation of TLR2 protein in PBLCs by novel-miR1. **(I)** Western blot assay results demonstrating the downregulation of TLR2 protein in PBLCs by novel-miR1 (fold change was calculated by the gray values of the image). ns, $p \geq 0.05$; **, $p \leq 0.01$; ***, $p \leq 0.001$; ****, $p \leq 0.0001$.

3.3 Novel-miR1 inhibits the TLR2 signaling pathway and NF-κB activation

TLR2 is a pattern recognition receptor that plays a critical role in initiating innate inflammatory responses and promoting adaptive immune responses (38, 39). To investigate the effect of novel-miR1 targeting TLR2 in rabbit PBLCs, novel-miR1 was overexpressed in rabbit PBLCs via transfection with novel-miR1 mimic. Subsequently, the expression of cytokines related to the TLR2 signaling pathway and NF-κB protein was assessed. The experimental outline is shown in Figure 3.

The qPCR results indicated significant downregulation of *TLR2, IL-6, TNF-α*, and *IL-1β* mRNA expression in rabbit PBLCs. As a control, TLR2 siRNA was transfected into rabbit PBLCs, which confirmed that the mRNA expression of *TLR2* was downregulated. Interestingly, the expression of *IL-6* and *TNF-α* was significantly downregulated (Figure 3A). Consistent with the qPCR results, Westen blot results showed that the protein expression of TLR2 IL-6, TNF-α, and IL-1β was also downregulated. Additionally, we observed downregulation of P65 and phosphorylated-P65 (pP65) protein levels (Figures 3B, C), indicating inhibition of the NF-κB pathway activation due to reduced TLR2 expression. These results collectively suggest that novel-miR1 inhibits the NF-κB pathway signaling by targeting TLR2.

Next, *C. pisiformis* exosomes were marked with DiD dye and cocultured with rabbit PBLCs, which revealed that *C. pisiformis* exosomes can enter rabbit PBLCs (Figure 4A). Furthermore, qPCR results suggested that the expression of novel-miR1 and TLR2 was inhibited by *C. pisiformis* exosomes (Figure 4B). Similarly, Western blot results showed that *C. pisiformis* exosomes downregulated the expression of TLR2, P65, and pP65 proteins (Figures 4C, D).

Lastly, rabbit PBLCs were isolated from the CPi and NC groups for detection and analysis. The results revealed consistent upregulation of novel-miR1 expression and downregulation of TLR2 mRNA during the initial 3 months (Figures 5A, B). Similarly, protein levels of TLR2, P65, pP65, IL-6, TNF-α, and IL-1β were downregulated (Figures 5C–E). In summary, these findings strongly support the release of novel-miR1 into the bloodstream through *C. pisiformis* exosomes in infected rabbits and demonstrate that novel-miR1 targets TLR2 to inhibit NF-κB pathway signaling.

4 Discussion

In our previous study, we observed a significant upregulation of novel-miR1 in rabbit serum through high-throughput sequencing of small RNA, which was further validated by qPCR. However, the sources of novel-miR1 within rabbit serum have not been well elucidated. In the present study, we conducted absolute quantification qPCR to assess total miRNA levels in samples from rabbit serum (CPi and NC), *C. pisiformis*, and *C. pisiformis* exosomes. The results indicated a significant enrichment of novel-miR1 in *C. pisiformis* exosomes. However, it is important to note that higher copy numbers observed in the NC group samples may be attributed to nonspecific sequence amplification.

To further elucidate the functions of novel-miR1, we employed transfection of novel-miR1 mimics and inhibitors into rabbit PBLCs. Interestingly, we were unable to detect any differences in novel-miR1 or novel-miR1 target gene expression in the groups transfected with novel-miR1 inhibitors (Supplementary Figures S1, S2). This finding suggests that novel-miR1 may not naturally exist within rabbit PBLCs and provides supporting evidence that rabbit serum novel-miR1 is released by *C. pisiformis*.

Our data revealed that the expression level of novel-miR1 increased up to 2 months and then decreased by the third month, while TLR2 mRNA expression followed an opposite trend, decreasing until the second month and subsequently increasing. The upregulation of novel-miR1 during the initial stages of infection and the subsequent decrease may be indicative of an ongoing enhancement of immune interactions between *C. pisiformis* and rabbits. After 2 months of infection, the immune response gradually weakens, facilitating continued parasitism by *C. pisiformis*. Additionally, the opposite expression trends observed between novel-miR1 and TLR2 provide evidence that TLR2 is a target gene of novel-miR1.

The findings in the present study highlight the significant immunoregulatory role of novel-miR1 by targeting rabbit PBLCs

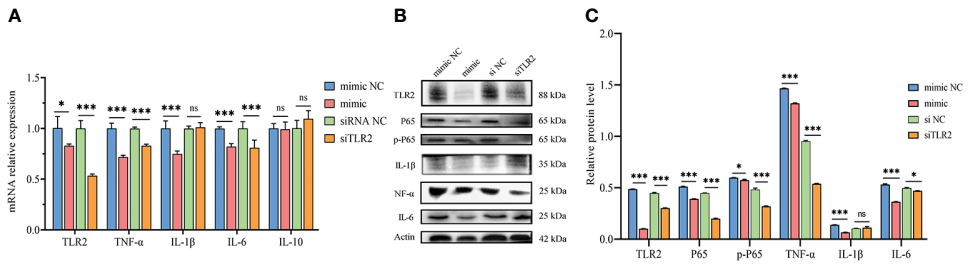

FIGURE 3
Inhibition of TLR2 signaling pathway and NF-κB activation by novel-miR1. **(A)** qPCR results demonstrate the reduction of *TLR2, TNF-α, IL-1β, and IL-6* mRNA levels by novel-miR1. Each test was performed in triplicate. Fold change was calculated based on qPCR results. **(B)** Western blot assay results indicate the decrease in TLR2, P65, pP65, TNF-α, IL-1β, and IL-6 protein levels by novel-miR1. **(C)** Western blot assay results showing the decrease in protein levels of TLR2, P65, pP65, TNF-α, IL-1β, IL-6 (fold change was calculated by the gray values of the image). ns, $p \geq 0.05$; *, $p \leq 0.05$; ***, $p \leq 0.001$.

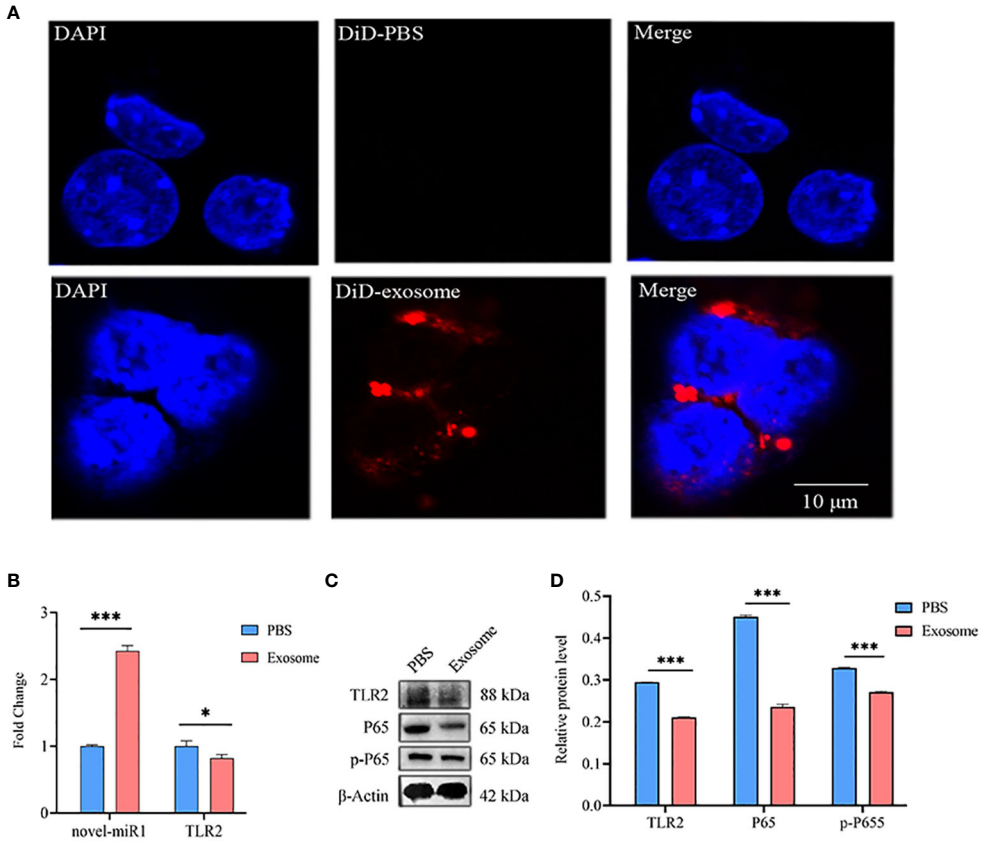

FIGURE 4
C. pisiformis exosomes inhibit the TLR2 signaling pathway and NF-κB activation. **(A)** *C. pisiformis* exosomes can enter rabbit PBLCs. **(B)** qPCR results demonstrate the increased expression of novel-miR1 and decreased *TLR2* mRNA level in rabbit PBLCs after treatment with *C. pisiformis* exosomes. Each test was performed in triplicate; fold change was calculated based on qPCR results. **(C)** Western blot assay results suggest that treatment with *C. pisiformis* exosomes decreased TLR2, P65, and pP65 protein expression levels. **(D)** Western blot assay results indicating the reduction in protein expression levels of TLR2, P65, and pP65 by *C. pisiformis* exosomes (fold change was calculated by the gray values of the image). *, $p \leq 0.05$; ***, $p \leq 0.001$.

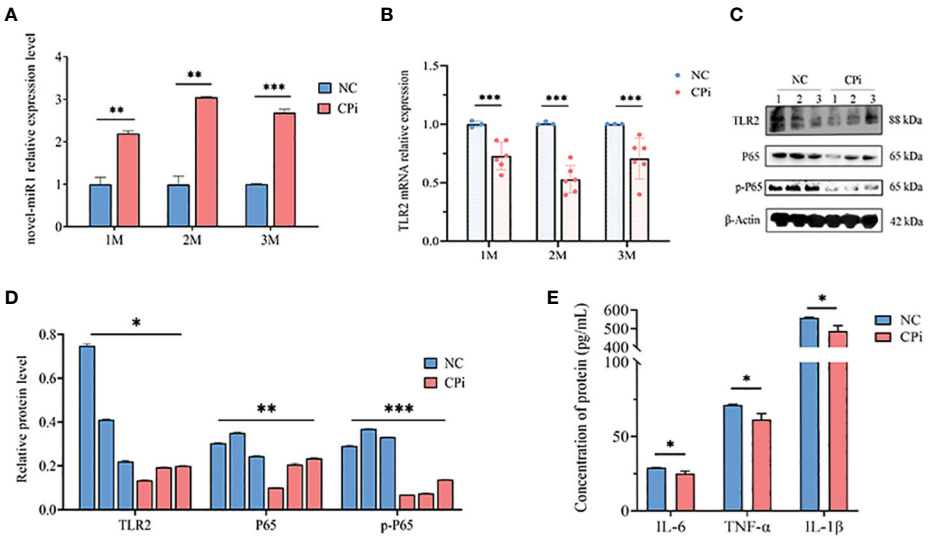

FIGURE 5
C. pisiformis inhibits the TLR2 signaling pathway and NF-κB activation. **(A)** Expression profile of novel-miR1 in rabbit PBLCs over a 3-month period. **(B)** Relative expression TLR2 mRNA in rabbit PBLCs during the initial 3-month period. **(C)** Western blot assay results indicate inhibition of TLR2, P65, and pP65 protein levels in *C. pisiformis*-infected rabbit PBLCs. **(D)** Western blot assay results demonstrating the inhibition of TLR2, P65, and pP65 protein levels in *C. pisiformis*-infected rabbit PBLCs (the fold change was calculated by the gray values of the image). **(E)** ELISA assay results indicate inhibition of IL-6, TNF-α, and IL-1β protein expression levels in *C. pisiformis*-infected rabbit PBLCs. *, $p \leq 0.05$; **, $p \leq 0.01$; ***, $p \leq 0.001$.

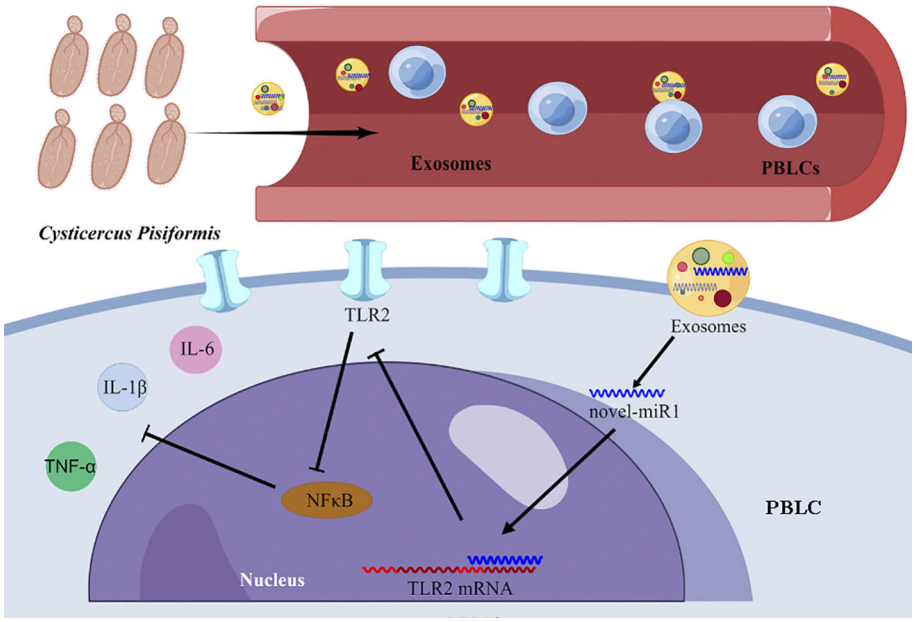

FIGURE 6
Graphical representation illustrating the mechanism of novel-miR1 targeting TLR2 in PBLCs to regulate the immune response in rabbits. The figure was created using Figdraw.

TLR2 during *C. pisiformis* infection. It has been reported that the miRNAs, as regulators of innate immunity, can regulate components of the TLR signaling pathway, including the TLRs themselves, associated signal proteins, regulatory molecules, transcription factors, and functional cytokines (40). For instance, mouse-derived mmu-miR-92a-2-5 can target TLR2 to inhibit *Schistosoma japonicum*-induced liver fibrosis and downregulate the expression of TLR2-related cytokines such as IL-4, IFN-γ, and TNF-α during *S. japonicum* infection in mice (41).

Further investigations have revealed that novel-miR1 can inhibit the expression of TNF-α-, IL-1β, and IL-6-related cytokines in rabbit PBLCs. Notably, novel-miR1 showed significant upregulation in rabbit PBLCs from 1 to 3 months during *C. pisiformis* infection in rabbits, while the corresponding expression of TLR2 was downregulated. TNF-α, IL-1β, and IL-6 play critical roles in regulating worm immune evasion. Cysteine protease inhibitors (cystatins) present in the ESPs of *Fasciola hepatica* were found to reduce the production of IL-6 and TNF-α in mouse macrophages (42). Similar findings have been reported in *S. japonicum* infections (43). Additionally, it has been reported that mice infected with *Echinococcus multilocularis* and treated with albendazole exhibited a reversal of elevated levels of IL-1β, IL-6, TNF-α, and IFN-γ in the liver (44). Inhibition of these inflammatory cytokines tends to regulate the host immune response toward Th2, and numerous studies have demonstrated the beneficial effects of helminths in inhibiting inflammatory cytokines for the management of auto-inflammatory/immune diseases (45–48).

Based on our study, we have identified that novel-miR1 has significant therapeutic potential for the treatment of allergic, inflammatory, and autoimmune disorders in rabbit. Furthermore, further investigation into the regulatory mechanisms governed by novel-miR1 holds potential for the prevention and treatment of human auto-inflammatory/immune diseases.

5 Conclusion

The results from the present study strongly indicate that *C. pisiformis*-derived exosomes serve as a means for the release of novel-miR1 into rabbit serum during parasite infection. Moreover, our results demonstrate that novel-miR1 exerts its regulatory effects by inhibiting the expression of TLR2, thereby modulating the production of pro-inflammatory factors via the NF-κB pathway. These observations support the notion that novel-miR1 plays a crucial role in facilitating parasite survival and establishment within the host (Figure 6).

Data availability statement

The original contributions presented in the study are included in the article/Supplementary Material. Further inquiries can be directed to the corresponding author.

Ethics statement

The animal study was reviewed and approved by Animal Ethics Committee of Lanzhou Veterinary Research Institute (SYXK 2020–0010).

Author contributions

GC and XNL conceived and designed the study, analyzed the data, drafted and critically revised the manuscript. GC, GP, LW performed the experiments. YL, LW, TL, HL, GP, SZ, XW, and XLL helped in the implementation of the study and performed and interpreted the computational analysis. All authors have read and approved the final manuscript.

Funding

This research was supported by grants from the National Natural Science Foundation of China (No. 32072889) and the National Key Research and Development Program of China (No.2017YFD0501303). The funders had no role in the design of the study, in the collection, analysis, or interpretation of data, in the writing of the manuscript, or in the decision to publish the results.

Acknowledgments

The authors wish to thank the Lanzhou Veterinary Research Institute for facilitating the implementation of this study.

Conflict of interest

The authors declare that the research was conducted in the absence of any commercial or financial relationships that could be construed as a potential conflict of interest.

Publisher's note

Supplementary material

The Supplementary Material for this article can be found online at: https://www.frontiersin.org/articles/10.3389/fimmu.2023.1201455/full#supplementary-material

SUPPLEMENTARY FIGURE 1
Relative expression of novel-miR1 in rabbit PBLCs treated with novel-miR1 inhibitors.

SUPPLEMENTARY FIGURE 2
qPCR results showing the relative expression of TLR2, TNF-α, IL-1β, IL-6, and IL-10 mRNA in rabbit PBLCs treated with novel-miR1 inhibitors.

SUPPLEMENTARY TABLE 1
Quantification of *C. pisiformis in* rabbits from CPi and NC groups.

SUPPLEMENTARY TABLE 2
Prediction of target genes for novel-miR1 using Targetscan, miRNADA and PITA.

SUPPLEMENTARY TABLE 3
Functional annotation clustering analysis of novel-miR1 target genes using GO.

SUPPLEMENTARY TABLE 4
KEGG pathway analysis of novel-miR1 target genes.

References

1. Samorek-Pieróg M, Karamon J, Brzana A, Bilska-Zając E, Zdybel J, Cencek T. Molecular confirmation of massive *Taenia pisiformis* cysticercosis in one rabbit in Poland. *Pathogens* (2021) 10(8):1029. doi: 10.3390/pathogens10081029

2. Chen GL, Wang LQ, Liu TL, Li YP, Zhang SH, Li H, et al. Identification and expression profiling of circulating MicroRNAs in serum of *Cysticercus pisiformis*-infected rabbits. *Genes (Basel)* (2021) 12(10):1591. doi: 10.3390/genes12101591

3. Hallal-Calleros C, Morales-Montor J, Orihuela-Trujillo A, Togno-Peirce C, Murcia-Mejía C, Bielli A, et al. *Taenia pisiformis* cysticercosis induces decreased prolificacy and increased progesterone levels in rabbits. *Vet Parasitol* (2016) 229:50–3. doi: 10.1016/j.vetpar.2016.09.015

4. Stancampiano L, Ravagnan S, Capelli G, Militerno G. Cysticercosis by *Taenia pisiformis* in brown hare (Lepus europaeus) in northern Italy: epidemiologic and pathologic features. *Int J Parasitol Parasites Wildl* (2019) 9:139–43. doi: 10.1016/j.ijppaw.2019.04.004

5. Arias-Hernández D, García-Jiménez S, Domínguez-Roldan R, Murcia-Mejía C, Báez-Saldaña A, Hallal-Calleros C, et al. Effects of *Taenia pisiformis* infection and obesity on clinical parameters, organometry and fat distribution in Male rabbits. *Pathogens* (2020) 9(11):861. doi: 10.3390/pathogens9110861

6. Wang LQ, Liu TL, Liang PH, Zhang SH, Li TS, Li YP, et al. Characterization of exosome-like vesicles derived from *Taenia pisiformis* cysticercus and their immunoregulatory role on macrophages. *Parasit Vectors* (2020) 13(1):318. doi: 10.1186/s13071-020-04186-z

7. Kalluri R, LeBleu VS. The biology, function, and biomedical applications of exosomes. *Science* (2020) 367(6478):eaau6977. doi: 10.1126/science.aau6977

8. Liang PH, Mao L, Zhang SH, Guo XL, Liu GX, Wang LQ, et al. Identification and molecular characterization of exosome-like vesicles derived from the *Taenia asiatica* adult worm. *Acta Trop* (2019) 198:105036. doi: 10.1016/j.actatropica.2019.05.027

9. Zhang X, Gong W, Cao S, Yin J, Zhang J, Cao J, et al. Comprehensive analysis of non-coding RNA profiles of exosome-like vesicles from the protoscoleces and hydatid cyst fluid of *Echinococcus granulosus*. *Front Cell Infect Microbiol* (2020) 10:316. doi: 10.3389/fcimb.2020.00316

10. Wu Z, Wang L, Li J, Wang L, Wu Z, Sun X. Extracellular vesicle-mediated communication within host-parasite interactions. *Front Immunol* (2019) 9:3066. doi: 10.3389/fimmu.2018.03066

11. Twu O, Johnson PJ. Parasite extracellular vesicles: mediators of intercellular communication. *PloS Pathog* (2014) 10(8):e1004289. doi: 10.1371/journal.ppat.1004289

12. Wang Z, Hao C, Zhuang Q, Zhan B, Sun X, Huang J, et al. Excretory/Secretory products from *Trichinella spiralis* adult worms attenuated DSS-induced colitis in mice by driving PD-1-Mediated M2 macrophage polarization. *Front Immunol* (2020) 11:563784. doi: 10.3389/fimmu.2020.563784

13. Gao X, Yang Y, Liu X, Wang Y, Yang Y, Boireau P, et al. Extracellular vesicles derived from *Trichinella spiralis* prevent colitis by inhibiting M1 macrophage polarization. *Acta Trop* (2021) 213:105761. doi: 10.1016/j.actatropica.2020.105761

14. Liang PH, Li YP, Mao L, Liu TL, Zhang SH, Ehsan M, et al. Transcriptome analysis and autophagy investigation of LoVo cells stimulated with exosomes derived from t. asiatica adult worms. *Microorganisms* (2021) 9(5):994. doi: 10.3390/microorganisms9050994

15. Abou-El-Naga IF. Emerging roles for extracellular vesicles in schistosoma infection. *Acta Trop* (2022) 232:106467. doi: 10.1016/j.actatropica.2022.106467

16. Buck AH, Coakley G, Simbari F, McSorley HJ, Quintana JF, Le Bihan T, et al. Exosomes secreted by nematode parasites transfer small RNAs to mammalian cells and modulate innate immunity. *Nat Commun* (2014) 5:5488. doi: 10.1038/ncomms6488

17. Cai MT, Ding JT, Li YT, He GT, Yang J, Liu TL, et al. *Echinococcus multilocularis* infection induces UBE2N suppression via exosomal emu-miR-4989. *Acta Trop* (2021) 223:106087. doi: 10.1016/j.actatropica.2021.106087

18. Tran N, Ricafrente A, To J, Lund M, Marques TM, Gama-Carvalho M, et al. *Fasciola hepatica* hijacks host macrophage miRNA machinery to modulate early innate immune responses. *Sci Rep* (2021) 11(1):6712. doi: 10.1038/s41598-021-86125-1

19. Wu J, Liao Y, Li DH, Zhu ZF, Zhang LC, Wu ZD, et al. Extracellular vesicles derived from *Trichinella spiralis* larvae promote the polarization of macrophages to M2b type and inhibit the activation of fibroblasts. *Front Immunol* (2022) 13:974332. doi: 10.3389/fimmu.2022.974332

20. Liu B, Li J, Cairns MJ. Identifying miRNAs, targets and functions. *Brief Bioinform* (2014) 15(1):1–19. doi: 10.1093/bib/bbs075

21. Li C, Wang Z, Chen S, Zhang J, Qu K, Liu C. MicroRNA-552 promotes hepatocellular carcinoma progression by downregulating WIF1. *Int J Mol Med* (2018) 42(6):3309–17. doi: 10.3892/ijmm.2018.3882

22. Kabekkodu SP, Shukla V, Varghese VK, D' Souza J, Chakrabarty S, Satyamoorthy K. Clustered miRNAs and their role in biological functions and diseases. *Biol Rev Camb Philos Soc* (2018) 93(4):1955–86. doi: 10.1111/brv.12428

23. He X, Pan W. Host-parasite interactions mediated by cross-species microRNAs. *Trends Parasitol* (2022) 38(6):478–488. doi: 10.1016/j.pt.2022.02.011

24. Zhou R, Gong AY, Eischeid AN, Chen XM. miR-27b targets KSRP to coordinate TLR4-mediated epithelial defense against *Cryptosporidium parvum* infection. *PloS Pathog* (2012) 8(5):e1002702. doi: 10.1371/journal.ppat.1002702

25. Jin X, Li Y, Yang X, Zheng Y. Modulatory effects of *Echinococcus multilocularis* emu-let-7-5p on the immunological functions of RAW264.7 macrophages. *Front Vet Sci* (2021) 8:663497. doi: 10.3389/fvets.2021.663497

26. Kawai T, Akira S. TLR signaling. *Semin Immunol* (2007) 19(1):24–32. doi: 10.1016/j.smim.2006.12.004

27. Zang R, Lian H, Zhong X, Yang Q, Shu HB. ZCCHC3 modulates TLR3-mediated signaling by promoting recruitment of TRIF to TLR3. *J Mol Cell Biol* (2020) 12(4):251–62. doi: 10.1093/jmcb/mjaa004

28. Hoppstädter J, Dembek A, Linnenberger R, Dahlem C, Barghash A, Fecher-Trost C, et al. Toll-like receptor 2 release by macrophages: an anti-inflammatory program induced by glucocorticoids and lipopolysaccharide. *Front Immunol* (2019) 10:1634. doi: 10.3389/fimmu.2019.01634

29. Rajasekaran S, Anuradha R, Bethunaickan R. TLR specific immune responses against helminth infections. *J Parasitol Res* (2017) 2017:6865789. doi: 10.1155/2017/6865789

30. Yan C, Fang F, Zhang YZ, Dong X, Wu J, Liu HL, et al. Recombinant CsHscB of carcinogenic liver fluke clonorchis sinensis induces IL-10 production by binding with TLR2. *PloS Negl Trop Dis* (2020) 14(10):e0008643. doi: 10.1371/journal.pntd.0008643

31. Wojtkowiak-Giera A, Derda M, Wandurska-Nowak E, Jagodziński PP, Kolasa-Wołosiuk A, Kosik-Bogacka D, et al. Changes in the expression of TLR2 during the intestinal phase of trichinellosis. *J Vet Res* (2020) 64(2):269–74. doi: 10.2478/jvetres-2020-0027

32. Reyes JL, González MI, Ledesma-Soto Y, Satoskar AR, Terrazas LI. TLR2 mediates immunity to experimental cysticercosis. *Int J Biol Sci* (2011) 7(9):1323–33. doi: 10.7150/ijbs.7.1323

33. Soleymani N, Taran F, Nazemshirazi M, Naghibi A, Torabi M, Borji H, et al. Dysregulation of ovine toll-like receptors 2 and 4 expression by hydatid cyst-derived antigens. *Iran J Parasitol* (2021) 16(2):219–28. doi: 10.18502/ijpa.v16i2.6271

34. Wang LQ, Liu TL, Chen GL, Li YP, Zhang SH, Mao L, et al. Exosomal microRNA let-7-5p from *Taenia pisiformis* cysticercus prompted macrophage to M2 polarization through inhibiting the expression of C/EBP δ. *Microorganisms* (2021) 9 (7):1403. doi: 10.3390/microorganisms9071403

35. Deng Y, Ediriwickrema A, Yang F, Lewis J, Girardi M, Saltzman WM. A sunblock based on bioadhesive nanoparticles. *Nat Mater* (2015) 14(12):1278–85. doi: 10.1038/nmat4422

36. Li S, Yuan L, Su L, Lian Z, Liu C, Zhang F, et al. Decreased miR-92a-3p expression potentially mediates the pro-angiogenic effects of oxidative stress-activated endothelial cell-derived exosomes by targeting tissue factor. *Int J Mol Med* (2020) 46 (5):1886–98. doi: 10.3892/ijmm.2020.4713

37. Livak KJ, Schmittgen TD. Analysis of relative gene expression data using real-time quantitative PCR and the 2(-delta delta C(T)) method. *Methods* (2001) 25(4):402–8. doi: 10.1006/meth.2001.1262

38. Wang X, Ha T, Liu L, Hu Y, Kao R, Kalbfleisch J, et al. TLR3 mediates repair and regeneration of damaged neonatal heart through glycolysis dependent YAP1 regulated miR-152 expression. *Cell Death Differ* (2018) 25(5):966–82. doi: 10.1038/s41418-017-0036-9

39. Hua Z, Hou B. TLR signaling in b-cell development and activation. *Cell Mol Immunol* (2013) 10(2):103–6. doi: 10.1038/cmi.2012.61

40. He X, Jing Z, Cheng G. MicroRNAs: new regulators of toll-like receptor signalling pathways. *BioMed Res Int* (2014) 2014:945169. doi: 10.1155/2014/945169

41. Zhao Y, Dang Z, Chong S. Mmu-miR-92a-2-5p targets TLR2 to relieve *Schistosoma japonicum*-induced liver fibrosis. *Int Immunopharmacol* (2019) 69:126–35. doi: 10.1016/j.intimp.2019.01.007

42. Zhang K, Liu Y, Zhang G, Wang X, Li Z, Shang Y, et al. Molecular characteristics and potent immunomodulatory activity of *Fasciola hepatica* cystatin. *Korean J Parasitol* (2022) 60(2):117–26. doi: 10.3347/kjp.2022.60.2.117

43. Yang X, Liu J, Yue Y, Chen W, Song M, Zhan X, et al. Cloning, expression and characterisation of a type II cystatin from *Schistosoma japonicum*, which could regulate macrophage activation. *Parasitol Res* (2014) 113(11):3985–92. doi: 10.1007/s00436-014-4064-9

44. Weingartner M, Stücheli S, Jebbawi F, Gottstein B, Beldi G, Lundström-Stadelmann B, et al. Albendazole reduces hepatic inflammation and endoplasmic reticulum-stress in a mouse model of chronic *Echinococcus multilocularis* infection. *PloS Negl Trop Dis* (2022) 16(1):e0009192. doi: 10.1371/journal.pntd.0009192

45. Christen U, Hintermann E. Pathogens and autoimmune hepatitis. *Clin Exp Immunol* (2019) 195(1):35–51. doi: 10.1111/cei.13203

46. Lerner A, Arleevskaya M, Schmiedl A, Matthias T. Microbes and viruses are bugging the gut in celiac disease. are they friends or foes? *Front Microbiol* (2017) 8:1392. doi: 10.3389/fmicb.2017.01392

47. Gazzinelli-Guimaraes PH, Nutman TB. Helminth parasites and immune regulation. *F1000Res* (2018) 7:F1000 Faculty Rev–1685. doi: 10.12688/f1000research.15596.1

48. Terrazas CA, Sánchez-Muñoz F, Mejía-Domínguez AM, Amezcua-Guerra LM, Terrazas LI, Bojalil R, et al. Cestode antigens induce a tolerogenic-like phenotype and inhibit LPS inflammatory responses in human dendritic cells. *Int J Biol Sci* (2011) 7 (9):1391–400. doi: 10.7150/ijbs.7.1391

frontiers | Frontiers in Immunology

TYPE Original Research
PUBLISHED 02 August 2023
DOI 10.3389/fimmu.2023.1215913

OPEN ACCESS

EDITED BY
William Harold Witola,
University of Illinois at Urbana–Champaign, United States

REVIEWED BY
Juan Diego Maya,
University of Chile, Chile
Juliana A. S. Gomes,
Federal University of Minas Gerais, Brazil

*CORRESPONDENCE
Antonio Osuna
aosuna@ugr.es

†These authors have contributed equally to this work

RECEIVED 02 May 2023
ACCEPTED 17 July 2023
PUBLISHED 02 August 2023

CITATION
Cornet-Gomez A, Moreira LR, Gomez-Samblás M and Osuna A (2023) Extracellular vesicles of *Trypanosoma cruzi* and immune complexes they form with sialylated and non-sialylated IgGs increase small peritoneal macrophage subpopulation and elicit different cytokines profiles.
Front. Immunol. 14:1215913.
doi: 10.3389/fimmu.2023.1215913

Extracellular vesicles of *Trypanosoma cruzi* and immune complexes they form with sialylated and non-sialylated IgGs increase small peritoneal macrophage subpopulation and elicit different cytokines profiles

Alberto Cornet-Gomez[1†], Lissette Retana Moreira[1,2,3†], Mercedes Gomez-Samblás[1] and Antonio Osuna[1*]

[1]Grupo de Bioquímica y Parasitología Molecular (CTS 183), Departamento de Parasitología, Instituto de Biotecnología, Universidad de Granada, Granada, Spain, [2]Departamento de Parasitología, Facultad de Microbiología, Universidad de Costa Rica, San José, Costa Rica, [3]Centro de Investigación en Enfermedades Tropicales (CIET), Universidad de Costa Rica, San José, Costa Rica

American trypanosomiasis, or Chagas disease, is caused by the protozoan parasite *Trypanosoma cruzi* and is characterized by the presence of cardiac or gastrointestinal symptoms in a large number of patients during the chronic phase of the disease. Although the origin of the symptoms is not clear, several mechanisms have been described involving factors related to *T. cruzi* and the host immune response. In this sense, the extracellular vesicles (EVs) secreted by the parasite and the immune complexes (ICs) formed after their recognition by host IgGs (EVs-IgGs) may play an important role in the immune response during infection. The aim of the present work is to elucidate the modulation of the immune response exerted by EVs and the ICs they form by analyzing the variation in the subpopulations of small and large peritoneal macrophages after intraperitoneal inoculation in mice and to evaluate the role of the sialylation of the host IgGs in this immunomodulation. Both macrophage subpopulations were purified and subjected to cytokine expression analysis by RT-qPCR. The results showed an increase in the small peritoneal macrophage subpopulation after intraperitoneal injection of parasite EVs, but a greater increase in this subpopulation was observed when sialylated and non-sialylated ICs were injected, which was similar to inoculation with the trypomastigote stage of the parasite. The cytokine expression results showed the ability of both subpopulations to express inflammatory and non-inflammatory cytokines. These results suggest the role of free EVs in the acute phase of the disease and the possible role of immune complexes in the immune response in the chronic phase of the disease, when the levels of antibodies against the parasite allow the formation of immune complexes. The differential expression of

interleukins showed after the inoculation of immune complexes formed with sialylated and non-sialylated IgGs and the interleukins expression induced by EVs, demonstrates that the IgG glycosilation is involved in the type of immune response that dominates in each of the phases of the Chagas disease.

KEYWORDS

extracellular vesicles, trypomastigotes, *Trypanosoma cruzi*, macrophages, interleukins, immune modulation

1 Introduction

Trypanosoma cruzi (*T. cruzi*) is the causative agent of American trypanosomiasis or Chagas disease, considered a neglected infectious disease by the World Health Organization. Recent studies estimate that there are 6-7 million people infected with this parasite, approximately 14,000 deaths per year by causes related to the infection, and approximately 80 million people at risk of infection (1, 2). Chagas disease was initially restricted to geographical areas where the natural biological cycle of the parasite was maintained, comprising 21 countries in the Americas; however, it has become a global health issue as a result of migratory movements. Besides transmission through contact with feces of infected triatomine bugs of the family Reduviidae (subfamily Triatominae), infection with the parasite can occur by oral, transfusional or through vertical routes, epidemiologically important in areas where vector-borne transmission does not occur (3, 4).

The course of Chagas disease presents two phases: acute and chronic. The acute phase corresponds to the first weeks of infection with this intracellular parasite, in which no clear pathognomonic symptoms are present, but high parasitemia can be observed. The chronic phase appears from the 3rd to the 8th week after infection and, during this phase, the presence of trypomastigotes (the infective stage of the parasite for the vertebrate host) in blood is drastically reduced; however, the individual remains infected for decades. It is estimated that only 30-40% of infected individuals will develop characteristic symptoms of the disease during the chronic phase (determinate form of the disease), including cardiac involvement or gastrointestinal megasyndromes (5, 6).

During an infection with *T. cruzi*, the immune system plays a crucial role; in this sense, the innate immune response is able to detect the pathogen-associated molecular patterns (PAMPs) present on the parasite`s surface, most of which are the glycosylphosphatidylinositol anchors derived from *T. cruzi* mucin-like glycoproteins (GPI-mucins). These molecules are recognized by Toll-like receptors (TLRs), which are part of a group of receptors called pattern recognition receptors (PRRs) (7, 8). Stimulation of TLRs is important in controlling parasitemia through the production of cytokines such as IL-12 and IFN-γ. During the acute phase of the disease, an increased production of inflammatory cytokines (IL-12, IL-6, IFN-γ and TNF-α) and chemokines (CCL2, CCL3, CCL4, CCL5 and CXCL10) is observed. Following PAMP recognition, antigen presenting cells (APCs) initiate the adaptive immune response necessary to control parasitemia, leading to the production of specific antibodies and the activation of CD4+ and CD8+ T lymphocytes. Moreover, during this phase, the inflammatory response (Th1 and Th17) also leads to the production of nitric oxide (NO), and this response is related to the resistance to *T. cruzi* infection and control of parasitemia (9–11). Although the inflammation process elicited during the acute phase of the disease is able to control parasitemia, it does not completely eliminate the parasite, leading to the chronic phase, in which a fine balance between inflammatory and anti-inflammatory cytokines and an effective cellular response needs to be reached to keep parasite levels in check while avoiding tissue damage (12).

Macrophages are considered to be part of the first barrier to prevent infections, acting as antigen-presenting cells to CD4+ T lymphocytes. Under normal physiological conditions, monocytes present a quiescent state (M0: CCL1-, CD163-, CD14+) (13); however, macrophages have been classified as M1 and M2, the former based on classical activation, and M2 designated for alternatively activated macrophages. M1 macrophages are mostly induced by TLR ligands (bacterial lipopolysaccharides, LPS) or by some cytokines, such as IFN-γ, TNF-α and GM-CSF. On the other hand, M2 macrophages refer to alternatively activated macrophages and can be polarized by various stimulatory factors, such as cytokines (IL-4, IL-10 and IL-13), glucocorticoids or immune complexes and LPS. This macrophage classification into M1 and M2 is maintained despite evidence that M2 designation encompasses cells with different physiological and biochemical patterns (14). Moreover, in 2010, Ghosn et al. described two subpopulations of peritoneal macrophages with physically, functionally and evolutionarily different immunological markers: i.) large peritoneal macrophages (LPM), of embrionary origin and that express high levels of CD11b and F4/80, and ii.) small peritoneal macrophages (SPM) of monocytic origin and that express lower levels of CD11b and F4/80 but higher levels of MHC-II. LPM are the majority subpopulation in unstimulated animals but, upon inflammatory stimuli, for example, with LPS, thyoglicolate or after inoculation of *T. cruzi* flagellate forms, SPM become the majority subpopulation (15, 16). SPM, but not LPM, have the ability to present antigens to naive CD4+ T cells *via* the activating receptor DNAM-1 (CD226) (17). These authors propose that SPM are functionally distinct from LPM and that DNAM-1

plays a co-stimulatory role in antigen presentation by SPM. An increased phagocytic capacity of SPM and differences in cytokine production have also been reported. Despite these facts, the role of each macrophage subset has never been described, making it impossible to fit them into the classical M1/M2 classification (18).

IgGs are traditionally recognized as mediators of the humoral immune response. Antibodies bind and neutralize antigens by their Fab region to promote complement-dependent cytotoxicity resulting from binding of antibodies *via* the Fab region to antigen epitopes and binding of Fc regions to complement, binding to specific receptors (FcR) present on the cell membranes of lymphoid cells and in particular of macrophages, which allows the opsonization of antigens and the initiation of phagocytosis of immune complexes by these phagocytic cells.

Based on these receptors present on the surface of macrophages, the effector functions initiated by antibodies and recognized as proinflammatory mediators of the humoral immune response are triggered by the Fc domain upon binding to FcR receptors. Fc γ receptor IIb (FcγRIIb) is the only inhibitory FcγR in the FcγR family (19). These effector functions are largely dependent on the N-terminally bound biantennary glycan of IgG heavy chains, which is located below the Ig hinge region (20, 21). This glycan is considered to hold the two Fc heavy chains in an open conformation necessary to interact with activating Fcγ receptors (FcγRs). However, the presence in the sugar chain of terminal sialic acid in the glycan has profound implications on the effector functions of Fc by inhibiting activation by cells (22), and it is the FcRγIIb receptors that would be responsible for binding to such immunoglobulins carrying sialic acid in their Fc region (23). The presence of sialic acid, bound in an α2,6 bond to the penultimate terminal galactose of the glycan reduces FcγR binding and converts IgG antibodies to anti-inflammatory mediators demonstrated activity (24, 25). Thus, glycosylated IgGs in Fc would be responsible for the *in vivo* anti-inflammatory activity of Intravenous immunoglobulin (IVIg) therapy (24). Where immune complexes with sialylated Fcs initiate an anti-inflammatory cascade *via* the receptor or lectin SIGN-R1 (26). Instead of binding to the FcγR, sialylated Fcs may rather interact with inflammatory cells by the FcR inhibitor, FcγRIIb, or *via* the lectin receptor SIGN-R1 or DC-SIGN and the initiate an anti-inflammatory cascade. This leads to an inhibitory FcγRIIb surface expression on inflammatory cells, thus attenuating the inflammation initiated by autoantibodies in autoimmune diseases where this type of therapy has been used (21). In addition, other authors have recently proposed the hypothesis that non-fucosylated IgGs in serum can saturate FcgRIIIa in immune cells due to its high affinity for the receptor and thus modulate immune responses, demonstrating how the anti-inflammatory activity of IVIG is mediated through activating blockade of the FcgR by galactosylated IgGs, modulating by inhibiting antibody dependent cellular cytotoxicity (ADCC). and complement-dependent cytotoxicity (27).

Extracellular vesicles (EVs) are small membrane-coated vesicles released into the extracellular milieu by all cell types, and classified according to their size, biogenesis and composition (28). In *T. cruzi*, the cargo of EVs is complex and includes nucleic acids (DNA, RNA and miRNA), proteins, lipids and different metabolites (29–32). In previous studies, our research group characterized some of the biological properties of EVs released by different stages of the parasite, studying some of their physical properties, the effects of the interaction between these EVs and cells at the molecular level, the localization and presence of *trans*-sialidases, the formation of immune complexes EVs-IgGs in the plasma of patients and the role they play in inhibiting the complement system; the presence of immune complexes in patients sera means that they could play a role a systemic level (33–36). Garcia-Silva et al. (37) studied the changes induced by EVs secreted by non-infective stages of *T. cruzi* over HeLa cells, finding that the expression of inflammatory interleukins IL-1, IL-6 and IL-18 was increased even after the stimulation with EVs secreted by these non-infective forms. Other groups have also evidenced the ability of EVs of the parasite to induce the release of proinflammatory cytokines (TNF-α and IL-6) and NO production by murine macrophages by interacting with TLR2 (38, 39). In this sense, it is well known that *T. cruzi* is present in biological fluids, including ascitic fluid, and is capable of forming nests of amastigotes and trypomastigotes in the peritoneal membrane, not only in the chronic phase but also in the acute phase of the infection (40). On the other hand, the histopathological presence of *T. cruzi* amastigotes nests have been described in different organs such as liver, spleen, pancreas or colon; high concentrations of *T. cruzi* DNA was found in the myocardium, urinary bladder, stomach, lymph nodes, adrenal gland, and colon (41–43).

In the present work, we present an analysis of the variation of peritoneal macrophage subpopulations after the intraperitoneal cavity inoculation of mice with EVs of tissue-culture cell-derived trypomastigotes of *T. cruzi*, including analyses of interleukin profiles expressed by these two populations after the EVs-stimulus. Stimulation of mice with immune complexes formed *in vitro* after the incubation of EVs of the parasite with sialylated or non-sialylated IgGs anti-*T. cruzi* are also included, assessing the potential differences that sialylated immunoglobulins could play in the activation processes. In the present work, using as a model of "inflammatory response" the variations in the populations of peritoneal macrophages in the presence of forms of *T. cruzi* already described by (15, 16), we study the role played by the immune complexes formed by the extracellular vesicles of the parasite recognized by sialylated and non-sialylated IgGs, all of them purified from an immunoserum against the parasite antigens, as well as the different expression of cytokines expressed by the different populations of peritoneal macrophages that emerged after intraperitoneal inoculation of the different stimuli.

2 Materials and methods

2.1 Cell culture and parasite strain

Vero cells (ECACC 84113001) were obtained from the cell bank of the "Centro Instrumentación Científica" of the University of Granada. The cells were cultured in 75 cm^2 surface area flasks (Thermo Fischer Scientific, Waltham, MA, USA) using Modified Eagle´s Medium (MEM) medium (Sigma Aldrich, St. Louis, MO,

USA) supplemented with 10% heat-inactivated (56 °C, 30 min) fetal bovine serum (iFBS) (Gibco, Waltham, MA, USA) plus antibiotics (penicillin 100 U/mL; streptomycin 100 µg/mL) and maintained at 37°C, in a moist atmosphere enriched with 5% CO_2.

For Vero cell infection with the infective trypomastigote stage of the parasite, or for the collection of its secreted products for EVs purification, the *T. cruzi* Pan4 (Tc Ia + Tc Id) strain (44) was used. This strain was isolated by our group in 2004, in collaboration with Dr. A. Ying of the University of Panama, and it is. maintained in culture and cryopreserved in our laboratory. Cell infections were performed as previously described (34, 45) and trypomastigotes derived from cell cultures were obtained for EVs collection. Briefly, Vero cell monolayers were disrupted with trypsin-EDTA solution, the cells were washed and then seeded on a new culture flask (1 x 10^6 cells/mL) using MEM + 10% iFBS + antibiotics. Once the cells had attached to the surface of the flask (12 hours), they were washed with sterile phosphate buffered saline (PBS) and subsequently infected with a suspension of the metacyclic forms obtained in culture and purified using Percoll, according to the methodology described by Castanys et al. (46). Cell cultures were incubated with parasites for 6 hours in MEM culture medium (parasite/cell ratio of 3 parasites per cell) and, after the incubation time, non-internalized parasites were removed, cell cultures were washed with PBS, and fresh MEM + 10% iFBS + antibiotics was added. After 96-120 hours of the intracellular development of the parasite, tissue-culture cell-derived trypomastigotes present in culture supernatant were harvested by centrifugation.

2.2 Purification of EVs secreted by trypomastigotes

Trypomastigotes were collected from the supernatant of infected cell cultures, in which the parasite had continuously completed a series of intracellular cycles of development. An initial centrifugation of the supernatant at 500 x g for 5 minutes was performed to remove cell debris and, once this centrifugation was completed, the resulting supernatant was centrifuged at 3,000 x g for 15 minutes to concentrate the trypomastigotes in the pellet. Then, the pellet with the parasites was washed 3 times in sterile PBS and 5 x 10^7 parasites were placed in 75 cm^2 surface area flasks (Thermo Fischer Scientific, Waltham, MA, USA) with 10 mL of MEM without iFBS (pH 7.2) for EVs secretion. Flasks with the parasites were incubated for 5 hours at 37 °C in 5% CO_2 enriched atmosphere. Thereafter, the supernatants were collected and centrifuged at 3,500 x g for 15 minutes at 4 °C to remove the parasites.

For EVs isolation and purification, the methodology previously described by our group was employed (34b; 35). Briefly, supernatants with the secreted products of trypomastigotes were subjected to a centrifugation step at 17,000 x g for 30 minutes at 4 °C to remove any apoptotic vesicles and cell debris. After this step, the supernatants obtained were filtered through sterile filters with a pore size of 0.22 µm (Sartorius, Göttingen, Germany, Germany) in order to select EVs with a diameter smaller than the pore size and to remove aggregates or other types of vesicles such as larger ectosomes. The ultrafiltrated samples were then ultracentrifuged at 100,000 x g for 4 hours at 4 °C in a CP100NX ultracentrifuge (Hitachi Koki, Tokyo, Japan) with a P70AT fixed-angle rotor for EVs isolation and, after this centrifugation step, the pellets containing EVs were washed three times by ultracentrifugation using sterile filtered PBS. Finally, EVs were concentrated by ultracentrifugation in a P50A3 fixed-angle rotor and resuspended in 100 µL of sterile filtered PBS.

The isolation procedure and purity of EVs samples were evaluated by transmission electron microscopy, nanoparticle tracking analysis and atomic force microscopy, following the methodologies described in previous works (34–36). The protein concentration of EVs was measured using the microBCA protein assay kit (Thermo Fischer Scientific, Waltham, MA, USA), following the manufacturer's instructions and the viability of trypomastigotes after the 5-hour period of EVs secretion was assessed by the trypan blue exclusion assay, maintaining a percentage close to 99% of live forms.

2.3 Animal handling and permission of the animal welfare and ethics committee

The use of animals was carried out according to institutional guidelines (Spanish Government Regulations: Royal Decree RD1201/05) and European Union guidelines (European Directive 2010/63/EU), having been approved by the Ethics Committee of the University of Granada (Ethics Committee, 235-CEEA-OH-2018), as well as by the authorities of the Regional Government of the Junta de Andalucía with number 12/11/2017/162.

2.4 Transmission electron microscopy

For visualization of EVs, samples obtained from the last ultracentrifugation step were resuspended in 30 µL Tris-HCl (pH 7.3) and 5 µL of the suspension was applied directly onto Formvar/carbon-coated grids. After 30 minutes, the grids were washed in PBS and fixed in 1% glutaraldehyde for 30 minutes. After the fixation step, the grids were washed again in PBS and stained and counterstained with 2% (v/v) uranyl acetate. Finally, the samples were observed under a Carl Zeiss SMT LIBRA 120 PLUS TEM microscope. The size of the nanoparticles was measured using the microscope's own measuring scale and Image J 1.41 software.

2.5 Nanoparticle tracking analysis

Distribution, size, and concentration of the EVs samples of *T. cruzi* were determined by measuring the rate of Brownian motion according to the particle size in a Nanosight NS300 (Malvern Instruments, UK). For this purpose, EVs samples were diluted in sterile filtered PBS up to 1 mL and loaded into the high-sensitivity EMCCD chamber for excitation with a 405 nm laser available on the instrument. The Brownian motion images were recorded in three 60-second videos on a camera and analyzed for each of the samples using the instrument's image analysis software, NTA 2.3

(NanoSight, UK). Measurement conditions were manually adjusted for both shutter, gain, brightness and threshold, all measured at 25 °C. The mean size distribution was calculated as the average of three independent size distributions.

2.6 Preparation of polyclonal anti-*T. cruzi* antibodies and separation of sialylated and non-sialylated IgGs

2.6.1 Preparation of polyclonal anti *T. cruzi* antibodies

Five male BALB/c mice were immunized with 20 µg per dose of a total trypomastigote extract of *T. cruzi* Pan4 to produce a polyclonal anti-*T. cruzi* antibody. The parasite extract was obtained from 10^9 trypomastigotes from cell cultures previously washed and concentrated by centrifugation as described above. The pellet containing the parasites was subjected to three cycles of freezing at -20 °C and slow thawing, and then sonicated in a Branson SLP sonifier (10 s intervals and 10 s pauses, for 2 min). The protein concentration of the lysate was quantified using the microBCA protein assay kit (Thermo Fischer Scientific, Waltham, MA, USA) and aliquoted to 20 µg per 250 µL of PBS.

For the first immunization, the antigen suspension was prepared by mixing it with Freund's complete adjuvant (Sigma, USA) in a 1:1 ratio (final volume: 500 µL). Freund's incomplete adjuvant (Sigma, USA) was used for subsequent immunizations up to a total of 7 (one per week). The antibody titers of the serum samples were determined weekly after the first two immunizations by indirect ELISA and, at the end of the immunization period (8 weeks) mice were euthanized under isoflurane. Whole blood samples were obtained by cardiac puncture and sera were collected using BD Microtainers® (BD, Franklin Lakes, New Jersey, USA). Final antibody titers were determined by enzyme-linked immunosorbent assay (ELISA) as described elsewhere.

2.6.2 Electrophoretic separation of proteins and Western blot

Proteins from EVs samples of *T. cruzi* were precipitated in acetone at -20 °C overnight. The precipitated samples were centrifuged at 13,000 x g for 10 minutes at 4 °C and washed twice with cold acetone. Finally, the acetone was evaporated under a nitrogen stream and the precipitated proteins were quantified using the MicroBCA protein assay kit (Thermo Fischer Scientific, Waltham, MA, USA). For electrophoresis, 30 µg of proteins of EVs were loaded onto 12% SDS-PAGE gels and then transferred to PVDF membranes (BioRad, Hercules, CA, USA) in a Turbo Trans-Blot transfer system (BioRad, Hercules, CA, USA). The membranes were immersed in blocking buffer (PBS, 0.1% Tween 20 and 4% nonfat dry milk) and incubated for 2 hours at 4 °C and under gentle shaking. The blocked membranes were then incubated with a 1:1,000 dilution of the polyclonal anti-*T. cruzi* antibodies overnight at 4 °C. After this incubation, the membranes were washed and incubated with peroxidase-conjugated goat anti-mouse IgG (1: 1,000) (Dako Agilent Pathology Solutions, USA) for 1 hour at room temperature. The detected bands were visualized using Clarity ECL Western Substrate (BioRad, Hercules, CA, USA) on a ChemiDoc Imaging system (BioRad, Hercules, CA, USA).

2.6.3 Purification of sialylated and non-sialylated IgGs

IgGs anti-*T. cruzi* were purified from polyclonal anti-*T. cruzi* antibodies using Melon gel chromatography gel monoclonal IgG purification kit (Thermo Fischer Scientific, Waltham, MA, USA), following the manufacturer's instructions. Microcolumns were prepared by placing 500 µL of gel in an empty cartridge that was centrifuged at 3,000 x g for 1 minute to densify the gel, followed by two washes with 300 µL of the purification buffer provided with the kit. Then, 0.5 mL of serum with polyclonal antibodies were diluted 1:10 with the purification buffer, added to the column and incubated for 5 minutes under agitation. The column was then centrifuged to collect the purified IgGs present in the elution.

In order to separate sialylated from non-sialylated IgGs, an affinity chromatography using minicolumns coupled to Sambucus nigra lectin (SNA, EBL) agarose (Vector Laboratories, Newark, CA, USA) was performed. For this purpose, 500 µL of Sambucus nigra lectin (SNA, EBL)-agarose were placed in an empty cartridge (Thermo Fischer Scientific, Waltham, MA, USA) and submitted to a centrifugation step at 3,000 x g for 1 minute to densify the matrix of these columns. Then, 3 washing steps of the column with PBS, followed by 3 washing steps with Hank`s solution (Sigma Aldrich, St. Louis, MO, USA) were performed. IgGs previously purified using the Melon Gel Chromatography Purification Kit were diluted in Hank's solution at a 1:1 ratio and added to the lectin for 10 minutes at room temperature with gentle agitation. Thereafter, the column was centrifuged at 3,000 x g for 1 minute and the eluate (containing non-sialylated IgGs) was collected. The column was washed 4 times with PBS, collecting the eluate after each step.

Elution of sialylated IgGs was performed by adding 2 volumes of 0.5 M lactose in PBS, followed by further washing with 2 volumes of 0.5 M lactose and 0.2 M acetic acid in PBS; once the sialylated IgGs was eluted, the pH of the samples was neutralized to 7.2 by adding Tris base. Both sialylated and non-sialylated IgGs were dialyzed against 0.1 M ammonium acetate for 24 hours with at least 4 changes of the dialysis fluid. The protein concentration of the samples was quantified using the microBCA protein assay kit (Thermo Fischer Scientific, Waltham, MA, USA) and after quantification, the samples were aliquoted and lyophilized. Before use, lyophilized IgGs were resuspended in sterile PBS. Both the purity of the samples and whether or not they were sialylated IgGs were assessed by 12.5% SDS-PAGE electrophoresis followed by Western blot.

For Western blot, 10 µg of sialylated and non-sialylated IgGs obtained as previously described were separated by 12.5% SDS-PAGE gel electrophoresis. After electrophoretic separation, transference to PVDF membranes (BioRad, Hercules, CA, USA) was performed using a Trans-Blot turbo transfer system (BioRad, Hercules, CA, USA). The membranes were then blocked and washed as previously described, and incubation with 5 µg/mL Sambucus nigra biotin-linked lectin (SNA, EBL) (Vector Laboratories, Newark, CA, USA) for 25 minutes at

room temperature was performed. After this incubation, the membranes were washed 6 times in PBS-Tween 20 0.1% and then incubated with streptavidin-HRP (1:8000) for 45 minutes at room temperature. Finally, the membranes were washed 6 times with PBS-Tween 20 0.1% and visualized on a ChemiDoc MP imaging system (BioRad, Hercules, CA, USA) (Figure 1C).

2.6.4 Recognition of EVs proteins by IgGs anti-*T. cruzi*

To evaluate the recognition and binding of proteins in EVs by polyclonal anti-*T. cruzi* IgGs, 30 µg of EVs were resolved by SDS-PAGE electrophoresis and analyzed by Western blot, as previously described. For this purpose, the analyses were performed using the anti-*T. cruzi* IgGs separated from the polyclonal anti-*T. cruzi* antibodies produced in mice (1:100). Goat anti-mouse IgGs conjugated with peroxidase (Agilent Technologies, Santa Clara, CA, USA) (1: 1,000) were used as secondary antibodies and visualization was performed in a ChemiDoc MP imaging system (BioRad, Hercules, CA, USA).

2.6.5 Preparation of immune complexes (ICs) EVs - IgGs anti-*T. cruzi* and inoculation of mice

To carry out the formation of immune complexes *in vitro* using EVs of trypomastigotes and IgGs anti-*T. cruzi*, a methodology previously described was applied, and the amount of proteins of EVs necessary to carry out the experiment was set at a rate of 38 µg of EVs per mouse (equivalent to approximately 5.087 x 10^8 EVs) (35).

Incubation of EVs and anti-*T. cruzi* IgGs (sialylated and non-sialylated IgGs) was performed under orbital shaking (10 rotations per minute) at 37 °C for 1 hour. Thereafter, the samples were washed 3 times by ultracentrifugation in sterile-filtered PBS plus

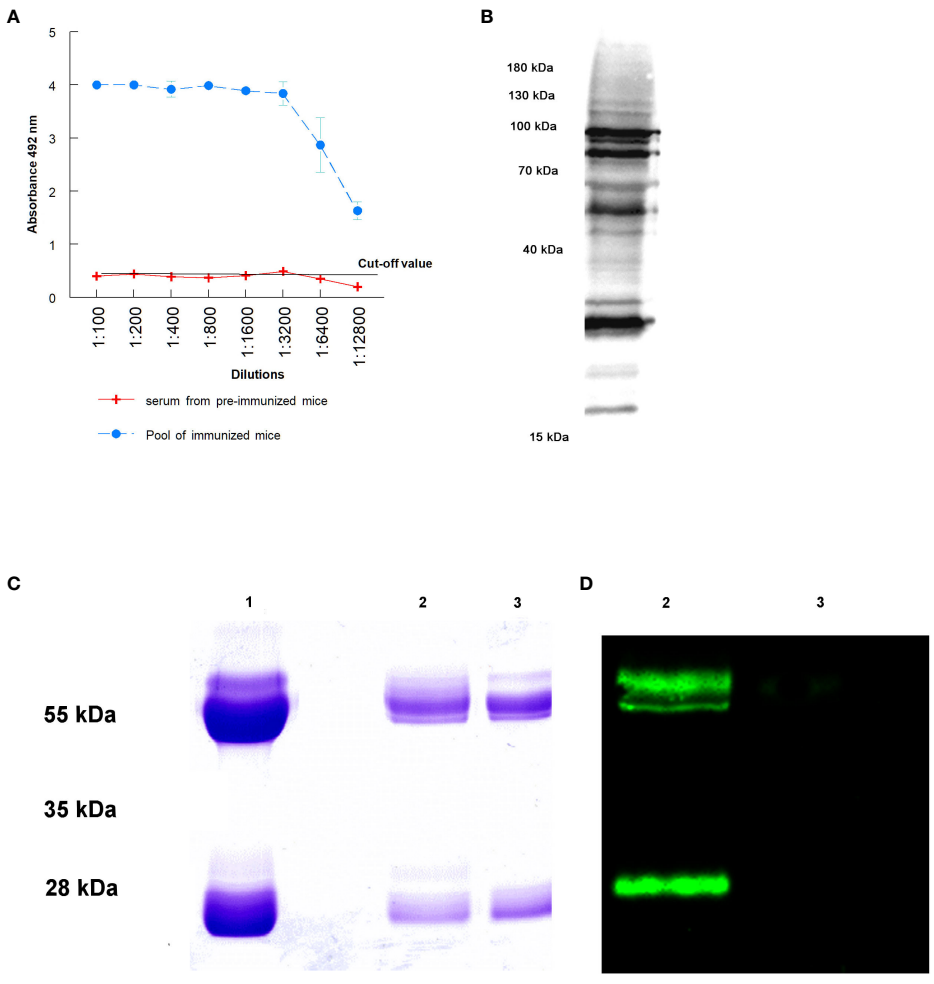

FIGURE 1
Purification of IgGs anti *T. cruzi* after the immunization of mice: **(A)** antibody titers obtained against total proteins of trypomastigotes of *T. cruzi*; **(B)** antibody recognition of total proteins from a lysate of trypomastigotes by Western blot; **(C)** SDS-PAGE electrophoresis of purified immunoglobulins: purification of total IgGs by Melon gel chromatography (1), sialylated (2) and non-sialylated IgGs (3) after affinity chromatography using Sambucus nigra lectin; **(D)** Western blot analysis using biotinilated Sambucus nigra lectin and revealed with streptavidin HRP: sialylated (2) and non-sialylated IgGs (3).

protease inhibitors (Roche, Switzerland) to remove unbound immunoglobulins and each pellet was then resuspended in 100 µL of sterile-filtered PBS and stored at 4 °C until inoculation into the animals. An aliquot of the immune complexes obtained was examined by atomic force microscopy (Figure 2).

For the intraperitoneal inoculation of mice with the previously prepared stimuli, 4 animals were used for each batch, which consisted of 250 µL of PBS containing an equivalent amount of proteins from each of the different fractions of the purified IgGs (sialylated or non-sialylated IgGs).

2.7 Atomic force microscopy

To visualize the binding of the anti-*T. cruzi* IgGs to the purified EVs released by trypomastigotes, atomic force microscopy analyses were performed, following the methodology previously described (36). For these experiments, 8 µL of the suspension of ICs formed *in vitro* (EVs-IgGs) were deposited onto the moscovite mica slide that served as the substrate, and the samples were incubated for 15 minutes. Then, 3 washing steps with milliQ ultrapure water (Millipore, Burlington, MA, USA) were performed and the samples were dried under a gentle stream of argon prior to the visualization.

Atomic force microscopy analysis was performed using non-contact and tapping modes, in NX-20 equipment (Park Systems, Suwon, Korea) and images were acquired and processed as described by Retana Moreira et al. (36), using the XEI software (Park Systems, Suwon, Korea). Samples of purified EVs were also analyzed.

2.8 Flow cytometry analysis for macrophage separation

For these experiments, six-week-old female C57BL/6 wild-type mice maintained under pathogen-free conditions were used and six different groups were established and inoculated with a final volume of 250 µL of the following preparations: 1) EVs (38 µg/mouse), 2) immune complexes EVs - sialylated IgGs, 3) immune complexes EVs - non-sialylated IgGs, 4) trypomastigotes derived from cell cultures and resuspended in PBS (10^6 parasites), and 5) LPS (10 µg). The last two preparations were included as positive controls, as described previously (16). A final batch of mice inoculated with 250 µL of PBS was also included as negative control. All inoculations were performed intraperitoneally in a final volume of 250 µL in PBS.

After 48 h of stimulation of the mice with the preparations previously described, the mice were anesthetized in isoflurane atmosphere, euthanized by cervical dislocation and peritoneal exudate cells (PEC) were collected by washing the peritoneal cavity of each animal with 5 mL of a cold 0.85 mM EDTA solution in sterile PBS. Peritoneal cells were centrifuged at 1,000 x g for 10 minutes at 4 °C and the pellets obtained from centrifugation were resuspended in ACK lysis buffer (0.15M NH_4Cl, 0.01M $KHCO_3$, 0.1mM Na_2EDTA, pH 7.2), where they were held for 5 minutes to lyse red blood cells contaminating the peritoneal exudate. After this lysis step, the cells were centrifuged at 1,000 x g for 5 minutes and the pellets were resuspended in 200 µL of PBS.

The cell suspensions were incubated for 20 minutes in the dark at room temperature with the labeled monoclonal antibodies included in Table S1. Incubations with each antibody were performed in separate and after each incubation, the cells were centrifuged at 1,000 x g for 5 minutes, unbound antibodies were removed and two washes with 500 µL sterile PBS were performed. With this panel of antibodies, the frequency of two different subpopulations of peritoneal macrophages was measured and a sorting separation of these populations into large peritoneal macrophages or LPM (CD19-, CD11c-, CD11bhi, F4/80hi and MHCIIlo) and small peritoneal macrophages or SPM (CD19-, CD11c-, CD11blo, F4/80lo and MHCIIhi) was carried out (15, 18). Briefly, for this separation and after the incubation with all the antibodies of the panel, singlets were chosen. Then, viable. B cells were removed, selecting CD19- cells. Dendritic cells were also removed gating CD11c- cells and finally, LPM and SPM were selected according to the expression levels of CD11b and F4/80.

2.9 Cytokine expression analyses in large and small peritoneal macrophages

After the separation and purification of both macrophage subpopulations, the cell suspensions were centrifuged at 1,000 x g for 10 minutes and the cell pellets were lysed and homogenized with TRIzol reagent (Thermo Fischer Scientific, Waltham, MA, USA) for RNA purification. After the extractions, incubation with DNase I, RNase-free (Thermo Fischer Scientific, Waltham, MA, USA) was performed according to the manufacturer's recommendations, and the absence of gDNA was confirmed by the absence of a positive amplicon in PCR amplification for the actin gene.

Once the RNAs were purified and quantified, the expression of cytokines and markers (*IL-1β, IL-2, IL-12, IL-18, TNF-α, IFN-γ, G-CSF, IL-6, IL-15, IL-10, TGF-β, IL-17, IL-38*, and nitric oxide synthase (*NOS*) was analyzed by RT-qPCR, using the iTaq™ universal SYBR® Green one-step universal SYBR® kit (BioRad, Hercules, CA, USA), employing *gapdh* as the reference gene. The sequences of the primers employed in this analysis are listed in Table S2; primer sequences were located across exon–exon borders, avoiding any interspecifically and intraspecifically variable positions. Moreover, a calibration curve was performed according to Gomez-Samblas et al. (47) to calculate the efficiency of each pair of primers,.

Reactions were performed in a CFX-96 RT-PCR system (BioRad, Hercules, CA, USA), using a final volume of 10 µL, which included 300 nM of each primer and 100 ng of RNA per reaction. The thermal cycling conditions consisted of retrotranscription at 50 °C for 10 minutes, followed by an enzymatic activation step and DNA denaturation at 95 °C for 1 minute, 40 cycles of denaturation at 95 °C for 10 seconds and an annealing and extension step at 60 °C for 30 seconds, followed by plate reading. At the end of the RT-qPCR reactions, a melting gradient was applied from 65 °C to 95 °C in 0.5 °C increments.

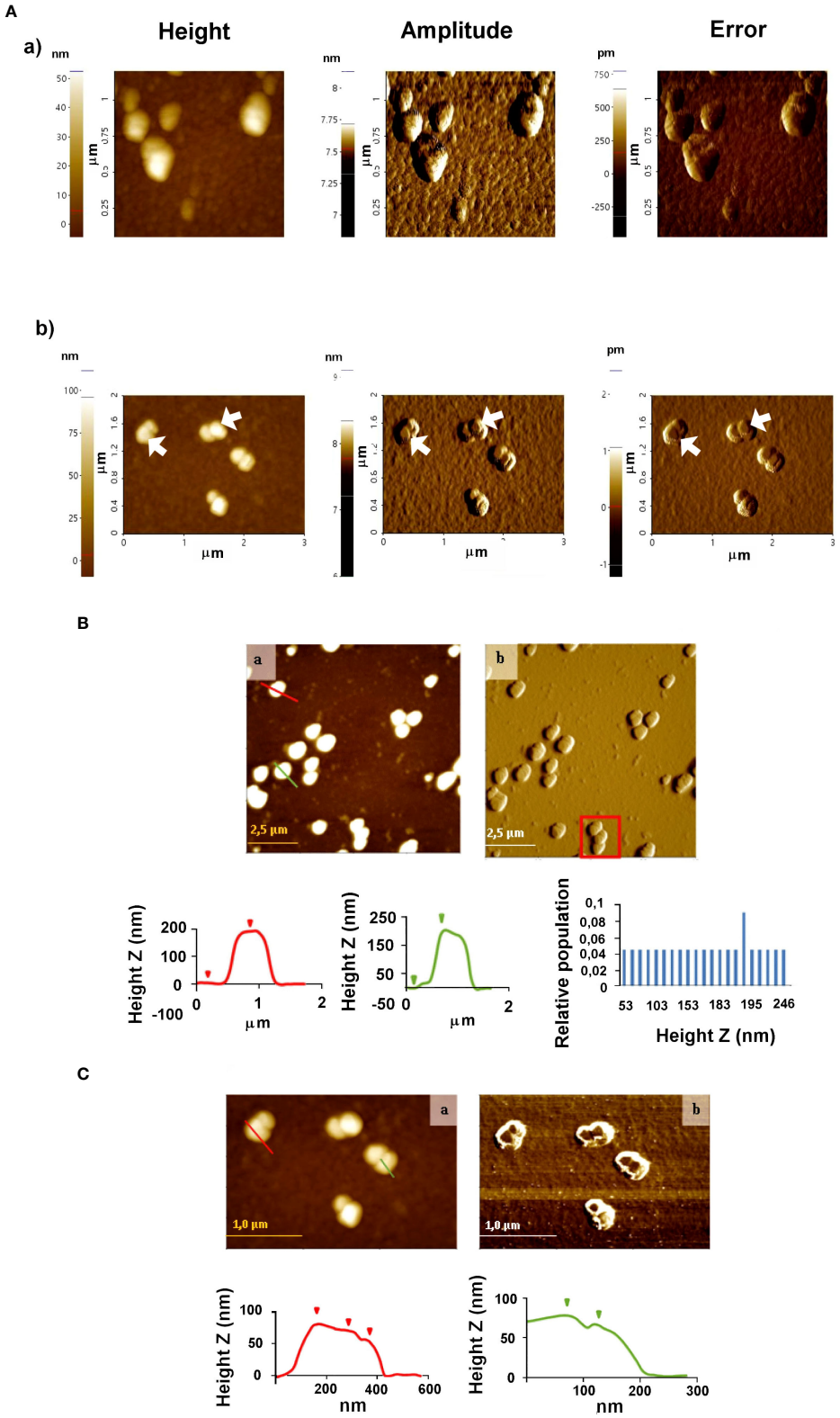

FIGURE 2
Atomic force microscopy analyses of EVs secreted by trypomastigotes of *T. cruzi* **(A)** and **(B)** immune complexes EVs-IgGs anti *T. cruzi* **(A)**. Non-contact **(B)** and tapping **(C)** modes were employed for the analysis of ICs. In C, the formation of ICs as a result of the binding of IgGs to EVs is evidenced by changes in the height profile as a result of that binding. Graphs show profile lines that correspond to topography images, in which changes in the profile are observed as changes in the heights of the particles identified (for the red profile: first step of 8.167 nm and second step of 10.082 nm in height; for the green profile: Z height of 11.220 nm).

Cytokine expression was also normalized against *gapdh* and the negative control (PBS-injected mice).

3 Results

3.1 Isolation and characterization of EVs

Extracellular vesicles of trypomastigotes of *T. cruzi* were obtained following a sequential process of differential centrifugation, filtration and ultracentrifugation, a method previously employed by our research group (35, 36). EVs isolation and characterization was performed following the Minimal Information for the Study of Extracellular Vesicles (MISEV) guidelines (28), recommended by the International Society for Extracellular Vesicles (ISEV) for all articles involving such vesicles. Transmission electron microscopy of the samples observed by negative staining, nanoparticle tracking analysis and atomic force confirmed the presence of vesicles of a size compatible with exosomes and smaller ectosomes of the infecting stage of the parasite, described by our group in previous publications (36) (Figure S1). In particular, TEM revealed a mean size of vesicles of 46.3 nm (median: 45.7 nm) (Figure S1A) and majority peaks of vesicles corresponding to 42 and 52 nm was observed using NTA (Figure S1B). In all of the analyses, aggregations of EVs were observed, especially in TEM and AFM (Figures S1A, C).

Western blot analysis using an antibody against cruzipain revealed the presence of bands of 35 kDa – 70 kDa, corresponding to this *T. cruzi*-specific enzyme in EVs (Figure S1D).

3.2 Purification of sialylated and non-sialylated IgGs and formation of immune complexes EVs – IgGs

The success in mice immunization with a total extract of trypomastigotes of *T. cruzi* and the consequent purification IgGs anti-*T. cruzi* from sera from infected mice is presented in Figure 1. Figure 1A shows antibody titers obtained by immunization of mice with the total extract of trypomastigotes obtained from cell cultures. From the ELISA, the 1: 12,800 dilution of the hyperimmune serum revealed an absorbance 3 times higher than that the titer of sera from non-immunized mice, in which the cut-off value was obtained. Figure 1B shows the antigenic recognition of antigens of *T. cruzi* in the total extract of trypomastigotes by sera of immunized mice using Western blot.

Figure 1C the Lane 1 shows the result of the purification of total IgGs from sera using Melon gel chromatography. In this Figure, bands corresponding to the heavy and light chains of the purified IgGs are observed. Moreover, affinity chromatography with Sambucus nigra lectin was performed to separate sialylated from non-sialylated IgGs; results from this process are shown in Figure 1C (2 and 3 lanes. In this Figure, lane 2 corresponds to sialylated-IgGs, which were retained and subsequently eluted with 0.5 M lactose, while lane 3 corresponds to non-sialylated-IgGs that were not retained in the previous affinity chromatography. Figure 1D shows a Western blot that confirms the proper purification of sialylated and non-sialylated IgGs, following the protocol described in Material and Methods section.

AFM was also employed to study the morphology and distribution of *T. cruzi* EVs and those with which immune complexes were formed by incubating purified IgGs from anti-*T. cruzi* sera with the purified EVs. Once the ICs resulting from this incubation were formed, they were purified and washed by ultracentrifugation, and non-covalently immobilized on the mica sheet for subsequent observation by AFM. The results obtained are shown in Figure 2, which also confirmed the presence and integrity of the vesicles. For EVs, homogeneous particles of 20-50 nm were observed (Figure 2A). In the case of the immune complexes (Figures 2A, B), larger structures were observed both in the non-contact (Figure 2B) and tapping modes (Figure 2C), suggesting that they could correspond to more than one IgGs aggregated with one or more different EVs, as length values between 0.8 µm and 1.5 µm were obtained (Figure 2B, red square); however, length values from 0.35 to 1.35 µm and height values from 50 to 250 nm prevailed. Figure 2C shows immune complexes of different globular shapes and sizes, with length values from 0.175 to 1.8 µm and height values from 50 to 246 nm. In the same Figure 2C, changes in the profile lines are evident, which can be interpreted as changes in the heights of the identified particles.

3.3 Flow cytometry analysis for macrophage separation

Figures S6-S11 show the separation of cell subpopulations in the peritoneal cavity of mice stimulated with different preparations using sorter flow cytometry. Results include both the number of events and the percentages of cell subpopulations 48 hours after the inoculation with the samples included in this study: EVs, immune complexes formed by the incubation of EVs of *T. cruzi* with sialylated or non-sialylated IgGs, LPS and trypomastigotes of *T. cruzi* (positive controls) and PBS (negative control). Results regarding the number of cells obtained for each stimulation are shown in Table S3. The same figures (Figures S6-S11) also show how cell subpopulations were selected using antibodies and flow cytometry.

Figure 3A shows the final plots of the different macrophage subpopulations recovered from the peritoneal cavity of the mice, 48 hours after the stimulation with the samples described above. In Figure 3B, macrophage subpopulations recovered after mice stimulation with the samples, as well as the statistical significance of the difference in the numbers of small and large peritoneal macrophages are presented in a bar graph. Results show that in the peritoneal cavity of mice inoculated with PBS (negative control), there is a larger population of LPM (86.2%) compared to 13.8% of SPM, while for LPS (positive control), the percentage of LPM is drastically reduced to 7.3% and SPM increased to 92.7%. When mice were stimulated with trypomastigotes of *T. cruzi*, the percentage of LPM decreased to 33.7% as compared to the

10.3389/fimmu.2023.1215913

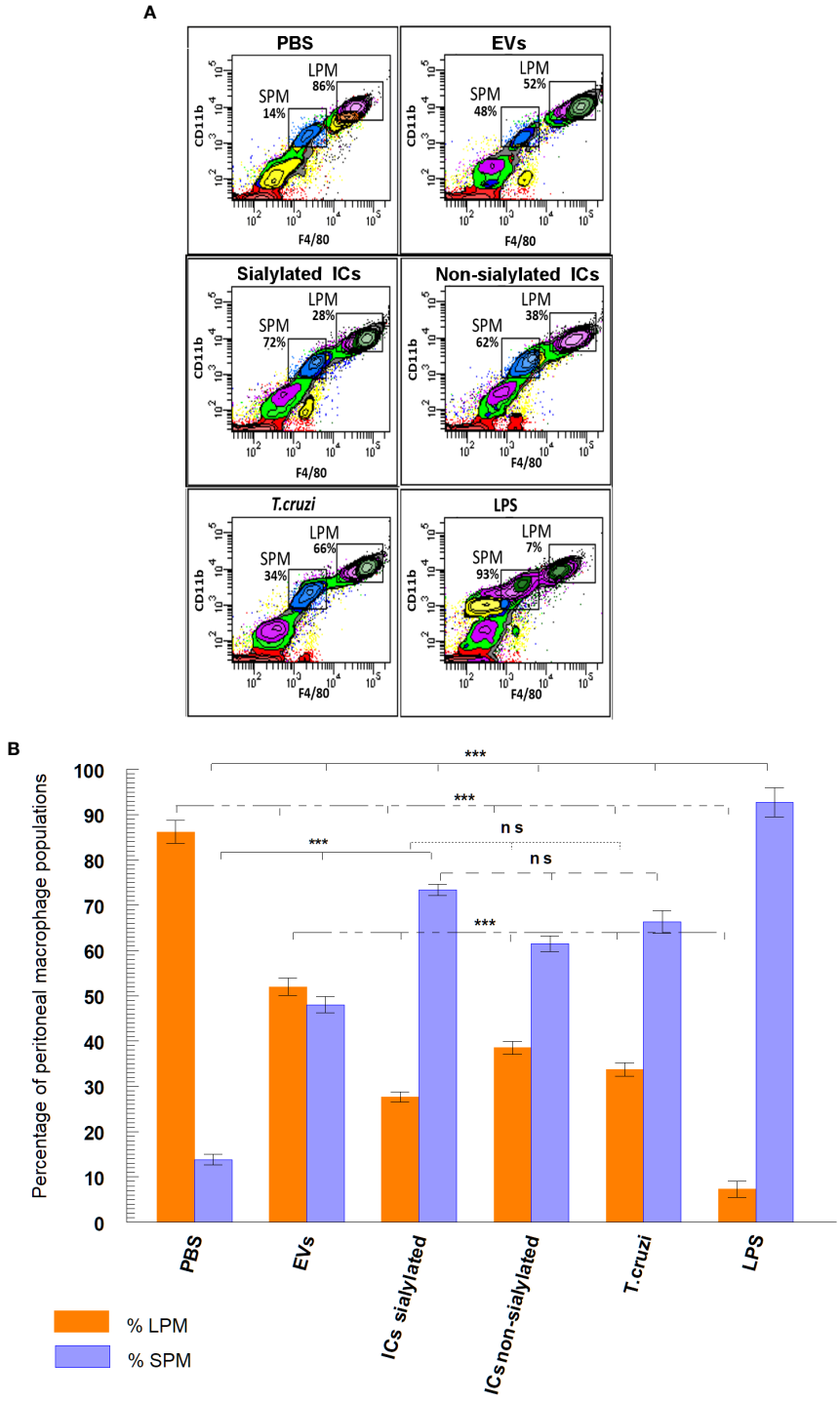

FIGURE 3
Separation **(A)** and percentage **(B)** of macrophage subpopulations (small and large peritoneal macrophages) collected from the peritoneal cavity of mice after different stimuli using flow cytometry: PBS, EVs (extracellular vesicles shed by trypomastigotes of *T. cruzi*), sialylated ICs (EVs - IgGs anti *T. cruzi* retained after affinity chromatography using Sambucus nigra lectin), non-sialylated ICs (EVs - IgGs not retained after affinity chromatography using Sambucus nigra lectin), *T. cruzi* (trypomastigotes) and LPS. The statistical test used was the Tukey-Kramer Multiple Comparisons Test (*** = $p < 0.001$).

negative control, while SPM reached 66.3%. However, when mice were stimulated with EVs secreted by this stage of the parasite, percentages of LPM and SPM tended to equalize (52% for LPM and 48% for SPM). A percentage of LPM significantly reduced with respect to the percentage of LPM obtained when mice were inoculated with immunoglobulin-free EVs (27.6%); for SPM, the percentage of cells reached 73.4% of the total population of macrophages. Finally, mice stimulated with ICs formed by the incubation of EVs with non-sialylated IgGs reached macrophage percentages of 38.5% for LPM and 61.5% for SPM.

3.4 Cytokine expression analyses in large and small peritoneal macrophages stimulated with EVs and immune complexes EVs - IgGs anti-*T. cruzi*

The differential expression of interleukins by the LPM and SPM populations, recovered from the peritoneal cavity of mice after the 48-hour stimulation with EVs and ICs and separated by the sorter, is shown in Figures 4, 5A. Figures 4A, B shows the cytokine expression in LPM after the stimulation with EVs or after forming immune complexes with sialylated or non-sialylated IgGs. In, Figures 4C, D shows the expression levels of the non-inflammatory interleukins in peritoneal macrophages after the stimulation with trypomastigotes of *T. cruzi* or LPS (positive controls). The expression of Th1 inflammatory interleukins reflects how, in general, the stimulation with EVs induces a higher expression of IFN-γ, TNF-α, IL-18 and IL-6. As can be observed in Figure 4A, there is an increase in the IL-1β expression in macrophages from the 3 conditions in which EVs of *T. cruzi* were used. This is followed by the stimulation produced by the immune complexes formed using sialylated IgGs, where an increased expression of IL-12 and TNF-α is induced. Moreover, the IFN-γ, IL1B and IL12 interleukins were upregulated when the peritoneal cavity of mice was stimulated by LPS (Figure 4C). For the case of trypomastigotes, expression of IL-6 and IL-18 resulted higher when compared to PBS control. Regarding IL-17 expression, LPM showed an increased expression level after stimulation with LPS, Figure 4C.

Figures 5A, B shows the relative expression levels of inflammatory and non-inflammatory interleukins produced by SPM after stimulation with EVs or immune complexes formed by sialylated or non-sialylated IgGs. Figure 5C shows the expression levels of inflammatory interleukins produced by SPM after stimulation with trypomastigote forms of the parasite or with LPS. Figure 5D shows the expression levels of non-inflammatory interleukins produced by sorter-purified SPM after stimulation of the peritoneal cavity with *T. cruzi* forms or with LPS (stimulation control). For IL-10, the highest level of expression occurred after the injection of the peritoneal cavity with EVs and in stimulation control experiments with LPS (Figures 5B, D, respectively). Other cytokines such as IL-15, IL-38 or G-CSF, also presented maximum expression levels after the stimulation with immune complexes formed with sialylated IgGs.

The SPM subpopulation underwent significant variations after the different stimuli (Figure 5), either with the ICs or after the challenge with trypomastigotes or LPS. In this sense, the highest expression levels of IFN-γ were obtained after the stimulation of these cells with the immune complexes with non-sialylated IgGs, while stimulation with EVs of the parasite induced maximal expression levels of TNF-α, IL-6 (Figures 5A, C), IL-10, IL-15 and TGF-β (Figures 5B, D), the stimulation with immune

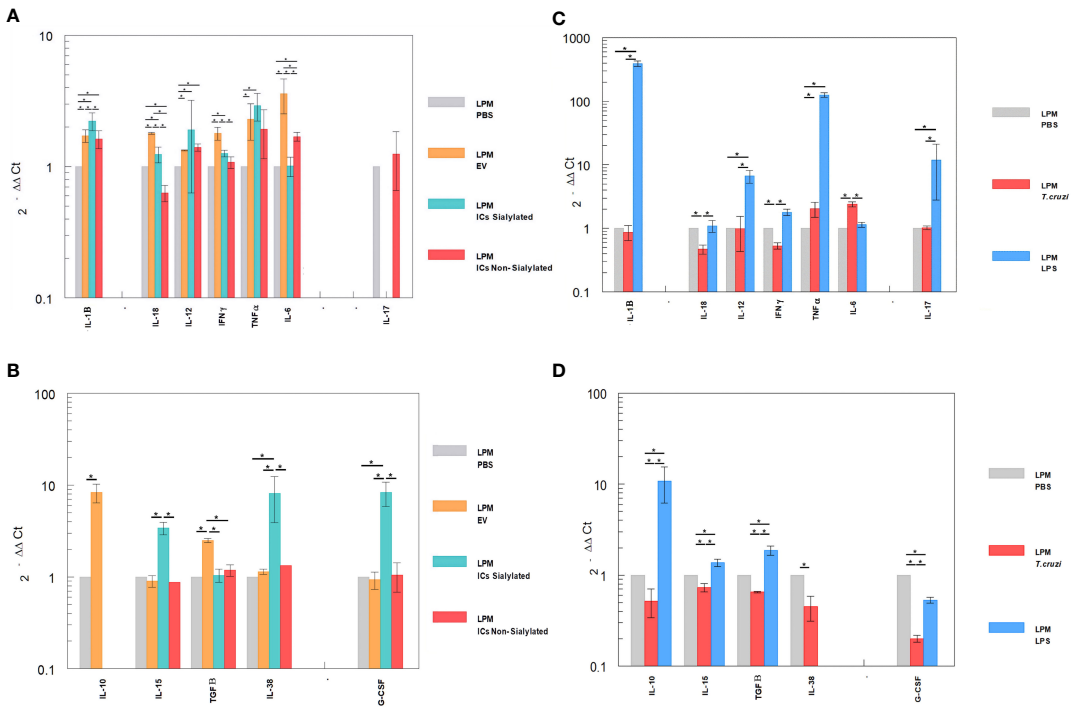

FIGURE 4
Relative interleukin expression of the LPM subpopulation after the stimuli of mice with EVs of *T. cruzi*, as well as sialylated and non-sialylated ICs (EVs – IgGs anti-*T. cruzi)* versus controls stimulated with trypomastigote forms of the parasite or LPS. **(A)**, relative expression levels of inflammatory interleukins produced by LPM after stimulation with EVs or immune complexes formed by sialylated or non-sialylated IgGs. **(B)** shows the expression levels of non-inflammatory interleukins produced by LPM after stimulation with EVs or ICs formed by sialylated or non-sialylated IgGs. **(C)** shows the expression levels of inflammatory interleukins produced by LPM after stimulation with trypomastigote forms of the parasite or with LPS (stimulation controls). **(D)** shows the expression levels of non-inflammatory interleukins produced by sorter-purified LPM after stimulation of the peritoneal cavity with *T. cruzi* forms or with LPS (stimulation controls). The statistical test used was the Tukey-Kramer Multiple Comparisons Test. (*= $p < 0.05$).

10.3389/fimmu.2023.1215913

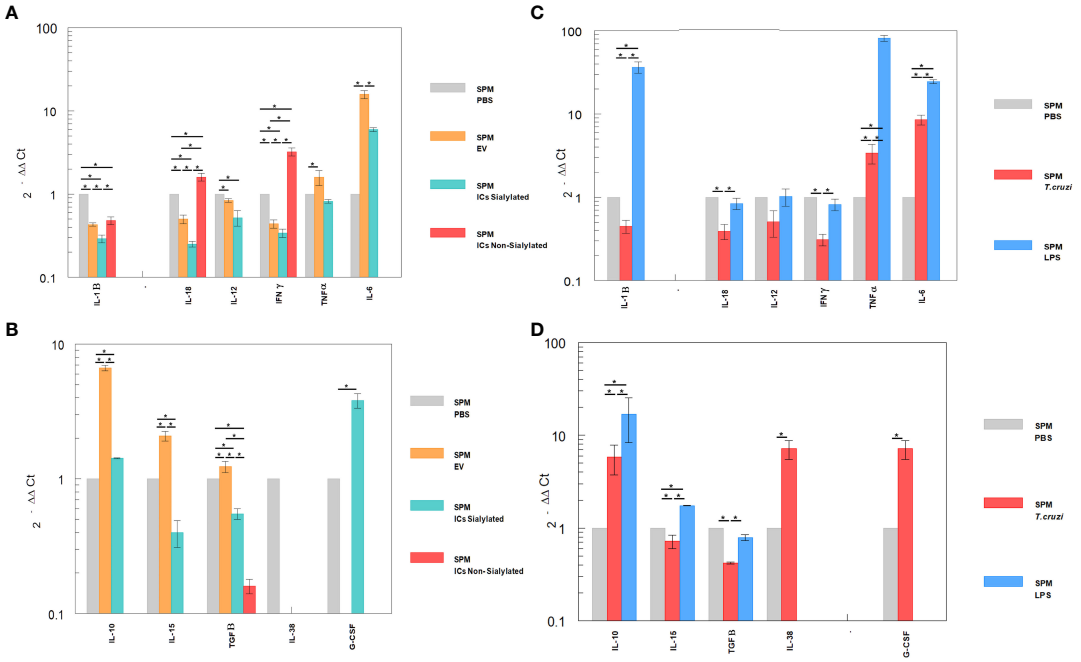

FIGURE 5
Relative interleukin expression by SPM subpopulation after the stimuli of mice with EVs of *T. cruzi*, as well as sialylated and non-sialylated ICs (EVs – IgGs anti-*T. cruzi*) versus control stimulated with trypomastigote forms of the parasite or LPS. **(A)**, relative expression levels of inflammatory interleukins produced by SPM after stimulation with EVs or immune complexes formed by sialylated or non-sialylated IgGs. **(B)** shows the expression levels of non-inflammatory interleukins produced by SPM after stimulation with EVs or ICs formed by sialylated or non-sialylated IgGs. **(C)** shows the expression levels of inflammatory interleukins produced by SPM after stimulation with trypomastigote forms of the parasite or with LPS (stimulation controls). **(D)** shows the expression levels of non-inflammatory interleukins produced by sorter-purified SPM after stimulation of the peritoneal cavity with *T. cruzi* forms or with LPS (stimulation control). The statistical test used was the Tukey-Kramer Multiple Comparisons Test. (*= $p < 0.05$).

complexes with sialylated IgGs induced increased expression of both the inflammatory interleukin IL-6 (Figure 5A) and the regulatory interleukins IL-10 and G-CSF (Figure 5B). For the latter, expression was not induced by either EVs or non-sialylated immune complexes, and in the case of control experiments, expression of G-CSF was only achieved when the stimulation was performed with trypomastigotes of *T. cruzi* (Figure 5D). The SPM did not express IL-17 in any case, and expression levels for interleukin IL-38 were obtained only when the stimulation was performed in the control experiment after the inoculation with trypomastigotes (Figure 5D).

Finally, the expression of NOS by large and small peritoneal macrophages of the control treatments is shown in Figure 6, where the stimulation with LPS or trypomastigotes of *T. cruzi* induces the expression of NOS in LPM at a higher level than SPM, which even showed lower expression levels than macrophages obtained after the injection of mice with PBS. Injection of either EVs or the two types of immune complexes in SPM did not induce NOS expression levels higher than the PBS control under our experimental conditions.

4 Discussion

Macrophages are considered to be part of the first barrier to prevent infections, acting as antigen-presenting cells to CD4+ T lymphocytes or as phagocytic cells of previously opsonized antigens. During an infection, monocytes/macrophages acquire the M1 phenotype (IL-10-, IL-12+, NOS+, CXCL9+), which are the major effector cells for the first line of host antibacterial defense (48). On the other hand, M2 macrophages refer to alternatively activated macrophages and can be polarized by various stimulatory factors; moreover, different M2 macrophage subtypes can be induced by different stimulatory factors (49). In 2008, Mosser and Edwards proposed that the classification of macrophages could be based on the functions in which they participate, including host defense, wound healing, and immune regulation (50). From subtypes of M2 macrophages, M2a (also referred to as wound healing macrophages) are induced by IL-4 and IL-13, and express high levels of mannose receptor (MR, also referred to as CD206), IL-1 decoy receptor (IL-R) and CCL17, which promote the secretion of pro-fibrotic factors such as TGF-β, insulin-like growth factor (IGF) and fibronectin to contribute to tissue repair (48). On the other hand, bacteria, viruses, and some protozoan parasites like Leishmania can increase the number and proportion of M2b macrophages in the peritoneal cavity (IL-10+, IL-12-, IL-6+, TNF-α+, CD11b+, MHCII+) (51, 52), which, despite their high phagocytic capacity, are not the main cells responsible for killing bacteria (53).

The secretion of EVs by trypomastigotes of *T. cruzi* favors the invasion process to the host cell and modulates the immune response so that parasitization can be successful. In a recent

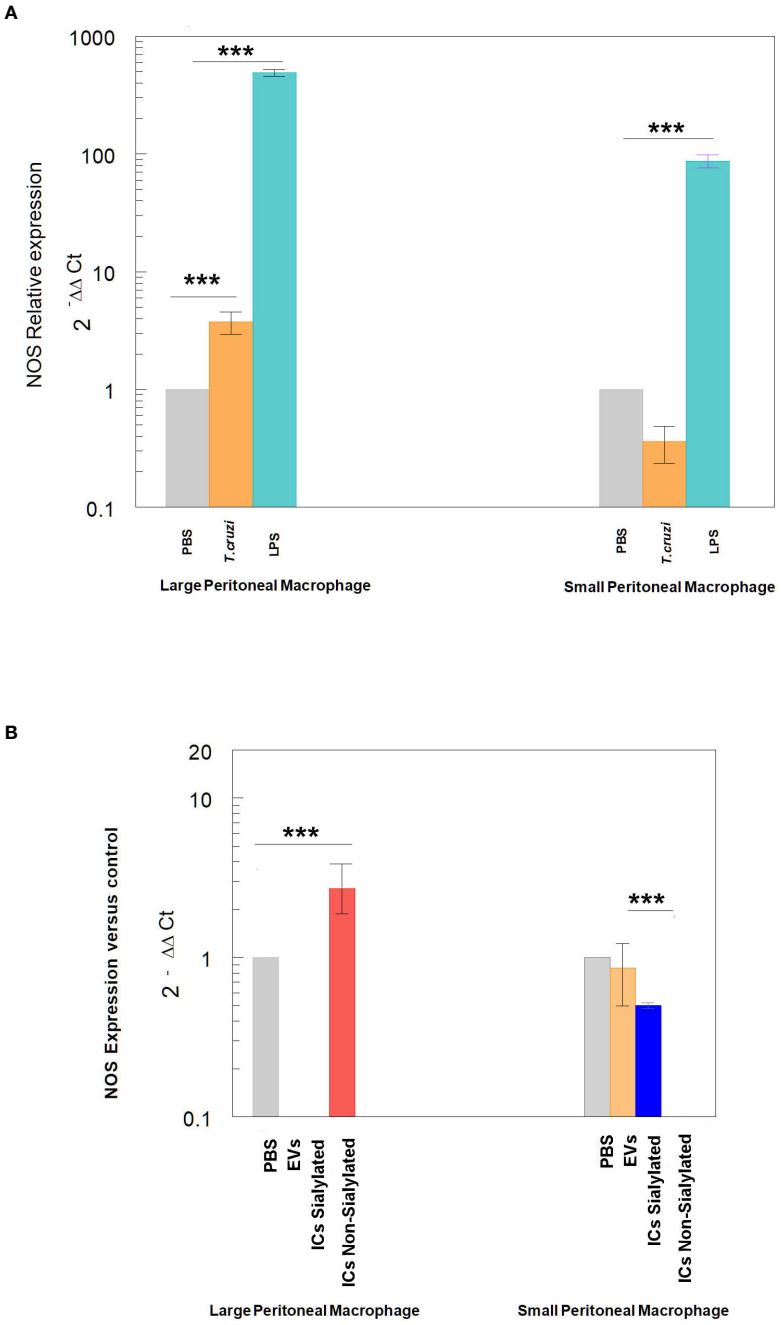

FIGURE 6
Relative expression of nitric oxide synthase (NOS) in SPM and LPM subpopulations after the stimuli of mice with: trypomastigotes of *T. cruzi* and LPS **(A)**, and EVs of *T. cruzi* and sialylated or non-sialylated ICs. **(B)** Relative expression of nitric oxide synthase (NOS) in LPM and SPM peritoneal macrophages. The statistical test used was the Tukey-Kramer Multiple Comparisons Test. (*** = $p < 0.001$).

publication, Cortes Serra et al. (54) review and discuss the role of EVs secreted during a *T. cruzi* infection and their immunomodulatory properties (54). It is also well known that EVs of the parasite induce physiological changes, including increases in the intracellular calcium concentration and modifications at the cytoskeletal level such as actin depolymerization (35), which could maybe alter macrophage migration and their phagocytic capacity. Moreover, EVs released by THP-1 cells that are in contact with the parasite are also able to modulate the immune response of the host by inhibiting C3 convertase; complement system inhibition is also achieved directly by EVs released by the parasite (34b).

The role of EVs of *T. cruzi* in inducing the release of pro-inflammatory cytokines (TNF-α and IL-6) *in vivo*, as well as the production of NO by murine macrophages after the interaction with TLR2 has been previously reported (38, 39). Moreover, in 2018, Lovo Martins et al. revealed that macrophages from the bone marrow stimulated with EVs of the parasite increased prostaglandin

E2 (PGE2) production and the formation of lipid bodies; the increase in PGE2 has been related to an augmented susceptibility of the host to *T. cruzi* invasion (55, 56). Moreover, PGE2 can also affect the antibody production by blocking the transformation of B lymphocytes into plasmatic cells, and inhibit the role of T cytotoxic cells and Th1 lymphocyte development (57). The ability of EVs of the parasite in inducing the release of proinflammatory cytokines has also been confirmed using *in vitro* models, in which the secretion of nitric oxide (NO) by THP-1 macrophages was also confirmed (39). Besides, Nogueira et al. (38) analyzed the immune response induced by these vesicles in peritoneal macrophages from C57BL/6 mice and their results coincide with increased expression levels of TNF-α and IL-6 in LPM of our study. On the other hand, it has also been described how the stimulation of animals with EVs of *T. cruzi* prior to the infection with trypomastigotes induced a decrease in NO production in plasma, as well as the production of TNF-α and IL-6 in spleen cells, but an increase in IL-4 and IL-10 in splenocytes and macrophages that induced high parasitemia and the death of the mice. It was confirmed in this study that peritoneal cells also synthetize IL-12, TNF-α and NO after EVs stimulation (56, 58).

Extracellular vesicles released by *T. cruzi* contain a repertoire of key components that are also capable of stimulating TLR (59) as it happens with the whole parasite. The cargo of these EVs includes nucleic acids, proteins with protease activity like GP63 and serine proteases, and GPI-anchored members of the large mucin family that include *trans*-sialidases, all of them capable of activating TLR2 and TLR9 and induce a pro-inflammatory response (60). The role of *trans*-sialidases in EVs over cell physiology and the modulation of the immune response has also been studied by our research group, and it is likely that these enzymes, capable of transferring sialic acid from the host cell to mucins of the parasite might be responsible, at least in part, for lymphoid cell modulation (36).

In this work, the exposure of extracellular vesicles of trypomastigotes of *T. cruzi* to the immune system could be considered an approach to the early stage of the infection (acute phase of the disease), while the injection of immune complexes EVs - IgGs anti *T. cruzi* could simulate the chronic stage, in which most of the circulating anti *T. cruzi* immunoglobulins are IgGs which must participate in the formation of these complexes, as previously reported by our group (34a). Results obtained under our experimental conditions show that the stimulation of C57BL/6 mice with trypomastigotes of the parasite and LPS triggered an increase in the proportion of SPM when compared to the negative control (PBS-stimulated mice) (Figure 3B); similar results as those obtained by 18 (18). When the stimulation was performed with EVs of the parasite, an increase in the proportion of SPM was also observed, but in a minor proportion as for trypomastigotes or LPS. However, when mice were challenged with both types of immune complexes (sialylated and non-sialylated ICs), the proportion of SPM was significantly higher than when the challenge was performed with EVs, which could suggest that even when EVs are an immunologic stimulus capable of increasing the SPM population, surface components of the vesicles that are not blocked by the Fab region of IgGs anti-*T. cruzi* are likely to suppress the stimulatory response in lymphoid cells of the peritoneal cavity of mice, which would impede the recruitment of circulating monocytes to the peritoneal cavity.

The separation of SPM and LPM subpopulations obtained from the peritoneal cavity of mice was successfully achieved by flow cytometry in this work, which allowed specific cytokine expression analyses in each macrophage subpopulation. Results obtained from these experiments showed that, even when the subpopulation of SPM increased after the inflammatory stimuli with EVs of the parasite (expressing high levels of pro-inflammatory cytokines like IL-1β, TNF-α and IL-6), an increased expression of regulatory cytokines such as IL-10, IL-15 and TGF- β by this subpopulation was also observed. A similar result was obtained when performing the expression analyses of cytokines from the subpopulation of LPM, in which both regulatory (IL-10, IL-15, IL-38 and TGF-β) and proinflammatory (IL-1β, IL-12, TNF-α, IL-6 and IL-17) cytokines were found to be increased. It should be highlighted that no expression of IL-2, IL-4, IL-9, IL-21, IL-23 and IL-25 was detected in SPM nor LPM subpopulations, even when the challenges were performed using trypomastigotes or LPS (positive controls). In this sense, our results confirm that SPM and LPM subpopulations could not be classified as M1 and M2, since both types of subpopulations are able to express pro-inflammatory and non-inflammatory cytokines as suggested elsewhere.

Differential expression levels of cytokines in mice stimulated with EVs or with the immune complexes EVs - IgGs anti *T. cruzi* were found, which could be related to the fact that IgGs present in these ICs interact with Fcγ receptors. IgGs bind to specific Fc receptors present on the cell membranes of macrophages and allow the opsonization of antigens and phagocytosis of immune complexes. Based on these receptors present on the surface of the cells, the effector functions initiated by antibodies are triggered by the Fc domain upon binding to FcR receptors, functions that are largely dependent on the N-terminally bound biantennary glycan of immunoglobulin heavy chains, located below the immunoglobulin hinge region. This glycan is considered to hold the two Fc heavy chains in an open conformation necessary to interact with activating Fcγ receptors (FcγRs). However, the presence in the sugar chain of terminal sialic acid in the glycan has profound implications on the effector functions of Fc by inhibiting activation by cells (22), as FcRγIIB receptors would be responsible for binding to such immunoglobulins carrying sialic acid in their Fc (23). In this sense, the presence of sialic acid, bound in an α2,6 bond to the penultimate terminal galactose of the glycan (24) reduces FcγR binding and converts IgGs antibodies to anti-inflammatory mediators (25), thus sialylated IgGs would be responsible for the anti-inflammatory activity of intravenous immunoglobulin (IVIg) therapy (25). IVIg therapy is based on the anti-inflammatory activity of immunoglobulins derived from plasma of healthy donors and is commonly employed in inflammatory pathologies such as autoimmune diseases (61) due to its regulatory properties, as it induces a polarization of M2 into M1 macrophages (especially in tumor-related macrophages). For this therapy, immune complexes with sialylated Fcs initiate an anti-inflammatory cascade *via* the receptor or lectin SIGN-R1 or DC-SIGN (26), which works as a receptor of IgGs enriched in sialic acid (24) in humans, and this would lead to a surface expression of the FcR

inhibitor (FcγRIIB) on inflammatory cells, thereby attenuating inflammation as it happens with B cells, in which this receptor negatively regulates activating signals (62). It has also been suggested that the effects of IVIg would depend on the activation/polarization state of macrophages; the strongest association between treatments with high doses of IgGs and macrophage polarization seems to depend on Fc receptors of immunoglobulins, which play a major role in macrophage regulation. For our study, it is important to highlight that B lymphocytes from C57BL/6 mice lack this receptor (23) and this could explain the differences in the proportion of LPM and SPM cell subpopulations obtained when mice were challenged with sialylated and non-sialylated ICs when compared to CD1 mice Figure S12), in which SPM subpopulation did not increase after the challenges. In this sense, a possible role of this receptor in immune modulation and probably in monocyte migration and transformation into SPM in the peritoneal cavity of C57BL/6 mice is suggested.

Our results reveal an opposite behavior in the expression of IL-1β in both macrophage subpopulations; in this regard, while this cytokine expression was reduced after all the stimuli performed in SPM, in LPM the expression was increased after all of the stimuli employed, especially in ICs formed with sialylated IgGs. However, an increased expression of IFN-γ was only observed in SPM after the challenge with ICs formed with non-sialylated IgGs. Regarding IL-12 and IFN-γ expression in SPM, the levels obtained were under the expression levels of the negative control, except for the IFN-γ expression after the stimulation with non-sialylated ICs which was increased; it is noteworthy that IL-12 induces the expression of IFN-γ (63). On the contrary, LPM stimulated with EVs showed increased levels of IFN-γ when compared to the negative control or when mice were stimulated with sialylated ICs. In the case of IL-12, all the employed stimuli increased the cytokine expression, and for TNF-α, expression levels in all cases were higher than the control in this subpopulation.

IL-18, a cytokine that belongs to the IL-1 superfamily, is produced by macrophages and other cell types (64, 65) and has pleiotrophic roles (66) including the regulation of IL-12 expression (67) and, thus, IFN-γ (68). In monocytes stimulated with IL-12 and IL-18, morphological changes in cells are observed, suggesting the role of these cytokines in differentiation and activation of monocytes into macrophages (69), increasing their phagocytic capacity (70). Under our experimental conditions, a diminished expression of this cytokine was observed in SPM of mice stimulated with EVs and sialylated ICs; however, in LPM, increased expression of this cytokine was observed under the same stimuli. The lower expression levels of IL-12 and the higher expression levels of IFN-γ in SPM of mice stimulated with non-sialylated ICs could correspond to an induction of IL-12 by IL-18, with the consequent induction of IFN-γ as a result of FcγR stimulation by non-sialylated Fc regions of IgGs. Overall results of IL-18 expression suggest that the route of activation of the Th1 response is different in both types of cells and might depend on Fc receptors and on PAMP activation after the phagocytosis of non-sialylated ICs (71).

As IL-18 and IL-12 trigger the production of IFN-γ during an infection, Berclaz et al. evaluated the role of these cytokines in the regulation of FCγR expression in cell membranes by GM-CSF/PU.1, which is related to increased IFN-γ expression in alveolar macrophages (72). In these cells, the expression of IL-18 was augmented by GM-CSF expression *in vivo*, which contributes to the expression of FCγR in the macrophage surface as GM-CSF is able to regulate the constitute expression of this type of receptors and thus, opsonization and phagocytosis. The effect of GM-CSF over FCγ receptors was also studied previously by Rossman et al. (73), revealing a significant increase only in the FCγRII receptor. These studies show how GM-CSF increases FCγRII expression in monocytes, favoring the clearance of the immune complexes; in this sense, a similar mechanism could be employed by LPM of the peritoneal cavity, especially when the stimulation is performed with EVs or sialylated ICs.

Regarding IL-6 expression, increased levels were observed in SPM of EVs-stimulated mice, followed by sialylated ICs; for non-sialylated ICs, undetectable levels were obtained. In the case of LPM of mice challenged with EVs and non-sialylated ICs, higher expression levels were obtained when compared to the control. The role of IL-6 in the immune response toward *T. cruzi* was studied by Sanmarco et al., who compared the expression of this cytokine in wild type mice vs. knockout mice and showed how IL-6 deficient mice produced higher amounts of NO in plasma, accompanied by increases in IL-1β and more inflammatory circulating monocytes (74). In our study, nitric oxide synthase (NOS) expression levels in LPM of mice stimulated with non-sialylated ICs were higher than levels obtained in the other study groups in which IL-6 was not detected, while NOS expression levels in mice stimulated with EVs and sialylated ICs were almost null, while IL-6 expression was increased. IL-6 can potentially exert an non-inflammatory response through inhibition of IL-1 and TNF-α synthesis by macrophages (75, 76), which could be considered a mechanism of regulation of the inflammatory Th17 response at low TGF-β concentrations. Results related to the decrease in the expression levels of cytokines associated to the Th1 response (IL-1, IFN-γ, IL-12 and TNF-α) in SPM, as well as IL-6 expression when mice were stimulated with EVs or sialylated ICs, could be explained by this mechanism.

In this study, the highest expression levels of IL-15 were observed in LPM of mice stimulated with sialylated ICs and in SPM of mice stimulated with EVs of the parasite. This cytokine is a potent autocrine regulator of the production of proinflammatory cytokines by monocytes and macrophages, which, at high concentrations, favors the production of TNF-α, IL-1 and IL-6, while, at low concentrations, favors the production of IL-10 (77). In LPM, the lowest expression of IL-15 induced by EVs and non-sialylated ICs, and the highest expression of IL-10 and TGF-β could be explained by this mechanism. Moreover, the increased expression of IL-15, TNF-α and IL-1β in LPM of mice stimulated with sialylated ICs was not found in SPM. IL-15, in combination with GM-CSF, can induce the differentiation of monocytes into immature dendritic cells (78); this could induce the differentiation of monocytes into SPM. In our study, sialylated ICs recruited more SPM to the peritoneal cavity, while non-sialylated ICs recruited more LPM and larger numbers of dendritic cells were obtained after this stimulus.

IL-10 antagonizes the expression of MHCII, co-stimulatory molecules B7.1/B7.2 (CD80/CD86) and proinflammatory cytokines IL-1β, IL-6, IL-8, TNF-α and, especially, IL-12 (79, 80). SPM is the subpopulation that expresses MHCII to a major extent and, after the challenge of mice with EVs and sialylated ICs, the expression levels of IL-10 presented the highest increase, with decreased expression of IL-1β and IL-12. Moreover, when employing non-sialylated ICs for the challenge of mice, the expression levels of IL-10 as well as other non-inflammatory cytokines is null or under the expression levels of the negative control. In LPM, IL-10 expression after the stimuli with both types of ICs was undetectable, a result that contrasts with the high expression of IL-38 obtained for this type of subpopulation, also considered a regulatory cytokine. In SPM, instead, high levels of IL-10 were observed after the challenge of mice with sialylated ICs; a fact that could be explained as a consequence of the interaction of sialylated groups in ICs with FcRgIIB and thus, the induction of this inhibitory cytokine.

The high expression levels of IL-38 in LPM after the challenge of mice with sialylated ICs contrasts with the absence of expression of this cytokine in SPM. IL-38 is considered an important anti-inflammatory cytokine, which significantly inhibits IL-6, IL-1β, CCL5, TNF-α and CXC10 (related to the Th1 response), as well as IFN-γ (81). From our results, high expression levels of IL-15 and GM-CSF in LPM of mice stimulated with sialylated ICs were observed; however, when the challenge was performed with non-sialylated ICs, this is the only subpopulation in which IL-17 expression levels were higher than in the control, possibly as a consequence of the stimulation through FcγR receptors. The role of IL-17 in Chagas disease has previously been studied and the presence of low parasitemia has been related to the effect of this cytokine (82). In this sense, in infected individuals with the indeterminate form of the disease or with mild cardiopathy, high levels of IL-17 and IL-10 were found, while high levels of IFN-γ and TNF-α were found in patients with severe cardiopathy. In this sense, it seems that IL-17 and IL-10 regulate the Th1 response in order to avoid cardiac involvement (83). LPM of mice challenged with non-sialylated ICs expressed IL-17 but not IL-10.

The results obtained from this work suggest that the immunological tolerance exerted by *T. cruzi* EVs and ICs by macrophages inhibits the response and decreases the secretion of proinflammatory cytokines. Which allow macrophages to control inflammation, avoiding tissue damage caused by an excessive inflammatory response (84) and could be related to the type of immune response that predominates in each phase of the disease (acute or chronic), and thus, to the pathology of chronic Chagas disease, as the Fc region of IgGs that form the ICs interact with FcγR (specially FcγRIIB), eliciting or inhibiting the immune response and favoring (or not) the presence of the parasite and clinic manifestations of the disease. However, the virulence and type of clinic manifestation presented will depend on the parasite strain, as well as the amount of IgGs and the isotypes that could be sialylated as it also happens in other inflammatory or autoimmune diseases.

Data availability statement

The original contributions presented in the study are included in the article/Supplementary Material. Further inquiries can be directed to the corresponding author.

Ethics statement

The animal study was reviewed and approved by Ethics Committee of the University of Granada (Ethics Committee, 235-CEEA-OH-2018), as well as by the authorities of the Regional Government of the Junta de Andalucía with number 12/11/2017/162.

Author contributions

Conceptualization, AO, AC-G, and LM; methodology, AC-G, LM, and MG-S; formal analysis, AC-G, LM, and AO; investigation, AC-G, LM, MG-S, and AO, writing—original draft preparation, AC-G, LM, and AO; writing—review and editing, AC-G, AO, LM, and MG-S; visualization, AC-G, AO, and LM; supervision, AO; funding acquisition, AO. All authors contributed to the article and approved the submitted version.

Funding

This research was funded by the ERANet program, Research in prevention of congenital Chagas disease: parasitological, placental and immunological markers (ERANet17/HLH-0142 (Cochaco). Instituto Carlos III, Ministerio de Sanidad, Gobierno de Espanãa; Fundacioín Ramoín Areces "Interactoma de las exovesículas de *T. cruzi* y de los inmunocomplejos que forman con las células del hospedador: implicaciones en la patología de la enfermedad de Chagas (2019)". Ministerio de Ciencia y Tecnología of the Government of Spain funded the project PGC2018-099424-B-I00)". Exovesiculas circulantes como marcadoras de diagnostico, PREcoz de la Enfermedad de CHAGas Fundación Ramón Areces del XXI Concurso Nacional para la adjudicación de Ayudas a la Investigación en Ciencias de la Vida y de la Materia (2022). Ministerio de Ciencia y Tecnologiía of the government of Spain funded the project PGC2018-099424-B-I00.

Acknowledgments

AC-G was supported by the "Contrato de Formación de Profesorado Universitario" of the Ministry of Science, Culture and Sports (Spain). LM was supported by the Oficina de Asuntos Internacionales y Cooperación Externa (OAICE) of Universidad de Costa Rica and Fundación Carolina (Spain). Transmission electron

microscopy, atomic force microscopy and flow cytometry were performed at the "Centro de Instrumentación Científica", and nanoparticle tracking analysis was performed at the "Departamento de Física Aplicada" of the Faculty of Sciences, both at the University of Granada.

Conflict of interest

The authors declare that the research was conducted in the absence of any commercial or financial relationships that could be construed as a potential conflict of interest.

Publisher's note

Supplementary material

The Supplementary Material for this article can be found online at: https://www.frontiersin.org/articles/10.3389/fimmu.2023.1215913/full#supplementary-material

References

1. Pérez-Molina JA, Molina I. Chagas disease. *Lancet* (2018) 391(10115):82–94. doi: 10.1016/S0140-6736(17)31612-4

2. WHO. *Chagas disease (also known as American trypanosomiasis)* (2022). Available at: https://www.who.int/news-room/fact-sheets/detail/chagas-disease-(american-trypanosomiasis).

3. Moncayo Á., Silveira AC. Current epidemiological trends for Chagas disease in Latin America and future challenges in epidemiology, surveillance and health policy. *Memórias Do Instituto Oswaldo Cruz 104(suppl* (2009) 1):17–30. doi: 10.1590/S0074-02762009000900005

4. Kemmerling U, Osuna A, Schijman AG, Truyens C. Congenital transmission of trypanosoma cruzi: A review about the interactions between the parasite, the placenta, the maternal and the fetal/neonatal immune responses. *Front Microbiol* (2019) 10:1854 (AUG). doi: 10.3389/fmicb.2019.01854

5. Coura JR. Chagas disease: what is known and what is needed - A background article. *Memórias Do Instituto Oswaldo Cruz 102(suppl* (2007) 1):113–22. doi: 10.1590/S0074-02762007000900018

6. Messenger LA, Gilman RH, Verastegui M, Galdos-Cardenas G, Sanchez G, Valencia E, et al. Toward improving early diagnosis of congenital chagas disease in an endemic setting. *Clin Infect Dis* (2017) 65(2):268–75. doi: 10.1093/cid/cix277

7. Ropert C, Gazzinelli RT. Signaling of immune system cells by glycosylphosphatidylinositol (GPI) anchor and related structures derived from parasitic protozoa. *Curr Opin Microbiol* (2000) 3(4):395–403. doi: 10.1016/S1369-5274(00)00111-9

8. Campos MAS, Almeida IC, Takeuchi O, Akira S, Valente EP, Procópio DO, et al. Activation of toll-like receptor-2 by glycosylphosphatidylinositol anchors from a protozoan parasite. *J Immunol* (2001) 167(1):416–23. doi: 10.4049/jimmunol.167.1.416

9. Machado FS, Martins GA, Aliberti JCS, Mestriner FLAC, Cunha FQ, Silva JS. Trypanosoma cruzi –infected cardiomyocytes produce chemokines and cytokines that trigger potent nitric oxide–dependent trypanocidal activity. *Circulation* (2000) 102 (24):3003–8. doi: 10.1161/01.CIR.102.24.3003

10. Gao W, Pereira MA. Interleukin-6 is required for parasite specific response and host resistance to Trypanosoma cruzi. *Int J Parasitol* (2002) 32(2):167–70. doi: 10.1016/S0020-7519(01)00322-8

11. Miyazaki Y, Hamano S, Wang S, Shimanoe Y, Iwakura Y, Yoshida H. IL-17 Is Necessary for Host Protection against Acute-Phase Trypanosoma cruzi Infection. *J Immunol* (2010) 185(2):1150–7. doi: 10.4049/jimmunol.0900047

12. Andrade DV, Gollob KJ, Dutra WO. Acute chagas disease: New global challenges for an old neglected disease. *PLoS Negl Trop Dis* (2014) 8(7):e3010. doi: 10.1371/journal.pntd.0003010

13. Tsuchimoto Y, Asai A, Tsuda Y, Ito I, Nishiguchi T, Garcia MC, et al. M2b monocytes provoke bacterial pneumonia and gut bacteria-associated sepsis in alcoholics. *J Immunol* (2015) 195(11):5169–77. doi: 10.4049/jimmunol.1501369

14. Edwards JP, Zhang X, Frauwirth KA, Mosser DM. Biochemical and functional characterization of three activated macrophage populations. *J Leukocyte Biol* (2006) 80 (6):1298–307. doi: 10.1189/jlb.0406249

15. Bou Ghosn EE, Cassado AA, Govoni GR, Fukuhara T, Yang Y, Monack DM, et al. Two physically, functionally, and developmentally distinct peritoneal macrophage subsets. *Proc Natl Acad Sci U S A* (2010) 107(6):2568–73. doi: 10.1073/pnas.0915000107

16. Cassado AdA, de Albuquerque JAT, Sardinha LR, Buzzo CdL, Faustino L, Nascimento R, et al. Cellular renewal and improvement of local cell effector activity in peritoneal cavity in response to infectious stimuli. *PLoS ONE* (2011) 6(7):22141. doi: 10.1371/journal.pone.0022141

17. Takenaka E, Van Vo A, Yamashita-Kanemaru Y, Shibuya A, Shibuya K. Selective DNAM-1 expression on small peritoneal macrophages contributes to CD4+ T cell costimulation. *Sci Rep* (2018) 8(1):15180. doi: 10.1038/s41598-018-33437-4

18. Cassado AA, D'Império Lima MR, Bortoluci KR. Revisiting mouse peritoneal macrophages: Heterogeneity, development, and function. *Front Immunol* (2015) 6:225 (MAY). doi: 10.3389/fimmu.2015.00225

19. Udompornpitak K, Bhunyakarnjanarat T, Charoensappakit A, Dang CP, Saisorn W, Leelahavanichkul A. Lipopolysaccharide-enhanced responses against aryl hydrocarbon receptor in fcgRIIb-deficient macrophages, a profound impact of an environmental toxin on a lupus-like mouse model. *Int J Mol Sci* (2021) 22(8):4199. doi: 10.3390/ijms22084199

20. da Silva AA, Teixeira TL, Teixeira SC, Machado FC, dos Santos MA, Tomiosso TC, et al. Galectin-3: A Friend but Not a Foe during Trypanosoma cruzi Experimental Infection. *Front Cell Infection Microbiol* (2017) 7:463. doi: 10.3389/fcimb.2017.00463

21. Vattepu R, Sneed SL, Anthony RM. Sialylation as an important regulator of antibody function. *Front Immunol* (2022) 13:818736(April). doi: 10.3389/fimmu.2022.818736

22. Anthony RM, Ravetch JV. A novel role for the igG fc glycan: The anti-inflammatory activity of sialylated igG fcs. *J Clin Immunol* (2010) 30(S1):9–14. doi: 10.1007/s10875-010-9405-6

23. Takai T, Ono M, Hikida M, Ohmori H, Ravetch JV. Augmented humoral and anaphylactic responses in FcγRII-deficient mice. *Nature* (1996) 379(6563):346–9. doi: 10.1038/379346a0

24. Anthony RM, Nimmerjahn F, Ashline DJ, Reinhold VN, Paulson JC, Ravetch JV. Recapitulation of IVIG anti-inflammatory activity with a recombinant igG fc. *Science* (2008) 320(5874):373–6. doi: 10.1126/science.1154315

25. Schwab I, Mihai S, Seeling M, Kasperkiewicz M, Ludwig RJ, Nimmerjahn F. Broad requirement for terminal sialic acid residues and FcγRIIB for the preventive and therapeutic activity of intravenous immunoglobulins in *vivo*. *Eur J Immunol* (2014) 44 (5):1444–53. doi: 10.1002/eji.201344230

26. O'Neill ASG, van den Berg TK, Mullen GED. Sialoadhesin - a macrophage-restricted marker of immunoregulation and inflammation. *Immunology* (2013) 138 (3):198–207. doi: 10.1111/imm.12042

27. Mimura Y, Mimura-Kimura Y, Saldova R, Rudd PM, Jefferis R. Enhanced immunomodulatory effect of intravenous immunoglobulin by fc galactosylation and nonfucosylation. *Front Immunol* (2022) 13:818382(January). doi: 10.3389/fimmu.2022.818382

28. Théry C, Witwer KW, Aikawa E, Alcaraz MJ, Anderson JD, Andriantsitohaina R, et al. Minimal information for studies of extracellular vesicles 2018 (MISEV2018): a position statement of the International Society for Extracellular Vesicles and update of the MISEV2014 guidelines. *J Extracellular Vesicles* (2018) 7(1):1535750. doi: 10.1080/20013078.2018.1535750

29. van der Pol E, Böing AN, Harrison P, Sturk A, Nieuwland R. Classification, functions, and clinical relevance of extracellular vesicles. *Pharmacol Rev* (2012) 64 (3:676–705. doi: 10.1124/pr.112.005983

30. Bayer-Santos E, Aguilar-Bonavides C, Rodrigues SP, Cordero EM, Marques AF, Varela-Ramirez A, et al. Proteomic analysis of trypanosoma cruzi secretome: Characterization of two populations of extracellular vesicles and soluble proteins. *J Proteome Res* (2013) 12(2):883–97. doi: 10.1021/pr300947g

31. Marcilla A, Martin-Jaular L, Trelis M, de Menezes-Neto A, Osuna A, Bernal D, et al. Extracellular vesicles in parasitic diseases. *J Extracellular Vesicles* (2014) 3(1). doi: 10.3402/jev.v3.25040

32. de Pablos Torró LM, Retana Moreira L, Osuna A. Extracellular vesicles in chagas disease: A new passenger for an old disease. *Front Microbiol* (2018) 9:1190. doi: 10.3389/fmicb.2018.01190

33. De Pablos LM, Díaz Lozano IM, Jercic MI, Quinzada M, Giménez MJ, Calabuig E, et al. The C-terminal region of Trypanosoma cruzi MASPs is antigenic and secreted *via* exovesicles. *Sci Rep* (2016) 6(1):27293. doi: 10.1038/srep27293

34. Díaz Lozano IM, De Pablos LM, Longhi SA, Zago MP, Schijman AG, Osuna A. Immune complexes in chronic Chagas disease patients are formed by exovesicles from Trypanosoma cruzi carrying the conserved MASP N-terminal region. *Sci Rep* (2017) 7 (November 2016):1–14. doi: 10.1038/srep44451

35. Retana Moreira L, Rodríguez Serrano F, Osuna A. Extracellular vesicles of Trypanosoma cruzi tissue-culture cell-derived trypomastigotes: Induction of physiological changes in non-parasitized culture cells. *PLoS Negl Trop Dis* (2019) 13 (2):e0007163. doi: 10.1371/journal.pntd.0007163

36. Retana Moreira L, Prescilla-Ledezma A, Cornet-Gomez A, Linares F, Jódar-Reyes AB, Fernandez J, et al. Biophysical and biochemical comparison of extracellular vesicles produced by infective and non-infective stages of trypanosoma cruzi. *Int J Mol Sci* (2021) 22(10). doi: 10.3390/ijms22105183

37. Garcia-Silva MR, Cabrera-Cabrera F, das Neves RF, Souto-Padrón T, de Souza W, Cayota A. Gene expression changes induced by Trypanosoma cruzi shed microvesicles in mammalian host cells: relevance of tRNA-derived halves. *Biomed Res Int* (2014) 2014:305239. doi: 10.1155/2014/305239

38. Nogueira PM, Ribeiro K, Silveira ACO, Campos JH, Martins-Filho OA, Bela SR, et al. Vesicles from different *Trypanosoma cruzi* strains trigger differential innate and chronic immune responses. *J Extracellular Vesicles* (2015) 4(1):28734. doi: 10.3402/jev.v4.28734

39. Van Hezel ME, Nieuwland R, Van Bruggen R, Juffermans NP. "The Ability of Extracellular Vesicles to Induce a Pro-Inflammatory Host Response." *International Journal of Molecular Sciences* (2017) 18(no. 6):1285. doi: 10.3390/ijms18061285

40. De Yarbuh AL, Cáceres K, Sulbarán D, Araujo S, Moreno E, Carrasco HJ, et al. Proliferation of Trypanosoma cruzi in the peritoneal membrane and ascitic liquid of mice with acute Infection. *BOLETÍN DE MALARIOLOGÍA Y SALUD AMBIENTAL* (2013) 53(2):146–56.

41. Williams JT, Mubiru JN, Schlabritz-Loutsevitch NE, Rubicz RC, VandeBerg JL, Dick EJ, et al. Polymerase chain reaction detection of Trypanosoma cruzi in Macaca fascicularis using archived tissues. *Am J Trop Med Hygiene* (2009) 81(2):228–34.

42. Penas FN, Cevey Á.C, Siffo S, Mirkin GA, Goren NB. Hepatic injury associated with Trypanosoma cruzi infection is attenuated by treatment with 15-deoxy-Δ 12,14 prostaglandin J 2. *Exp Parasitol* (2016) 170:100–8. doi: 10.1016/j.exppara.2016.09.015

43. Ward AI, Olmo F, Atherton RL, Taylor MC, Kelly JM. Trypanosoma cruzi amastigotes that persist in the colon during chronic stage murine infections have a reduced replication rate. *Open Biol* (2020) 10(12). doi: 10.1098/rsob.200261

44. Cura CI, Mejía-Jaramillo AM, Duffy T, Burgos JM, Rodriguero M, Cardinal MV, et al. Trypanosoma cruzi I genotypes in different geographical regions and transmission cycles based on a microsatellite motif of the intergenic spacer of spliced-leader genes. *Int J Parasitol* (2010) 40(14):1599–607. doi: 10.1016/j.ijpara.2010.06.006

45. De Pablos LM, González GG, Parada JS, Hidalgo VS, Lozano IMD, Samblás MMG, et al. Differential expression and characterization of a member of the mucin-associated surface protein family secreted by Trypanosoma cruzi. *Infection Immun* (2011) 79(10):3993–4001. doi: 10.1128/IAI.05329-11

46. Castanys S, Osuna A, Gamarro F, Ruiz-Perez LM. Purification of metacyclic forms ofTrypanosoma cruzi by Percoll discontinuous gradient centrifugation. *Z Parasitenkunde Parasitol Res* (1984) 70(4):443–9. doi: 10.1007/BF00926684

47. Gomez-Samblas M, Bernal D, Bolado-Ortiz A, Vilchez S, Bolás-Fernández F, Espino AM, et al. Intraperitoneal administration of the anti-IL-23 antibody prevents the establishment of intestinal nematodes in mice. *Sci Rep* (2018) 8(1):7787. doi: 10.1038/s41598-018-26194-x

48. Wang L, Zhang S, Wu H, Rong X, Guo J. M2b macrophage polarization and its roles in diseases. *J Leukocyte Biol* (2019) 106(2):345–58. doi: 10.1002/JLB.3RU1018-378RR

49. Gordon S. Alternative activation of macrophages. *Nat Rev Immunol* (2003) 3 (1):23–35. doi: 10.1038/nri978

50. Mosser DM, Edwards JP. Exploring the full spectrum of macrophage activation. *Nat Rev Immunol* (2008) 8(12):958–69. doi: 10.1038/nri2448

51. Lefèvre L, Lugo-Villarino G, Meunier E, Valentin A, Olagnier D, Authier H, et al. The C-type lectin receptors dectin-1, MR, and SIGNR3 contribute both positively and negatively to the macrophage response to leishmania infantum. *Immunity* (2013) 38(5):1038–49. doi: 10.1016/j.immuni.2013.04.010

52. Zhao X, Dai J, Xiao X, Wu L, Zeng J, Sheng J, et al. PI3K/Akt signaling pathway modulates influenza virus induced mouse alveolar macrophage polarization to M1/M2b. *PloS One* (2014) 9(8):e104506. doi: 10.1371/journal.pone.0104506

53. Atri C, Guerfali F, Laouini D. Role of human macrophage polarization in inflammation during infectious diseases. *Int J Mol Sci* (2018) 19(6):1801. doi: 10.3390/ijms19061801

54. Cortes-Serra N, Gualdron-Lopez M, Pinazo M-J, Torrecilhas AC, Fernandez-Becerra C. Extracellular Vesicles in Trypanosoma cruzi Infection: Immunomodulatory Effects and Future Perspectives as Potential Control Tools against Chagas Disease. *J Immunol Res* (2022) 2022:1–11. doi: 10.1155/2022/5230603

55. D'Avila H, Freire-de-Lima CG, Roque NR, Teixeira L, Barja-Fidalgo C, Silva AR, et al. Host cell lipid bodies triggered by trypanosoma cruzi infection and enhanced by the uptake of apoptotic cells are associated with prostaglandin E2 generation and increased parasite growth. *J Infect Dis* (2011) 204(6):951–61. doi: 10.1093/infdis/jir432

56. Lovo-Martins MI, Malvezi AD, Zanluqui NG, Lucchetti BFC, Tatakihara VLH, Mörking PA, et al. Extracellular vesicles shed by trypanosoma cruzi potentiate infection and elicit lipid body formation and PGE2 production in murine macrophages. *Front Immunol* (2018) 9:896. doi: 10.3389/fimmu.2018.00896

57. Kalinski P. Regulation of immune responses by prostaglandin E 2. *J Immunol* (2012) 188(1):21–8. doi: 10.4049/jimmunol.1101029

58. Trocoli Torrecilhas AC, Tonelli RR, Pavanelli WR, da Silva JS, Schumacher RI, de Souza W, et al. Trypanosoma cruzi: parasite shed vesicles increase heart parasitism and generate an intense inflammatory response. *Microbes Infection* (2009) 11(1):29–39. doi: 10.1016/j.micinf.2008.10.003

59. Bafica A, Santiago HC, Goldszmid R, Ropert C, Gazzinelli RT, Sher A. Cutting edge: TLR9 and TLR2 signaling together account for myD88-dependent control of parasitemia in trypanosoma cruzi infection. *J Immunol* (2006) 177(6):3515–9. doi: 10.4049/jimmunol.177.6.3515

60. Tarleton RL. Immune system recognition of Trypanosoma cruzi. *Curr Opin Immunol* (2007) 19(4):430–4. doi: 10.1016/j.coi.2007.06.003

61. Galeotti C, Kaveri SV, Bayry J. IVIG-mediated effector functions in autoimmune and inflammatory diseases. *Int Immunol* (2017) 29(11):491–8. doi: 10.1093/intimm/dxx039

62. Schwab I, Nimmerjahn F. Intravenous immunoglobulin therapy: how does IgG modulate the immune system? *Nat Rev Immunol* (2013) 13(3):176–89. doi: 10.1038/nri3401

63. Hamza T, Barnett JB, Li B. Interleukin 12 a key immunoregulatory cytokine in infection applications. *Int J Mol Sci* (2010) 11(3):789–806. doi: 10.3390/ijms11030789

64. Stoll S, Jonuleit H, Schmitt E, Müller G, Yamauchi H, Kurimoto M, et al. Production of functional IL-18 by different subtypes of murine and human dendritic cells (DC): DC-derived IL-18 enhances IL-12-dependent Th1 development. *Eur J Immunol* (1998) 28(10):3231–9. doi: 10.1002/(SICI)1521-4141(199810)28:10<3231::AID-IMMU3231>3.0.CO;2-Q

65. Chen L, Li C, Peng† Z, Zhao† J, Gong‡ G, Tan D. miR-197 expression in peripheral blood mononuclear cells from hepatitis B virus-infected patients. *Gut Liver* (2013) 7(3):335–42. doi: 10.5009/gnl.2013.7.3.335

66. Yasuda K, Nakanishi K, Tsutsui H. Interleukin-18 in health and disease. *Int J Mol Sci* (2019) 20(3):649. doi: 10.3390/ijms20030649

67. Wawrocki S, Druszczynska M, Kowalewicz-Kulbat M, Rudnicka W. Interleukin 18 (IL-18) as a target for immune intervention. *Acta Biochim Polonica* (2016) 63(1):59–63. doi: 10.18388/abp.2015_1153

68. Dinarello CA. Novel targets for interleukin 18 binding protein. *Ann Rheumatic Dis* (2001) 60(suppl 3):iii18–24. doi: 10.1136/ard.60.90003.iii18

69. Coma G, Peña R, Blanco J, Rosell A, Borras FE, Esté JA, et al. Treatment of monocytes with interleukin (IL)-12 plus IL-18 stimulates survival, differentiation and the production of CXC chemokine ligands (CXCL)8, CXCL9 and CXCL10. *Clin Exp Immunol* (2006) 145(3):535–44. doi: 10.1111/j.1365-2249.2006.03145.x

70. Xu H, Toyota N, Xing Y, Fujita Y, Huang Z, Touma M, et al. Enhancement of phagocytosis and cytotoxicity in macrophages by tumor-derived IL-18 stimulation. *BMB Rep* (2014) 47(5):286–91. doi: 10.5483/BMBRep.2014.47.5.152

71. Kaplanski G. Interleukin-18: Biological properties and role in disease pathogenesis. *Immunol Rev* (2018) 281(1):138–53. doi: 10.1111/imr.12616

72. Berclaz P-Y, Shibata Y, Whitsett JA, Trapnell BC. GM-CSF, *via* PU.1, regulates alveolar macrophage FcγR-mediated phagocytosis and the IL-18/IFN-γ–mediated molecular connection between innate and adaptive immunity in the lung. *Blood* (2002) 100(12):4193–200. doi: 10.1182/blood-2002-04-1102

73. Rossman MD, Ruiz P, Comber P, Gomez F, Rottem M, Schreiber AD. Modulation of macrophage Fc gamma receptors by rGM-CSF. *Exp Hematol* (1993) 21(1):177–83.

74. Sanmarco LM, Ponce NE, Visconti LM, Eberhardt N, Theumer MG, Minguez Á.R, et al. IL-6 promotes M2 macrophage polarization by modulating purinergic signaling and regulates the lethal release of nitric oxide during Trypanosoma cruzi infection. *Biochim Biophys Acta (BBA) - Mol Basis Dis* (2017) 1863(4):857–69. doi: 10.1016/j.bbadis.2017.01.006

75. Dienz O, Eaton SM, Bond JP, Neveu W, Moquin D, Noubade R, et al. The induction of antibody production by IL-6 is indirectly mediated by IL-21 produced by CD4+ T cells. *J Exp Med* (2009) 206(1):69–78. doi: 10.1084/jem.20081571

76. Akdis M, Burgler S, Crameri R, Eiwegger T, Fujita H, Gomez E, et al. Interleukins, from 1 to 37, and interferon-γ: Receptors, functions, and roles in diseases. *J Allergy Clin Immunol* (2011) 127(3):701–721.e70. doi: 10.1016/j.jaci.2010.11.050

77. Alleva DG, Kaser SB, Monroy MA, Fenton MJ, Beller DI. IL-15 functions as a potent autocrine regulator of macrophage proinflammatory cytokine production: evidence for differential receptor subunit utilization associated with stimulation or inhibition. *J Immunol (Baltimore Md. : 1950)* (1997) 159(6):2941–51.

78. Anguille S, Smits EL, Cools N, Goossens H, Berneman ZN, Van Tendeloo VF. Short-term cultured, interleukin-15 differentiated dendritic cells have potent immunostimulatory properties. *J Trans Med* (2009) 7(1):109. doi: 10.1186/1479-5876-7-109

79. Pestka S, Krause CD, Sarkar D, Walter MR, Shi Y, Fisher PB. Interleukin-10 and related cytokines and receptors. *Annu Rev Immunol* (2004) 22:929–79. doi: 10.1146/annurev.immunol.22.012703.104622

80. Saraiva M, O'Garra A. The regulation of IL-10 production by immune cells. *Nat Rev Immunol* (2010) 10(3):170–81. doi: 10.1038/nri2711

81. Gresnigt MS, Rösler B, Jacobs CWM, Becker KL, Joosten LAB, van der Meer JWM, et al. The IL-36 receptor pathway regulates Aspergillus fumigatus- induced Th1 and Th17 responses. *Eur J Immunol* (2013) 43(2):416–26. doi: 10.1002/eji.201242711

82. Guedes PMM, Gutierrez FRS, Silva GK, Dellalibera-Joviliano R, Rodrigues GJ, Bendhack LM, et al. Deficient regulatory T cell activity and low frequency of IL-17-producing T cells correlate with the extent of cardiomyopathy in human chagas' Disease. *PLoS Negl Trop Dis* (2012) 6(4):e1630. doi: 10.1371/journal.pntd.0001630

83. Braga YLL, Neto JRC, Costa AWF, Silva MVT, Silva MV, Celes MRN, et al. Interleukin-32γ in the control of acute experimental chagas disease. *J Immunol Res* (2022) 2022:1–9. doi: 10.1155/2022/7070301

84. Zubair K, You C, Kwon G, Kang K. Two faces of macrophages: Training and tolerance. *Biomedicines* (2021) 9(11):1596. doi: 10.3390/biomedicines9111596

frontiers | Frontiers in Immunology

TYPE Original Research
PUBLISHED 03 August 2023
DOI 10.3389/fimmu.2023.1218965

OPEN ACCESS

EDITED BY
Hua Cong,
Shandong University, China

REVIEWED BY
Natasa Ilic,
Institute for the Application of Nuclear Energy (INEP), Serbia
Laila Gutierrez Kobeh,
National Autonomous University of Mexico, Mexico

*CORRESPONDENCE
Yaowapa Maneerat
yaowapa.man@mahidol.ac.th

†These authors have contributed equally to this work and share first authorship

RECEIVED 08 May 2023
ACCEPTED 14 July 2023
PUBLISHED 03 August 2023

CITATION
Puasri P, Dechkhajorn W, Dekumyoy P, Yoonuan T, Ampawong S, Reamtong O, Boonyuen U, Benjathummarak S and Maneerat Y (2023) Regulation of immune response against third-stage *Gnathostoma spinigerum* larvae by human genes. *Front. Immunol.* 14:1218965. doi: 10.3389/fimmu.2023.1218965

Regulation of immune response against third-stage *Gnathostoma spinigerum* larvae by human genes

Pattarasuda Puasri[1†], Wilanee Dechkhajorn[1†], Paron Dekumyoy[2], Tippayarat Yoonuan[2], Sumate Ampawong[1], Onrapak Reamtong[3], Usa Boonyuen[3], Surachet Benjathummarak[4] and Yaowapa Maneerat[1*]

[1]Department of Tropical Pathology, Faculty of Tropical Medicine, Mahidol University, Bangkok, Thailand, [2]Department of Helminthology, Faculty of Tropical Medicine, Mahidol University, Bangkok, Thailand, [3]Department of Molecular Tropical Medicine and Genetics, Faculty of Tropical Medicine, Mahidol University, Bangkok, Thailand, [4]Center of Excellence for Antibody Research (CEAR), Faculty of Tropical Medicine, Mahidol University, Bangkok, Thailand

Background: Gnathostomiasis is an important zoonosis in tropical areas that is mainly caused by third-stage *Gnathostoma spinigerum* larvae (*G. spinigerum* L3).

Objectives: This study aimed to prove whether *G. spinigerum* L3 produces extracellular vesicles (EVs) and investigate human gene profiles related to the immune response against the larvae.

Methods: We created an immune cell model using normal human peripheral blood mononuclear cells (PBMCs) co-cultured with the larvae for 1 and 3 days, respectively. The PBMCs were harvested for transcriptome sequencing analysis. The EV ultrastructure was examined in the larvae and the cultured medium.

Results: Extracellular vesicle-like particles were observed under the larval teguments and in the pellets in the medium. RNA-seq analysis revealed that 2,847 and 3,118 genes were significantly expressed on days 1 and 3 after culture, respectively. The downregulated genes on day 1 after culture were involved in pro-inflammatory cytokines, the complement system and apoptosis, whereas those on day 3 were involved in T cell-dependent B cell activation and wound healing. Significantly upregulated genes related to cell proliferation, activation and development, as well as cytotoxicity, were observed on day 1, and genes regulating T cell maturation, granulocyte function, nuclear factor-κB and toll-like receptor pathways were predominantly observed on day 3 after culture.

Conclusion: *G. spinigerum* L3 produces EV-like particles and releases them into the excretory-secretory products. Overall, genotypic findings during our 3-day observation revealed that most significant gene expressions were related to T and B cell signalling, driving T helper 2 cells related to chronic infection, immune evasion of the larvae, and the pathogenesis of gnathostomiasis. Further in-depth

studies are necessary to clarify gene functions in the pathogenesis and immune evasion mechanisms of the infective larvae.

KEYWORDS

Gnathostoma spinigerum, gene expression, extracellular vesicles, immune evasion, pathogenesis, gnathostomiasis, third stage *G. spinigerum* larvae

1 Introduction

Human Gnathostomiasis is a zoonosis caused by third-stage *Gnathostoma* spp. larvae (L3). At least five of the 12 species in the genus (*G. binucleatum*, *G. doloresi*, *G. hispidum*, *G. nipponicum* and *G. spinigerum)* cause human disease. The species most frequently found in humans and most widely distributed around the world is *G. spinigerum. G. binucleatum* is found in the Americas (1). Sporadic cases caused by *G. doloresi, G. hispidum*, and *G. nipponicum* have been documented in Asia. *G. spinigerum* is the most common cause of the disease worldwide, particularly in Southeast Asia and Thailand (1). The disease can develop through 3 modes of transmission including oral, transplacental and skin wounds. Among the human cases, more than 90% caused by ingestion of raw or undercooked meat of intermediate hosts, such as fish, frogs, snakes or poultry, which contains *G. spinigerum* L3.

Epidemiological studies have revealed that *Gnathostoma* spp. is distributed worldwide. About 5,000 cases of human gnathostomiasis have been reported globally. The first case was described in Thailand, in 1889. The disease is endemic to Japan and Thailand, and has been reported sporadically in many countries around the world. Three thousand, one hundred and eighty-two (3,182) cases of human gnathostomiasis were detected in Japan between 1911 and 1995. In Thailand, 1,079 cases of human gnathostomiasis have been reported. The seroprevalence of Gnathostoma in humans was 62.5% (531/849) in Bangkok, Thailand, between 2000 and 2005. The high prevalence of gnathostomiasis among this population might be due in part to the local custom of eating raw fish. The first case of human gnathostomiasis in China was reported in Xiamen, Fujian Province, in 1919. Eighty-three cases (of which 80 were caused by *G. spinigerum*, two by *G. hispidum* and one by *G. doloresi*) were reported between 1918 and 2014, mostly in southern and eastern China (reviewed in (2)).

Although the infective larvae cannot develop into the adult stage in humans, they migrate within the host's body and provoke an inflammatory reaction and associated clinical symptoms. Cutaneous gnathostomiasis is relatively common, and is characterised by intermittent migratory swelling, usually in the trunk and upper limbs. Visceral larval migrans is a more serious condition but less frequently found. It occurs when the L3 (mostly *G. spinigerum*) migrate throughout various organs, such as the eyes, ears, breasts, lungs, gastrointestinal tract, thoracic spinal cord, genito-urinary system and central nervous system (CNS). Human cerebral gnathostomiasis with neurological manifestations, such as eosinophilic encephalomyelitis, intracranial haemorrhage and tract haemorrhage, can cause sudden death (1–3). Our current understanding of the host immune response and the larval immune evasion strategies remains unclear.

Previous studies of helminthic diseases reported the association of cutaneous and visceral migrans with excretory-secretory products (ESPs) from infective larvae (4–6). ESPs are composed of many essential molecules, such as protease and hyaluronidase, responsible for tissue invasion, protein degradation and anticoagulation inhibition, as well as acting as anti-inflammatory agents and modulators of the host immune response or causing the pathology of helminthic diseases (5–10). Until now, the role of *G. spinigerum* L3 ESPs in larvae migrans, immune evasion and pathogenesis has not been fully elucidated.

Extracellular vesicles (EVs) are membrane-enclosed structures secreted by various cell types. During their biogenesis, EVs may selectively capture cell-specific proteins, lipids, RNAs or even DNA, which may become a part of the EV membrane or molecular cargo (11). EVs play key roles in both homeostasis and disease pathogenesis by participating in intercellular signalling and communication. Several parasite species, including the adult and larval stages of some helminths, produce EVs and release them into ESPs (12). EVs are classified into three major subtypes: exosomes, microvesicles (MVs) and apoptotic bodies (11). EVs are found in body fluids, such as blood and urine. It was reported that EVs modulate host cells to enhance pathogenesis and/or inhibit immune responses. Due to the resemblance of the composition of EVs with the parental cell, circulating EVs have attracted considerable interest as a potential source of undiscovered biomarkers (12). Several recent intensive studies have revealed that parasite EVs are composed of bioactive contents, including proteins, microRNA (miRNA), noncoding RNA, and lipid. Nowadays, the mechanisms of EV uptake and cargo delivery into the cytosol of target cells in the infected host remain incompletely clarified. Previous studies demonstrated that bioactive molecules secreted by parasitic nematodes, packaged in exosomes, function as cell-to-cell effectors in the host-parasite interaction and immunomodulator in immune cells. For example, proteins and small RNA species in EVs secreted by *Heligmosomoides polygyrus* (*H. polygyrus)* alter gene expression in host cells and suppress innate immune responses, and reduce eosinophilia in the lungs of mice. *O. viverrini* EVs on human cholangiocytes found that they enhanced cell proliferation and induced the development of cholangiocarcinoma in liver fluke-infected patients. *Brugia malayi* EVs contain migration inhibitory factor for macrophage activation. (reviewed in (13)). There

is currently no evidence to prove whether *G. spinigerum* L3 produce EVs that are released into ESPs. Moreover, in-depth bioinformatics studies of host immunity against infective *G. spinigerum* L3 are crucial to understand the pathogenesis of human gnathostomiasis. Such studies can be performed using next-generation sequencing (NGS) analysis, which efficiently sequences the whole genome and detects abnormalities, including copy number changes and variations. Compared with traditional DNA sequencing, NGS is cheaper, has a faster turnaround time and requires a smaller amount of DNA (14).

The aims of this study were two-fold: 1) to prove whether *G. spinigerum* L3 produces EVs and 2) to explore human gene profiling related to the immune response to *G. spinigerum* L3. We co-cultured peripheral blood mononuclear cells (PBMCs) obtained from healthy buffy coats with live *G. spinigerum* L3 for 3 days. On days 1 and 3 after culture, the PBMCs were collected for RNA extraction and subsequent transcriptomic analyses using NGS. Gene profiling of human PBMC's response against *G. spinigerum* L3 will provide a better understanding of gnathostomiasis pathogenesis and may be advantageous for future studies of immunotherapeutic strategies.

2 Materials and methods

2.1 Study design and subjects

This study was performed at the Faculty of Tropical Medicine, Mahidol University. The study was approved by 1) the Ethics Committees of the Faculty of Tropical Medicine, Mahidol University (MUTM 2021-069-01), 2) the Thai Red Cross Society, Bangkok, Thailand (NBC 21/2021), and 3) Faculty of Tropical Medicine- Animal Care and Use Committee (FTM-ACUC 008/2020E). Normal PBMC were separated from healthy buffy coats provided by the Thai Red Cross Society. These PBMCs were used as a human immune cell model for the present study. The experimental design is summarised in Figure 1.

2.2 *G. spinigerum* L3 preparation from eel liver

G. spinigerum L3 were obtained from the livers of naturally infected eels by 1% acid -pepsin digestion (15). After treatment, the larvae in the eel liver suspension were collected under a dissecting microscope, washed several times with normal saline solution, and finally with sterile distilled water before use.

2.3 Examination of parasite and EVs morphology

2.3.1 Examination of EVs in ESP from the *G. spinigerum* L3 cultivation

To investigate whether EVs were found in the ES product, a pellet was collected from ultracentrifugation of the pooled 7-day *G. spinigerum L3* cultured media and processed as described previously (16). The pellets were fixed with 2.5% glutaraldehyde in PBS for 1 hour (h), then washed in PBS. Ten microliters of pellet suspension in sucrose phosphate buffer (SPB) pH 7.4 was dropped on Formvar grids. After negative staining with uranyl acetate, the morphology and size of EV-like particles were observed under a transmission electron microscope (TEM) (Hitachi; model HT7700, Japan).

2.3.2 Examination of EVs in *G. spinigerum* L3 by TEM

To prove that *G. spinigerum* L3 could produce EVs, day 3-cultured larvae were harvested and processed as described previously (17). Briefly, the larvae were fixed with 2.5% glutaraldehyde for at least 1 h, then washed 3 times for 10-15 minutes (min) each in sucrose phosphate buffer (SPB) pH 7.4. The larvae were then soaked in 1% osmium tetroxide for 1 h, then washed 3 times for 10-15 min each with SPB. The larvae were dehydrated twice in graded ethanol for 15 min each. The larvae were then infiltrated with Epon (EMS, Hatfield, PA, USA) in acetone and then embedded in a capsule beam. After that, the embedded larvae were polymerized in a 60 °C incubator blocks for 72 h and then cut into 90–100-nm thick sections. The sections were negative-stained using uranyl acetate, and then observed under a TEM.

2.3.3 Identification of *G. spinigerum* L3 by SEM

To examine the characteristics of *G. spinigerum* L3, five larvae were randomly collected and processed (18). The larvae were fixed with 2.5% glutaraldehyde for 1 h and then post-fixed with osmium tetroxide for 1 h. Samples were then dehydrated twice in graded ethanol for 10 min each. After dehydration, the samples were put into a critical point dryer (CPD) and then placed on an aluminum stub sputtered with gold in the coating unit (model K550, Emitech Ltd., Kent, England), and examined under a scanning electron microscope (model JSM-6610LV, JEOL Ltd., Tokyo, Japan).

2.4 Live *G. spinigerum L3* co-cultured with human PBMCs

3×10^6 PBMCs (CD27-)/well in 6 well plates were co-cultured with one live *G. spinigerum* L3 in complete medium (RPMI1640 supplemented with 10% heat-inactivated fetal bovine serum) at 37° C in an atmosphere of 5% CO_2. On days 0, 1, or 3 after incubation, cultured PBMCs were harvested, and washed 3 times with D-PBS (Thermo Fisher Scientific, Waltham, MA, USA) for RNA extraction. In this study, two independent experiments were performed in duplicate.

2.5 RNA extraction

Total RNA was extracted from PBMC pellets (15). Briefly, after washing, PBMC pellets were completely lysed with 1 ml of Trizol™ (Invitrogen, Carlsbad, CA, USA). Two hundred microliters of chloroform were added to the lysate, vortexed and incubated at room temperature for 10 min. Total RNA was extracted from each

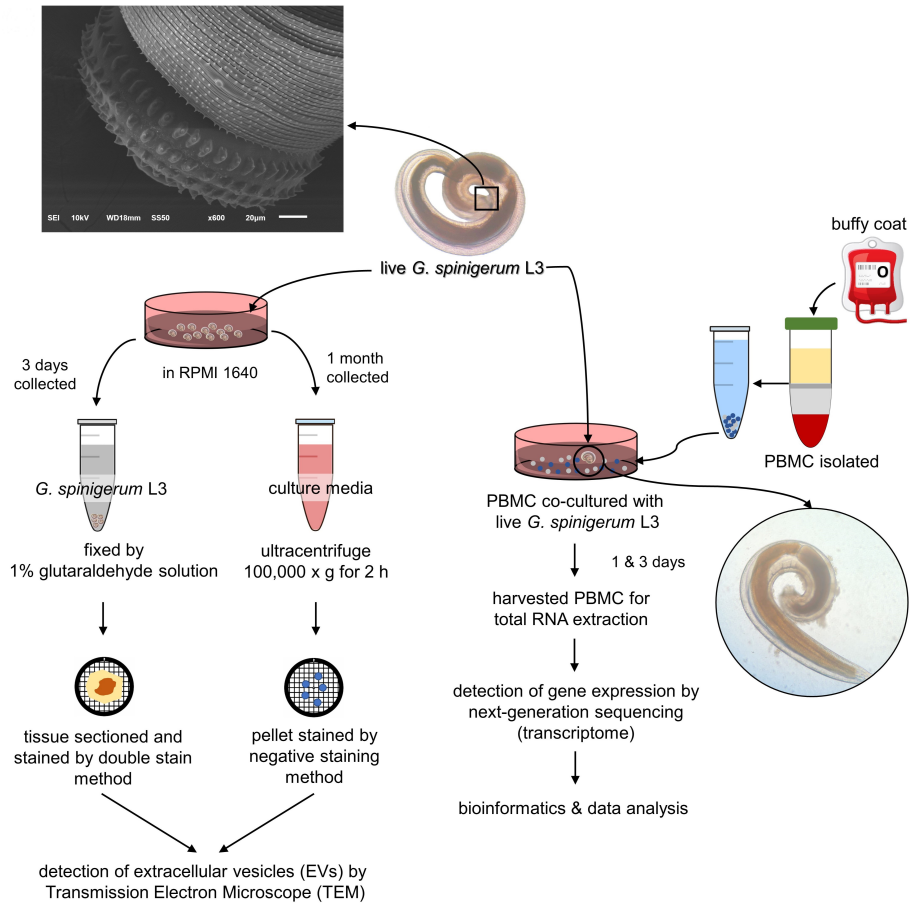

FIGURE 1
Experimental design was divided into 2 parts according to aims of the study. 1) to prove whether third stage *G. spinigerum* larvae (*G. spinigerum* L3) could produce extravascular vesicles (EVs), live *G. spinigerum* L3, obtained from eel livers, were cultured for excretory secretory product (ES) collection. Extracellular vesicles (EVs) in the ultra-centrifuged pellets of the collected cultured medium and in larvae were processed and examined by transmission electron microscopy; and 2) to inspect human gene profiling related to the immune response to *G. spinigerum* L3, peripheral blood mononuclear cells (PBMCs) obtained from healthy buffy coats were co-cultured with live *G. spinigerum* L3 for 3 days. At day 1 and 3 after cultivation, the cultured PBMCs were collected for RNA extraction and further performed next generation sequencing based transcriptomic analyses. Gene profiling and corresponding proteins were selected and discussed their roles and interplays in immune response against the larvae and possible pathogenesis of human gnathostomiasis.

lysate using a phenol-chloroform method, as previously described (15, 19). RNA pellets were washed with 75% ethanol, dried and resuspended with sterile distilled water. Total RNA was measured by Qubit 4 Fluorometer (Thermo Fisher, Waltham, MA, USA). Samples were used for cDNA library construction.

2.6 cDNA library construction and sequencing by NGS technique

The procedure was performed as mentioned previously (20). The amount and quality of total RNA samples were determined before analysis. The integrity of the total RNA was assessed using an Agilent 2100 Bioanalyzer (Agilent Technologies, Santa Clara, CA, United States). Approximately 500 ng of the total RNA from each sample were used to create individually indexed strand-specific RNA-seq libraries using a TruSeq stranded mRNA library preparation kit (Illumina Inc., San Diego, CA, United States). Briefly, poly-A-containing mRNA molecules were captured using magnetic oligo (dT) beads, purified, and directed to cDNA synthesis. AMPure XP beads (Beckman Coulter Genomic, Atlanta, GA, United States) were used to separate the cDNA from the reaction mix. Indexing adapters were ligated to the cDNA, and all cDNA libraries were checked for quality using an Agilent 2100 Bioanalyzer and quantified using a fluorometer (DeNovix Inc., Wilmington, DE, United States). The indexed sequencing libraries were pooled in equimolar quantities and subjected to cluster generation and paired-end 2 × 75 nucleotide read sequencing on an Illumina NextSeq 500 sequencer. The sequencing process was carried out at Omics Sciences and Bioinformatics Center, Chulalongkorn University, Bangkok, Thailand.

2.7 Differential expression analyses of RNA-seq data and statistical methods

Bioinformatics analyses were performed according to the instructions from the manufacturers and as described previously

(20). Briefly, the analyses comprised an initial quality check of the raw data files using FASTQC software (Bioinformatics Group, Babraham Institute, Cambridge, United Kingdom). Adapter and low-quality reads were depleted using Trimmomatic (21) http://www.usadellab.org/cms/index.php?page=trimmomatic. The filtered reads were aligned to a human reference genome using HISAT2 aligner software (Center for Computational Biology, Johns Hopkins University, Baltimore, MD, United States). StringTie (Center for Computational Biology, Johns Hopkins University) was used to assemble transcripts from RNA-seq reads that were aligned to the genome. Fold change ≥ 1, p-value < 0.05, and false discovery rate (FDR) < 0.05 was interpreted statistically significant. Gene profiling with fold change ± 4.0 were selected for further analyses in the current study. The gffcompare utility (22) (Center for Computational Biology, Johns Hopkins University, Baltimore, MD, United States), StringTie was used to discover a novel transcript. Gene Ontology (GO) and pathway enrichment analyses were done using a web-based bioinformatics tool DAVID (OmicX, Seine Innopolis, Le-Petit-Quevilly, France).

2.8 Correlate functions of some interesting genes to pathogenesis or immuno-evasion strategies of *G. spinigerum* L3 in Gnathostomiasis

Significant differential gene profiles expressed in *G. spinigerum* L3 co-cultured PBMCs on day 1 or day 3 were selected to explore properties and functions based on a reference database and linked to pathogenesis and/or immune-evasion strategies in human gnathostomiasis.

3 Results

3.1 Ultrastructural characteristics of *G. spinigerum* L3

The cultured larvae were examined under a scanning electron microscope (model JSM-6610LV, JEOL, Japan). They were identified as *G. spinigerum* L3, having morphological characteristics consistent with those mentioned previously (15, 23).

3.2 *G. spinigerum* L3 produces and releases EVs

The presence of EVs and typical morphology in the pellets of *G. spinigerum* L3 in the culture medium and under the larval teguments are shown in Figures 2A, B, respectively. EV-like vesicles were found in the pellets (Figure 2A). Both exosome-like vesicles (EX) (size = 27.90 ± 1.75 nm), small MV like vesicles (146.71 ± 13.76 nm) (MV) and large MV like vesicles (583.02 ± 136.03 nm) (pictures not shown) were observed. Examination of the larvae revealed the presence of some exosome- and MV-like vesicles under the cuticles (Figure 2B). The average sizes of the exosome and MV-like vesicles were 47.22 ± 8.17 nm (EX) and 471.33 ± 136.70 nm (MV), respectively. The double membranes of these vesicles were not obvious, but the vesicle sizes fell within the ranges of exosomes and MVs, respectively.

3.3 Gene expression selection from PBMCs co-cultured with *G. spinigerum* L3

After RNA-seq analysis, the raw data files were exported and the data were sorted using a bioinformatics platform. In this study, only gene profiles that were significantly expressed on day 1 (2,847 genes) or day 3 (3,118 genes) after culture, in comparison with those expressed on day 0, were investigated further. There were 2,358 genes co-expressed on both days 1 and 3, meaning that they were expressed throughout the 3 days of culture (Figure 3A) and were thus not the focus of the present study. A number of up- and down-regulated genes from the 2,874 genes from day 1 and 3,118 genes from day 3 after culture are shown in Figure 3B.

3.4 Gene ontology analysis

Gene ontology (GO) analysis is a representative set of contigs in particular metabolic networks. GO classification considers three categories: molecular function, biological process and cellular component. The most substantial enrichments (p value < 0.05) in function and process are shown in Figure 3C.

3.5 Kyoto Encyclopaedia of Genes and Genomes (KEGG) analysis

The results of the KEGG database analysis are presented in Supplementary Table 1. There were significant changes in pathways related to *G. spinigerum* L3 infection. On day 1 after culture, the nucleotide-binding and oligomerisation domain-like receptor signalling pathway was significantly expressed, while on day 3, expression of the B cell receptor (BCR) signalling pathway and apoptosis pathway dominated.

3.6 Reactome analysis

Analysis using the Reactome pathway databases revealed the significant expression of 18 pathways related to immune response on day 1 (Figure 4; Supplementary Table 2), but only seven pathways on day 3 after culture (Figure 5; Supplementary Table 3). Among the pathways identified as significant, the immune system pathway (REACT:R-HSA-168256) was significantly expressed on day 1 after culture, with the highest member count of 298 on day 1 and 276 counts on day 3 after culture. All non-human identifiers were converted to their human equivalent. The report was also filtered to only show results for the species 'Homo sapiens', and resources were set to 'all resources'. The gene profiles from these data were grouped, and the association of those genes of interest that were

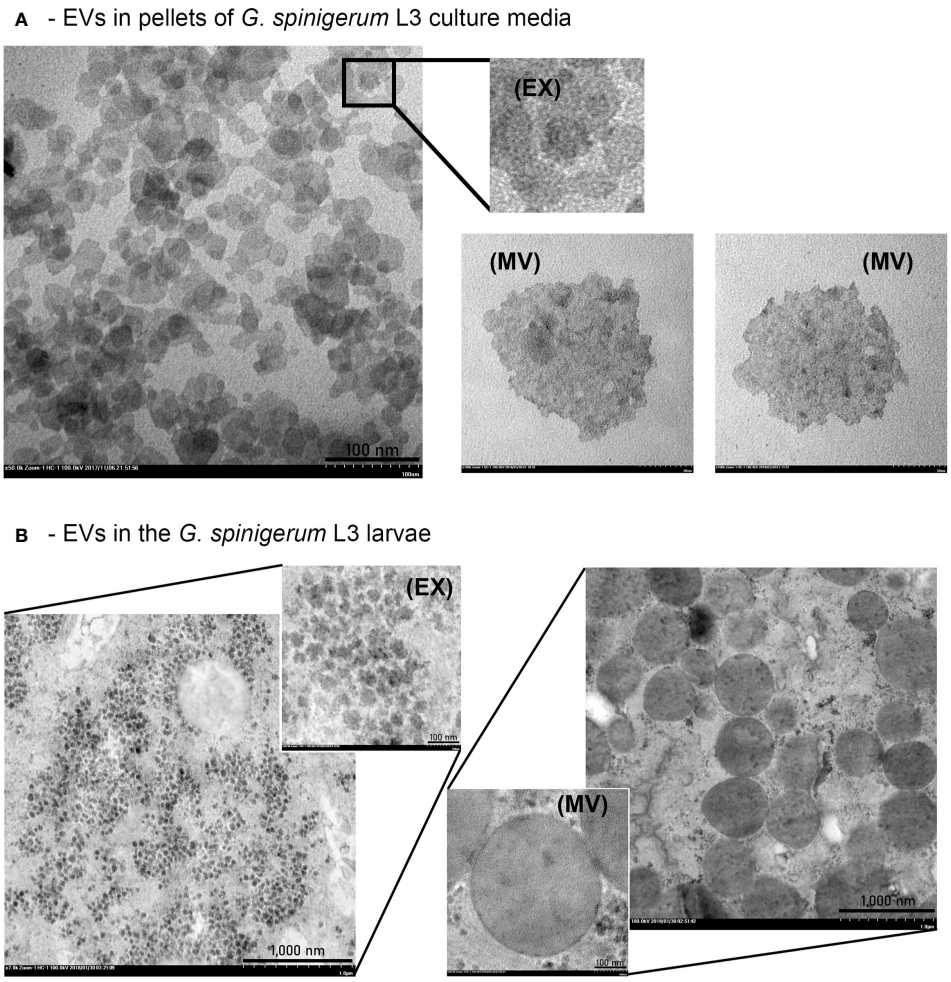

FIGURE 2
G. spinigerum L3 produce and release the EVs. Ultrastructural examination under transmission microscope: **(A)** The presence of EVs like vesicles in pellets of the larval cultured medium. Both exosome (EX) liked vesicles (size = 27.90 ± 1.75 nm), and microvesicle (MV)-like vesicles with small size (146.71 ± 13.76 nm) were observed, and **(B)** Some EX and MV-like vesicles were noted under cuticles of the larvae. The average sizes were 47.22 ± 8.17 nm, and 471.33 ± 136.70 nm, respectively.

involved in the immune response and were statistically significant on day 1 and day 3 after culture (p value < 0.05, FDR < 0.05) and related with gnathostomiasis caused by *G. spinigerum* L3 are shown in Tables 1, 2, respectively. Proteins that showed significant changes in transcript levels on days 1 and 3 after culture were classified as involved in innate immunity, adaptive immunity, cytokine signalling in the immune system and others (Figures 6A, B).

4 Discussion

Current knowledge about the pathogenesis, host-parasite interaction and immunity in human gnathostomiasis remains unclear.

In this study, the ultrastructural results revealed that EV-like particles were found both inside the *G. spinigerum* L3 body and the ESP pellet. The presence of EV-like vesicles in the parasite body was confirmed using transmission electron microscopy (TEM). In the present study, isolated EVs from *G. spinigerum* L3 were identified under TEM and presented the morphological characteristics as previously described (11, 12) We found that the vesicle sizes were consistent with exosomes and MVs reported in previous studies (11, 12), although the morphology and double membrane were not always obvious. This limitation may depend on the procedure used to prepare and process the samples for ultrastructural investigation. In a previous study, fresh *H. polygyrus* larvae were collected and transferred into a culture medium for only 5 h prior to staining for electron microscopy (12). In contrast, we examined a 3-day culture instead of fresh larvae. We suggest that the longer delay in examining the harvested larvae may have increased the degradation of the parasite organelles and cells. Additionally, most studies used ultracentrifugation for EV isolation and purification (12). Although this is the gold standard, high-speed centrifugation without preservation by sucrose gradient solution (24) can damage the EV membrane, as observed in the present study. However, alternative techniques, such as immunohistochemistry with antibody to EVs markers and molecular markers, are required to clarify our findings.

A previous study showed that 31 of 51 identified proteins in exosomes in *Schistosoma mansoni* (*S. mansoni*) ESPs (24). *S.*

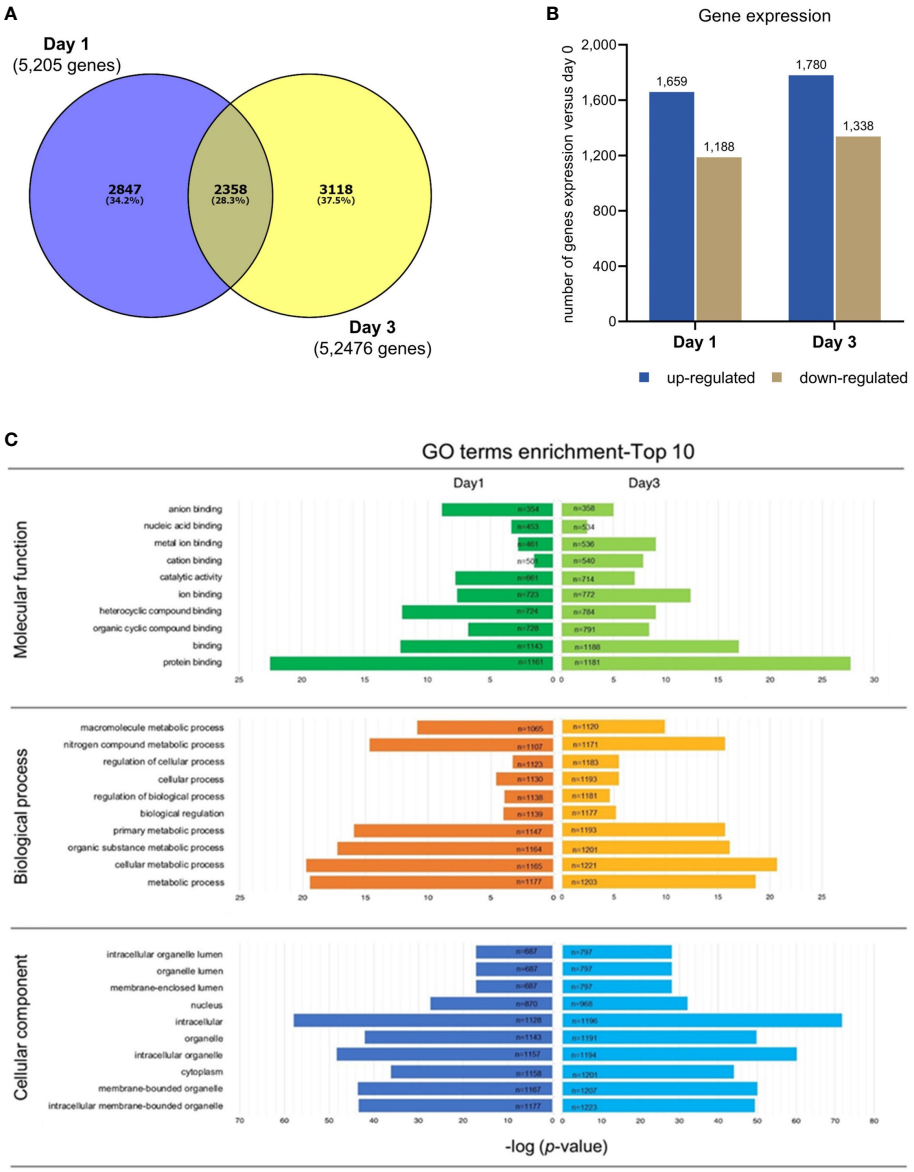

FIGURE 3
RNA-Seq analysis in PBMC co-cultured with *G. spinigerum* L3. **(A)** The venn diagram shows numbers of genes significantly expressed at day 1 (2,847 genes) or day 3 (3,118 genes), in comparison with those at day 0 of cultivation. These genes were further investigated. The 2,358 intersected genes were not focused in this study. **(B)** The bar graph indicates a number of up- and down regulated genes from 2,874 genes expressed at day 1, and 3,118 genes at day 3. **(C)** The illustration of gene ontology (GO) analysis. The GO classification considers 3 categories including molecular function, biological process, and cellular component. The most substantial enrichments ($p < 0.05$) in function and process. Expression and functions of genes at day1 and 3 of culture are shown in the left and right panels, respectively. Protein binding (n = 1161) was the most predominant term in "Molecular function", both at day1 and day3. Metabolic process (n = 1177) was the top GO term identified in "Biological process", while intracellular membrane (n = 1128) was the most predominant term in "Cellular component" at day 1. The enrichment of GO term at day 3 shows the same results as day 1, by which protein binding (n = 1181), metabolic process (n = 1171) and intracellular membrane (n = 1196) were the most abundant.

japonicum-derived EVs showed a high proportion of membrane- and tegument-associated proteins (25). The genetic and phenotypic profiles of EVs of several important pathogenic helminths have been reported (12). Here we did not perform any in-depth investigations to clarify and validate the functions and properties of the genome, transcriptome, and proteome in the EVs. However, this information is necessary to contribute to understanding the correlation of EVs and ESPs with the pathological effects, immunomodulation and immune evasion mechanisms of *G. spinigerum* L3.

The present study focused on exploring the gene expression related to both the innate and adaptive immune response against *G. spinigerum* L3 *in vitro* using PBMCs as an immune cell model. The human gene profiling results related to the immune response were obtained from NGS of PBMCs that were co-cultured with live *G. spinigerum* L3 for 3 days. Therefore, the PBMCs are representative of first-line immune cells in response to an infection. Additionally, PBMCs detect pathogen-associated molecular patterns (PAMPs) on the pathogen surfaces, transmitting signals into the cell to activate gene expression of pro-inflammatory and anti-inflammatory

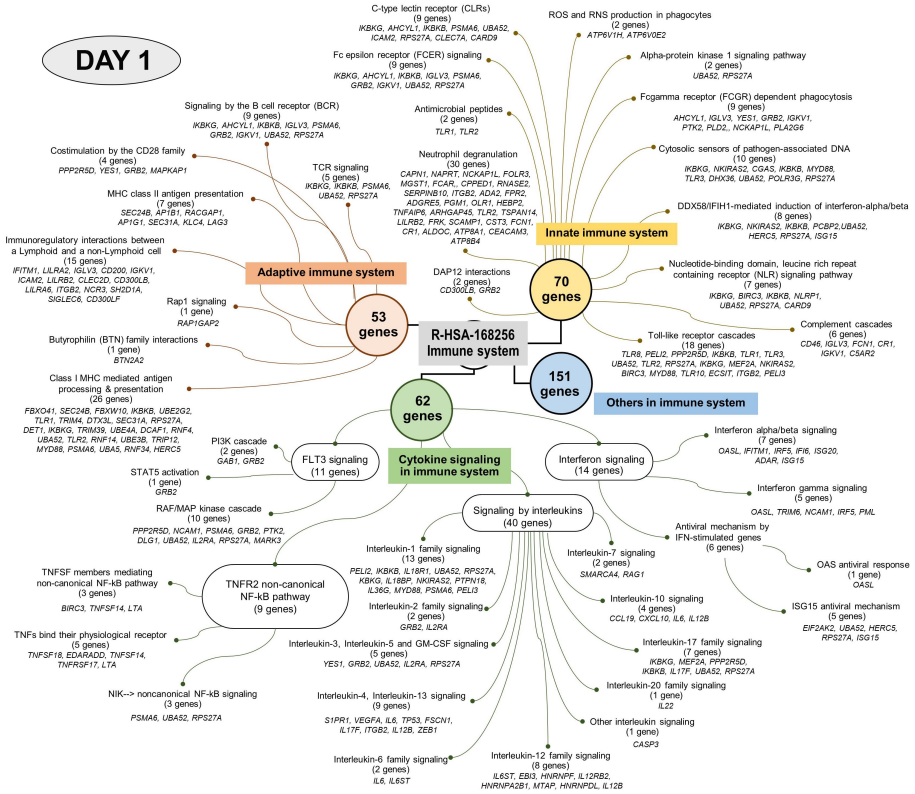

FIGURE 4
Visualised graph of immune system term (REAG : HAS-168256) of reactome database in PBMC co-cultured with *G. spinigerum* L3 at day 1.

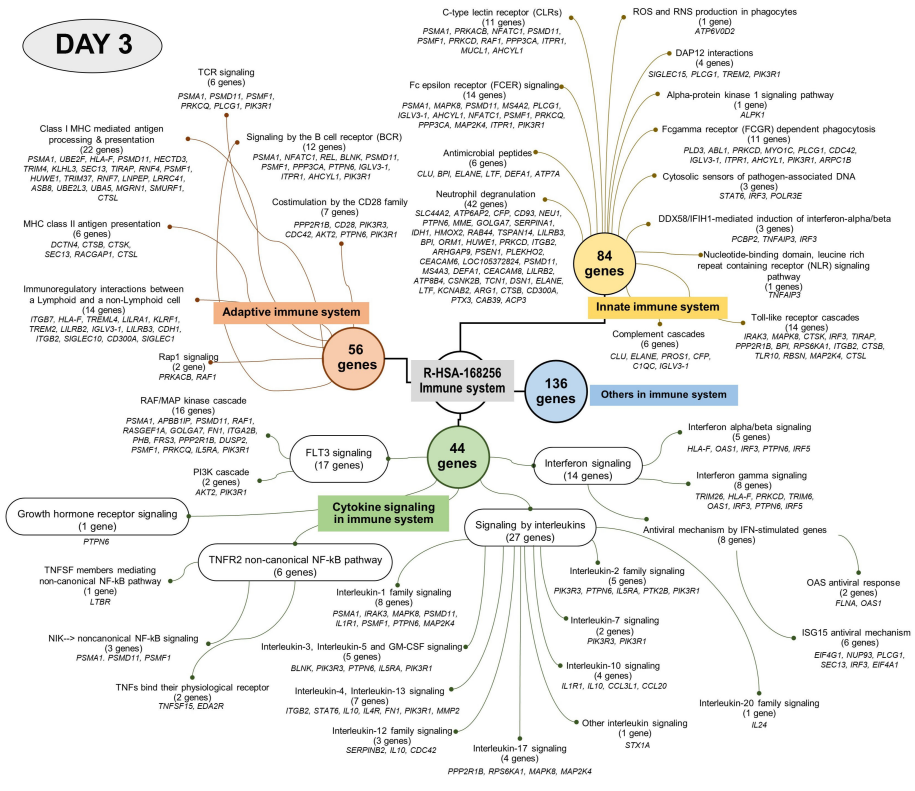

FIGURE 5
Visualised graph of immune system term (REAG : HAS-168256) of reactome database in PBMC co-cultured with *G. spinigerum* L3 at day 3.

10.3389/fimmu.2023.1218965

TABLE 1 Significant regulated genes expression related to immune system in PBMC co-cultured with *G. spinigerum* L3 at day 1 of stimulation ($p < 0.05$ and FDR < 0.05).

Ensembl Transcript ID	Symbol	Description	logFC	*p*-value	FDR	Regulation
Toll like receptors						
ENST00000504367	*TLR3*	toll like receptor 3	11.19036612	2.41064E-05	0.000405919	up
ENST00000311912	*TLR8*	toll like receptor 8	4.990818373	0.002322798	0.016875361	up
ENST00000308979	*TLR1*	toll like receptor 1	4.824035063	0.003285048	0.022943438	up
ENST00000642580	*TLR2*	toll like receptor 2	-13.05858833	9.65844E-07	4.19988E-05	down
C-type lectins						
ENST00000438351	*CLEC5A*	C-type lectin domain containing 5A	4.546921524	0.005836801	0.037626389	up
ENST00000290855	*CLEC2D*	C-type lectin domain family 2 member D	4.041883774	0.008074238	0.049625056	up
Ubiquitine genes						
ENST00000461934	*UBA3*	ubiquitin like modifier activating enzyme 3	9.60663781	0.000358854	0.003131692	up
ENST00000450743	*UBE2D4*	ubiquitin conjugating enzyme E2 D4 (putative)	6.244955135	0.000535236	0.004449826	up
ENST00000449510	*UBE3B*	ubiquitin protein ligase E3B	4.246364235	0.007344852	0.045688205	up
ENST00000330942	*UBE2G2*	ubiquitin conjugating enzyme E2 G2	-5.625077179	0.001620904	0.012236419	down
ENST00000431736	*UBE4A*	ubiquitination factor E4A	-7.004217532	8.7854E-05	0.00108468	down
Proteasome						
ENST00000389993	*PSME4*	proteasome activator subunit 4	13.56332621	4.03346E-07	2.44619E-05	up
ENST00000559042	*PSME2*	proteasome activator subunit 2	5.396570406	0.001279515	0.009904009	up
ENST00000559741	*PSME1*	proteasome activator subunit 1	5.48867216	0.002764619	0.01896649	up
ENST00000592169	*PSME3*	proteasome activator subunit 3	-5.84535768	0.000459179	0.003754016	down
Caspase						
ENST00000490682	*CASP8*	caspase 8	5.024180794	0.001651213	0.012446583	up
ENST00000619992	*CASP2*	caspase 2	-11.56850313	1.26397E-05	0.000253086	down
ENST00000489932	*CARD9*	caspase recruitment domain family member 9	-9.872026654	0.000227724	0.002219461	down
IRF						
ENST00000528413	*IRF7*	interferon regulatory factor 7	4.128725299	0.007116144	0.044512773	up
LILRs						
ENST00000473156	*LILRA1*	leukocyte immunoglobulin like receptor A1	-14.96020652	3.59684E-08	6.66447E-06	down
ENST00000430421	*LILRA6*	leukocyte immunoglobulin like receptor A6	-10.95645976	3.60864E-05	0.00055212	down
Pro-inflammatory cytokines						
ENST00000259205	*IL36G*	interleukin 36 gamma	15.34778506	1.8383E-08	5.06752E-06	up
ENST00000648487	*IL12RB2*	interleukin 12 receptor subunit beta 2	11.25678998	2.14701E-05	0.000372734	up
ENST00000336123	*IL17F*	interleukin 17F	10.67675085	5.83948E-05	0.0007954	up
ENST00000538666	*IL22*	interleukin 22	9.784421306	0.000264562	0.002497361	up
ENST00000258743	*IL6*	interleukin 6	4.682488472	0.00287209	0.020372635	up
ENST00000379959	*IL2RA*	interleukin 2 receptor subunit alpha	4.160496605	0.006759739	0.042611299	up
ENST00000409599	*IL18R1*	interleukin 18 receptor 1	-12.16996757	4.47137E-06	0.000120186	down
ENST00000620017	*IL18BP*	interleukin 18 binding protein	-10.12432144	0.000149619	0.00160778	down

(Continued)

10.3389/fimmu.2023.1218965

TABLE 1 Continued

Ensembl Transcript ID	Symbol	Description	logFC	*p*-value	FDR	Regulation
KIRs						
ENST00000336077	*KIR2DL1*	killer cell immunoglobulin like receptor, two Ig domains and long cytoplasmic tail 1	-12.809832	1.4849E-06	5.49861E-05	down
ENST00000463062	*KIR2DL4*	killer cell immunoglobulin like receptor, two Ig domains and long cytoplasmic tail 4	5.451300899	0.002834143	0.020140316	up
ENST00000479407	*NKIRAS2*	NFKB inhibitor interacting Ras like 2	-5.856937956	0.000910973	0.007277095	down
Complements components						
ENST00000472581	*CFB*	complement factor B	4.907049998	0.00322678	0.022580291	up
ENST00000595464	*C5AR2*	complement component 5a receptor 2	-12.36066091	3.22355E-06	9.53967E-05	down
ENST00000592860	*CFD*	complement factor D	-11.93525773	6.71648E-06	0.000159895	down
Surface proteins (CD)						
ENST00000473539	*CD200*	CD200 molecule	6.499255811	0.001050189	0.008284146	up
ENST00000528435	*CD3E*	CD3e molecule	4.415287189	0.007812412	0.048203957	up
ENST00000443761	*CD1C*	CD1c molecule	-5.272358835	0.002385781	0.017278145	down
ENST00000322875	*CD46*	CD46 molecule	-4.536967506	0.003832954	0.026264202	down
Others						
ENST00000433677	*CPPED1*	calcineurin like phosphoesterase domain containing 1	-13.39690662	5.3798E-07	2.89361E-05	down
ENST00000637481	*MEF2C*	myocyte enhancer factor 2C	-14.88729372	4.08259E-08	7.24487E-06	down

TABLE 2 Significant regulated genes expression related to immune system in PBMC co-cultured with *G. spinigerum* L3 at day 3 of stimulation ($p < 0.05$ and FDR < 0.05).

Ensembl Transcript ID	Symbol	Description	logFC	*p*-value	FDR	Regulation
Ubiquitine genes						
ENST00000346330	*UBE2A*	ubiquitin conjugating enzyme E2 A	9.447272478	0.000466677	0.003803408	up
ENST00000442670	*UBE2E1*	ubiquitin conjugating enzyme E2 E1	7.770827761	3.41012E-05	0.000517072	up
ENST00000414443	*UBE2F*	ubiquitin conjugating enzyme E2 F (putative)	6.335637296	0.000391682	0.003284291	up
ENST00000520595	*UBE2V2*	ubiquitin conjugating enzyme E2 V2	5.725884142	0.001874872	0.013466752	up
ENST00000545681	*UBE2L3*	ubiquitin conjugating enzyme E2 L3	4.277789464	0.007493316	0.044852236	up
ENST00000513098	*UBE2D3*	ubiquitin conjugating enzyme E2 D3	-6.097929538	0.000511692	0.004127887	down
Proteasome						
ENST00000559741	*PSME1*	proteasome activator subunit 1	5.48867216	0.002764619	0.01896649	up
ENST00000592169	*PSME3*	proteasome activator subunit 3	-5.84535768	0.000459179	0.003754016	down
Caspase						
ENST00000527979	*CASP1*	caspase 1	-12.28343431	3.67906E-06	0.000100176	down
IRF						
ENST00000597198	*IRF3*	interferon regulatory factor 3	-9.819519142	0.000247822	0.00230753	down
LILRs						
ENST00000391750	*LILRB3*	leukocyte immunoglobulin like receptor B3	12.63548282	2.00566E-06	6.59219E-05	up

(Continued)

TABLE 2 Continued

Ensembl Transcript ID	Symbol	Description	logFC	*p*-value	FDR	Regulation
ENST00000430952	*LILRB4*	leukocyte immunoglobulin like receptor B4	4.053443852	0.00790473	0.046871459	up
ENST00000391749	*LILRB2*	leukocyte immunoglobulin like receptor B2	-6.379914479	0.000168318	0.001717255	down
ENST00000251372	*LILRA1*	leukocyte immunoglobulin like receptor A1	-4.406010665	0.004825174	0.030807165	down
Anti- inflammatory cytokine						
ENST00000170630	*IL4R*	interleukin 4 receptor	5.154344032	0.001360231	0.010104634	up
ENST00000423557	*IL10*	interleukin 10	4.677601477	0.002936296	0.020020635	up
ENST00000391929	*IL24*	interleukin 24	4.567393135	0.004273952	0.02782438	up
ENST00000615950	*ILF2*	interleukin enhancer binding factor 2	-12.04247883	5.57705E-06	0.000135081	down
ENST00000416750	*IL1B*	interleukin 1 beta	-10.16892142	0.000137239	0.001470078	down
ENST00000383846	*IL5RA*	interleukin 5 receptor subunit alpha	-9.740896694	0.000282929	0.002562356	down
ENST00000472292	*IL1RN*	interleukin 1 receptor antagonist	-7.719125693	6.47064E-05	0.000834787	down
Complement complement						
ENST00000510260	*C1QB*	complement C1q B chain	10.6966174	5.6334E-05	0.000750665	up
ENST00000418949	*C2*	complement C2	8.521279704	3.54456E-05	0.000533091	up
ENST00000461983	*C1S*	complement C1s	5.525285908	0.00113524	0.008587219	up
ENST00000374640	*C1QC*	complement C1q C chain	5.044784209	0.001624009	0.011845263	up
Surface proteins						
ENST00000458610	*CD28*	CD28 molecule	4.820673844	0.002695362	0.018547355	up
ENST00000492627	*CD81*	CD81 molecule	4.724752731	0.003205828	0.021622473	up
ENST00000310828	*CD300A*	CD300a molecule	-6.445742921	0.000283966	0.002570811	down
ENST00000246006	*CD93*	CD93 molecule	-5.359648103	0.000934207	0.007186163	down
B-cell						
ENST00000413476	*BLNK*	B cell linker	9.66225397	0.00032541	0.00284507	up
Others						
ENST00000394236	*PROS1*	protein S	10.9802551	3.4689E-05	0.00052329	up

cytokines and chemokines (26–28). Therefore, PBMCs are influential biological sensors of infection, making them suitable for use as immune cell models for studying immune response against various antigen, for examples, studies in innate and adaptive immunity, immunoregulation, immunomodulation, and acute/chronic infection (29). However, sampling of mRNA levels obtained from PBMCs reflects a static point in time and may not illustrate the complete expression pattern (29). Similar to previous studies, we observed the expression of genes related to innate and adaptive immune responses at day 1 (30, 31) and day 3 after culture, respectively (32). Innate immune response can occur rapidly after innate immune cells are exposed to antigens. Previous studies in innate immunity, e.g. monocyte and NK cell activation, and pro-inflammatory cytokine secretion, observed the related gene expression at day 1 of stimulation. Adaptive immunity, such as T and B cell activation and antibody production, is noted about 7 days or later. Duration time to study adaptive immune gene expression is optimal from day 3 of incubation (33). So, in the present study we designed to investigate gene expression of innate and adaptive immunity at days 1 and 3 of stimulation. The previous study suggested that the PBMC expression profiles were drawn from a mixed population of cells and, therefore could not be attributed to a specific cell type or lineage (29). The composition of this profile reflects the conditions in the periphery and not those in germinal centres (GCs), lymph nodes or remote sites of infection and inflammation (29). In the present study, we selected genes of interest that were related to the immune response against *G. spinigerum* L3 on days 1 and 3 after culture and linked to conceivable pathogenesis, immunomodulation and immune evasion mechanisms in human gnathostomiasis.

Table 1 summarises gene expression in human PBMCs against *G. spinigerum* L3 on day 1 after culture. The expression of several genes is related to immunity. Genes coding for toll-like receptors (TLRs), including *TLR1*, *TLR3* and *TLR8*, were mostly upregulated. TLRs are pathogen recognition receptors (PRRs). *TLR* upregulation drives T helper (Th) 2 or regulatory responses in *Acanthocheilonema viteae*

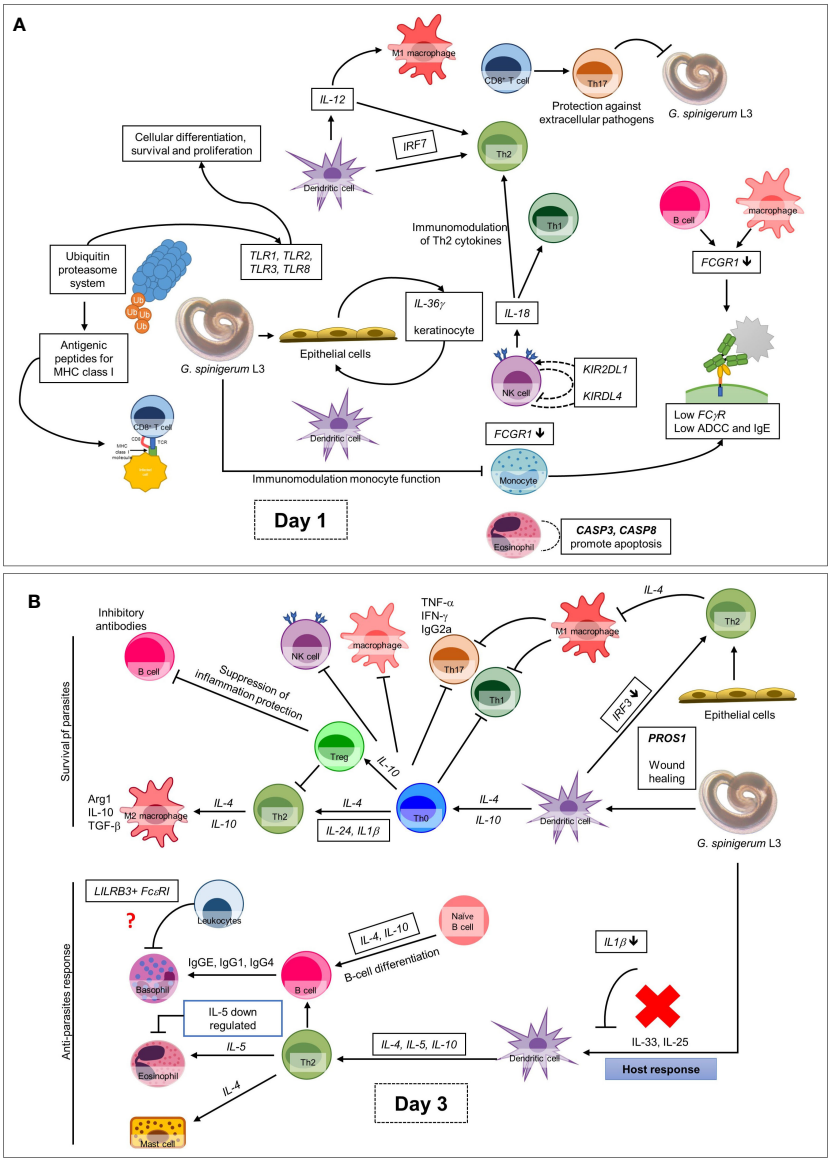

FIGURE 6
Overall up and down-regulated gene expression in PBMC co-cultured with *G. spinigerum* L3 **(A)** At day 1 after cultivation, gene expression profile trends to related to dominant innate immunity that play roles in pathogenesis, immunomodulation and contribute to evasion of *G. spinigerum* L3. The genes which play roles in pathogen recognition, proteolysis, NF-kB antigenic peptides generation for MHC I, NK cells, cytotoxic T cells activation, regulatory T cell, M1 macrophages, pro-inflammatory cytokines were up-regulated. Some of these can also drive type 2 immunity. Genes related to activation of NK cells, phagocytosis and complement system were down-regulated. **(B)** The genes expressed at day 3 of cultivation include genes related to regulation of T-cell activation and development, TCR and BCR which drive to Th 2 response, B cell development and antibody production, anti-inflammatory cytokines, wound healing and most of complement system were up-regulated. Genes play roles in phagocytosis function of monocyte, eosinophil, NK cell apoptosis, M2 macrophage and Th1/Th17 were down-regulated.

infection (34) and schistosomiasis (35). TLRs also transduce signalling to promote the expression of genes coding for pro-inflammatory cytokines and type I interferons (IFNs; including IFN-α and IFN-β). They also promote innate immunity by activating the signalling transduction cascades for nuclear factor-κB (NF-κB), mitogen-activated protein kinases and interferon regulatory factor (IRF) 3 cascades (36). *TLR2* downregulation has been suggested to increase the ability to promote a Th2-type response (35). TLR2 is a key molecule required for innate immunity and is involved in the recognition of a wide range of viruses, bacteria, fungi and parasites. A cysticercosis experiment in a previous study demonstrated that the lack of Th1-dominant adaptive immunity in $TLR2^{-/-}$ mice were associated with significantly elevated parasite burdens. While $TLR2^{+/+}$ mice were resistant to infection (37). Furthermore, this Th2-type response is elicited by most helminth infections e.g. schistosomiasis, and stimulates the production of cytokines and interleukins (ILs), antibody isotypes (IgG1, IgG4 and IgE) (38) and expanded populations of eosinophils, basophils, mast cells, type 2 innate lymphoid cells and alternatively activated macrophages (M2) (39). In our previous study, human B cells separated from PBMCs were co-cultured with crude Ag derived from *G. spinigerum* L3 for 2 wks. The results revealed that cultured B

cell function was impaired to produce specific IgM and IgG against the parasite antigens (19). The finding may contribute to *G. spinigerum* L3's survival from the host's immune response.

Earlier studies identified a family of membrane-bound TLRs (TLR1–TLR13), and mouse genetic studies revealed that TLRs generally serve as PRRs that recognise a wide range of PAMPs, including lipids, lipoproteins, proteins, glycans and nucleic acids and play a central role in initiating innate immune responses (40). In animal model studies, a loss-of-function mutation of the mouse homolog of hToll was subsequently unable to promote innate immune responses against bacterial lipopolysaccharides (41). Similarly, our present findings revealed *TLR2* downregulation, which may explain the defect in innate immunity in gnathostomiasis.

Similar to the expression of TLRs, CLR genes *CLEC5A* and *CLEC2D* code for C-type lectin, which served as PRRs were up-regulated on day 1 after culture. CLR proteins have a diverse range of functions, including cell-cell adhesion, immune response to pathogens and apoptosis (42). CLEC2D is a receptor for KLRB1, a natural killer (NK) cell receptor that protects target cells against NK cell-mediated lysis (43). CLEC5A, also known as myeloid DAP12-associating lectin 1(MDL-1), is highly expressed in myeloid lineages, such as neutrophils, monocytes and macrophages, as well as osteoclasts, microglia and dendritic cells (44). Both CLEC2 and CLEC5A are critical in microbe-induced "neutrophil extracellular trap" (NET) formation (a form of neutrophil activity to destroy pathogens) and proinflammatory cytokine production in viral infections (45). For example, dengue virus (DV) and H5N1 influenza A virus (IAV) could activate CLEC2 to induce the release of EVs, which further enhance damage in infected cells by NET (NETosis) and proinflammatory cytokine production *via* CLEC5A and TLR2 (45). In *Listeria monocytogenes* (*L. monocytogenes*) infection, CLEC5A induce NET formation and the production of proinflammatory cytokines and reactive oxygen species (ROS). Inoculation of *Clec5a* −/− mice with *L. monocytogenes* develops rapid bacterial spread, increased bacterial loads in the circulation and liver, and severe liver necrosis. In these knockout mice, IL-1β, IL-17A, and TNF production is suppressed (46). It is possible that *TLR* expression in the present study may have contributed to the ability of immune cells to recognise and eliminate parasites *via* the Th2 response. *TLR* and *NF-κB* expression protect against pathogenic infection by orchestrated gene expression programmes. Moreover, TLR ligands are potent activators of the NF-κB pathway that promote degradation of inhibitory IκBα, resulting in NF-κB activation (47). In the present study, *NKIRAS2*, which codes for NF-κB inhibitor interacting Ras-like 2, was downregulated, leading to NF-κB activation. NF-κB controls the transcription of cytokines and genes that regulate cellular differentiation, survival and proliferation. Additionally, it regulates the expression of various genes involved in innate and adaptive immune responses (48). Similarly, an in-vitro study in mouse macrophage co-cultured with ES from adult *Toxocara canis* revealed that NF-κB were expressed at both transcriptional and translational levels after 9 h of incubation. The production of pro-inflammatory cytokines, including TNF-α, IL-1β and IL-6 released by the stimulated macrophages, were modulated (49).

Ubiquitin (Ub) was originally named ATP-dependent proteolysis factor 1. Mammals have four Ub genes. *UBA52* and *RPS27A* code for Ub-ribosomal fusion proteins L40 and S27a, respectively, and *UBB* and *UBC* code for polyubiquitin precursor proteins (50). Ubiquitination refers to the conjugation of Ub to a target protein. This is a multi-step process that requires three enzymes: a Ub-activating enzyme (E1), a Ub-conjugating enzyme (E2) (51) and a Ub ligase (E3) (52). Ubiquitination is an energy-dependent, post-translational modification process and is suggested as essential for the initiation, maintenance and termination of the immune system's response (50, 53). Ubiquitination affects cellular processes by regulating protein degradation *via* proteosomes (PSMEs) and lysosomes, coordinating the cellular localisation of proteins, activating and inactivating proteins and modulating protein-protein interactions. In response to the eradication of invading pathogens and to reduce concomitant host damage due to pathogen infection, the Ub system tunes the host's innate immune system, including inflammatory signalling, phagosomal maturation, autophagy and apoptosis (53). Additionally, Ub mediates regulation of the TLR, retinoic acid-inducible gene-I-like receptor and tumour necrosis factor (TNF)-α signalling pathways. However, pathogens have evolved strategies to evade host innate immunity by usurping the Ub system to favour their own survival (54).

The PSME, a profoundly complicated protease complex, performs selective, efficient and processive hydrolysis of client proteins. PSME collaborates with Ub, which polymerises to form a marker for regulated proteolysis in eukaryotic cells (55). IFN-γ-inducible PSMEs or immunoproteasomes are a type of proteasome that degrades Ub-labelled proteins found in the cytoplasm under conditions of oxidative stress and in cells exposed to pro-inflammatory stimuli. Additionally, the immunoproteasome influences inflammatory disease pathogenesis through its ability to regulate T cell polarisation (55). The immunoproteasome contributes to the production of peptide epitopes for cytotoxic T cells and has been highlighted in the major histocompatibility complex (MHC) class I-restricted antigen-processing pathway and cell-mediated immunity (55, 56).

The degradation of ubiquitinated proteins is mediated by the Ub–proteasome system (UPS). Degradation of proteins by the UPS is the first step in the generation of MHC I-presented peptides (56). Protein degradation through the UPS is the major pathway of non-lysosomal proteolysis of intracellular proteins. It plays important roles in a variety of fundamental cellular processes, such as the regulation of cell cycle progression, division, development and differentiation; apoptosis; cell trafficking and modulation of the immune and inflammatory responses. Aberrations in this system lead to the dysregulation of cellular homeostasis and the development of various diseases (55, 57).

A recent transcriptomic and proteomic analysis in the immature stage liver fluke revealed that ubiquitin related genes were predominated. These genes regulate proteins at the cellular level *via* the ubiquitin proteasome system. It is specifically important for controlling cell cycle progression during intensified cell growth and proliferation in fascioliasis. In *Fasciola hepatica* infection, the major pathogenesis associated with results from the

extensive tissue damage caused by immature fluke migration, growth and development in the liver. This is compounded by the pathology caused by host innate and adaptive immune responses against infection and repair tissue damage (58).

In this study, *UBA3*, *UBE2D4* and *UBE3B* were upregulated, while *UBE2G2* and *UBE4* were downregulated. Our findings indicated that Ub genes regulate functions by balancing the expression of Ub-activating, Ub-conjugating and Ub ligase enzymes. In agreement with our findings, Qureshi et al, suggested that alterations in the UPS would profoundly affect immune responses, including the regulation of an array of inflammatory cytokines. Additionally, the proteasome acts as a central regulator of inflammation and macrophage function *via* several pathways (59).

PSME1, PSME2 and *PSME4* were significantly upregulated during our 3-day observation, while *PSME3* was significantly downregulated. Previous studies have suggested that IFN-γ-inducible PSME1 and PSME2 are components of the immunoproteasomes that play a crucial role in the generation of antigenic peptides for presentation on MHC I molecules and activation of the NF-κB pathway (55, 56, 59). Thus, our findings suggest that *G. spinigerum* L3-derived antigenic peptides were generated for MHC I presentation.

The IRFs are a family of transcription factors that play essential roles in various aspects of the immune response, including immune cell development and differentiation and regulating responses to pathogens. *IRF3, IRF5* and *IRF7* are vital to IFN-I production downstream of PRRs, and *IRF9* regulates IFN-driven gene expression. Additionally, *IRF4, IRF8* and *IRF5* regulate myeloid cell development and phenotype, thereby regulating inflammatory responses. IRF release during infection enhances the expression of IFN-I genes, IFN-stimulated genes and other pro-inflammatory cytokines/chemokines (60). Webb et al, reported that during *S. mansoni* infection, the parasite eggs stimulate plasmacytoid dendritic cells (pDCs) to potently induce IFN-I signalling, thereby driving Th2-type immunity, which is essential against helminthic infection (61). Acute *S. mansoni* infection and the upregulation of IFN-I enhance DCs, which activate T cell function (39, 61). *IRF7* upregulation was noted in the lymphoid tissue, and largely pDC activation (60). In the infection of lymphoid tissues, the majority of *IRF7* is expressed in pDC. Therefore, the *IRF7* upregulation observed in the present study suggests that increased IFN-I drives Th2-type immunity, leading to T cell activation against *G. spinigerum* L3 infection.

The leukocyte immunoglobulin-like receptors (LILRs) are in a family of immunoregulatory receptors comprising inhibitory (*LILRB 1–5*) and activating receptors (*LILRA 1–6*, excluding *LILRA 3*) (62, 63). (*LILRs* are expressed by haematopoietic cells, including monocytes, macrophages, dendritic cells, granulocytes, NK cells, T cells and B cells and non-immune cells such as endothelial cells and neurons (63). The inhibitory receptors contain an immunoreceptor tyrosine-based inhibitory motif, while the activating receptors couple with an immunoreceptor tyrosine-based activating motif ITAM)-bearing FcεRI-γ (62). *LILRs* also modulate TLR signalling and functions. Thus, *LILRs* can modulate a broad set of immune functions, including immune cell function, cytokine release, antibody production, and antigen presentation. Additionally, LILRs in neutrophils activate and suppress antimicrobial responses. However, several human pathogens take advantage of these inhibitory receptors for immune evasion. In this study, downregulation of activating receptors, *LILAR1* and *LIAR6*, may contribute to *G. spinigerum* L3 evasion from host immune response.

Fc receptors for IgG (FcγRs) are broadly expressed by haematopoietic cells and consist of one inhibitory and several activating receptors that differ in their affinity and specificity for immunoglobulin subclasses (64). Our earlier study suggested that the level of FcγRI (CD 64) expression on monocytes was depleted by *G. spinigerum* L3 ESPs, leading to impaired phagocytic function (30). This agreed with our finding of the downregulation of *FCGR1*, which codes for FcγRI, during the first 24 hours of the co-culture of *G. spinigerum* L3 with PBMCs. FcγRI is an activating receptor with a high affinity for IgG and is expressed on monocytic DCs and monocytes/macrophages. The cross-linking of FcγRI (also called CD64) and antigen-antibody complex initiates signal transduction cascades for phagocytosis, cytokine production and antibody-dependent cell-mediated cytotoxicity (ADCC) (65). ADCC is dependent on eosinophils, neutrophils, macrophages or platelets as effector cells and IgE, IgG or IgA as antibodies. It also immobilises nematode larval stages as they migrate through the gut mucosa (66). In the present study, *FCGR1* downregulation suggests that the larvae modulate host immunity by impairing monocyte capacity and ADCC mechanisms. However, our findings suggest less efficiency in disrupting *G. spinigerum* L3 migration in human gnathostomiasis. Furthermore, *in vitro* co-culture of *H. polygyrus* larvae and bone marrow (BM)-derived macrophages found that the larval immobilisation was largely independent of CD11b and, instead, required the activating IgG receptor FcγRI. FcγRI signalling also contributed to the upregulation of macrophage Arg1 expression. IgG2a/c was the major IgG subtype in early immune sera bound by FcγRI on the macrophage surface (66). In addition, purified IgG2c and Arg1 expressed by macrophages elicited larval immobilisation (67).

Killer cell immunoglobulin-like receptors (*KIRs*) are expressed on NK cells and subsets of $CD8^+$ T cells. KIRs inhibit the ability of cytotoxic cells to lyse cells with self-expressed MHC I alleles and are key regulators of the development, tolerance and activation of NK cells. KIR2DL4, composed of two Ig domains and long cytoplasmic tail 4, is a unique long-tailed activating KIR, and KIR2DL4 is only expressed on CD56 high NK cells. *KIR2DL4* expression results in a more potent activator of cytokine production rather than cytotoxicity and is associated with the ITAM-bearing FcεRI-γ adaptor and LILRs. There are multiple similarities between KIRs and LILRs in terms of Ig domain-based structure, gene location and the ability to recognise MHC I (68). The present study revealed that *KIR2DL4* was upregulated, while the inhibitor receptor KIR2DL1, composed of two Ig domains and long cytoplasmic tail 1, was downregulated. KIR inhibitory receptors recognise self-MHC I molecules on target cells and consequently activate signalling pathways to prevent the cytolytic function of NK cells (68). However, KIRs that recognise the same MHC I molecule are usually not expressed by the same NK cell. Our observation of up- and downregulation to both inhibit and activate KIR balance

suggests the modulation of NK cell capacity in natural infections of *G. spinigerum* L3. Moreover, our recent study in PBMCs exposed to ES from *G. spinigerum* L3 during the 7-day observation revealed low amounts of ES modulated NK cells by decreasing *IFNG* mRNA expression and IFN-γ production, and upregulating the expression of *NKG2A* and *NKG2D* encoded for C type killer cell lectin-like receptor (KLR), inhibitory receptor (NKG2A), and activating receptor (NKG2D). KLRs require some adaptors to initiate signalling transduction and cellular activation in NK cell cytotoxicity (43). Consistently, mice infected with *Echinococcus multilocularis* (*E. multilocularis*) larvae showed decreased NK cell frequencies and increased NKG2A expression on NK cells. These changes in NK cells during alveolar echinococcosis resulted in low cytotoxic activity through decreased IFN-γ secretion (69).

In the current study, *CD3E*, which controls cell surface proteins, was upregulated. CD3E proteins form the T cell receptor-CD3 complex, which plays an important role in coupling antigen recognition to several intracellular signal transduction pathways. It is also essential for T cell development (70). We found that *CD1C* and *CD46* were downregulated. Earlier studies suggested that CD1C molecules survey for lipid antigens throughout the endocytic system (71, 72). *CD46* codes for the complement regulatory protein C46. This is a cofactor of the CD3 T cell receptor, which is a receptor for complement components C3b and C4b. CD46 interferes with the inactivation and cleavage of C3b and C4b *via* serum factor I. CD46 protects the host cell from damage by complement *via* membrane-binding proteins and opsonisation (73). Therefore, the downregulated *CD46* expression observed in this study suggests that host tissue damage occurs due to complement activation. A previous study showed that helminth lipids, such as schistosome phosphatidylserine (PS), are also implicated in immune modulation. The schistosome PS induces DCs to polarise IL-4-/IL-10-producing T cells (74). It appears consistently that these expressions of gene-controlled cell surface proteins in this study may promote antigen recognition and T cell development.

The complement system is an effective host defence against initial infection by opsonisation, killing pathogenic organisms and recruiting inflammatory cells. The system is composed of three pathways of complement activation: the classical pathway, mannose-binding lectin pathway and alternative pathway (AP). Among the three pathways, the AP accounts for most of the complement activation. Complement factor B (FB), coded by *CFB*, is a major protease of the AP and circulates in the blood as a single-chain polypeptide. Upon activation of the AP pathway, FB is cleaved by complement factor D (FD), yielding the noncatalytic chain Ba and the catalytic subunit Bb. The active subunit Bb is a serine protease that associates with C3b to form the AP C3 convertase and proceed to the next step of parasite killing (75). Bb is involved in the proliferation of pre-activated B lymphocytes, while Ba inhibits their proliferation. *CFB* is localised in the MHC III region on chromosome 6 (76). In the present study, *CFB* was upregulated on day 1 after culture, while *CFD*, which codes for FD, was downregulated. These observations may be due to the low efficiency of FB cleavage, leading to impaired activation of the AP on day 1. Our finding agrees with a previous study. TsPmy is a paramyosin secreted by *Trichinella spiralis* (*T. spiralis*) on the surface of larvae and adult worms. Only P2 peptide of 9 peptides covering TsPmy241-280aa could interact with complement components C1q and C8/C9 to compromise their activation and functions. The binding of P2 peptide to C1q significantly inhibited both C1q-initiated complement classical activation and C1q-induced macrophage chemotaxis. This finding contributes to the ability of *T. spiralis* to evade host immunity (77).

Caspases are a class of cysteinyl proteases that play key roles in programmed cell death and inflammation. The human caspase gene family contains 11 members that are classified into three groups. Group 1 (*CASP1, CASP4* and *CASP5*) comprises enzymes involved in inflammation regulation. Group 2 (*CASP2, CASP3* and *CASP7*) and group 3 (*CASP6, CASP8, CASP9* and *CASP10*) comprise caspases that regulate apoptosis. Caspases play a central role in the execution phase of cell apoptosis. CASP8 is essential for death receptor-induced apoptosis (78) and initiates the extrinsic pathway, while CASP9 initiates the intrinsic apoptosis pathway, which is activated by dimerization induced when the activation and recruitment domain (CARD) of CASP9 binds to the adapter protein apoptotic protease-activating factor-1 (79). Active CASP9 then initiates apoptosis by cleaving and thereby activating executioner caspases. In this study, the initiator caspase (*CASP8*) and the executioner caspase (*CASP3*) were upregulated, while *CASP2* and *CARD9* were downregulated on day 1 after culture. These findings suggest that *G. spinigerum* L3-induced apoptosis of PBMCs occurs *via* extrinsic rather than intrinsic pathways. Supporting this, our previous study reported that *G. spinigerum* L3 ESPs also induced apoptosis of PBMC *via* the extrinsic pathway during a 48 hour-observation (80). Early apoptosis in ESP-induced PBMC was noted within 90 min post-exposure, and the greatest effects were found at 18-24 h. The regulatory genes involved in the apoptotic processes were expressed, including several caspases, especially *CASP3, CASP8*, and *CASP9*. In addition, the expression of 7 genes associated with extrinsic apoptotic pathways were increased, including *DAPL1, FADD, FAS, TNFRSF9, TNFSF8*, and *XIAP* (80). Similarly, *Paragonimus westermani* ESP products induced CASP3-mediated apoptosis of human eosinophils (81).

ILs are cytokines produced by leukocytes and several other body cells. They regulate cell growth, differentiation and motility and are particularly important in stimulating immune responses like inflammation (82). In this study, most genes that controlled pro-inflammatory cytokines, such as *IL-6, IL-12, IL-17, IL-22* and *IL-36*, were upregulated on day 1 after culture. In sepsis, the upregulation of these ILs probably activated or modulated the activity of various immune cells, such as IL-12-enhanced Th1 differentiation, NK cell activation, and classical macrophage (M1) activation. IL-17 prevents parasite evasion, IL-6 modifies regulatory T cells (Tregs), IL-22 is involved in parasite expulsion and IL-36 regulates keratinocytes in wound healing (82). In contrast, IL-18 was downregulated on day 3 after culture. IL-18 stimulation is mediated by IL-18 receptors. The binding of IL-18 to these receptors relays signals from myeloid differentiation primary response protein 88, a primary adapter protein for many TLR and IL-1R family members. IL-12 or IL-2 enhance the effect of IL-18 in immune cell activation. Together with IL-12, IL-18 promotes IFN-γ production from Th1 and B cells. Meanwhile, IL-18 alone is

sufficient to induce the production of IFN-γ by NK cells. IL-18 not only induces Th1 cytokine production but also activates the humoral immune response *via* Th2 cytokine production (82, 83). Therefore, IL-18 downregulation may interfere with the complex interplay between cytokines related to IL-18 in the host cell-mediated or humoral immune response.

In schistosomiasis, biomolecules secreted by skin-penetrating cercariae, migrating schistosomulae, larval and adult worms, and their eggs, modulate both innate and adaptive immune responses. The overall interactions include the down- or up-regulated cytokines that activate or inhibit inflammation, and switches between the Th1 and Th2 immune response. Once infected with skin-penetrating cercariae, the initial response (for about 6 weeks) within infected tissues and plasma is characterised by type-1 inflammation, which is driven by IL-1, IL-12, TNF-α and IFN-γ. Subsequently, chronic schistosomiasis is developed mainly by the Th2 response to soluble antigens secreted by the eggs, and is driven by IL-4, IL-5, IL-10, and IL-13. IL-10 is an important element in disease progression by inducing inflammation through down-regulation of the Th1 response, while also preventing severe disease during the Th2 response (36).

In the present study, genes related to the nervous system were upregulated. *PSEN1* encodes the protein presenilin 1, which is described as the proteolytic subunit of γ-secretase (84). The γ-secretase complex is involved in processing amyloid precursor protein (APP). APP is manufactured in the brain and other tissues and is involved in the formation of neurons in the brain both before and after birth as well as in normal immune system function. β-amyloid (Aβ) is derived from β-APP through sequential cleavage by β- and γ-secretases. One of the most critical pathological features of Alzheimer disease is the accumulation of Aβ peptides that form extracellular senile plaques in the brain (84). In this study, the upregulated *PSEN1* may contribute to damage or degeneration during parasite migration in nerve tissues. However, further in-depth studies are required.

Table 2 summarises gene expression in human PBMCs against L3 on day 3 of culture. The expression of several genes is related to immunity. E2s play a role in Ub size by twisting and attaching Ub to cellular proteins. Humans have approximately 40 E2s that are involved in Ub or Ub-like protein transfer (51). In the present study, most of the genes encoding E2s, including *UBE2A*, *UBE2E1*, *UBE2F*, *UBE2V2* and *UBE2L3*, were significantly upregulated on day 3 of culture. This suggests that the attachment of Ub to cellular protein may be increased. The expression of *UB* genes on both days 1 and 3 resulted in the movement of important proteins in the cells. On day 1 of culture, Ub was involved in the synthesis of new proteins for host defence, such as TLRs. Additionally, defective proteins are destroyed by ubiquitination.

On day 3 of culture, *PSME1* was upregulated, while *PSME3* was downregulated. Only PSME3 can promote NF-κB activity (56). Therefore, NF-κB activation may decline on day 3. Although Ub-related genes were highly upregulated, the expression level of *PSMEs* was low. The imbalance between the expression of *UB* and *PSME* genes may result in impaired protein degradation. In contrast to *PSME* expression on day 1 after culture, the lack of IFN-γ-inducible PSME2 may lead to incompletely formed immunoproteasomes. Additionally, hyperactivation of *IRF3* (85) was downregulated, leading to low expression of type I IFNs. These findings on day 3 possibly induced the decrease in MHC I antigenic peptide generation, which may lead to increased susceptibility to *G. spinigerum* L3 infection.

LILRB3 and *LILRB4* were predominantly upregulated, and *LILRA1* was downregulated. The function of these ligands is unknown. The LILRB subfamily is considered immune checkpoint receptors that are crucial for maintaining self-tolerance and modulating the length and magnitude of physiological immune responses in peripheral tissues (86, 87). Lu et al, demonstrated that LILRB4 inhibited TNF-α release *via* FcγRI signalling and also inhibited inflammatory cytokine production (87). *CASP1*, which plays a major role in cytokine maturation (88), was downregulated. These findings support the modulation of cytokine involvement on day 3 of culture. Cytokines are important components of the immune system. They modulate the balance between humoral and cell-mediated immunity. Furthermore, they regulate the maturation, growth and responsiveness of immune cell populations. *BLNK*, which controls B cell development and B cell linker protein (89), was upregulated on day 3 of culture.

On day 3 after culture, *IL-4R*, *IL-10* and *IL-24* expression of cytokines was upregulated. Several studies have suggested that Th2 function is activated by IL-4, IL-24 and IL-1β (82). B cell differentiation and IgE production are activated by IL-4 and IL-10 (82). Furthermore, IL-10 production promotes the downregulation of Th1 cells, NK cells and macrophages and suppresses Th1/Th17 during helminthic infection (90). Additionally, IL-4 expression enhances MHC II expression. In contrast, the downregulation of *IL1B* observed on day 3 probably results in IL-25 and IL-33 suppression, supporting chronic helminthic infection. Moreover, IL-5 acts as an eosinophil chemoattractant factor. For example, in early infection, *S. mansoni* eggs induce IL-5 function in recruiting eosinophils to the site of antigen deposition (91, 92).

The TNF-encoding genes *TNFSF15*, *TNFAIP3* and *TNFRSF1B* were downregulated on day 3 after culture. TNF is used by the immune system for cell signalling and can induce fever, apoptotic cell death and inflammation (90). TNF-α functions through the regulation of IL-4 and IL-13 receptor expression, and it was reported to regulate Th2 cytokine responses that have protective immunity against *Trichuris muris* and *T. spiralis* infections (90). In the present study, the downregulation of *TNF* on day 3 of culture may be immunomodulation caused by the parasite, enabling survival in host cells.

Complement activation was predominant on day 3. *C2*, *C1s*, *C1QB* and *C1QC* were upregulated. Consequently, the elimination of the invading parasites may occur through the formation of a membrane attack complex *via* the classical pathway and promoting inflammatory reactions on the parasite's surface. It has also been reported that several parasites secrete calreticulin, a Ca^{2+}-binding chaperone protein. This protein mainly resides in the endoplasmic reticulum but is also found in other cellular compartments, including the plasma membrane. Some studies have demonstrated that calreticulin from helminth infections, such as *T. spiralis* (93),

Necator americanus (94) and *E. multilocularis* (95), bind to C1q to interfere with the activation of the classical complement pathway. This phenomenon is one of the immune evasion strategies of these helminths, but there is no report of this in human gnathostomiasis. The present study found that genes related to the AP were downregulated on day 1. This suggests that the efficiency of the AP to kill parasites was decreased. Thus, our findings assumed that the classical complement pathway played a dominant role in the immune response during our 3-day observation.

On day 3 after culture, we found that genes regulating wound healing, particularly *PROS1*, which encodes protein S, were upregulated. Protein S is important for controlling blood clotting and a cofactor for activated protein C, which helps to prevent coagulation and stimulates fibrinolysis in the wound healing process (96). In contrast, the knockdown of *PROS1* in human glioma cells (LN18) caused the activation of both extrinsic and intrinsic apoptotic pathways and the inhibition of migration and invasion. This finding contributes to an important role in the development of glioblastoma multiforme, which is an aggressive brain tumour with poor prognosis (97). This knowledge may explain that up-regulated *PROS1* expression in the present study supports the migration and invasion of *G. spinigerum* L3

CD28 and *CD81* were upregulated on day 3 of culture. CD81 is a tetraspanin protein, which is a type of protein consistently found within exosomes. CD81 has been identified as a marker for EVs and exosomes (98, 99). It is widely expressed on immune cells, such as B cells, T cells, NK cells, monocytes and eosinophils. Some studies have suggested that *CD81* shows the highest expression levels on GC B cells. On B cells, CD81 exists in a complex with CD19, CD21 and Leu13. CD81 plays a role in segregating the CD19/CD21–BCR complexes to lipid rafts to activate signal transduction. It is also involved in antigen presentation, T cell signalling, activation, motility and adhesion (100) and BCR signalling, B cell development and lymphocyte proliferation (101).

The expression of CD28 on T cells provides co-stimulatory signals required for T cell activation and survival (102). Furthermore, *CD28*−/− mice consistently showed increased susceptibility to *S. mansoni* infection by impaired Th2 response and also had reduced levels of immunoglobulin secretion (103).

Our findings revealed the downregulation of *CD93* and *CD300A*. CD93 is a receptor implicated in cell adhesion and cytoskeletal organisation and is expressed on developing B cells in the BM and on plasma cells but not on naive B cells, B cells in GCs and memory B cells (104). CD93 contributes to the long life of BM plasma cells (105). CD93 is also strongly expressed in platelets, megakaryocytes, endothelial cells, NK cells and monocytes. It is a C1q receptor of phagocytosis involving apoptotic bodies but does not bind directly to C1q (106). CD93 plays a role in cell adhesion, proliferation and migration, as well as in the regulation of inflammatory responses. Under inflammatory conditions, CD93 is proteolytically cleaved from the cell surface of myeloid cells and, as a soluble protein, is involved in opsonising apoptotic cells for efferocytosis by mouse and human macrophages. Efferocytosis is the effective clearance of apoptotic cells by professional and nonprofessional phagocytes. The process is mechanically different from other forms of phagocytosis and involves the localisation, binding, internalisation and degradation of apoptotic cells. Furthermore, it is important for inflammation resolution and homeostasis restoration (107). In mice, CD93 plays a role in the control of innate and adaptive immunity in the CNS (108). In the present study, we supposed that phagocytosis by monocytes and macrophages and apoptosis by NK cells might decrease due to the downregulation of *CD93* expression. Similarly, the uptake of apoptotic cells was impaired in mice with deficient CD93 expression (109).

CD300a is a member of the CD300 glycoprotein receptor family of cell surface proteins found on leukocytes, including monocytes, DCs, NK cells, neutrophils, basophils and T cells. Unlike CD93, CD300a acts as an inhibitory receptor and is involved in the diverse signalling pathways of both innate and adaptive immune cells. CD300a controls processes such as cellular differentiation and viability, cytokine/chemokine secretion, phagocytosis, inflammation and chemotaxis (110). The role of the CD300a receptor during *Leishmania* infection has been reported. The parasite induces CD300a receptors on the host's phagocytic cells and antigen-presenting cells to counter the host's defence mechanisms, which eventually facilitates parasite survival. The blocking of CD300a signals in *Leishmania* antigen-activated macrophages and dendritic cells enhances the production of nitric oxide and pro-inflammatory cytokines along with MHCI/II gene expression and reduces parasitic uptake (111). The inhibition of CD300a signals in mice infected with *Leishmania* also induced antigen-experienced cells (i.e. $CD4^+CD44^+$ and $CD8^+CD44^+$ T cells) to produce more pro-inflammatory cytokines and was helpful in the early clearance of parasites from visceral organs (111).

The present study had some limitations (1): we did not confirm EVs by immunostaining with antibodies to their markers (2); we did not identify EV components and validate their roles; and (3) we did not select important genes to verify whether they correlated with the pathogenesis of human gnathostomiasis. The pathogenesis of the disease is complex, resulting from the host's immune response and the mechanisms of several larval factors to evade host attack. Further studies are strongly needed to clarify the effects of the larvae and their various biomolecules on host immunity, particularly type 1 and type 2 immunity, cytokine profiles, the network interplay of cytokines, immune cells and effector cells, and the mechanisms of the complement system and signalling pathways.

5 Conclusion

First, *G. spinigerum* L3 produce EVs and release them into the ESPs. However, the present study did not assess its components. Thus, further studies are necessary to identify the components and verify their roles in the pathogenesis and immunomodulation of human gnathostomiasis.

Second, human gene profiling of the immune response to the live larvae for 3 days revealed that the gene expression profile on day 1 of

culture appeared to involve pathogenesis, immunomodulation and evasion. This includes the upregulation of genes that play roles in pathogen recognition, proteolysis, NF-κB antigenic peptide generation for MHC I, NK cells, cytotoxic T cell activation, Treg cell activation, regulatory T cells, M1 macrophages and pro-inflammatory cytokines, some which also drive type 2 immunity. However, genes related to innate immunity, particularly NK cells, phagocytosis and complement activation, were downregulated. On day 3 after culture, the genes that regulate T cell activation and development, T cell receptors and BCRs, which drive the Th2 response, gene-regulated B cell development, antibody production, anti-inflammatory cytokines, most of the complement systems and wound healing, were upregulated. In contrast, the phagocytosis function of monocytes, eosinophils, NK cell apoptosis, M2 macrophages and Th1/Th17 were downregulated. These findings may explain the immune evasion mechanisms of the larvae and the expression of some genes involved in adaptive immunity and others related to antibody production. Additionally, the results showed that most signalling from T and B cells drives Th2 immunity related to chronic infection and its pathogenesis.

Collectively, the findings of our investigation represent current knowledge, so that further in-depth studies are necessary to clarify how *G. spinigerum* L3 modulate the human immune response and the pathogenesis of gnathostomiasis.

Data availability statement

The datasets presented in this study can be found in online repositories. The names of the repository/repositories and accession number(s) can be found below: https://www.ncbi.nlm.nih.gov/, PRJNA853915.

Ethics statement

The studies involving human participants were reviewed and approved by the Ethics Committees of the Faculty of Tropical Medicine, Mahidol University. Written informed consent for participation was not required for this study in accordance with the national legislation and the institutional requirements. The animal study was reviewed and approved by Faculty of Tropical Medicine- Animal care and use committee.

Author contributions

PP and WD were responsible for laboratory work including blood collection and culture experiments. TY collected and cultured third-stage *G. spinigerum* larvae. SB conducted RNA extraction and determined quality of RNA. PP, OR, and UB analysed the NGS data. WD worked on data analysis and statistical calculations. YM, PD, OR, and UB participated in the study design, conceived the study, and coordination. PP, WD, and YM wrote the manuscript. All authors contributed to the article and approved the submitted version.

Funding

This study was supported by a Research Grant from the Faculty of Tropical Medicine, Mahidol University, Fiscal Year 2017 for YM, and financial support from a DAAD scholarship for PP.

Acknowledgments

We thank the funders for their support. We also thank Supaporn Nuamtanong and Urusa Thaenkham for part of the collection of third-stage *G. spinigerum* larvae. We appreciate Enago Author Service (www.enago.com) for editing a draft of this manuscript and Mr. Paul R. Adams for editing the revised manuscript.

Conflict of interest

The authors declare that the research was conducted in the absence of any commercial or financial relationships that could be construed as a potential conflict of interest.

Publisher's note

Supplementary material

The Supplementary Material for this article can be found online at: https://www.frontiersin.org/articles/10.3389/fimmu.2023.1218965/full#supplementary-material

References

1. Diaz JH. Gnathostomiasis: an emerging infection of raw fish consumers in gnathostoma nematode-endemic and nonendemic countries. *J Travel Med* (2015) 22 (5):318–24. doi: 10.1111/jtm.12212

2. Liu GH, Sun MM, Elsheikha HM, Fu YT, Sugiyama H, Ando K, et al. Human gnathostomiasis: a neglected food-borne zoonosis. *Parasit Vectors*. (2020) 13(1):616. doi: 10.1186/s13071-020-04494-4

3. Moore DA, McCroddan J, Dekumyoy P, Chiodini PL. Gnathostomiasis: an emerging imported disease. *Emerg Infect Dis* (2003) 9(6):647–50. doi: 10.3201/eid0906.020625

4. Anthony RM, Rutitzky LI, Urban JFJr., Stadecker MJ, Gause WC. Protective immune mechanisms in helminth infection. *Nat Rev Immunol* (2007) 7(12):975–87. doi: 10.1038/nri2199

5. Joshi P, Mishra PKK. Functional diversity of the excretory/secretory proteins of nematode parasites. *Acta Parasitol* (2022) 67(2):619–27. doi: 10.1007/s11686-022-00523-7

6. Mulcahy G, O'Neill S, Fanning J, McCarthy E, Sekiya M. Tissue migration by parasitic helminths - an immunoevasive strategy? *Trends Parasitol* (2005) 21(6):273–7. doi: 10.1016/j.pt.2005.04.003

7. Barbosa AP, Campos DM, Semerene AR, Teixeira AR, Santana JM. Lagochilascaris minor third-stage larvae secrete metalloproteases with specificity for fibrinogen and native collagen. *Microbes Infect* (2006) 8(12-13):2725–32. doi: 10.1016/j.micinf.2006.08.001

8. Basavaraju SV, Zhan B, Kennedy MW, Liu Y, Hawdon J, Hotez PJ. Ac-FAR-1, a 20 kDa fatty acid- and retinol-binding protein secreted by adult Ancylostoma caninum hookworms: gene transcription pattern, ligand binding properties and structural characterisation. *Mol Biochem Parasitol* (2003) 126(1):63–71. doi: 10.1016/s0166-6851(02)00253-0

9. Bennuru S, Semnani R, Meng Z, Ribeiro JM, Veenstra TD, Nutman TB. Brugia malayi excreted/secreted proteins at the host/parasite interface: stage- and gender-specific proteomic profiling. *PloS Negl Trop Dis* (2009) 3(4):e410. doi: 10.1371/journal.pntd.0000410

10. Hotterbeekx A, Perneel J, Vieri MK, Colebunders R, Kumar-Singh S. The secretome of filarial nematodes and its role in host-parasite interactions and pathogenicity in onchocerciasis-associated epilepsy. *Front Cell Infect Microbiol* (2021) 11:662766. doi: 10.3389/fcimb.2021.662766

11. Doyle LM, Wang MZ. Overview of extracellular vesicles, their origin, composition, purpose, and methods for exosome isolation and analysis. *Cells* (2019) 8(7):1–24. doi: 10.3390/cells8070727

12. Buck AH, Coakley G, Simbari F, McSorley HJ, Quintana JF, Le Bihan T, et al. Exosomes secreted by nematode parasites transfer small RNAs to mammalian cells and modulate innate immunity. *Nat Commun* (2014) 5:5488. doi: 10.1038/ncomms6488

13. Drurey C, Coakley G, Maizels RM. Extracellular vesicles: new targets for vaccines against helminth parasites. *Int J Parasitol* (2020) 50(9):623–33. doi: 10.1016/j.ijpara.2020.04.011

14. Qin D. Next-generation sequencing and its clinical application. *Cancer Biol Med* (2019) 16(1):4–10. doi: 10.20892/j.issn.2095-3941.2018.0055

15. Khetsuphan T, Chaisri U, Dechkhajorn W, Benjathummarak S, Dekumyoy P, Ampawong S, et al. Effects of Gnathostoma spinigerum infective stage larva excretory-secretory products on NK cells in peripheral blood mononuclear cell culture: focused on expressions of IFN-gamma and killer cell lectin-like receptors. *Parasitol Res* (2020) 119(3):1011–21. doi: 10.1007/s00436-019-06593-3

16. Scarff CA, Fuller MJG, Thompson RF, Iadanza MG. Variations on negative stain electron microscopy methods: tools for tackling challenging systems. *J Vis Exp* (2018) (132). doi: 10.3791/57199

17. Kengkoom K, Angkhasirisap W, Kanjanapruthipong T, Tungtrakanpoung R, Tuentam K, Phansom N, et al. Streptozotocin induces alpha-2u globulin nephropathy in male rats during diabetic kidney disease. *BMC Vet Res* (2021) 17(1):105. doi: 10.1186/s12917-021-02814-z

18. Kanjanapruthipong T, Ampawong S, Thaenkham U, Tuentam K, Watthanakulpanich D. Survival of immature pre-adult Gnathostoma spinigerum in humans after treatment with albendazole. *PloS One* (2022) 17(3):e0264766. doi: 10.1371/journal.pone.0264766

19. Somthana K, Eshita Y, Kumsiri R, Dekumyoy P, Waikagul J, Kalambaheti T, et al. Roles of partially purified antigens from Gnathostoma spinigerum larvae on antibody production by human B cell culture. *Southeast Asian J Trop Med Public Health* (2011) 42(4):772–81.

20. Prasongsukarn K, Dechkhajorn W, Benjathummarak S, Maneerat Y. TRPM2, PDLIM5, BCL3, CD14, GBA genes as feasible markers for premature coronary heart disease risk. *Front Genet* (2021) 12:598296. doi: 10.3389/fgene.2021.598296

21. Bolger AM, Lohse M, Usadel B. Trimmomatic: a flexible trimmer for Illumina sequence data. *Bioinformatics* (2014) 30(15):2114–20. doi: 10.1093/bioinformatics/btu170

22. Pertea G, Pertea M. GFF utilities: GffRead and GffCompare. *F1000Res* (2020) 9:1–20. doi: 10.12688/f1000research.23297.2

23. Chai JY, Sohn WM, Na BK, Park JB, Jeoung HG, Hoang EH, et al. Larval Gnathostoma spinigerum Detected in Asian Swamp Eels, Monopterus albus, Purchased from a Local Market in Yangon, Myanmar. *Korean J Parasitol* (2015) 53 (5):619–25. doi: 10.3347/kjp.2015.53.5.619

24. Samoil V, Dagenais M, Ganapathy V, Aldridge J, Glebov A, Jardim A, et al. Vesicle-based secretion in schistosomes: Analysis of protein and microRNA (miRNA) content of exosome-like vesicles derived from Schistosoma mansoni. *Sci Rep* (2018) 8 (1):3286. doi: 10.1038/s41598-018-21587-4

25. Zhu L, Liu J, Dao J, Lu K, Li H, Gu H, et al. Molecular characterization of S. japonicum exosome-like vesicles reveals their regulatory roles in parasite-host interactions. *Sci Rep* (2016) 6:25885. doi: 10.1038/srep25885

26. Gazzinelli RT, Ropert C, Campos MA. Role of the Toll/interleukin-1 receptor signaling pathway in host resistance and pathogenesis during infection with protozoan parasites. *Immunol Rev* (2004) 201:9–25. doi: 10.1111/j.0105-2896.2004.00174.x

27. Janeway CAJr., Medzhitov R. Innate immune recognition. *Annu Rev Immunol* (2002) 20:197–216. doi: 10.1146/annurev.immunol.20.083001.084359

28. Pasare C, Medzhitov R. Toll-like receptors: linking innate and adaptive immunity. *Microbes Infect* (2004) 6(15):1382–7. doi: 10.1016/j.micinf.2004.08.018

29. Ockenhouse CF, Hu WC, Kester KE, Cummings JF, Stewart A, Heppner DG, et al. Common and divergent immune response signaling pathways discovered in peripheral blood mononuclear cell gene expression patterns in presymptomatic and clinically apparent malaria. *Infect Immun* (2006) 74(10):5561–73. doi: 10.1128/IAI.00408-06

30. Benjathummarak S, Kumsiri R, Nuamtanong S, Kalambaheti T, Waikagul J, Viseshakul N, et al. Third-stage Gnathostoma spinigerum larva excretory secretory antigens modulate function of Fc gamma receptor I-mediated monocytes in peripheral blood mononuclear cell culture. *Trop Med Health* (2016) 44:5. doi: 10.1186/s41182-016-0005-x

31. Traber KE, Dimbo EL, Shenoy AT, Symer EM, Allen E, Mizgerd JP, et al. Neutrophil-derived oncostatin M triggers diverse signaling pathways during pneumonia. *Infect Immun* (2021) 89(4):1–19. doi: 10.1128/IAI.00655-20

32. Han Z, Liu Y, Wang G, He Y, Hu S, Li Y, et al. Comparative analysis of immune responses in pigs to high and low pathogenic porcine reproductive and respiratory syndrome viruses isolated in China. *Transbound Emerg Dis* (2015) 62(5):e1–e10. doi: 10.1111/tbed.12190

33. Ateba-Ngoa U, Adegnika AA, Zinsou JF, Kassa Kassa RF, Smits H, Massinga-Loembe M, et al. Cytokine and chemokine profile of the innate and adaptive immune response of Schistosoma haematobium and Plasmodium falciparum single and co-infected school-aged children from an endemic area of Lambarene, Gabon. *Malar J* (2015) 14:94. doi: 10.1186/s12936-015-0608-4

34. Goodridge HS, Marshall FA, Else KJ, Houston KM, Egan C, Al-Riyami L, et al. Immunomodulation *via* novel use of TLR4 by the filarial nematode phosphorylcholine-containing secreted product, ES-62. *J Immunol* (2005) 174(1):284–93. doi: 10.4049/jimmunol.174.1.284

35. Dibo N, Liu X, Chang Y, Huang S, Wu X. Pattern recognition receptor signaling and innate immune responses to schistosome infection. *Front Cell Infect Microbiol* (2022) 12:1040270. doi: 10.3389/fcimb.2022.1040270

36. Masamba P, Kappo AP. Immunological and biochemical interplay between cytokines, oxidative stress and schistosomiasis. *Int J Mol Sci* (2021) 22(13):1–22. doi: 10.3390/ijms22137216

37. Reyes JL, Gonzalez MI, Ledesma-Soto Y, Satoskar AR, Terrazas LI. TLR2 mediates immunity to experimental cysticercosis. *Int J Biol Sci* (2011) 7(9):1323–33. doi: 10.7150/ijbs.7.1323

38. Hoffmann KF, Wynn TA, Dunne DW. Cytokine-mediated host responses during schistosome infections; walking the fine line between immunological control and immunopathology. *Adv Parasitol* (2002) 52:265–307. doi: 10.1016/s0065-308x(02)52014-5

39. Li J, Liu H, Jiang J, She X, Niu Y, Ming Y. The potential role of schistosome-associated factors as therapeutic modulators of the immune system. *Infect Immun* (2020) 88(8):1–13. doi: 10.1128/IAI.00754-19

40. Akira S, Uematsu S, Takeuchi O. Pathogen recognition and innate immunity. *Cell* (2006) 124(4):783–801. doi: 10.1016/j.cell.2006.02.015

41. Poltorak A, He X, Smirnova I, Liu MY, Van Huffel C, Du X, et al. Defective LPS signaling in C3H/HeJ and C57BL/10ScCr mice: mutations in Tlr4 gene. *Science* (1998) 282(5396):2085–8. doi: 10.1126/science.282.5396.2085

42. Gijzen K, Cambi A, Torensma R, Figdor CG. C-type lectins on dendritic cells and their interaction with pathogen-derived and endogenous glycoconjugates. *Curr Protein Pept Sci* (2006) 7(4):283–94. doi: 10.2174/138920306778018016

43. Scur M, Parsons BD, Dey S, Makrigiannis AP. The diverse roles of C-type lectin-like receptors in immunity. *Front Immunol* (2023) 14:1126043. doi: 10.3389/fimmu.2023.1126043

44. Batliner J, Mancarelli MM, Jenal M, Reddy VA, Fey MF, Torbett BE, et al. CLEC5A (MDL-1) is a novel PU.1 transcriptional target during myeloid differentiation. *Mol Immunol* (2011) 48(4):714–9. doi: 10.1016/j.molimm.2010.10.016

45. Sung PS, Hsieh SL. CLEC2 and CLEC5A: pathogenic host factors in acute viral infections. *Front Immunol* (2019) 10:2867. doi: 10.3389/fimmu.2019.02867

46. Chen ST, Li FJ, Hsu TY, Liang SM, Yeh YC, Liao WY, et al. CLEC5A is a critical receptor in innate immunity against Listeria infection. *Nat Commun* (2017) 8(1):299. doi: 10.1038/s41467-017-00356-3

47. Kawai T, Akira S. The roles of TLRs, RLRs and NLRs in pathogen recognition. *Int Immunol* (2009) 21(4):317–37. doi: 10.1093/intimm/dxp017

48. Hayden MS, Ghosh S. NF-kappaB in immunobiology. *Cell Res* (2011) 21 (2):223–44. doi: 10.1038/cr.2011.13

49. Li F, Li XL, Chen SJ, Tan C, Mei SP, Jia HG, et al. Excretory/secretory proteins of adult Toxocara canis induce changes in the expression of proteins involved in the NOD1-RIP2-NF-kappaB pathway and modulate cytokine production in mouse macrophages. *Exp Parasitol* (2021) 229:108152. doi: 10.1016/j.exppara.2021.108152

50. Kimura Y, Tanaka K. Regulatory mechanisms involved in the control of ubiquitin homeostasis. *J Biochem* (2010) 147(6):793–8. doi: 10.1093/jb/mvq044

51. Reyes-Turcu FE, Ventii KH, Wilkinson KD. Regulation and cellular roles of ubiquitin-specific deubiquitinating enzymes. *Annu Rev Biochem* (2009) 78:363–97. doi: 10.1146/annurev.biochem.78.082307.091526

52. Li W, Bengtson MH, Ulbrich A, Matsuda A, Reddy VA, Orth A, et al. Genome-wide and functional annotation of human E3 ubiquitin ligases identifies MULAN, a mitochondrial E3 that regulates the organelle's dynamics and signaling. *PloS One* (2008) 3(1):e1487. doi: 10.1371/journal.pone.0001487

53. Mukhopadhyay D, Riezman H. Proteasome-independent functions of ubiquitin in endocytosis and signaling. *Science* (2007) 315(5809):201–5. doi: 10.1126/science.1127085

54. Liu X, Wang Q, Chen W, Wang C. Dynamic regulation of innate immunity by ubiquitin and ubiquitin-like proteins. *Cytokine Growth Factor Rev* (2013) 24(6):559–70. doi: 10.1016/j.cytogfr.2013.07.002

55. Tanaka K. The proteasome: overview of structure and functions. *Proc Jpn Acad Ser B Phys Biol Sci* (2009) 85(1):12–36. doi: 10.2183/pjab.85.12

56. Wang J, Maldonado MA. The ubiquitin-proteasome system and its role in inflammatory and autoimmune diseases. *Cell Mol Immunol* (2006) 3(4):255–61.

57. Zhang H, Liu J, Ying Z, Li S, Wu Y, Liu Q. Toxoplasma gondii UBL-UBA shuttle proteins contribute to the degradation of ubiquitinylated proteins and are important for synchronous cell division and virulence. *FASEB J* (2020) 34(10):13711–25. doi: 10.1096/fj.202000759RR

58. Cwiklinski K, Robinson MW, Donnelly S, Dalton JP. Complementary transcriptomic and proteomic analyses reveal the cellular and molecular processes that drive growth and development of Fasciola hepatica in the host liver. *BMC Genomics* (2021) 22(1):46. doi: 10.1186/s12864-020-07326-y

59. Qureshi N, Morrison DC, Reis J. Proteasome protease mediated regulation of cytokine induction and inflammation. *Biochim Biophys Acta* (2012) 1823(11):2087–93. doi: 10.1016/j.bbamcr.2012.06.016

60. Zarrin AA, Monteiro RC. Editorial: the role of inhibitory receptors in inflammation and cancer. *Front Immunol* (2020) 11:633686. doi: 10.3389/fimmu.2020.633686

61. Webb LM, Phythian-Adams AT, Costain AH, Brown SL, Lundie RJ, Forde-Thomas J, et al. Plasmacytoid Dendritic Cells Facilitate Th Cell Cytokine Responses throughout Schistosoma mansoni Infection. *Immunohorizons* (2021) 5(8):721–32. doi: 10.4049/immunohorizons.2100071

62. Dushek O, Goyette J, van der Merwe PA. Non-catalytic tyrosine-phosphorylated receptors. *Immunol Rev* (2012) 250(1):258–76. doi: 10.1111/imr.12008

63. Veillette A, Latour S, Davidson D. Negative regulation of immunoreceptor signaling. *Annu Rev Immunol* (2002) 20:669–707. doi: 10.1146/annurev.immunol.20.081501.130710

64. Harrison PT, Davis W, Norman JC, Hockaday AR, Allen JM. Binding of monomeric immunoglobulin G triggers Fc gamma RI-mediated endocytosis. *J Biol Chem* (1994) 269(39):24396–402. doi: 10.1016/S0021-9258(19)51097-3

65. Nimmerjahn F, Ravetch JV. Fcgamma receptors as regulators of immune responses. *Nat Rev Immunol* (2008) 8(1):34–47. doi: 10.1038/nri2206

66. Esser-von Bieren J, Volpe B, Kulagin M, Sutherland DB, Guiet R, Seitz A, et al. Antibody-mediated trapping of helminth larvae requires CD11b and Fcgamma receptor I. *J Immunol* (2015) 194(3):1154–63. doi: 10.4049/jimmunol.1401645

67. Esser-von Bieren J, Mosconi I, Guiet R, Piersgilli A, Volpe B, Chen F, et al. Antibodies trap tissue migrating helminth larvae and prevent tissue damage by driving IL-4Ralpha-independent alternative differentiation of macrophages. *PloS Pathog* (2013) 9(11):e1003771. doi: 10.1371/journal.ppat.1003771

68. Campbell KS, Purdy AK. Structure/function of human killer cell immunoglobulin-like receptors: lessons from polymorphisms, evolution, crystal structures and mutations. *Immunology* (2011) 132(3):315–25. doi: 10.1111/j.1365-2567.2010.03398.x

69. Abulizi A, Shao Y, Aji T, Li Z, Zhang C, Aini A, et al. Echinococcus multilocularis inoculation induces NK cell functional decrease through high expression of NKG2A in C57BL/6 mice. *BMC Infect Dis* (2019) 19(1):792. doi: 10.1186/s12879-019-4417-1

70. Shah K, Al-Haidari A, Sun J, Kazi JU. T cell receptor (TCR) signaling in health and disease. *Signal Transduct Target Ther* (2021) 6(1):412. doi: 10.1038/s41392-021-00823-w

71. Heger L, Hofer TP, Bigley V, de Vries IJM, Dalod M, Dudziak D, et al. Subsets of CD1c(+) DCs: dendritic cell versus monocyte lineage. *Front Immunol* (2020) 11:559166. doi: 10.3389/fimmu.2020.559166

72. Sugita M, van der Wel N, Rogers RA, Peters PJ, Brenner MB. CD1c molecules broadly survey the endocytic system. *Proc Natl Acad Sci U S A.* (2000) 97(15):8445–50. doi: 10.1073/pnas.150236797

73. Riley-Vargas RC, Gill DB, Kemper C, Liszewski MK, Atkinson JP. CD46: expanding beyond complement regulation. *Trends Immunol* (2004) 25(9):496–503. doi: 10.1016/j.it.2004.07.004

74. van der Kleij D, Latz E, Brouwers JF, Kruize YC, Schmitz M, Kurt-Jones EA, et al. A novel host-parasite lipid cross-talk. Schistosomal lyso-phosphatidylserine activates toll-like receptor 2 and affects immune polarization. *J Biol Chem* (2002) 277 (50):48122–9. doi: 10.1074/jbc.M206941200

75. Abbas AK, Lichtman AH, Pillai S. *Cellular and Molecular Immunology. 6th, editor*. in Philadelphia: Elsevier Saunders (2010).

76. Sultan EY, Rizk DE, Kenawy HI, Hassan R. A small fragment of factor B as a potential inhibitor of complement alternative pathway activity. *Immunobiology* (2021) 226(4):152106. doi: 10.1016/j.imbio.2021.152106

77. Wang Z, Hao C, Huang J, Zhuang Q, Zhan B, Zhu X. Mapping of the complement C1q binding site on Trichinella spiralis paramyosin. *Parasit Vectors.* (2018) 11(1):666. doi: 10.1186/s13071-018-3258-x

78. Varfolomeev EE, Schuchmann M, Luria V, Chiannilkulchai N, Beckmann JS, Mett IL, et al. Targeted disruption of the mouse Caspase 8 gene ablates cell death induction by the TNF receptors, Fas/Apo1, and DR3 and is lethal prenatally. *Immunity* (1998) 9(2):267–76. doi: 10.1016/s1074-7613(00)80609-3

79. Shiozaki EN, Chai J, Shi Y. Oligomerization and activation of caspase-9, induced by Apaf-1 CARD. *Proc Natl Acad Sci U S A.* (2002) 99(7):4197–202. doi: 10.1073/pnas.072544399

80. Viseshakul N, Dechkhajorn W, Benjathummarak S, Nuamtanong S, Maneerat Y. Excretory-secretory product of third-stage Gnathostoma spinigerum larvae induces apoptosis in human peripheral blood mononuclear cells. *Parasitol Res* (2017) 116 (10):2783–94. doi: 10.1007/s00436-017-5589-5

81. Min DY, Lee YA, Ryu JS, Ahn MH, Chung YB, Sim S, et al. Caspase-3-mediated apoptosis of human eosinophils by the tissue-invading helminth Paragonimus westermani. *Int Arch Allergy Immunol* (2004) 133(4):357–64. doi: 10.1159/000077355

82. Justiz Vaillant AA, Qurie A. *Interleukin*. Treasure Island (FL: StatPearls (2023).

83. Dinarello CA, Fantuzzi G. Interleukin-18 and host defense against infection. *J Infect Dis* (2003) 187 Suppl 2:S370–84. doi: 10.1086/374751

84. Zhang X, Li Y, Xu H, Zhang YW. The gamma-secretase complex: from structure to function. *Front Cell Neurosci* (2014) 8:427. doi: 10.3389/fncel.2014.00427

85. Jefferies CA. Regulating IRFs in IFN driven disease. *Front Immunol* (2019) 10:325. doi: 10.3389/fimmu.2019.00325

86. Lewis Marffy AL, McCarthy AJ. Leukocyte immunoglobulin-like receptors (LILRs) on human neutrophils: modulators of infection and immunity. *Front Immunol* (2020) 11:857. doi: 10.3389/fimmu.2020.00857

87. Lu HK, Rentero C, Raftery MJ, Borges L, Bryant K, Tedla N. Leukocyte Ig-like receptor B4 (LILRB4) is a potent inhibitor of FcgammaRI-mediated monocyte activation *via* dephosphorylation of multiple kinases. *J Biol Chem* (2009) 284 (50):34839–48. doi: 10.1074/jbc.M109.035683

88. Van Opdenbosch N, Lamkanfi M. Caspases in cell death, inflammation, and disease. *Immunity* (2019) 50(6):1352–64. doi: 10.1016/j.immuni.2019.05.020

89. Tsukada S, Baba Y, Watanabe D. Btk and BLNK in B cell development. *Adv Immunol* (2001) 77:123–62. doi: 10.1016/s0065-2776(01)77016-2

90. Redpath SA, Fonseca NM, Perona-Wright G. Protection and pathology during parasite infection: IL-10 strikes the balance. *Parasite Immunol* (2014) 36(6):233–52. doi: 10.1111/pim.12113

91. Costain AH, Phythian-Adams AT, Colombo SAP, Marley AK, Owusu C, Cook PC, et al. Dynamics of host immune response development during schistosoma mansoni infection. *Front Immunol* (2022) 13:906338. doi: 10.3389/fimmu.2022.906338

92. Sabin EA, Kopf MA, Pearce EJ. Schistosoma mansoni egg-induced early IL-4 production is dependent upon IL-5 and eosinophils. *J Exp Med* (1996) 184(5):1871–8. doi: 10.1084/jem.184.5.1871

93. Shao S, Hao C, Zhan B, Zhuang Q, Zhao L, Chen Y, et al. Trichinella spiralis calreticulin S-domain binds to human complement C1q to interfere with C1q-mediated immune functions. *Front Immunol* (2020) 11:572326. doi: 10.3389/fimmu.2020.572326

94. Kasper G, Brown A, Eberl M, Vallar L, Kieffer N, Berry C, et al. A calreticulin-like molecule from the human hookworm Necator americanus interacts with C1q and the cytoplasmic signalling domains of some integrins. *Parasite Immunol* (2001) 23 (3):141–52. doi: 10.1046/j.1365-3024.2001.00366.x

95. Xian S, Chen L, Yan Y, Chen J, Yu G, Shao Y, et al. Echinococcus multilocularis calreticulin interferes with C1q-mediated complement activation. *Trop Med Infect Dis* (2023) 8(1):1–12. doi: 10.3390/tropicalmed8010047

96. Heeb MJ. Role of the PROS1 gene in thrombosis: lessons and controversies. *Expert Rev Hematol* (2008) 1(1):9–12. doi: 10.1586/17474086.1.1.9

97. Che Mat MF, Abdul Murad NA, Ibrahim K, Mohd Mokhtar N, Wan Ngah WZ, Harun R, et al. Silencing of PROS1 induces apoptosis and inhibits migration and

invasion of glioblastoma multiforme cells. *Int J Oncol* (2016) 49(6):2359–66. doi: 10.3892/ijo.2016.3755

98. Kowal J, Arras G, Colombo M, Jouve M, Morath JP, Primdal-Bengtson B, et al. Proteomic comparison defines novel markers to characterize heterogeneous populations of extracellular vesicle subtypes. *Proc Natl Acad Sci U S A.* (2016) 113 (8):E968–77. doi: 10.1073/pnas.1521230113

99. Norouzi M, Pirestani M, Arefian E, Dalimi A, Sadraei J, Mirjalali H. Exosomes secreted by Blastocystis subtypes affect the expression of proinflammatory and anti-inflammatory cytokines (TNFalpha, IL-6, IL-10, IL-4). *Front Med (Lausanne).* (2022) 9:940332. doi: 10.3389/fmed.2022.940332

100. Luo RF, Zhao S, Tibshirani R, Myklebust JH, Sanyal M, Fernandez R, et al. CD81 protein is expressed at high levels in normal germinal center B cells and in subtypes of human lymphomas. *Hum Pathol* (2010) 41(2):271–80. doi: 10.1016/j.humpath.2009.07.022

101. Hemler ME. Tetraspanin functions and associated microdomains. *Nat Rev Mol Cell Biol* (2005) 6(10):801–11. doi: 10.1038/nrm1736

102. Slavik JM, Hutchcroft JE, Bierer BE. CD28/CTLA-4 and CD80/CD86 families: signaling and function. *Immunol Res* (1999) 19(1):1–24. doi: 10.1007/BF02786473

103. King CL, Xianli J, June CH, Abe R, Lee KP. CD28-deficient mice generate an impaired Th2 response to Schistosoma mansoni infection. *Eur J Immunol* (1996) 26 (10):2448–55. doi: 10.1002/eji.1830261027

104. Greenlee MC, Sullivan SA, Bohlson SS. CD93 and related family members: their role in innate immunity. *Curr Drug Targets.* (2008) 9(2):130–8. doi: 10.2174/138945008783502421

105. Chevrier S, Genton C, Kallies A, Karnowski A, Otten LA, Malissen B, et al. CD93 is required for maintenance of antibody secretion and persistence of plasma cells in the bone marrow niche. *Proc Natl Acad Sci U S A.* (2009) 106(10):3895–900. doi: 10.1073/pnas.0809736106

106. Bohlson SS, O'Conner SD, Hulsebus HJ, Ho MM, Fraser DA. Complement, c1q, and c1q-related molecules regulate macrophage polarization. *Front Immunol* (2014) 5:402. doi: 10.3389/fimmu.2014.00402

107. Boada-Romero E, Martinez J, Heckmann BL, Green DR. The clearance of dead cells by efferocytosis. *Nat Rev Mol Cell Biol* (2020) 21(7):398–414. doi: 10.1038/s41580-020-0232-1

108. Griffiths MR, Botto M, Morgan BP, Neal JW, Gasque P. CD93 regulates central nervous system inflammation in two mouse models of autoimmune encephalomyelitis. *Immunology* (2018) 155(3):346–55. doi: 10.1111/imm.12974

109. Norsworthy PJ, Fossati-Jimack L, Cortes-Hernandez J, Taylor PR, Bygrave AE, Thompson RD, et al. Murine CD93 (C1qRp) contributes to the removal of apoptotic cells in *vivo* but is not required for C1q-mediated enhancement of phagocytosis. *J Immunol* (2004) 172(6):3406–14. doi: 10.4049/jimmunol.172.6.3406

110. Cao Y, Ao T, Wang X, Wei W, Fan J, Tian X. CD300a and CD300f molecules regulate the function of leukocytes. *Int Immunopharmacol.* (2021) 93:107373. doi: 10.1016/j.intimp.2021.107373

111. Singh R, Anand A, Rawat AK, Saini S, Mahapatra B, Singh NK, et al. CD300a receptor blocking enhances early clearance of leishmania donovani from its mammalian host through modulation of effector functions of phagocytic and antigen experienced T cells. *Front Immunol* (2021) 12:793611. doi: 10.3389/fimmu.2021.793611

frontiers | Frontiers in Immunology

TYPE Original Research
PUBLISHED 05 October 2023
DOI 10.3389/fimmu.2023.1272221

OPEN ACCESS

EDITED BY
Xiang Wu,
Central South University, China

REVIEWED BY
Fangli Lu,
Sun Yat-sen University, China
Perle Latre de Late,
University of Missouri, United States

*CORRESPONDENCE
Yasuhiro Suzuki
yasu.suzuki@uky.edu

RECEIVED 03 August 2023
ACCEPTED 18 September 2023
PUBLISHED 05 October 2023

CITATION
Mani R, Abdelaziz MH, Ochiai E, Sa Q, Fox BA, Bzik DJ and Suzuki Y (2023) Dense granule protein 3 of *Toxoplasma gondii* plays a crucial role in the capability of the tissue cysts of the parasite to persist in the presence of anti-cyst CD8$^+$ T cells during the chronic stage of infection. *Front. Immunol.* 14:1272221. doi: 10.3389/fimmu.2023.1272221

Dense granule protein 3 of *Toxoplasma gondii* plays a crucial role in the capability of the tissue cysts of the parasite to persist in the presence of anti-cyst CD8$^+$ T cells during the chronic stage of infection

Rajesh Mani[1], Mohamed H. Abdelaziz[1], Eri Ochiai[1], Qila Sa[1], Barbara A. Fox[2], David J. Bzik[2] and Yasuhiro Suzuki[1*]

[1]Department of Microbiology, Immunology and Molecular Genetics, University of Kentucky College of Medicine, Lexington, KY, United States, [2]Deaprtment of Microbiology and Immunology, Geisel School of Medicine at Dartmouth, Lebanon, NH, United States

Toxoplasma gondii establishes chronic infection by forming tissue cysts, and this chronic infection is one of the most common parasitic infections in humans. Our recent studies revealed that whereas CD8$^+$ T cells of genetically resistant BALB/c mice have the capability to remove the tissue cysts of the parasite through their perforin-mediated activities, small portions of the cysts are capable of persisting in the presence of the anti-cyst CD8$^+$ T cells. It is currently unknown how those small portions of the cysts resist or escape the T-cell immunity and persist in the hosts. In the present study, we discovered that the cysts, which persisted in the presence of the perforin-mediated CD8$^+$ T-cell immunity, have significantly greater mRNA levels for four dense granule proteins, GRA1, GRA2, GRA3, and GRA7, and one rhoptry protein, ROP35, than the total population of the cysts present in the absence of the T cells. In addition, increased levels of mRNA for GRA1, GRA3, and ROP35 in the cysts significantly correlated with their successful persistence through the condition in which greater degrees of reduction of the cyst burden occurred through anti-cyst CD8$^+$ T cells. In addition, GRA3-deficient *T. gondii* displayed significantly enhanced elimination of the cysts by anti-cyst CD8$^+$ T cells when compared to the wild-type parasite. These results indicate that GRA3 is a key molecule that mediates in the capability of *T. gondii* cysts to persist by resisting or evading the anti-cyst activity of CD8$^+$ T cells during the later stage of infection.

KEYWORDS

***Toxoplasma gondii*, cyst, dense granule protein, rhoptry protein, immune evasion**

Introduction

Toxoplasma gondii is an obligate intracellular protozoan parasite capable of establishing a persisting chronic infection. This chronic infection is widespread in humans worldwide, with one-third of the population being estimated to be infected (1). During the acute stage of the infection, IFN-γ-mediated protective immunity controls the proliferation of tachyzoites (the acute stage form of the parasite) (2). However, a part of the tachyzoites differentiates into tissue cysts in various organs, especially in the brain, and establishes chronic infection. Since individuals chronically infected with *T. gondii* usually remain seropositive for this parasite for decades or possibly life, it was generally considered that the immune system is unable to recognize or target the cyst stage of this parasite. However, our recent studies uncovered that $CD8^+$ T cells have the capability to remove *T. gondii* cysts through a perforin-mediated mechanism from the brains of chronically infected BALB/c mice (3–5), which are genetically resistant to the infection (6, 7). However, even in the presence of the anti-cyst T-cell immunity, small numbers of cysts still persist in the infected hosts. It is currently unknown how these *T. gondii* cysts are able to avoid their elimination by the $CD8^+$ T cell-mediated protective immunity. Since there is currently no drug available to target the cyst stage of *T. gondii*, it is crucial to elucidate the mechanisms by which *T. gondii* cysts persist in the presence of the anti-cyst protective immunity and generate the basis for developing a method that disrupts the persisting mechanism(s) of the cysts for their eradication.

The rhoptry and the dense granules are two major secretory organelles of *T. gondii*, which are critical for the pathogenesis of this parasite. The rhoptry proteins (ROPs) are secreted to assist the invasion of tachyzoites into host cells (8). Dense granule proteins (GRAs) are secreted after their invasion into host cells and support the formation of the parasitophorous vacuoles (PV), in which the parasite resides and proliferates within infected cells. When the intracellular tachyzoites transform to bradyzoites for developing tissue cysts, the PV transforms to the cyst wall (9). Since the bradyzoites maintain expressions of GRA and ROP proteins (9, 10), and since some of GRA and ROP proteins have been shown to disrupt the effector mechanisms of IFN-γ-mediated protective immunity against tachyzoites (11–13), it would be possible that certain GRA and/or ROP proteins mediate the evasion of *T. gondii* cysts from the perforin-mediated anti-cyst $CD8^+$ T-cell immunity.

In the present study, we examined mRNA expression levels for eight GRAs (GRA1–GRA8) and five ROPs (ROP5, ROP16, ROP17, ROP18, and ROP35) in *T. gondii* cysts that persisted in the presence of anti-cyst $CD8^+$ T cells. We found that mRNA levels for GRA1, GRA2, GRA3, GRA7, and ROP35 are significantly greater in *T. gondii* cysts that persisted in the presence of the perforin-mediated anti-cyst $CD8^+$ T cells than a total population of cysts that persisted in the absence of those T cells. We further identified that tissue cysts of the GRA3-deficient mutant strain of *T. gondii* have a significantly increased susceptibility to anti-cyst activity of $CD8^+$ T cells and display enhanced removal by the T cells. Thus, the present study revealed that GRA3 plays a crucial role in the capability of *T. gondii* cysts to persist by resisting or evading the anti-cyst activity of $CD8^+$ T cells in chronically infected hosts.

Materials and methods

Mice

BALB/c-background SCID, which lack T cells, and RAG1-knockout ($RAG1^{-/-}$) mice, which lack both T and B cells, and wild-type (WT) BALB/c mice were from the Jackson Laboratory (Bar Harbor, ME). BALB/c-background perforin-deficient ($Prf1^{-/-}$) mice (14) were originally provided by John T. Harty (University of Iowa) and bred in our animal facility. Female mice were used for all studies. SCID or $RAG1^{-/-}$ mice were used as recipients of $CD8^+$ T cells from WT or $Prf1^{-/-}$ BALB/c mice. There were three to five mice in each experimental group. Mouse care and experimental procedures were performed under specific pathogen-free conditions in accordance with established institutional guidance and approved protocols from the Institutional Animal Care and Use Committee.

T. gondii strains

The ME49 strain of *T. gondii* was maintained by infecting Swiss-Webster mice intraperitoneally with 10 cysts obtained from the brains of chronically infected mice of this strain (3–5). The WT and GRA3-deficient (ΔGRA3) Prugniaud (Pru) strains of the parasite were maintained as tachyzoites in their cultures with monolayers of human foreskin fibroblasts in DMEM medium (Gibco/Thermo Fisher Scientific, Waltham, MA) containing 10% fetal bovine serum (Gibco). Both the ME49 and Pru strains belong to the genotype II of *T. gondii*.

Infection of mice with *T. gondii*

Mice were infected with 10 cysts (for T-cell donors) or 20 cysts (for T-cell recipients) of the ME 49 strain of *T. gondii* orally by gavage. SCID and $RAG1^{-/-}$ mice were treated with sulfadiazine (Sigma-Aldrich, St. Louis, MO) in the drinking water (400 mg/L) beginning at 9 days after infection for the entire periods of the experiments to control proliferation of tachyzoites and establish a chronic infection (5, 15). The $Prf1^{-/-}$ mice received sulfadiazine in the same manner beginning at 26 days after infection. In a part of the experiments, SCID mice were infected intraperitoneally with 2×10^3 tachyzoite of the WT or ΔGRA3 Pru strains (16) and treated with sulfadiazine in the drinking water beginning at 7 days after infection to establish chronic infection, and sulfadiazine dose was increased to 1 g/L in drinking water from 13 days after infection to maintain the chronic stage of the infection.

Purification and transfer of $CD8^+$ T cells

Spleen cells were obtained from WT and $Prf1^{-/-}$ mice chronically infected with the ME49 strain and suspended in Hanks' balanced salt solution (Hyclone, Logan, UT) with 2% fetal bovine serum (Sigma). $CD8^+$ immune T cells were purified from the spleen cells using MACS with microbeads-conjugated anti-mouse CD8 (53-6.7) monoclonal antibody (Miltenyi Biotec, Auburn, CA)

(5, 17). As a control, $CD8^+$ normal T cells were purified from the spleens of uninfected WT mice in the same manner. Infected SCID and $RAG1^{-/-}$ mice received the purified $CD8^+$ T cells ($2.1–3.5 \times 10^6$ cells) intravenously from a tail vein at 3 weeks after infection (5).

Quantification of cyst numbers in the brain

At 1 day before (Day −1) or 7 days after (Day 7) the transfer of $CD8^+$ normal or immune T cells, half of each brain of infected SCID and $RAG1^{-/-}$ mice was triturated with a mortar and pestle in 0.5 mL of PBS (3, 5), and the number of cysts in at least three aliquots (20 µl each) of each brain suspension was counted microscopically.

Quantification of amount of mRNA for selected *T. gondii* molecules

RNA was purified from half of each brain of infected SCID and $RAG1^{-/-}$ mice obtained at Day −1 or Day 7 of the $CD8^+$ T-cell transfer, and the amount of mRNA for 13 secretory molecules (GRA1–8, ROP5, ROP16–18, and ROP35), bradyzoite antigen 1 (BAG1), and bradyzoite-specific surface antigen 2C (SAG2C) was measured by reverse transcription real-time PCR (RT-PCR) using the StepOne Plus real-time PCR system with TaqMan reagents (Allied Biosystems, Norwalk, CT) (5, 15). BAG1 was used as a molecule constitutively expressed only in the bradyzoites stage of *T. gondii*, and its mRNA levels were used to indicate the cyst burden in the brains of infected mice. SAG2C is a bradyzoite-specific molecule expressed on the surface of the bradyzoites and used as a control molecule for comparison with the secretory GRA and ROP molecules. In infection with the WT Pru and ΔGRA3 strains of *T. gondii*, mRNA levels for GRA3 were also measured to confirm the absence of GRA3 mRNA in the brains of mice infected with the ΔGRA3 strain. Sequences of the primers and probe for each of these *T. gondii* molecules are described in Table 1. Relative expression levels of GRA1–8, ROP5, ROP16–18, ROP35, and SAG2C in the cysts were calculated as ratios of their mRNA levels to BAG1 mRNA levels. The mRNA levels for mouse CD8β and Prf1 were also measured using ready-made primer and probes from Applied Biosystems.

Statistical analysis

Levels of difference between experimental groups were determined by one-way ANOVA with Tukey's multiple comparison test or Mann–Whitney test (GraphPad Prism software, version 9.3.1). Levels of significance in correlations between the degree of increased expression levels of selected GRA and ROP molecules and the successful persistence of *T. gondii* cysts through the condition in which greater portions of cysts from their total populations are eliminated were determined by Pearson test (GraphPad Prism software). The correlations that provided $p < 0.05$ were considered significant.

Results

T. gondii cysts that persisted in the presence of $CD8^+$ immune T cells have increased mRNA levels for five selected GRA and ROP proteins

SCID mice lacking T cells were infected with *T. gondii* and treated with sulfadiazine to establish and maintain the tissue cysts of

TABLE 1 Sequences of the primers and probes employed in quantitative real-time RT-PCR for the *T. gondii* molecules examined.

Gene	Forward Primer 5'→ 3'	Reverse Primer 5'→ 3'	Probe 5'→ 3'BAG1
BAG1	TCACGTGGAGACCCAGAGT	CTGGCAAGTCAGCCAAAATAATCAT	TTTGCTGTCGAACTCC
SAG2c	CGCACAGTCATTCAACCAAAAAGTT	TGGAGGTGACCGCTACAGT	TTGTGTCGTTCAGATAAATG
GRA1	ACAGGCAACCCGGACTTG	GACTTCGCTGTACGATCCATCT	ATCGCCATTAAAACTTC
GRA2	GCCAAAGAAGCAGCTGGAA	CTCCACATTCGCGAGTTTCTTG	ACGGTCACCATGCCCC
GRA3	GAGTCGGATAAGGTGGACAATCAG	CAACTCCTCTTCGACCTTCTTCAT	ACGCTCACCTCCCTCC
GRA4	CAGCCTCTTCGCACACAAG	GGGAGGAGGAGCTGCTG	ACGGCCACCTATTATC
GRA5	AAAGTGAAGACCGATCGTTATTCGA	CTGCAGTCCTCACTGGATGTC	CCGCTGCTCTTCCCCT
GRA6	CCGCGCTGGCGAATG	GCCCTGTTCTTCGATTCTTTCCT	CCTCCGACTTCCCC
GRA7	CACGAGACGAAAGGGTGGTT	GCCGCTGTTCTCGACAAAGA	CCTGGCAGCATCACGT
GRA8	CATGCCACAGCCAGAGGTT	CTGGAGTACCCACTGGATATGGA	CCGCCACTTCAGCATC
ROP5	ACTATGGGTGCCGAGAATTCC	GCCGCAAAAGTCGCTTCAT	CAACCGCTCCAGCTCT
ROP16	GAAGAGGGTCTGGAAGAAGTTCAG	GTCCGGAACCGCTACGA	CTGCCGCACAGCTT
ROP17	GCGGCTTTGGTCTTGTGTAC	CCTCATTGTTCATCACCCGTTGA	CCACAGGGCAACCAT
ROP18	TGGCTGTTAAGGTTTTCATGTCAGA	CCTCTGCAAGTCACGCATAGTC	ATCGGTGGGCTCCTTT
ROP35	CACACCTCGTCCAAGTTTCCA	CTTCGCCCCTCTTGTTTCTTG	CCGGACATGTTTCCTG

the parasite in their brains (3–5). At 3 weeks after infection, one mouse group received a systemic transfer of $CD8^+$ immune T cells (3.5×10^6 cells) purified from the spleens of WT mice chronically infected with the parasite. Another group of mice received $CD8^+$ normal T cells from uninfected WT mice as a control in the same manner. Two additional groups of infected SCID mice did not receive any T cells as another control, and cyst numbers and mRNA levels for bradyzoite (cyst)-specific BAG1 in their brains were measured at 1 day before (Day −1) and 7 days after (Day 7) the T-cell transfer. The cyst burden and BAG1 mRNA levels in the brains of the recipients of the $CD8^+$ T cells were measured at Day 7. We also performed an independent experiment using $RAG1^{-/-}$ mice that lack both T and B cells as the recipients of the $CD8^+$ T cells (3.2×10^6 cells) from infected and uninfected control WT mice in the same manner.

Cyst numbers in the control group without any T-cell transfer did not differ between Day −1 and Day 7, indicating that their cyst numbers were stable during this time period in the absence of T cells (Figure 1A, the data from both SCID and $RAG1^{-/-}$ mice are combined). In contrast, the number of cysts in the recipients of the $CD8^+$ immune T cells was 21 times less than that in the control mice with no T-cell transfer at Day 7 ($p < 0.001$) (Figure 1A). Consistently, cerebral mRNA levels for BAG1 in the $CD8^+$ immune T-cell recipients were 27 times less than the control mice with no T-cell transfer at Day 7 ($p < 0.001$) (Figure 1B, the data from both SCID and $RAG1^{-/-}$ mice are combined). In contrast, both cyst numbers and BAG1 mRNA levels in the brains of the mice that had received the normal T cells did not differ from those of the control mice without any T-cell transfer (Figures 1A, B). Thus, $CD8^+$ immune T cells eliminated a majority (95%) of *T. gondii* cysts from the brains of the recipients within 7 days after the transfer of T cells. In other words, a small population (5%) of cysts had successfully persisted despite the presence of the anti-cyst T-cell immunity that had eliminated a majority (95%) of the cysts.

We also examined whether cerebral BAG1 mRNA levels directly correlate with *T. gondii* cysts numbers in the brains of these mice. In this analysis, we applied the BAG1 mRNA level and cyst number of each mouse in all of the experimental groups at Day 7 described above. The BAG1 mRNA levels strongly correlated with the cyst numbers ($p = 0.0018$, Figure 1C), indicating that cerebral BAG1 mRNA levels are an effective indicator for cyst burdens in the brains of these mice with and without the transfer of $CD8^+$ normal and immune T cells.

We next address a possibility that the small portion (5%) of the cysts, which successfully persisted in the presence of $CD8^+$ immune T cells, have a unique molecular expression profile when compared to the total cyst population that persisted in the absence of those T cells in the control group. *T. gondii* has two major groups of secretory proteins, ROPs and GRAs. The ROPs are secreted during an invasion of the parasite into host cells (8), whereas GRAs are secreted after the parasite invaded into host cells to assist the formation of the PV and the cyst wall (9). We examined whether relative mRNA expression levels for eight GRAs (GRA1–8) and five ROPs (ROP5, ROP16–18, and ROP35) differ between the total population of cysts, which existed in the absence of T cells in the control mice, and the small portion of the cysts that successfully persisted for 7 days in the presence of the $CD8^+$ immune T cells. Among GRA proteins, GRA1–8 were chosen since they are not only secretory proteins but also known to be present in the cysts and/or the cyst wall detected in the brains of infected mice (18) and their absence often disrupts the cyst wall integrity and/or number of cysts in infected mice (16, 19, 20). Regarding ROP proteins, ROP5, ROP17, ROP18, and ROP35 were chosen, since the absence of any of these molecules results in marked decreases in the number of cysts in infected mice (21). ROP16 was used as a control for the other four ROPs, since a deletion of this molecule rather increases the number of cysts in the brains of infected mice (21). SAG2C was used as a control molecule that is not a secretory protein and expressed on the surface of the bradyzoites present within the cysts (22).

We calculated the relative expression levels of the mRNA levels for each of the eight GRAs, five ROPs, and the control molecule, SAG2C, in the ratios to BAG1 mRNA levels. Since BAG1 mRNA levels indicate cerebral cyst burden in infected mice as shown in Figures 1A–C, the relative expression levels of mRNA for the GRAs and ROPs in ratios to BAG1 mRNA levels indicate relative expression levels of these secretory molecules in the cysts present in the brains of these mice.

The relative expression levels of the control molecule, SAG2C, to BAG1 mRNA levels did not differ between the total population of the cysts present in the absence of T cells and the small portion of the cysts that successfully persisted in the presence of the $CD8^+$ immune T cells in both SCID and $RAG1^{-/-}$ mice (Figure 1D). In contrast, relative expression levels of mRNA for four GRAs (GRA1, GRA2, GRA3, and GRA7) and one ROP (ROP35) consistently showed significantly greater mRNA levels in the cysts that successfully persisted in the presence of the $CD8^+$ immune T cells than the cysts that persisted in the absence of any T cells in both SCID and $RAG1^{-/-}$ mice ($p < 0.05$, $p < 0.01$, $p < 0.001$, or $p < 0.0001$, Figures 1E–I). In contrast, the relative mRNA expression levels for these five secretory molecules in the cysts that persisted in the recipients of $CD8^+$ normal T cells from uninfected mice did not differ from the cysts present in the control mice that did not receive T cells in both SCID and $RAG1^{-/-}$ mice (Figures 1E–I). The transfer of the normal T cells did not induce significant reduction of cyst numbers and BAG1 mRNA levels as described earlier (Figures 1A, B). These results indicate that the elimination of a majority of *T. gondii* cysts by anti-cyst activity of $CD8^+$ immune T cells resulted in a selection of the cysts that express significantly increased mRNA levels for at least the five selected secretory molecules, GRA1, GRA2, GRA3, GRA7, and ROP35, suggesting that these GRA and ROP proteins could mediate in the capability of *T. gondii* cysts to persist in the presence of anti-cyst $CD8^+$ T-cell immunity.

Perforin-mediated activity of $CD8^+$ immune T cells is required for the selection of a particular population of *T. gondii* cysts that have increased mRNA expression levels for the five selected GRA and ROP proteins

We previously demonstrated that perforin is required for the activity of $CD8^+$ immune T cells to remove *T. gondii* cysts from the

10.3389/fimmu.2023.1272221

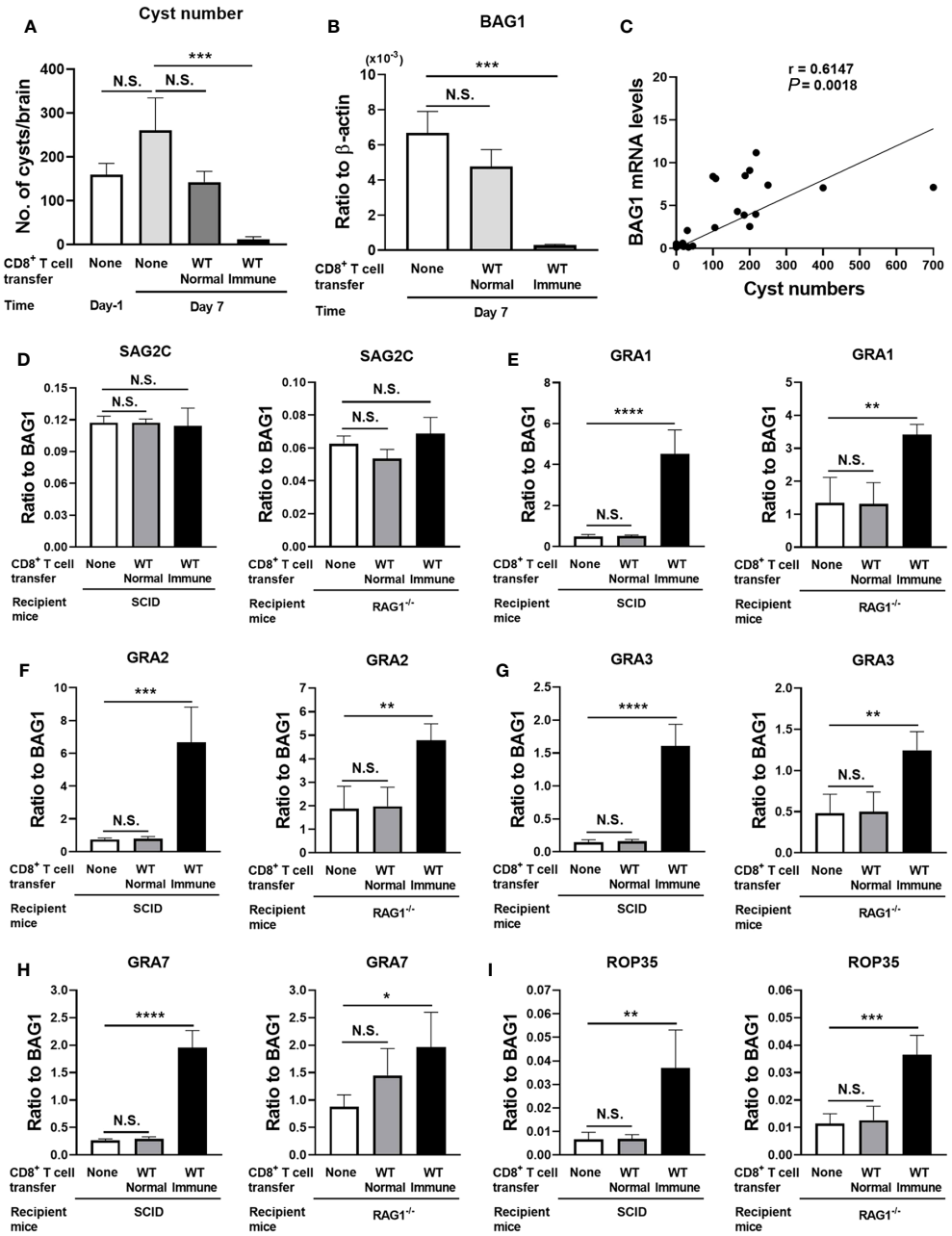

FIGURE 1
T. gondii cysts that persisted in the presence of $CD8^+$ immune T cells express increased levels of mRNA for five selected GRA and ROP molecules (GRA1, 2, 3, and 7 and ROP35) when compared to the cysts that existed in the absence of the T cells. SCID mice were infected orally with 20 cysts of the ME49 strain and treated with sulfadiazine in drinking water (400 mg/L) beginning at 9 days after infection for the entire period of the experiment. At 3 weeks after the infection, $CD8^+$ immune T cells (3.5×10^6 cells) purified from the spleens of infected WT mice or $CD8^+$ normal T cells from uninfected WT mice were injected intravenously from a tail vein into the SCID mice. Two additional groups of infected, sulfadiazine-treated SCID mice did not receive any T cells as a control, and their brains were collected at 1 day before (Day –1) and 7 days after the time of the T-cell transfer. The brains of the infected SCID mice that received the $CD8^+$ normal or immune T cells were collected at Day 7. Half of each of these brains was applied for cyst count, and another half was applied for RT-PCR to measure mRNA levels for bradyzoite (cyst)-specific BAG1 and SAG2C, and 13 secretory proteins (8 GRAs [GRA1–8] and 5 ROPs [ROP5, ROP16–18, and ROP35]). We performed an independent replicate study using $RAG1^{-/-}$ mice as the recipients of the $CD8^+$ normal and immune T cells in the same manner except for the number of $CD8^+$ T cells (3.2×10^6 cells) transferred in this experiment. **(A)** Cyst numbers in the brain, **(B)** cerebral mRNA levels for BAG1, and **(C)** a correlation between the cyst numbers and BAG1 mRNA levels at Day –1 and Day 7 in the control mice and the recipients of the $CD8^+$ T cells (data from both SCID and $RAG1^{-/-}$ mice are combined). Relative expression levels of mRNA for **(D)** bradyzoite-specific surface molecule (SAG2C) and **(E–I)** GRA1, GRA2, GRA3, GRA7, and ROP35 in ratios to BAG1 mRNA levels at Day 7 in the brains of SCID and $RAG1^{-/-}$ mice with and without a transfer of $CD8^+$ normal or immune T cells. There were four or five mice in each experimental group in each of the studies with SCID and $RAG1^{-/-}$ mice. Data represent the mean ± SEM. $^*p < 0.05$, $^{**}p < 0.01$, $^{***}p < 0.001$, and $^{****}p < 0.0001$. *N.S.*: Not significant.

10.3389/fimmu.2023.1272221

brains of infected mice (5, 23). Therefore, we examined whether the persistence of the cysts with upregulated expressions of mRNA for GRA1, GRA2, GRA3, GRA7, and ROP35 occur only when the immune T cells express perforin. Infected and sulfadiazine-treated SCID mice received $CD8^+$ immune T cells from chronically infected WT and $Prf1^{-/-}$ mice. As a control, an additional group of infected SCID mice did not receive any T cells.

Seven days after the T-cell transfer, BAG1 mRNA levels in the brains of the recipients of WT $CD8^+$ T cells were significantly less than those of the control mice that did not receive T cells ($p < 0.01$, Figure 2A), whereas BAG1 mRNA levels in the brains of the mice that received $Prf1^{-/-}$ $CD8^+$ T cells did not differ from those of the control mice with no T-cell transfer (Figure 2A). Their cerebral BAG1 mRNA levels significantly correlated with cyst numbers in their brains (Figure 2B), which is consistent with the results shown in Figure 1C, confirming that cerebral BAG1 mRNA levels are an effective indicator of the cyst burden in the brain of these mice as well.

We then examined mRNA expression levels for the four selected GRAs (GRA1, GRA2, GRA3, and GRA7), one ROP (ROP35), and one control molecule (SAG2C) of *T. gondii* molecules between the cysts that persisted in the presence and the absence of the perforin-mediated anti-cyst activity in $CD8^+$ immune T cells. The relative expression levels of mRNA for the control molecule, SAG2C, in ratios to BAG1 mRNA levels did not differ between the recipients of WT $CD8^+$ immune T cells and the control mice that did not receive T cells (Figure 2C). Similarly, the ratios of SAG2C mRNA levels to BAG1 mRNA levels did not differ between the recipients of the $Prf1^{-/-}$ T cells and the control mice with no T-cell transfer (Figure 2C). In contrast, the relative expression levels of mRNA levels for GRA1, GRA2, GRA3, GRA7, and ROP35 in ratios to BAG1 mRNA levels were markedly and significantly greater in the brains of the recipients of WT $CD8^+$ immune T cells than the control mice with no T-cell transfer ($p < 0.01$ for each of these GRA and ROP proteins, Figure 2D). Notably, the relative expression levels of mRNA levels for these selected GRA and ROP proteins in ratios to BAG1 mRNA levels did not differ between the recipients of $Prf1^{-/-}$ $CD8^+$ T cells and the control mice with no T-cell transfer (Figure 2D). These results together indicate that the selection of the cysts with increased mRNA expression for GRA1, GRA2, GRA3, GRA7, and ROP35 occurred when the perforin-mediated anti-cyst activity in $CD8^+$ immune T cells is present. Therefore, it would be possible that increased expression of these selected secretory molecules plays important roles in immune evasion of *T. gondii* cysts from the perforin-mediated protective activity of $CD8^+$ T cells for the successful survival of those selected population of *T. gondii* cysts.

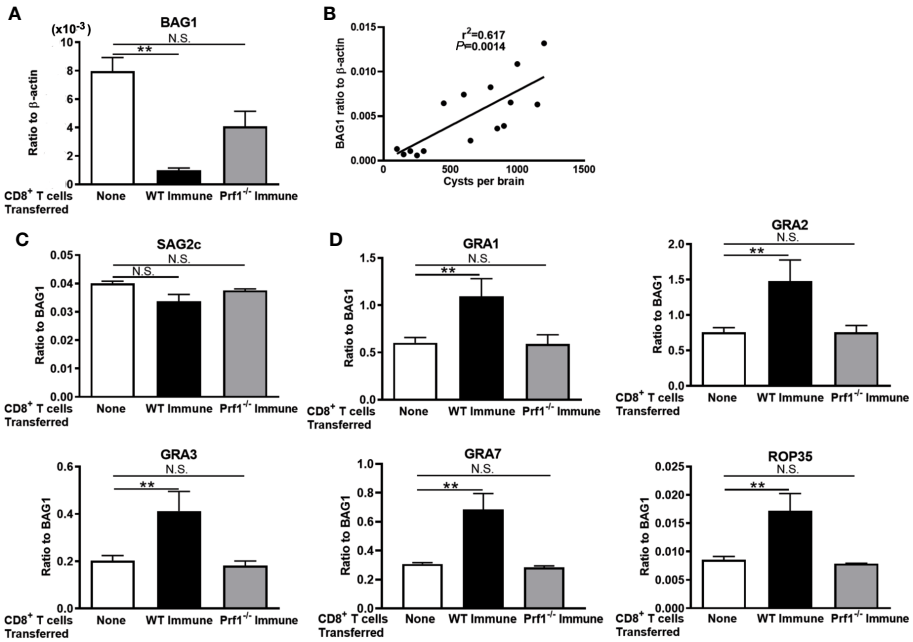

FIGURE 2
The perforin-mediated activity of $CD8^+$ T cells is required for a selection of *T. gondii* cysts that have increased mRNA levels for GRA1, GRA2, GRA3, GRA7, and ROP35 for their persistence in the presence of the T cells. SCID mice were infected orally with 20 cysts of the ME49 strain and treated with sulfadiazine in drinking water (400 mg/L) beginning at 9 days after infection for the entire period of the experiment. At 3 weeks after the infection, $CD8^+$ immune T cells (2.1×10^6 cells) purified from the spleens of infected WT or $Prf1^{-/-}$ mice were injected intravenously from a tail vein into the SCID mice. Seven days later, their brains were applied for determining **(A)** mRNA levels for BAG1 and **(B)** a correlation between the cyst numbers and BAG1 mRNA levels at Day 7. The relative expression levels of mRNA for **(C)** SAG2C and **(D)** GRA1, GRA2, GRA3, GRA7, and ROP35 in ratios to BAG1 mRNA levels were also measured. There were three or four mice in each experimental group. Data represent the mean ± SEM. $^{**}p < 0.01$. *N.S.*: Not significant.

10.3389/fimmu.2023.1272221

Greater expression levels of mRNA for GRA1, GRA3, and ROP35 in *T. gondii* cysts correlate with their successful persistence through the condition in which greater portions of cysts are eliminated from their total population by $CD8^+$ T cells

To further address the possibility that increased expressions of GRA1, GRA2, GRA3, GRA7, and ROP35 are involved in the immune evasion of *T. gondii* cysts to successfully persist in the presence of the perforin-mediated anti-cyst $CD8^+$ T-cell immunity, we examined whether the degree of increase in the relative mRNA expression levels for GRA1, GRA2, GRA3, GRA7, and ROP35 in the cysts directly correlates with their capability to successfully persist through the immune environment in which greater portions of cysts are eliminated. We applied the data from SCID and $RAG1^{-/-}$ mice that received $CD8^+$ T cells from uninfected and infected WT mice and infected $Prf1^{-/-}$ mice shown in Figures 1 and 2 in this analysis. SAG2C was included as a non-secretory control molecule whose expression level does not correlate with the capability of *T. gondii* cysts to persist in the presence of anti-cyst $CD8^+$ immune T cells.

In this analysis, the mean value of the relative mRNA levels of GRA1, GRA2, GRA3, GRA7, and ROP35 in ratios to BAG1 mRNA levels in the control mice that did not receive any T cells was used as the base value, and the fold increases in the relative expression levels of these selected secretory molecules in the cysts that had persisted in the presence of $CD8^+$ normal T cells and $CD8^+$ immune T cells from infected WT and $Prf1^{-/-}$ mice were calculated as their ratios to their base values in the control mice with no T-cell transfer. The degree of the decrease in the cyst burden was calculated as the fold decreases in cerebral BAG1 levels in the recipients of the normal T cells and immune T cells from infected WT and $Prf1^{-/-}$ mice in comparison with the mean value of BAG1 mRNA levels in the control mice with no T-cell transfer.

Greater expression levels of only GRA1, GRA3, and ROP35 in ratios to BAG1 mRNA levels significantly correlated with their persistence through the condition in which greater degrees of reduction of BAG1 mRNA levels occurred in the recipients of the $CD8^+$ T cells ($p < 0.05$ for GRA1 and GRA3, and $p < 0.001$ for ROP35, Figure 3). GRA7 also shows a tendency of the correlation (Figure 3), but the degree of the correlation did not reach significance ($p = 0.1074$, Figure 3). GRA2 did not show any trend of the correlation ($p = 0.9426$, Figure 3). The degree of increased expression of SAG2C mRNA levels did not correlate with the efficiency of cysts to persist in the presence of the T cells as expected ($p = 0.5864$, Figure 3). Thus, GRA1, GRA3, and ROP35 appear to be the most likely candidates for the *T. gondii* molecules that play important roles in the immune evasion of the cyst stage of the parasite to persist in the presence of anti-cyst $CD8^+$ immunity in infected hosts.

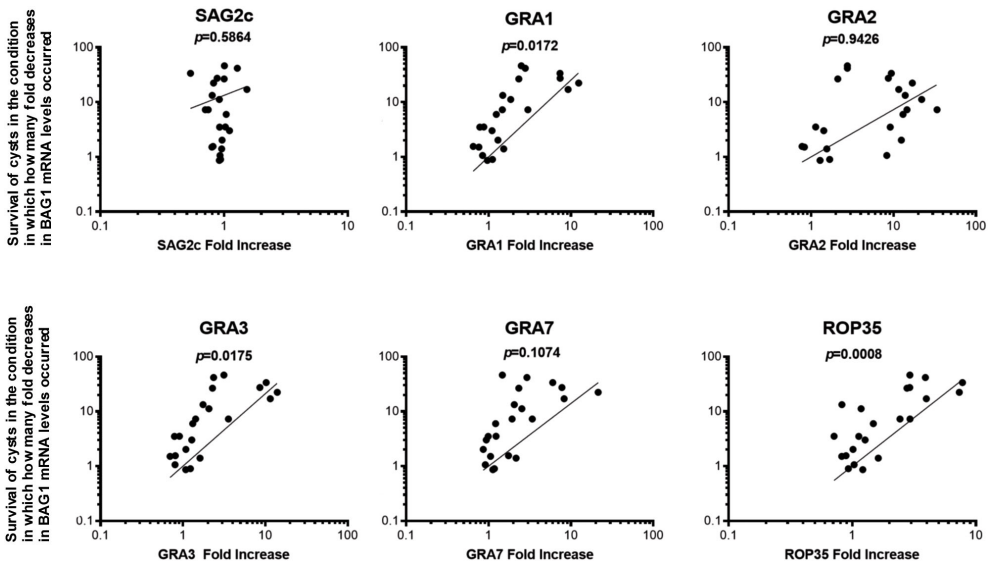

FIGURE 3
Greater expression levels of GRA1, GRA3, and ROP35 mRNA correlate with the successful persistence of *T. gondii* cysts through the condition in which greater portions of the cysts are eliminated from a total cyst populations by $CD8^+$ immune T cells. SCID and $RAG1^{-/-}$ were infected orally with 20 cysts of the ME49 strain and treated with sulfadiazine in drinking water (400 mg/L) beginning at 9 days after infection for the entire period of the experiment. At 3 weeks after the infection, $CD8^+$ normal and immune T cells (3.5 and 3.2 × 10^6 cells) purified from the spleens of normal and infected WT mice were injected intravenously from a tail vein into the SCID and $RAG1^{-/-}$ mice, respectively. In another experiment, SCID mice were infected and treated with sulfadiazine in the same manner and received a systemic transfer of $CD8^+$ immune T cells (2.1 × 10^6 cells) purified from the spleens of infected WT or $Prf1^{-/-}$ mice. The degree of increase in the mRNA expression levels for SAG2C GRA1, GRA2, GRA3, GRA7, and ROP35 in the cysts that persisted in the presence of these T cells was determined by the number of fold increases in their relative expression levels to BAG1 mRNA levels in those cysts in the recipients of $CD8^+$ T cells when compared to the cysts that persisted in the control mice that did not receive any T cells. The degrees of elimination of *T. gondii* cysts were determined by the number of fold decreases in the cyst burden (BAG1 mRNA levels) occurred in these T-cell recipients in comparison with the mean value of BAG1 mRNA levels in the control mice that did not receive any T cells.

Deficiency of GRA3 facilitates an elimination of *T. gondii* cysts by CD8$^+$ immune T cells

Among the three molecules, GRA1, GRA3, and ROP35, that showed significant correlations between the degrees of their increased expressions and increased survival rates of *T. gondii* cysts in the presence of CD8$^+$ T cells in Figure 3, GRA3 has been shown to be present in both cyst wall and the space within the cysts detected in the brains of infected mice (18, 24), and was suggested to play a structural or organizational role during cyst development or in cyst maintenance (16). Thus, we examined whether a deficiency of GRA3 ablates the capability of *T. gondii* cysts to persist in the presence of anti-cyst activity of CD8$^+$ immune T cells. Two groups of SCID mice were infected with 2×10^3 tachyzoites of the ΔGRA3 mutant strain, and two additional groups of mice were infected with the WT Pru strain in the same manner. The ΔGRA3 strain was generated from the WT Pru strain (16), which belongs to the genotype II of *T. gondii* as does the ME49 strain that was used in the studies shown in Figures 1–3. The mice received sulfadiazine treatment beginning at 7 days after infection for the entire period of the study. At 3 weeks after infection, one of the two groups of each of the WT Pru- and ΔGRA3-infected SCID mice received CD8$^+$ immune T cells (3×10^6 cells) from WT mice infected with the ME49 strain, and another group of each of the WT Pru- and ΔGRA3-infected SCID mice did not receive any T cells as a control.

The brains of the control group with no T-cell transfer in both the WT Pru- and ΔGRA3-infected SCID mice were obtained at 1 day before the T-cell transfer to indicate the cyst burden at the time of the T-cell transfer. The brains of the mice that received CD8$^+$ immune T cells were obtained at 1 week after the T-cell transfer to determine the degrees of reduction of cerebral cyst burden when compared to the time of the T-cell transfer in the control group. Equivalent BAG1 mRNA levels were detected in the brains of the control group without the T-cell transfer in the WT Pru- and ΔGRA3-infected mice (Figure 4A). One week after the CD8$^+$ immune T-cell transfer, the cerebral BAG1 mRNA levels in the ΔGRA3-infected mice were five times less than those in the control mice at the time of the T-cell transfer ($p < 0.05$, Figure 4A). In contrast, the cerebral BAG1 mRNA levels of the WT Pru-infected mice at 7 days after the CD8$^+$ T-cell transfer were slightly greater than half of those of the control mice at the time of the T-cell transfer, and the difference did not reach statistical significance ($p = 0.208$, Figure 4A). These results indicate that ΔGRA3 *T. gondii* cysts have a significantly increased susceptibility to anti-cyst activity of CD8$^+$ immune T cells for their elimination in the brain of infected mice.

To confirm the deficiency of GRA3 expression in ΔGRA3 *T. gondii* strain, we measured mRNA levels for GRA3 in the brains of SCID mice infected with the WT Pru and ΔGRA3 strains of the parasite. Large amounts of GRA3 mRNA were detected in the brains of the WT Pru-infected mice in parallel with those of BAG1 mRNA (Figure 4B). In the brains of the ΔGRA3-infected mice, GRA3 mRNA was somehow not completely absent but at the levels close to a detection limit (more than 3,500 times less than the levels detected in the WT Pru-infected mice) in the RT-PCR (Figure 4B). Even though trace amounts of GRA3 mRNA were detected in ΔGRA3 cysts, the marked reduction of the cyst burden in the ΔGRA3-infected SCID mice after receiving CD8$^+$ immune T cells indicates that GRA3 plays an important role in the capability of *T. gondii* cysts to persist in the presence of anti-cyst CD8$^+$ immune T cells.

In contrast to the notable differences in the reduction of BAG1 mRNA levels between the WT Pru- and ΔGRA3-infected SCID mice after receiving CD8$^+$ immune T cells, the mRNA levels for CD8β did not differ between these two groups of mice (Figure 4C), suggesting that the transferred CD8$^+$ immune T cells efficiently migrated into the brains of both WT Pru- and ΔGRA3-infected recipient mice in a similar manner. These results further support that GRA3 plays a critical role in the capability of *T. gondii* cysts to evade or resist anti-cyst CD8$^+$ T-cell immunity and persist in the brains of infected hosts in the presence of those T cells.

The reason for the inefficient removal of the cysts of the WT Pru strain by CD8$^+$ immune T cells in this study is unclear. One possible reason is that the CD8$^+$ immune T cells were purified from mice infected with the ME49 strain, whereas the recipient SCID mice were infected with the Pru strain. Although both the Pru and ME49 strains belong to the genotype II of *T. gondii* as mentioned earlier, there could be some variations in the amino acid sequences and structures of a part of the parasite molecules that anti-cyst CD8$^+$ T cells recognize, between these two strains of the parasite. These differences may have reduced the efficiencies of the CD8$^+$ immune T cells obtained from mice infected with the ME49 strain to eliminate the cysts of the Pru strain.

Discussion

The tissue cysts are the basis of the persistence of *T. gondii* during the chronic stage of infection. The cyst stage of the parasite is able to persist in immunocompetent hosts during the chronic stage of infection. Although CD8$^+$ T cells of infected mice have the capability to recognize the cyst-harboring cells and eliminate a majority of them through perforin-mediated mechanisms (3, 5, 23), small potions of the cysts are able to avoid their elimination by the T cells and persist in the presence of the anti-cyst T-cell immunity (3, 5, 23) through unknown mechanisms. The present study uncovered that the selected population of *T. gondii* cysts that successfully persisted in the brains of infected SCID or RAG1$^{-/-}$ mice after an adoptive transfer of perforin-sufficient CD8$^+$ immune T cells have markedly increased mRNA expression levels of five secretory proteins, GRA1, GRA2, GRA3, GRA7, and ROP35, among eight GRAs (GRA1–GRA8) and five ROPs (ROP5, ROP16–ROP18, and ROP35) tested. Notably, such increased expressions of these selected secretory proteins did not occur following a transfer of normal CD8$^+$ T cells from uninfected mice or CD8$^+$ immune T cells from infected Prf1$^{-/-}$ mice. These observations provided the novel evidence that *T. gondii* cysts that successfully persisted in the presence of the perforin-mediated anti-cyst CD8$^+$ T-cell immunity are a uniquely selected population that have notably

10.3389/fimmu.2023.1272221

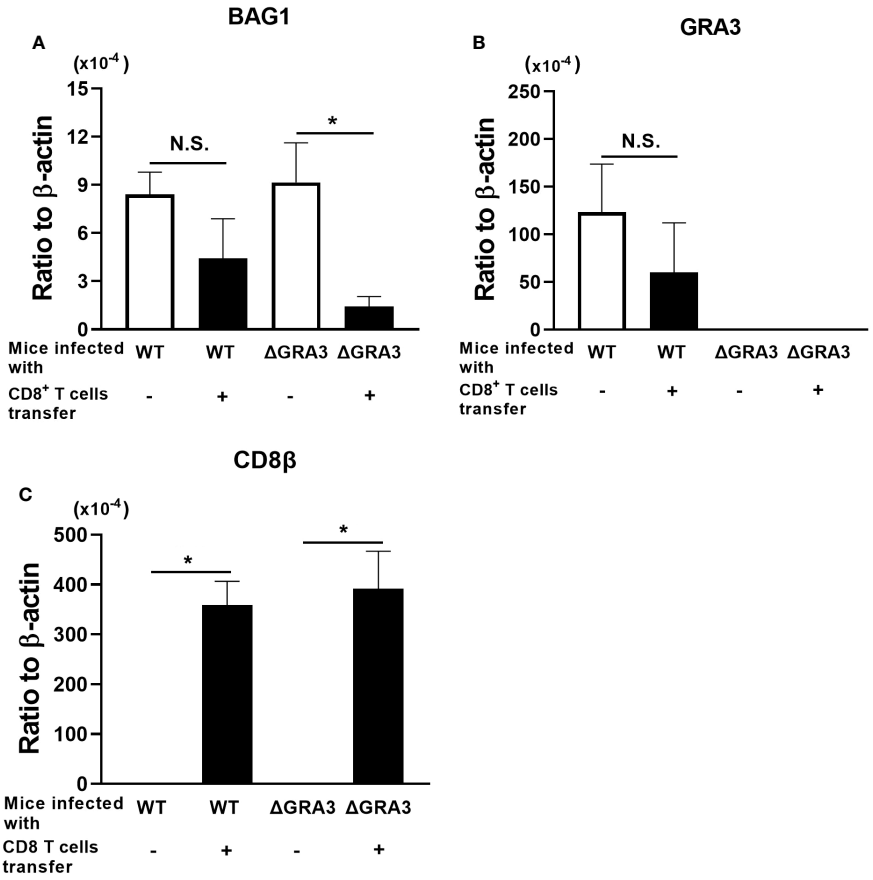

FIGURE 4
A deficiency in GRA3 in *T. gondii* facilitates an elimination of tissue cysts of the parasite by $CD8^+$ immune T cells. SCID mice were infected intraperitoneally with 2×10^3 tachyzoites of the WT Pru or ΔGRA3 strains of *T. gondii* and treated with sulfadiazine in drinking water (400 mg/L) beginning at 7 days after infection to establish chronic infection in their brains. At 3 weeks after the infection, mice received $CD8^+$ immune T cells (3×10^6 cells) purified from WT mice infected with the ME49 strain of *T. gondii*, intravenously from a tail vein. The Pru and ME49 strains both belong to the genotype II of the parasite. As a control, one group of each of the SCID mice infected with the WT Pru or ΔGRA3 strains did not receive any T cells. The mRNA levels for **(A)** BAG1 were measured in the brains of the recipients of the $CD8^+$ immune T cells at 7 days after the T-cell transfer. These mRNA levels in the brains of the control SCID mice without the T-cell transfer were measured at 1 day before the time of the T-cell transfer to demonstrate the base levels of mRNA for these molecules at the time of the T-cell transfer and to determine how much of these mRNA levels decrease in the T-cell recipients at 7 days after the T-cell transfer. The mRNA levels for **(B)** GRA3 and **(C)** CD8β were also measured in the brains of these mice. Data represent the mean ± SEM. $*p < 0.05$. *N.S.*: Not significant.

increased mRNA expressions for those selected GRA and ROP proteins when compared to the general population of cysts that exist in the absence of the protective immunity.

In contrast to the selected secretory molecules, GRA1, GRA2, GRA3, GRA7, and ROP35, whose mRNA levels are notably upregulated in the cysts that persisted in the presence of anti-cyst $CD8^+$ immune T cells, the present study also revealed that mRNA levels for the non-secretory control molecule, SAG2C, expressed on the surface of bradyzoites were not elevated in those cysts capable of persisting under the host immunity. A recent study demonstrated that a mutant strain of *T. gondii* with a deletion of the *SAG2CDYX* cluster of genes maintain significantly fewer cysts in the brains of infected mice at 4 and 9 weeks after infection (22). Since a previous study showed that *T. gondii*-infected humans do not induce IgG antibody responses to SAG2C (25), the presence of the fewer cysts in the SAG2CDYX-deletion mutant strain in infected mice may not be related to the immune evasion of *T. gondii cysts* for their persistence during the chronic stage of infection.

Among the five selected secretory proteins, GRA1, GRA2, GRA3, GRA7, and ROP35, the present study identified that the degree of increased mRNA expression levels for only GRA1, GRA3, and ROP35 in the cysts significantly correlated with their successful persistence of *T. gondii* cysts through the condition in which greater portions of cysts from their total population are eliminated by $CD8^+$ immune T cells. Notably, our study further revealed that the tissue cysts of the ΔGRA3 mutant strain of *T. gondii* have an increased susceptibility to the anti-cyst activity of $CD8^+$ immune T cells and display their accelerated elimination from the brains of infected mice by T cells. To our knowledge, *T. gondii* molecules that mediate the capability of tissue cysts to persist in the presence of the protective immunity have not been reported before.

GRA3 is present within both the PV and the cyst wall (9, 18). A recent study (16) demonstrated that a deficiency in GRA3 results in

a marked reduction of cyst numbers in the brains of infected mice, and suggested that GRA3 plays a structural or organizational role during cyst development or in cyst maintenance. Therefore, it is possible that increased levels of GRA3 enhance the integrity of the cyst wall and contribute to resisting the anti-cyst activity of $CD8^+$ T cells. Another recent study (26) using *in vitro* cultures of bone-marrow-derived macrophages and dendritic cells infected with ovalbumin (OVA)-expressing tachyzoites demonstrated that these antigen-presenting cells infected with OVA-expressing tachyzoites deficient in GRA3 stimulate OVA-specific $CD8^+$ T cells more potently than the antigen-presenting cells infected with the OVA-expressing wild-type control tachyzoites, indicating an immunosuppressive activity of GRA3 to downregulate the antigen-presenting activity of infected macrophages and dendritic cells to activate $CD8^+$ T cells. Thus, GRA3 present in *T. gondii* cysts may also play a similar pathogenic role in cyst-harboring cells to suppress their antigen presentation activity for avoiding their recognition by anti-cyst $CD8^+$ T cells. Similarly, another recent study (27) using tachyzoites demonstrated that GRA3 located in the PV interacts with the Golgi, leading to the formation of tubules and the entry of host Golgi materials into the PV and dysregulation of anterograde transport in infected cells. The Golgi network plays critical roles in antigen presentation by the major histocompatibility complex (MHC) class I molecules to stimulate $CD8^+$ T cells. Therefore, it is possible that GRA3 located in the cyst wall interacts with the Golgi in a similar manner as this molecule in the PV does and inhibits the antigen presentation by the MHC class I molecules to evade the anti-cyst activity of $CD8^+$ T cells. It is also possible that the GRA3-mediated disruption of the Golgi transport suppresses the secretion of immune molecules critical for inducing anti-cyst activity of $CD8^+$ T cells.

The results in the present study do not exclude a possible involvement of *T. gondii* molecules other than GRA3 in the immune evasion of the cysts to avoid the attack by $CD8^+$ immune T cells. GRA1, GRA2, GRA7, and ROP35 could be those candidate molecules that have a potential to be involved in the immune evasion of *T. gondii* cysts. There are currently no drugs available to target the cyst stage of *T. gondii*. One-third of the human population worldwide is estimated be chronically infected with this parasite (1) as mentioned earlier. It is well appreciated that the tissue cysts are the source of reactivation of the infection with this parasite, which causes the development of life-threatening toxoplasmic encephalitis in immunocompromised patients (1). In addition, even in immunocompetent individuals, recent epidemiological studies reported increased incidence of cancers in the individuals who are seropositive to (infected with) *T. gondii* when compared to seronegative (uninfected) people (28, 29). Therefore, it is critical to develop a method that allows us to target *T. gondii* cysts for their elimination and a cure for the chronic infection with this parasite. The evidence in the present study has the potential to provide a valuable basis to begin understanding how *T. gondii* cysts are able to persist in the presence of the anti-cyst protective T-cell immunity during the chronic stage of infection and to design a novel method for disrupting the immune evasion mechanism(s) of *T. gondii* cysts and their eradication to eliminate this widespread chronic infection.

Data availability statement

The original contributions presented in the study are included in the article/supplementary material. Further inquiries can be directed to the corresponding author.

Ethics statement

The animal study was approved by Institutional Animal Care and Use Committee of University of Kentucky. The study was conducted in accordance with the local legislation and institutional requirements.

Author contributions

YS: Conceptualization, Data curation, Formal Analysis, Funding acquisition, Investigation, Project administration, Supervision, Validation, Visualization, Writing – original draft, Writing – review & editing. RM: Formal Analysis, Investigation, Visualization, Writing – review & editing. MA: Investigation, Writing – review & editing. EO: Investigation, Writing – review & editing. QS: Investigation, Writing – review & editing. BF: Investigation, Writing – review & editing. DB: Supervision, Writing – review & editing.

Funding

The authors declare financial support was received for the research, authorship, and/or publication of this article. The studies are supported in part by NIH grants (AI095032, AI134323, AI136821, AI078756, and AI152687 to Y. S. and AI172811 to D. J. B.).

Acknowledgments

We appreciate Rancie Hannah for his technical assistance and preparing some figures.

Conflict of interest

The authors declare that the research was conducted in the absence of any commercial or financial relationships that could be construed as a potential conflict of interest.

Publisher's note

References

1. Montoya JG, Liesenfeld O. Toxoplasmosis. *Lancet* (2004) 363:1965–76. doi: 10.1016/S0140-6736(04)16412-X

2. Suzuki Y, Sa Q, Gehman M, Ochiai E. Interferon-gamma- and perforin-mediated immune responses for resistance against *Toxoplasma gondii* in the brain. *Expert Rev Mol Med* (2011) 13:e31. doi: 10.1017/S1462399411002018

3. Ochiai E, Sa Q, Perkins S, Grigg ME, Suzuki Y. $CD8^+$ T cells remove cysts of *Toxoplasma gondii* from the brain mostly by recognizing epitopes commonly expressed by or cross-reactive between type II and type III strains of the parasite. *Microbes Infect* (2016) 18:517–22. doi: 10.1016/j.micinf.2016.03.013

4. Sa Q, Ochiai E, Tiwari A, Mullins J, Shastri N, Mercier C, et al. Determination of a key antigen for immunological intervention to target the latent stage of toxoplasma gondii. *J Immunol* (2017) 198:4425–34. doi: 10.4049/jimmunol.1700062

5. Suzuki Y, Wang X, Jortner BS, Payne L, Ni Y, Michie SA, et al. Removal of *Toxoplasma gondii* cysts from the brain by perforin-mediated activity of CD8+ T cells. *Am J Pathol* (2010) 176:1607–13. doi: 10.2353/ajpath.2010.090825

6. Suzuki Y, Joh K, Orellana MA, Conley FK, Remington JS. A gene(s) within the H-2D region determines the development of toxoplasmic encephalitis in mice. *Immunology* (1991) 74:732–9.

7. Brown CR, Hunter CA, Estes RG, Beckmann E, Forman J, David C, et al. Definitive identification of a gene that confers resistance against *Toxoplasma* cyst burden and encephalitis. *Immunology* (1995) 85:419–28.

8. Ben Chaabene R, Lentini G, Soldati-Favre D. Biogenesis and discharge of the rhoptries: Key organelles for entry and hijack of host cells by the Apicomplexa. *Mol Microbiol* (2021) 115:453–65. doi: 10.1111/mmi.14674

9. Mercier C, Cesbron-Delauw MF. Toxoplasma secretory granules: one population or more? *Trends Parasitol* (2015) 31:60–71. doi: 10.1016/j.pt.2014.12.002

10. Weiss LM, Kim K. The development and biology of bradyzoites of *Toxoplasma gondii*. *Front Biosci* (2000) 5:D391–405. doi: 10.2741/Weiss

11. Virreira Winter S, Niedelman W, Jensen KD, Rosowski EE, Julien L, Spooner E, et al. Determinants of GBP recruitment to *Toxoplasma gondii* vacuoles and the parasitic factors that control it. *PLoS One* (2011) 6:e24434. doi: 10.1371/journal.pone.0024434

12. Khaminets A, Hunn JP, Konen-Waisman S, Zhao YO, Preukschat D, Coers J, et al. Coordinated loading of IRG resistance GTPases on to the *Toxoplasma gondii* parasitophorous vacuole. *Cell Microbiol* (2010) 12:939–61. doi: 10.1111/j.1462-5822.2010.01443.x

13. Fentress SJ, Behnke MS, Dunay IR, Mashayekhi M, Rommereim LM, Fox BA, et al. Phosphorylation of immunity-related GTPases by a *Toxoplasma gondii*-secreted kinase promotes macrophage survival and virulence. *Cell Host Microbe* (2010) 8:484–95. doi: 10.1016/j.chom.2010.11.005

14. White DW, MacNeil A, Busch DH, Pilip IM, Pamer EG, Harty JT. Perforin-deficient $CD8^+$ T cells: in *vivo* priming and antigen-specific immunity against *Listeria monocytogenes*. *J Immunol* (1999) 162:980–8. doi: 10.4049/jimmunol.162.2.980

15. Ochiai E, Sa Q, Brogli M, Kudo T, Wang X, Dubey JP, et al. CXCL9 is important for recruiting immune T cells into the brain and inducing an accumulation of the T cells to the areas of tachyzoite proliferation to prevent reactivation of chronic cerebral infection with *Toxoplasma gondi*i. *Am J Patol* (2015) 185:314–24. doi: 10.1016/j.ajpath.2014.10.003

16. Fox BA, Guevara RB, Rommereim LM, Falla A, Bellini V, Petre G, et al. *Toxoplasma gondii* parasitophorous vacuole membrane-associated dense granule proteins orchestrate chronic infection and GRA12 underpins resistance to host gamma interferon. *mBio* (2019) 10(4):e00589–19. doi: 10.1128/mBio.00589-19

17. Kang H, Suzuki Y. Requirement of non-T cells that produce gamma interferon for prevention of reactivation of *Toxoplasma gondii* infection in the brain. *Infect Immun* (2001) 69:2920–7. doi: 10.1128/IAI.69.5.2920-2927.2001

18. Ferguson DJ. Use of molecular and ultrastructural markers to evaluate stage conversion of *Toxoplasma gondii* in both the intermediate and definitive host. *Int J Parasitol* (2004) 34:347–60. doi: 10.1016/j.ijpara.2003.11.024

19. Fox BA, Falla A, Rommereim LM, Tomita T, Gigley JP, Mercier C, et al. Type II Toxoplasma gondii KU80 knockout strains enable functional analysis of genes required for cyst development and latent infection. *Eukaryot Cell* (2011) 10:1193–206. doi: 10.1128/EC.00297-10

20. Guevara RB, Fox BA, Falla A, Bzik DJ. *Toxoplasma gondii* intravacuolar-network-associated dense granule proteins regulate maturation of the cyst matrix and cyst wall. *mSphere* (2019) 4(5):e00487–19. doi: 10.1128/mSphere.00487-19

21. Fox BA, Rommereim LM, Guevara RB, Falla A, Hortua Triana MA, Sun Y, et al. The *toxoplasma gondii* rhoptry kinome is essential for chronic infection. *MBio* (2016) 7 (3):e00193–16. doi: 10.1128/mBio.00193-16

22. Saeij JP, Arrizabalaga G, Boothroyd JC. A cluster of four surface antigen genes specifically expressed in bradyzoites, SAG2CDXY, plays an important role in *Toxoplasma gondii* persistence. *Infect Immun* (2008) 76:2402–10. doi: 10.1128/IAI.01494-07

23. Tiwari A, Hannah R, Lutshumba J, Ochiai E, Weiss LM, Suzuki Y. Penetration of $CD8^+$ cytotoxic T cells into large target, tissue cysts of *Toxoplasma gondii*, leads to its elimination. *Am J Pathol* (2019) 189:1594–607. doi: 10.1016/j.ajpath.2019.04.018

24. Lemgruber L, Lupetti P, Martins-Duarte ES, De Souza W, Vommaro RC. The organization of the wall filaments and characterization of the matrix structures of *Toxoplasma gondii* cyst form. *Cell Microbiol* (2011) 13:1920–32. doi: 10.1111/j.1462-5822.2011.01681.x

25. Di Cristina M, Del Porto P, Buffolano W, Beghetto E, Spadoni A, Guglietta S, et al. The *Toxoplasma gondii* bradyzoite antigens BAG1 and MAG1 induce early humoral and cell-mediated immune responses upon human infection. *Microbes Infect* (2004) 6:164–71. doi: 10.1016/j.micinf.2003.11.009

26. Rommereim LM, Fox BA, Butler KL, Cantillana V, Taylor GA, Bzik DJ. Rhoptry and dense granule secreted effectors regulate $CD8^+$ T cell recognition of *Toxoplasma gondii* infected host cells. *Front Immunol* (2019) 10:2104. doi: 10.3389/fimmu.2019.02104

27. Deffieu MS, Alayi TD, Slomianny C, Tomavo S. The *Toxoplasma gondii* dense granule protein TgGRA3 interacts with host Golgi and dysregulates anterograde transport. *Biol Open* (2019) 8(3):bio039818. doi: 10.1242/bio.039818

28. Thomas F, Lafferty KD, Brodeur J, Elguero E, Gauthier-Clerc M, Misse D. Incidence of adult brain cancers is higher in countries where the protozoan parasite Toxoplasma gondii is common. *Biol Lett* (2012) 8:101–3. doi: 10.1098/rsbl.2011.0588

29. Cong W, Liu GH, Meng QF, Dong W, Qin SY, Zhang FK, et al. *Toxoplasma gondii* infection in cancer patients: prevalence, risk factors, genotypes and association with clinical diagnosis. *Cancer Lett* (2015) 359:307–13. doi: 10.1016/j.canlet.2015.01.036

frontiers | Frontiers in Immunology

TYPE Original Research
PUBLISHED 08 November 2023
DOI 10.3389/fimmu.2023.1291379

OPEN ACCESS

EDITED BY
William Harold Witola,
University of Illinois at Urbana–Champaign, United States

REVIEWED BY
Guanghui Zhao,
Northwest A&F University, China
Laila Gutierrez Kobeh,
National Autonomous University of Mexico, Mexico

*CORRESPONDENCE
Xiangrui Li
lixiangrui@njau.edu.cn

†These authors have contributed equally to this work

RECEIVED 09 September 2023
ACCEPTED 25 October 2023
PUBLISHED 08 November 2023

CITATION
Zhang Y, Lu M, Zhang Z, Huang X, Huang J, Liu J, Huang J, Song X, Xu L, Yan R and Li X (2023) The microneme adhesive repeat domain of MIC3 protein determined the site specificity of *Eimeria acervulina*, *Eimeria maxima*, and *Eimeria mitis*. *Front. Immunol.* 14:1291379. doi: 10.3389/fimmu.2023.1291379

The microneme adhesive repeat domain of MIC3 protein determined the site specificity of *Eimeria acervulina*, *Eimeria maxima*, and *Eimeria mitis*

Yang Zhang†, Mingmin Lu†, Zhenchao Zhang, Xinmei Huang, Jingwei Huang, Jiabin Liu, Jianmei Huang, Xiaokai Song, Lixin Xu, Ruofeng Yan and Xiangrui Li*

The Ministry of Education Joint International Research Laboratory of Animal Health and Food Safety, College of Veterinary Medicine, Nanjing Agricultural University, Nanjing, China

Understanding the determinants of host and tissue tropisms among parasites of veterinary and medical importance has long posed a substantial challenge. Among the seven species of *Eimeria* known to parasitize the chicken intestine, a wide variation in tissue tropisms has been observed. Prior research suggested that microneme protein (MIC) composed of microneme adhesive repeat (MAR) domain responsible for initial host cell recognition and attachment likely dictated the tissue tropism of *Eimeria* parasites. This study aimed to explore the roles of MICs and their associated MARs in conferring site-specific development of *E. acervuline*, *E. maxima*, and *E. mitis* within the host. Immunofluorescence assays revealed that MIC3 of *E. acervuline* (EaMIC3), MIC3 of *E. maxima* (EmMIC3), MIC3 of *E. mitis* (EmiMIC3), MAR3 of EaMIC3 (EaMIC3-MAR3), MAR2 of EmMIC3 (EmMIC3-MAR2), and MAR4 of EmiMIC3 (EmiMIC3-MAR4), exhibited binding capabilities to the specific intestinal tract where these parasites infect. In contrast, the invasion of sporozoites into host intestinal cells could be significantly inhibited by antibodies targeting EaMIC3, EmMIC3, EmiMIC3, EaMIC3-MAR3, EmMIC3-MAR2, and EmiMIC3-MAR4. Substitution experiments involving MAR domains highlighted the crucial roles of EaMIC3-MAR3, EmMIC3-MAR2, and EmiMIC3-MAR4 in governing interactions with host ligands. Furthermore, animal experiments substantiated the significant contribution of EmiMIC3, EmiMIC3-MAR4, and their polyclonal antibodies in conferring protective immunity to *Eimeria*-affiliated birds. In summary, EaMIC3, EmMIC3, and EmiMIC3 are the underlying factors behind the diverse tissue tropisms exhibited by *E. acervuline*, *E. maxima*, and *E. mitis*, and EaMIC3-MAR3, EmMIC3-MAR2, and EmiMIC3-MAR4 are the major determinants of MIC-mediated tissue tropism of each parasite. The results illuminated the molecular basis of the modes of action of *Eimeria* MICs, thereby facilitating an understanding and rationalization of the marked differences in tissue tropisms among *E. acervuline*, *E. maxima*, and *E. mitis*.

KEYWORDS

MIC3 protein, MAR, site specificity, *Eimeria*, chicken

Introduction

Avian coccidiosis, a consequence of *Eimeria* infections, is renowned for its high morbidity and mortality, with significant implications for poultry health and welfare (1, 2). The primary bird species affected by *Eimeria* include chickens (both in layer and broiler systems), turkeys, and fowls. Globally, the annual expenditure for the treatment and control of chicken coccidiosis is estimated to be up to $14.5 billion (3). Seven species of *Eimeria*, namely *E. tenella*, *E. acervulina*, *E. mitis*, *E. brunetti*, *E. praecox*, *E. necatrix*, and *E. maxima*, are recognized to infect chickens, each differing in pathogenicity (4). *E. tenella*, *E. acervulina*, *E. necatrix*, and *E. maxima* are highly pathogenic, while *E. mitis* and *E. praecox* are less infectious (5). The life cycle of *Eimeria* parasites comprises two distinct phases: the exogenous phase and the endogenous phase (1). Once ingested by chickens, the oocysts release sporozoites, the initial infective units specialized for invading host intestinal cells (6, 7). The endogenous reproductive stage commences with schizogony (asexual reproduction), followed by gametogony (sexual differentiation) (5). In the schizogony stage, free sporozoites replicate within host cells to form schizonts, while in the gametogony stage, the final generation of mature merozoites differentiates into gametes, which unite to generate zygotes, ultimately maturing into oocysts (6, 7).

Host and tissue tropisms are the ability of a given parasite to preferentially target a particular host or tissue, and the study of host and tissue tropisms has been a central topic for our understanding of parasitology as well as parasitic diseases. Although the phenomenon of aforementioned tropisms has long been observed from a variety of parasites of veterinary and medical significance, including helminths and protozoa, the general mechanism description of parasitic tropisms has posed a grand challenge for decades. For example, the coccidian parasite *Toxoplasma gondii* could infect almost each of warm-blooded vertebrates (8, 9), whereas *Eimeria* parasites within the same coccidia sub-class are individually highly host-specific (9). Moreover, the parasites that belong to the same *Eimeria* genus even display widely varying tissue tropisms, as demonstrated by chicken coccidia spp. These obligatory intracellular parasites are recognized to vary in site-specificity of development in the intestinal tract of birds. *E. acervulina* and *E. praecox* parasitize in the upper intestine, and *E. maxima* and *E. necatrix* develop in the mid intestine. In stark contrast, *E. brunetti* and *E. mitis* infected cells of the lower intestine, and *E. tenella* infected cells of the ceca (10) However, the molecular basis for tissue tropisms of these *Eimeria* parasites manifested long-term unresolved mysteries in the disease pathogenesis of avian coccidiosis.

Generally, the mechanisms of *Eimeria* to invade the chicken intestinal epithelial cells have been considered identical to the cell entry machinery of other apicomplexans (11, 12). Coccidia initially glided over the surface of a host cell and then reoriented to place its apical end in close contact with the host cell membrane. After initial attachment, a circumferential ring of adhesion (called the moving or tight junction) was formed, through which the parasite actively propelled itself while concurrently depressing the host-cell membrane to create a nascent protective vacuole (13). Of particular significance in this context is the adhesion process, which allows the further establishment of forced rapid invasion of host cells by *Eimeria* parasites. Secretory organelles, including micronemes and rhoptries, have been described to release a spectrum of proteins to help *Eimeria* parasites adhere to the host cell (14). Beyond that, micronemes proteins (MICs) also contribute to the invasion machinery by complexing with rhoptry proteins, and the complexes were later targeted into host cells.

To date, a spectrum of MICs of *Eimeria* spp. of chicken was identified and characterized, including ten of *E. tenella* (EtMIC1-7 and EtAMA1-3) (15–22), seven of *E. acervulina* (EaMIC2, EaMIC3, EaMIC5, EaMIC7, EaMIC13, EaMIC14 and EaAMA1 (23–25), six of *E. maxima* (EmMIC1, EmMIC2, EmMIC3, EmTFP250, EmMIC5, EmMIC7, and EmAMA1) (26–31), five of *E. mitis* (EmiMIC2, EmiMIC3, EmiMIC7, EmiAMA1, and EmiEtmic-2/7h) (32), six of *E. necatrx* (EnMIC2, EnMIC3, EnMIC5, EnMIC7, EnMIC13, EnAMA1) and two of *E. brunetti* (EbMIC2 and EbAMA1) (33). Although their functional roles in host-parasite interactions have not been fully elucidated, a few of these MICs have been reported to allow *Eimeria* spp. to bind a diverse range of oligosaccharide epitopes of host cells to drive parasite invasion (34, 35). For instance, MIC3 of *E. tenella* (EtMIC3), through the recognition of sialyl glycans, could guide the parasite to the site of invasion in the ceca.

Like MICs of *Neospora caninum* and *Toxoplasma gondii*, *Eimeria* MICs also bear the microneme adhesive repeat domain (MAR). All apicomplexan MARs were classified into Types I and II domains based on their subtle structural differences. The latter has an additional C-terminal β-finger chain, while Type I MARs have an extended α-loop chain. Both Types I and II MARs have been identified in *Toxoplasma* and *Plasmodium* MICs. However, *Eimeria* MICs appear to possess only Type I domains, which may be associated with the host and site specificity of *Eimeria* parasites. For example, MIC3 of *E. mitis* (EmiMIC3) contained nine Type I MARs (MARs1-9), and EtMIC3 consists of seven Type I MAR domains, namely, MAR1a, MAR1b, three repeated MAR1c, MAR1d, and MAR1e (36). Identically, Type I MAR domains of *Eimeria* MICs mediate parasite recognition of host cell molecules. Their sequence divergence alongside structural differences of MAR domains may account for differential binding properties. For *E. tenella*, there is considerable variability in the binding capability of all MARs of EtMIC3 to cell surface sialyl glycans, while MAR1b exhibits more robust binding signals than MAR1a, MAR1c, MAR1d, and MAR1e and may govern tissue tropisms of *E. tenella* (37, 38).

Sequence alignment analysis showed that two common LxxY and HxT/HxS motifs were shared by all MARs of EtMIC3, which were responsible for the specific binding of EtMIC3 protein to sialyl acid saccharide on host cells and may help *E. tenella* target chicken cecal epithelial cells. However, this is not the case for other *Eimeria* parasites. Specifically, the LxxY motif was presented in the MAR1,

Abbreviations: MAR, microneme adhesive repeat; EtMIC3, *E. tenella* microneme protein 3; EmMIC3, *E. maxima* microneme protein 3; EmiMIC3, *E. mitis* microneme protein 3; EtAMA1, ELISA, enzyme linked immunosorbent assay; RACE, rapid-amplification of cDNA ends; ORF, open reading frame; IFA, immunofluorescence assay; BSA, bovine serum albumin; TBST, tris-buffered saline with Tween 20; DAPI, 4,6-diamidino-2-phenylin-dole; PBS, phosphate buffer saline; TMB, 3,3',5,5'-Tetramethylbenzidine; HBSS, Hanks Balanced Salt Solution.

MAR2, MAR3 and MAR8 domains of EmiMIC3, whereas the motif of HxT/HxS was identified in MAR2, MAR3, MAR4, MAR5, MAR6, and MAR7 domains of EmiMIC3 (32). The predominant sequence difference in MARs of EtMIC3 and EmiMIC3 suggested that the key factors or the molecules that governed the site specificities of *Eimeria* spp. (parasitizing in the small intestine or the ceca) might be completely different. The tissue tropism machinery of coccidia parasites goes beyond the general conceptual framework of the apicomplexan invasion process and includes the binding specificity of *Eimeria* MICs, as well as their unique Type I MARs. Although recent studies have revealed the engagement of EtMICs in the invasion machinery of *E. tenella*, the diversified roles of EmiMICs, MICs of *E. maxima* (EmMICs), and MICs of *E. acervuline* (EaMICs) remain largely unknown. As such, the objective of this study was to identify the roles of EmiMICs, EmMICs, and EaMICs, alongside their unique MARs in the site specificities of *E. acervulina*, *E. maxima*, and *E. mitis*.

Results

EaMIC3, EmMIC3 and EmiMIC3 selectively bind to the upper, mid and lower intestines

To evaluate the binding specificity of different EaMICs, EmMICs, and EmiMICs to host tissues, intestinal samples were taken from throughout the chicken gut (the upper, mid, and lower intestine, and caecum), and immunofluorescence staining of EaMICs, EmMICs, and EmiMICs with specific anti-EaMICs, anti-EmMICs, and anti-EmiMICs antibodies was performed respectively. As shown in Figure 1C, substantial red fluorescence from labeling EaMIC3 was observed in sections of the upper intestines (Figure 1, c1) but not those of the mid and lower intestines and caecum. In addition, we did not observe any red fluorescence from either EaMIC2-treated (Figure 1A) or EaMIC5-treated (Figure 1B) histological sections taken from the upper, mid, and lower intestines and caecum, which indicated that EaMIC3 but not EaMIC2 or EaMIC5 could bind to the upper intestine and may play a key role in directing *E. acervulina* to this specific location.

Moreover, the tissue staining pattern was also investigated for EmMIC3 (Figure 1D), EmMIC2 (Figure 1E), and EmAMA1 (Figure 1F). In sections taken from the mid intestines, there was intense red fluorescence resulting from tagging EmMIC3 with anti-EmMIC3 pAbs (Figure 1, d2), suggesting that EmMIC3 could remain in close contact with host epithelial cell derived from the mid intestines. However, no red fluorescence was identified in rEmMIC3-treated sections of the upper and lower intestines and caecum (Figure 1, d1, d3, d4). As for EmMIC2 and EmAMA1, no red fluorescence was detected from any EmMIC2-treated or EmAMA1-treated gut sections (Figures 1E, F). In addition, incubation of these gut sections with rEmiMIC3 (Figure 1G), rEmiMIC2 (Figure 1H), rEmiAMA1 (Figure 1I), rEmiEtmic-2/7 (Figure 1J) showed an abundance of EmiMIC3 staining in sections taken from the lower intestines (Figure 1, g3). The absence of binding signals of EmiMIC2, EmiAMA1, and EmiEtmic-2/7 to the section derived from throughout the chicken gut suggested a specific binding pattern for EmiMIC3, and the binding was predominantly to the lower intestines.

The MARs of EaMIC3, EmMIC3, and EmiMIC3 have relatively conserved binding domains

Given that EaMIC3, EmMIC3, and EmiMIC3 might be responsible for guiding *E. maxima*, *E. acervulina*, and *E. mitis* to corresponding invasion sites in the chicken gut, respectively, we further aligned MARs from EaMIC3, EmMIC3, and EmiMIC3 so as

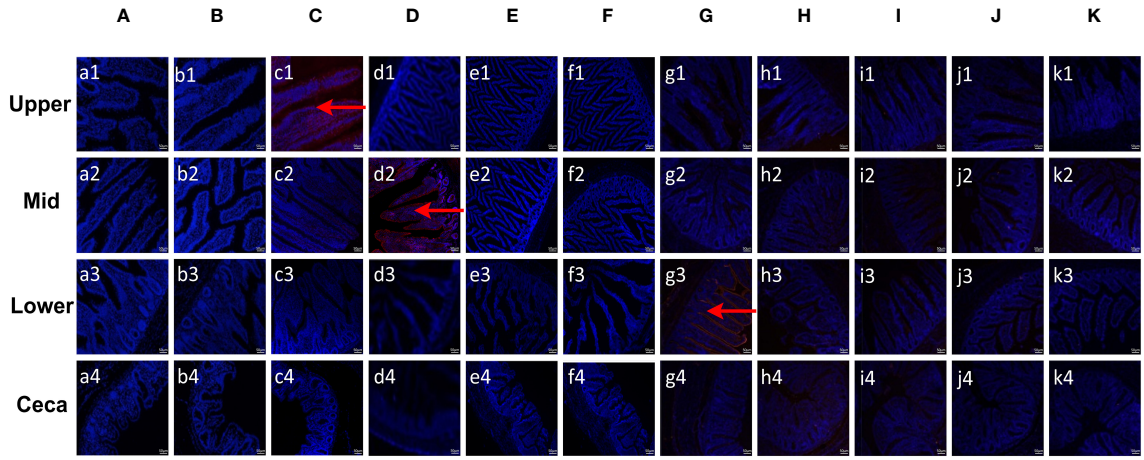

FIGURE 1
Binding properties of *Eimera* microneme proteins to different small intestine segments. The upper, mid, lower intestine, and caecum tissues were removed from 2-week-old chicken. The substantial red fluorescence from labeling EaMIC3 **(C)** was observed in sections of the upper intestines, red fluorescence resulting from tagging EmMIC3 **(D)** with anti-EmMIC3 pAbs, and the red fluorescence from labeling EmiMIC3 **(G)** was observed in sections of the lower intestines, while EaMIC2 **(A)**, EaMIC5 **(B)**, EmMIC2 **(E)**, EmAMA1 **(F)**, EmiMIC2 **(H)**, EmiAMA1 **(I)**, EmiEtmic-2/7 **(J)**, and pET-32a **(K)**, no red fluorescence was identified. Scale bars: 50 µm.

10.3389/fimmu.2023.1291379

to predict their potential binding properties. The EaMIC3-MAR1 and EaMIC3-MAR7 of EaMIC3, EmMIC3-MAR5 of EmMIC3, and EmiMIC3-MAR9 of EmiMIC3 were incomplete repeating sequences. Most of the EaMIC3-MARs, EmMIC3-MARs, and EmiMIC3-MARs contain seven cysteine (C) residues (Figures 2A–C, green boxes) except for EaMIC3-MAR1 and EaMIC3-MAR7 which lack the first three C residues and EmMIC3-MAR5 which lack the third one. Most MARs from EaMIC3, EmMIC3, and EmiMIC3 exhibit the conserved signatures of Type I MAR of *Eimeria* parasites. The LxxY motif within the α1-helix/loop extension of Type I MAR identified in EaMIC3-MAR2, EaMIC3-MAR3, EaMIC3-MAR4, EaMIC3-MAR5 and EaMIC3-MAR6 of EaMIC3, EmMIC3-MAR1, EmMIC3-MAR2, EmMIC3-MAR3 and EmMIC3-MAR4 of EmMIC3, and EmiMIC3-MAR1, EmiMIC3-MAR2, EmiMIC3-MAR3 and EmiMIC3-MAR8 of EmiMIC3 were relatively conserved (Figures 2A–C, red boxes). Moreover, the HxT/HxS signature that directly coordinates binding to sialyl saccharides found in EaMIC3-MAR2, EaMIC3-MAR3, EaMIC3-MAR4, EaMIC3-MAR5 and EaMIC3-MAR6 of EaMIC3, EmMIC3-MAR2, EmMIC3-MAR3 and EmMIC3-MAR4 of EmMIC3, and EmiMIC3-MAR2, EmiMIC3-MAR3, EmiMIC3-MAR4, EmiMIC3-MAR5, EmiMIC3-MAR6, EmiMIC3-MAR7 and EmiMIC3-MAR8 of EmiMIC3 were also considerably conserved (Figures 2A–C, blue boxes). The results from multiple sequence alignment suggested that most MARs from EaMIC3, EmMIC3, and EmiMIC3 have pretty high conservation in their binding motifs.

EaMIC3-MAR3, EmMIC3-MAR2, and EmiMIC3-MAR4 exerted strong binding abilities to differing intestinal tissues

To determine more precisely which MAR of EaMIC3, EmMIC3, and EmiMIC3 functions in tissue binding, the binding capability of different EaMIC3-MARs, EmMIC3-MARs, and EmiMIC3-MARs was compared using IFA assays. Among seven EaMIC3-MARs, EaMIC3-MAR3 gave the most robust binding to the upper intestine sections (red fluorescence) (Figure 3C, c1), but not to other gut sections, whilst the remaining EaMIC3-MARs and the pET-32a tag protein did not show significant binding to intestinal tissues (Figures 3A–H). This indicates that EaMIC3-MAR3 is the dominating domain in the EaMIC3 binding. As for EmMIC3, incubation of gut sections with different EmMIC3-MARs revealed an abundance of EmMIC3-MAR2 staining in sections taken from the mid intestines (Figure 4B, b2). Another striking finding was that no red fluorescence was observed from gut sections treated with the pET-32a tag protein, EmMIC3-MAR1, EmMIC3-MAR3, EmMIC3-MAR4, and EmMIC3-MAR5 (Figures 4A, C–F), demonstrating the predominant role of EmMIC3-MAR2 in tissue binding of EmMIC3. In addition, a unique binding pattern was presented by EmiMIC3-MAR4, showing strong binding to the lower intestines rather than to other gut tissues (Figure 5D, d3). Notably, the other eight EmiMIC3-MARs and the pET-32a tag protein gave no binding to any gut section (Figures 5A–C, E–J). This tissue binding pattern of EmiMIC3-MARs suggested that EmiMIC3-MAR4 was a potent domain of EmiMIC3.

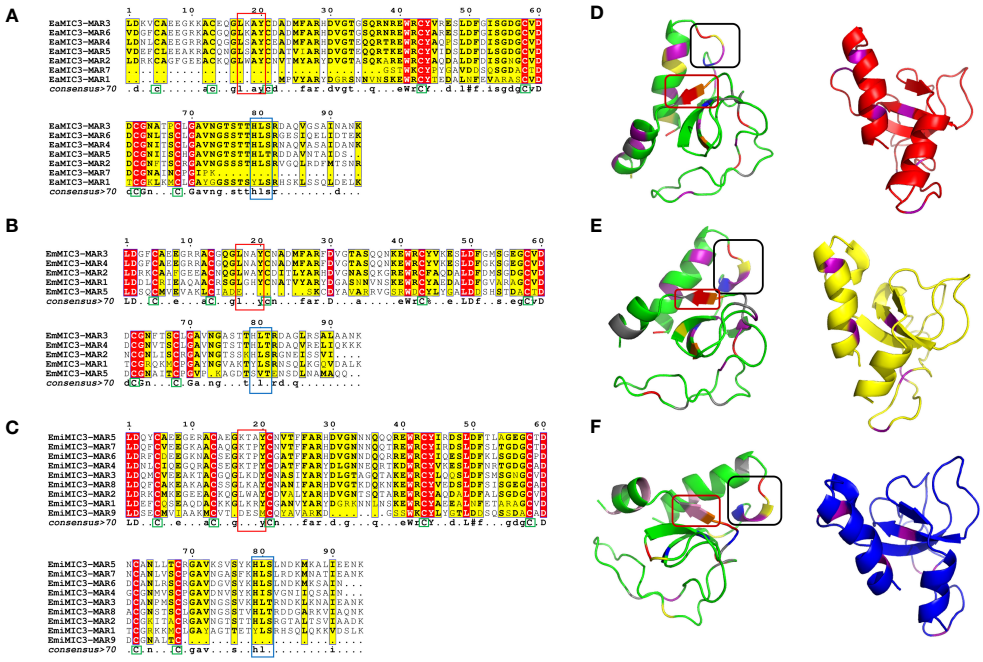

FIGURE 2
Alignment of MAR domains and the three-dimensional structure of the EaMIC3-MAR3, EmMIC3-MAR2, and EmiMIC3-MAR4. MAR domains from EaMIC3 (7 repeats) **(A)**, MAR domains from EmMIC (5 repeats) **(B)**, MAR domains from EmiMIC3 (9 repeats) **(C)**. The high similarity is represented by different intensities of red/yellow, respectively. Green boxes indicate conserved cysteines **(C)**, red boxes indicate LxxY residue with the α1-helix/loop extension of MAR type I; blue boxes indicate HxT/HxS residue coordinating binding to the sialic acid saccharides. The left structures of EaMIC3-MAR3 **(D)**, EmMIC3-MAR2 **(E)**, EmiMIC3-MAR4 **(F)** represent the spatial distribution of the LxxY and HxS/HXT motif, and the black frame indicates the LxxY motif and the red border indicates the HxS/HXT motif. The right images represent the cysteine distribution region, and the purple sections are cysteine.

10.3389/fimmu.2023.1291379

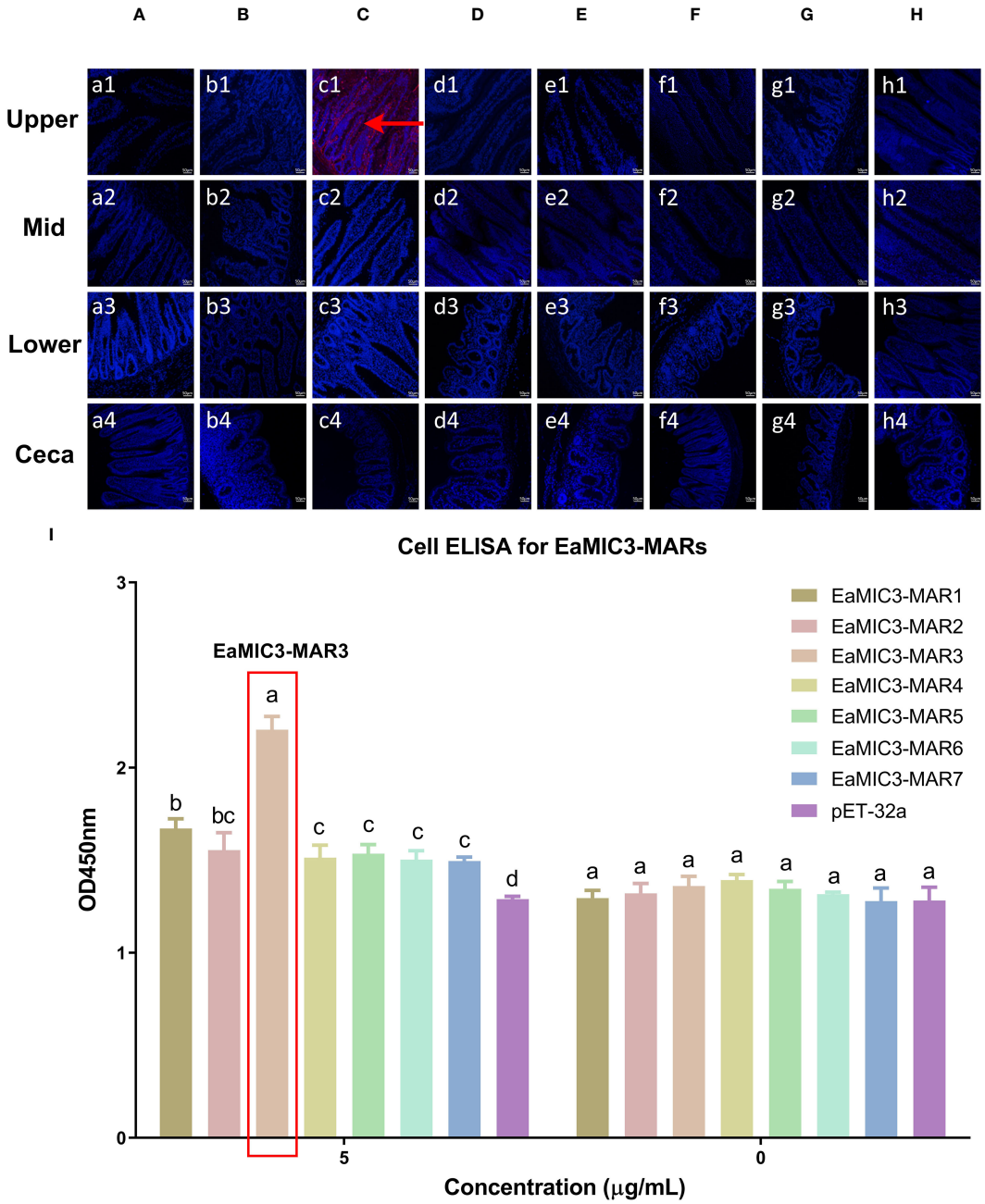

FIGURE 3
Binding properties of EaMIC3-MARs to different intestine segments. The upper, mid, lower intestine, and caecum tissues were removed from 2-week-old chicken. EaMIC3-MAR3 **(C)** gave the most robust binding to the upper intestine sections (red fluorescence), while EaMIC3-MAR1 **(A)**, EaMIC3-MAR2 **(B)**, EaMIC3-MAR4 **(D)**, EaMIC3-MAR5 **(E)**, EaMIC3-MAR6 **(F)**, EaMIC3-MAR7 **(G)**, and pET-32a **(H)** did not show significant binding to intestinal tissue. Scale bars: 50 μm. The upper intestinal epithelial cells were isolated and cultivated from 2-week-old chickens. The chicken upper epithelial cells were co-cultured respectively with the recombinant EaMIC3-MARs (0 μg/mL or 5 μg/mL). EaMIC3-MAR3 exhibited the most robust binding signals to the upper epithelial cells in a dose-dependent manner **(I)**. Among different MARs, the significant difference within the group was shown by different letters ($p < 0.05$).

EaMIC3-MAR3, EmMIC3-MAR2, and EmiMIC3-MAR4 exhibited robust interactions with epithelial cells derived from various intestinal tissues

To further validate the tissue staining pattern observed for MARs from EaMIC3, EmMIC3, and EmiMIC3, cell-based ELISA assays were developed and performed using intestine epithelial cells. All of the seven EaMIC3-MARs at varying concentrations could bind to intestinal epithelial cells derived from the upper intestines (Figure 3I, Supplementary File 1). Compared to the other six EaMIC3-MARs, EaMIC3-MAR3 exhibited the most robust binding signals to epithelial cells in a dose-dependent manner, which is consistent with the IFA results (Figure 3I, Supplementary

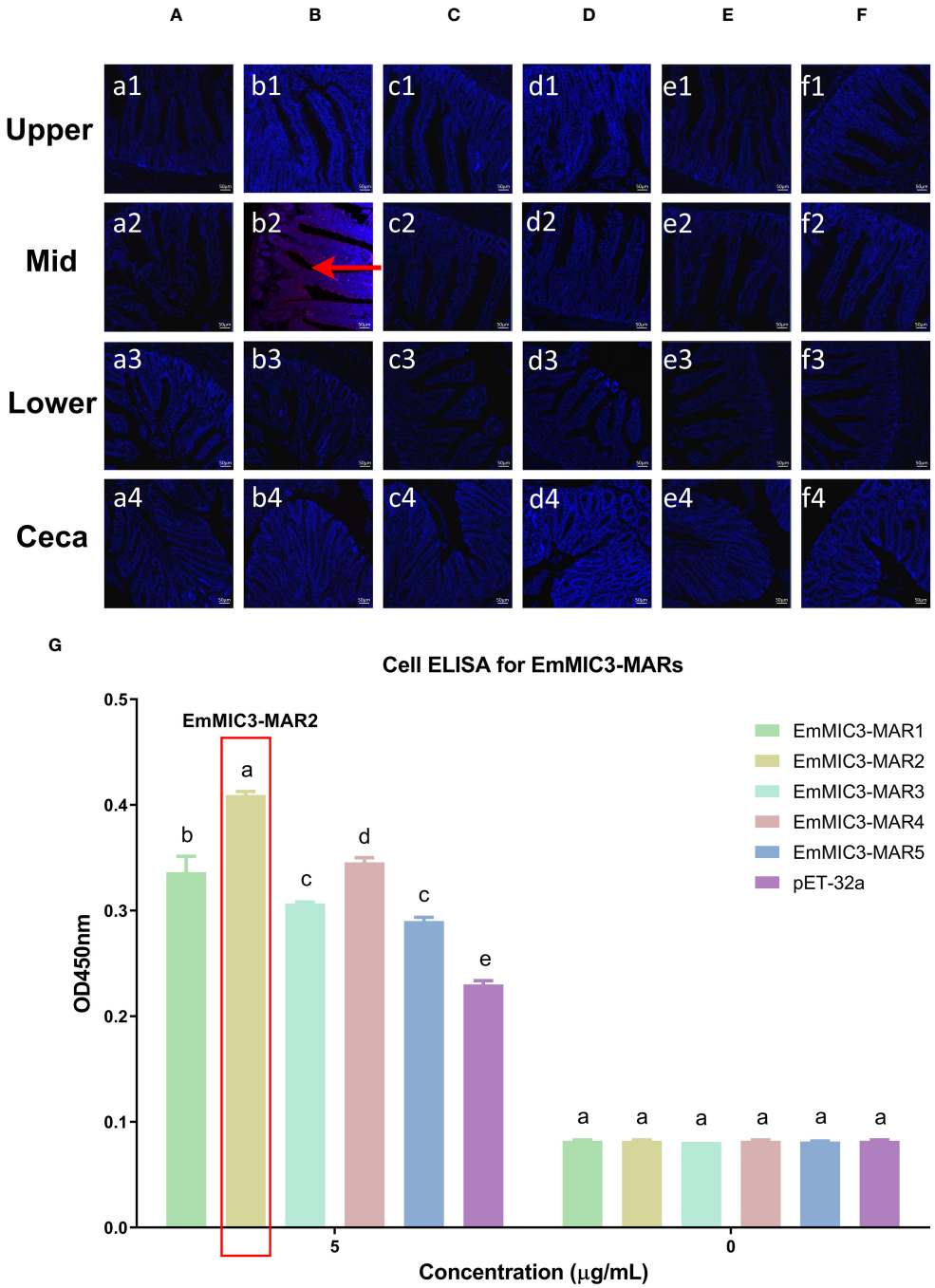

FIGURE 4
Binding properties of EmMIC3-MARs to different intestine segments. The upper, mid, lower intestine, and caecum tissues were removed from 2-week-old chicken. The substantial red fluorescence from labeling EmMIC3-MAR2 **(B)** was observed in sections of the mid intestines, whilst the EmMIC3-MAR1 **(A)**, EmMIC3-MAR3 **(C)**, EmMIC3-MAR4 **(D)**, EmMIC3-MAR5 **(E)** and pET-32a **(F)**, did not show significant binding to intestinal tissues. Scale bars: 50 μm. The mid intestinal epithelial cells were isolated and cultivated from 2-week-old chickens. The chicken mid intestinal epithelial cells were co-cultured respectively with the recombinant EmMIC3-MARs (0 μg/mL or 5 μg/mL). EmMIC3-MAR2 was most highly active for binding to mid intestinal epithelial cells among all EmMIC3-MARs, of which was concentration-dependent **(G)**. Among different MARs, the significant difference within the group was shown by different letters ($p < 0.05$).

File 1). For five EmMIC3-MARs, a sequential two-fold dilution of each EmMIC3-MAR interacted with host epithelial cells isolated from the mid intestines (Figure 4G, Supplementary File 2). Beyond that, EmMIC3-MAR2 was most highly active for cell binding among all EmMIC3-MARs, which was concentration-dependent (Figure 4G, Supplementary File 2). Each EmiMIC3-MAR domain could also bind to epithelial cells separated from the lower intestine, and a comparison of the binding capabilities of different EmiMIC3-MARs reveals that EmiMIC3-MAR4 has the strongest binding to cells (Figure 5K, Supplementary File 3). Therefore, these

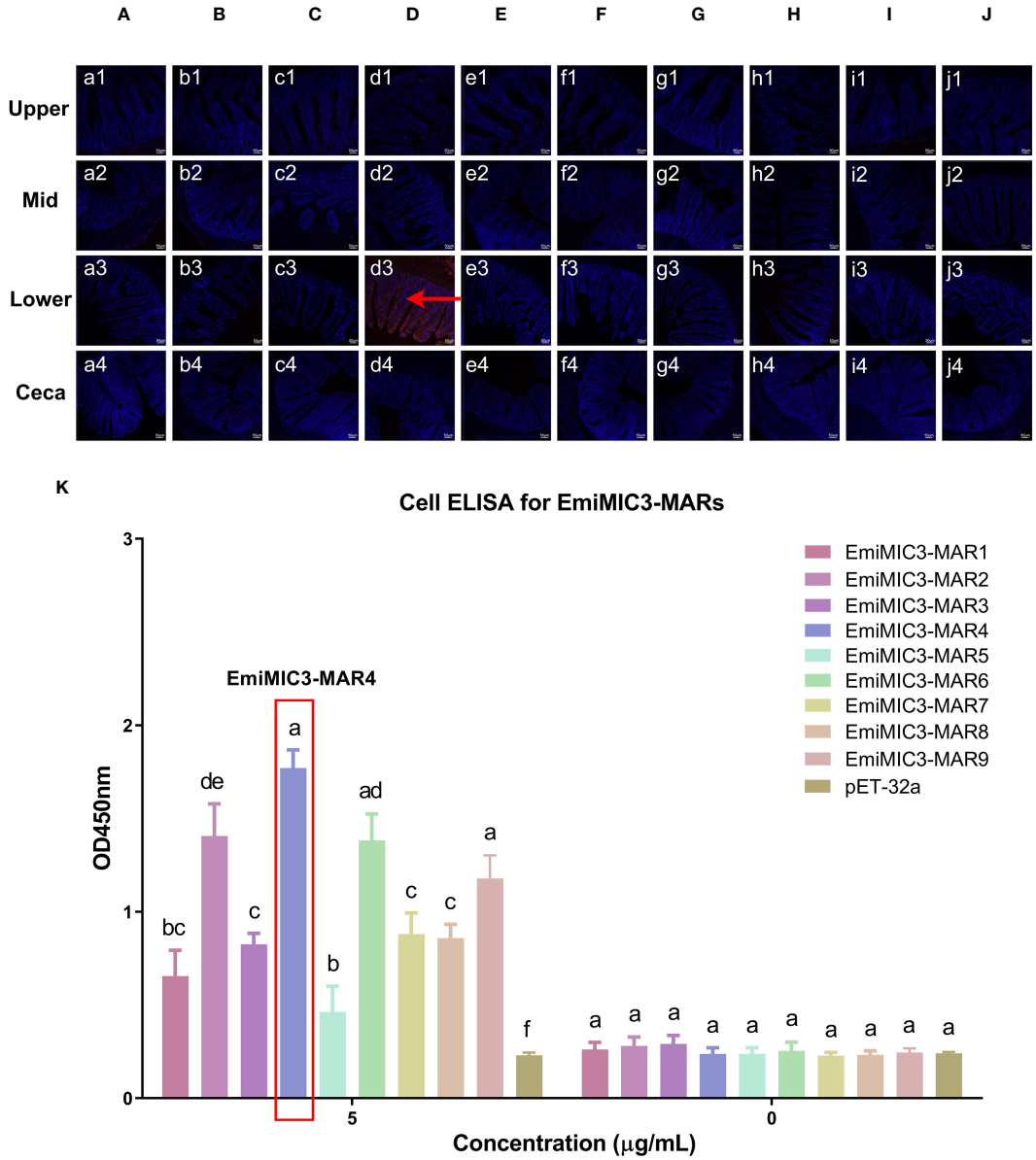

FIGURE 5
Binding properties of EmiMIC3-MARs to different intestine segments. The upper, mid, lower intestine, and caecum tissues were removed from 2-week-old chickens. EmiMIC3-MAR4 **(D)** showed stronger binding to the lower intestines rather than to other gut tissues (red fluorescence), whilst EmiMIC3-MAR1 **(A)**, EmiMIC3-MAR2 **(B)**, EmiMIC3-MAR3 **(C)**, EmiMIC3-MAR5 **(E)**, EmiMIC3-MAR6 **(F)**, EmiMIC3-MAR7 **(G)**, EmiMIC3-MAR8 **(H)**, EmiMIC3-MAR9 **(I)**, and pET-32a **(J)** did not show significant binding to intestinal tissues. Scale bars: 50μm. The lower intestinal epithelial cells were isolated and cultivated from 2-week-old chickens. The chicken lower intestinal epithelial cells were co-cultured respectively with the recombinant EmiMIC3-MARs (0 μg/mL or 5 μg/mL). EmiMIC3-MAR4 has the strongest binding to lower intestinal epithelial cells **(K)**. Among different MARs, the significant difference within the group was shown by different letters ($p < 0.05$).

observations provide more detailed evidence of the roles of EaMIC3-MAR3, EmMIC3-MAR2, and EmiMIC3-MAR4, respectively, for EaMIC3, EmMIC3, and EmiMIC3 binding within the gut of chicken.

To provide a structural basis for the recognition of EaMIC3-MAR3, EmMIC3-MAR2, and EmiMIC3-MAR4, we carried out the three-dimensional structural characterization of these MARs. The three-dimensional structures of the EaMIC3-MAR3, EmMIC3-MAR2, and EmiMIC3-MAR4 are relatively identical, containing α-helix and β-sheet; moreover, the three domains can overlap with each other to a certain extent (Figures 2D–F). By characterizing the arrangement of the LxxY and HxS/HxT motifs in three-dimensional space, it was found that the spatial distribution of these two motifs within the EaMIC3-MAR3, EmMIC3-MAR2, and EmiMIC3-MAR4 domains are considerably similar. However, they have slightly different secondary structures; the LxxY motif forms random coils on the EaMIC3-MAR3 (Figure 2D), while the α-helix forms on the EmMIC3-MAR2 (Figure 2E). The HxS/HxT motif forms a β-sheet on EaMIC3-MAR3, EmMIC3-MAR2, and EmiMIC3-MAR4, respectively (Figures 2D–F).

10.3389/fimmu.2023.1291379

The antibodies against EaMIC3-MAR3, EmMIC3-MAR2, and EmiMIC3-MAR4 significantly inhibited the invasions of sporozoites into the intestine epithelial cells

Given the binding specificity of EaMIC3, EmMIC3, and EmiMIC3, as well as associated MAR domains, we further carried out an inhibition assay using antibodies against different MICs and MARs to assess their roles in sporozoite invasion. As shown in Figure 6A, the treatment of anti-EaMIC2, anti-EaMIC3, and anti-EaMIC5 pAbs significantly inhibited the invasion of *E. acervulina* sporozoites to host upper intestines ($P < 0.05$ for each). Moreover, the treatment of anti-EaMIC3 pAbs (90.24%) gave a much higher inhibition rate than anti-EaMIC2 (14.15%) and anti-EaMIC5 pAbs (14.93%) (Figure 6A). In addition, *E. maxima* sporozoite invasion of cultured mid intestine tissues could be inhibited by anti-EmMIC2, anti-EmMIC3, and anti-EmAMA1 pAbs ($P < 0.05$), and anti-EmMIC3 pAbs (64.5%) exert much stronger inhibitory activity than anti-EmMIC2 and anti-EmAMA1 pAbs ($P < 0.05$) (Figure 6B). Besides, *E. mitis* sporozoites pre-exposed to anti-EmiMIC2, anti-EmiMIC3, ani-EmiEtmic2/7h, and ani-EmiAMA1 pAbs had much lower invading activity compared to the mock control ($P < 0.05$), and anti-EmiMIC3 pAbs was a more potent inhibitor of *E. mitis* sporozoite invasion in the lower intestines (53.09%) (Figure 6C).

Likewise, varying anti-MARs antibodies were also prepared to evaluate their inhibitory activity on corresponding MARs during the invasion of sporozoites of three *Eimeria* spp. Of all seven EaMIC3-MARs, EaMIC3-MAR3 serum exhibited the highest inhibitory activity in the invasion of *E. acervulina* sporozoites ($P < 0.05$), and the inhibition rate was 70% (Figure 6D). Meanwhile, both anti-EmMIC3-MAR1 and anti-EmMIC3-MAR2 pAbs could inhibit *E. maxima* sporozoite invasion in cultured mid intestines ($P < 0.05$), and more robust inhibitory activity was observed with EmMIC3-MAR2 antibody compared with EmMIC3-MAR1 antibody in the inhibition experiments (70.91%) ($P < 0.05$) (Figure 6E). Additionally, of all nine EmiMIC3-MARs, we found significant inhibition of *E. mitis* sporozoite invasion in the lower intestines following the treatment of EmiMIC3-MAR4 antibody ($P < 0.05$), while the other eight EmiMIC3-MAR antibodies did not show any inhibitory activities (Figure 6F).

Binding domain substitutions revealed MAR-mediated site specificity of *Eimeria* invasion

To further elucidate the predominant roles of EaMIC3-MAR3, EmMIC3-MAR2, and EmiMIC3-MAR4 in EaMIC3-mediated, EmMIC3-mediated, and EmiMIC3-mediated tissue binding, we selected the EaMIC3-MAR3 domain and EtMIC3-MAR1b

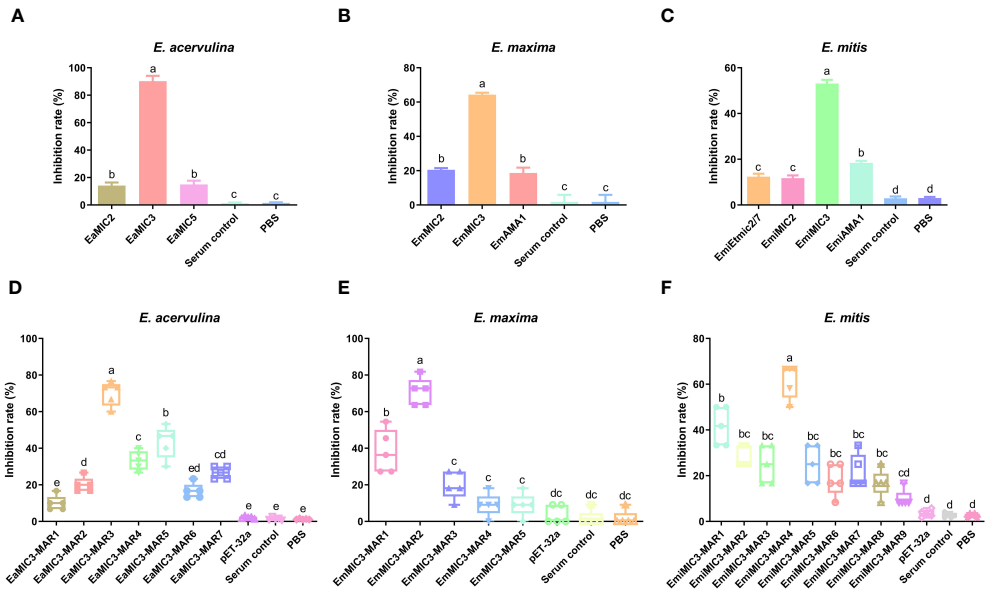

FIGURE 6
The inhibition effects of sera against MICs and MARs on *Eimeria* sporozoite invasion. *E acervulina* sporozoites were treated with rat anti-EaMIC2, -EaMIC3, -EaMIC5, and -EaMIC3-MARs pAbs, respectively. The sporozoites of *E maxima* were treated with rat anti-EmMIC2, -EmMIC3, -EmAMA1, and -EmMIC3-MARs pAbs, respectively, while *E mitis* sporozoites were blocked with rat anti-EmiMIC3, -EmiMIC2, -EmiEtmic2/7h, -EmiAMA, or -EmiMIC3-MARs pAbs, respectively. The treatment of anti-EaMIC3 pAbs presents the higher inhibition rate than anti-EaMIC2 and anti-EaMIC5 pAb **(A)**. The treatment of anti-EmMIC pAbs exerts much stronger inhibitory activity than anti-EmMIC2 and anti-EmAMA1 pAbs **(B)**. The treatment of anti-EmiMIC3 pAbs was a more potent inhibitor of *E mitis* sporozoite invasion in the lower intestines **(C)**. EaMIC3-MAR3 serum exhibited the highest inhibitory activity in the invasion of *E acervulina* sporozoites **(D)**. Both anti-EmMIC3-MAR1 and anti-EmMIC3-MAR2 pAbs could inhibit *E maxima* sporozoite invasion in cultured mid intestines, and more robust inhibitory activity was observed with EmMIC3-MAR2 antibody compared with EmMIC3-MAR1 antibody in the inhibition experiments **(E)**. The significant inhibition of *E mitis* sporozoite invasion in the lower intestines following the treatment of EmiMIC3-MAR4 antibody **(F)**. The significant difference was shown with different letters ($p < 0.05$).

domain to construct chimeric EaMIC3-EtMIC3 and EtMIC3-EaMIC3 proteins (Figure 7A) for comparison studies. The immunohistochemical assay indicated that, unlike EtMIC3 with a MAR1b domain which primarily binds to the caecum, EtMIC3-EaMIC3 with a unique EaMIC3-MAR3 domain could solely give a robust binding to the upper intestine (Figure 7B, a1). Besides, instead of binding to the upper intestine, EaMIC3-EtMIC3 protein with a particular EtMIC3-MAR1b domain can bind to the caecum only (Figure 7B, b4). Notably, all these observations suggested that without the core MAR domain, either EaMIC3 or EtMIC3 would lose binding specificity to host tissues. Collectively, the EaMIC3-MAR3 domain indeed contributed to EaMIC3-mediated tissue tropisms for *E. acervuline* within the gut of chicken.

EmiMIC3-MAR4 elicited partial protection against *Eimeria mitis* infection

To explore whether immunization with EmiMIC3, EmiMIC3-MAR4, and EmiMIC3-MAR5 could induce protection against *E. mitis* infection, we performed active and passive immunization trials in chickens. The protective efficacy of recombinant EmiMIC3, EmiMIC3-MAR4, and EmiMIC3-MAR5 and their pAbs were described in Tables 1 and 2, respectively. In the active vaccination trial, compared to the challenge control group, birds immunized with recombinant EmiMIC3, EmiMIC3-MAR4, and EmiMIC3-MAR5 had much-improved body weight gains ($P < 0.05$) (Table 1). Following the challenge with *E. mitis* oocysts, there was a statistically significant reduction in oocyst shedding in EmiMIC3-vaccinated, EmiMIC3-MAR4-vaccinated, and EmiMIC3-MAR5-vaccinated groups of birds compared to challenged control groups ($P < 0.05$) (Table 1). It was noted that the EmiMIC3 protein conferred substantially higher protection efficacy than EmiMIC3-MAR4 and EmiMIC3-MAR5 ($P < 0.05$) (Table 1), and EmiMIC3-MAR4 was more potent in inducing protection against *E. mitis* than EmiMIC3-MAR5 ($P < 0.05$) (Table 1). In the passive immunization trial, a similar protection pattern was observed. Immunization with antibodies against EmiMIC3, EmiMIC3-MAR4, and EmiMIC3-MAR5 elicited encouraging levels of protection in *E. mitis*-challenged birds, as instanced by much better body weight gain ($P < 0.05$) and reduced oocyst output ($P < 0.05$) in the feces compared to challenged controls (Table 2).

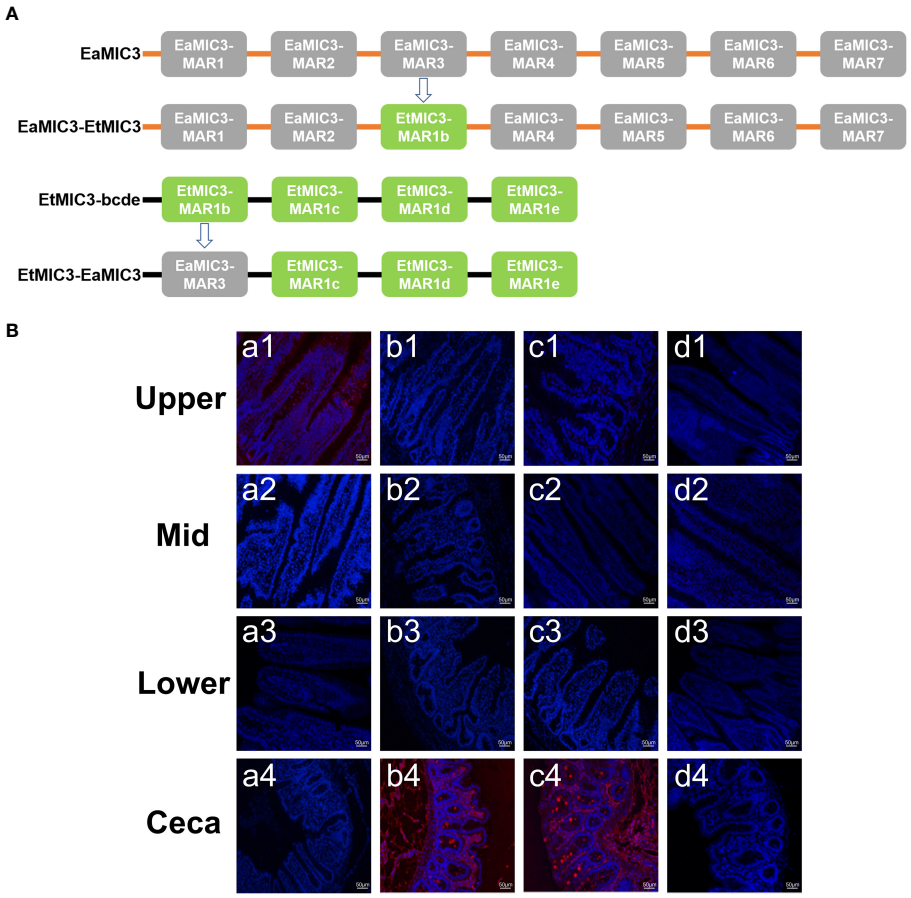

FIGURE 7
Binding capacity of chimeric proteins to different intestine segments. The structure of EaMIC3-EtMIC3 and EtMIC3-EaMIC3 **(A)**. The upper, mid, lower intestine, and caecum were removed from 2-week-old chicken. The immunohistochemical assay indicated that unlike EtMIC3 with a MAR1b domain which primarily binds to the caecum, EtMIC3-EaMIC3 with a unique EaMIC3-MAR3 domain could solely give a robust binding to the upper intestine **(B)**, a1). Instead of binding to the upper intestine, EaMIC3-EtMIC3 with a particular EtMIC3-EaMIC3 domain can bind to the caecum only **(B)** b4. EtMAR1b can bind to the caecum only **(B)** c4. pET-32a can not bind to any intestinal tissues **(B)**, d1-d4. Scale bars: 50 μm.

10.3389/fimmu.2023.1291379

Discussion

The distinct host and tissue tropisms of chicken coccidia parasites have been an unresolved debate in poultry studies, with far-reaching implications for understanding the invasion machinery of these parasites and developing novel therapeutics. Unlike *T. gondii* and *N. caninum* which can infect any warm-blooded nucleated cells, the vast majority of *Eimeria* spp., including all of the economically important ones that cause disease in poultry, replicate only within epithelial enterocytes of the different host intestinal tracts, by contrast (9). In recent years, slow but significant progress has been made to reveal the molecular basis for the site specificity of *Eimeria* parasites, and various molecules contributing to cell recognition and invasion, such as MICs, have been identified. Still, research on how *Eimeria* parasites build their invasion machinery lags far behind that of *Toxoplasma*, in addition to *Plasmodium*. Of all seven chicken coccidia parasites, the invasion machinery of *E. tenella* was best studied, and detailed characterization of EtMIC repertoire was carried out from structural and functional aspects, mainly for EtMIC3. However, limited investigations on MICs of other chicken *Eimeria* parasites have hindered the elucidation of their specific molecular interactions with hosts and the characterization of their roles at the host-parasite interface. Thus, it has prompted our group to further study EaMICs, EmMICs, and EmiMICs to find rationalization of differing host and tissue tropisms for *E. acervuline*, *E. maxima*, and *E. mitis*. We compared binding profiles of varying EaMICs, EmMICs, and EmiMICs to host intestines and determined the key MAR domain from EaMIC3, EmMIC3, and EmiMIC3 in MIC biology to demonstrate the molecular basis for host tissue tropisms of *E. acervuline*, *E. maxima*, and *E. mitis*.

MICs released from the secretory organelles mediate the initial specific high-affinity interaction between host cells and apicomplexan parasites and play an important role in host cell recognition and attachment. They are critically involved in the invasion process of apicomplexan parasites, allowing parasites to target a diverse range of cell surface oligosaccharide epitopes. Therefore, the host specificity and tissue tropism of apicomplexan parasites appear to be associated with the repertoire and specificity of the MICs that they produce. A family of MICs has been characterized in *E. acervuline*, *E. maxima*, and *E. mitis*, respectively, including seven EaMICs, six EmMICs, and five EmiMICs. Given that *E. acervuline*, *E. maxima*, and *E. mitis* exert distinct tissue tropisms (*E. acervuline* invades the upper intestine; *E. maxima* develops within the mid intestine; *E. mitis* parasitizes the lower intestine) and EaMICs, EmMICs, and EmiMICs are likely to be major determinants for this; therefore, we determined the binding specificity of EaMICs, EmMICs, and EmiMICs to different gut segments in this study. The immunohistochemical assay revealed a restricted tissue staining pattern: of all EaMICs, only EaMIC3 could bind to sections of the upper intestine; EmMIC3 could solely bind to the mid intestine, whereas other EmMICs showed no binding to any intestinal tissues; EmiMIC3 was the only EmiMIC that could bind to the lower intestine. All the tissue binding profiles suggested that EaMIC3, EmMIC3, and EmiMIC3, respectively, may play a key role in directing *E. acervuline*, *E. maxima*, and *E. mitis* to their specific parasitism location. Taking that the deployment of EtMIC3 governs host cell recognition and attachment into account, we speculated that all the MIC3s of *Eimeria* play a dominant role in determining the site specificity of different *Eimeria* parasites during the invasion. However, it warrants further investigation.

MICs are characterized by their composition of a modular arrangement of adhesive domains, such as the Apple/PAN motif, epidermal growth factor (EGF-like) domain, Galectin-like domain,

TABLE 1 Protective efficacy of recombinant EmiMIC3, EmiMIC3-MAR4 and EmiMIC3-MAR5 proteins against challenge infection with *E. mitis*.

Groups	Average body weight gains (g)	Oocyst output (lg)	Oocyst decrease ratio (%)
Unchallenged control	84.90 ± 6.25^{d}	0.00 ± 0.00^{a}	100
pET-32a protein control	19.29 ± 6.74^{a}	4.34 ± 1.22^{c}	28.14
Recombinant EmiMIC3 protein	74.75 ± 1.71^{c}	1.59 ± 0.23^{b}	73.67
Recombinant EmiMIC3-MAR4 protein	70.89 ± 4.65^{bc}	2.06 ± 0.90^{b}	65.89
Recombinant EmiMIC3-MAR5 protein	65.76 ± 5.04^{b}	3.47 ± 0.55^{b}	42.54
Challenged control	19.11 ± 7.18^{a}	6.04 ± 2.26^{d}	0.00

The difference ($p < 0.05$) between groups is shown in each column with different letters.

TABLE 2 Protective efficacy of recombinant EmiMIC3, EmiMIC3-MAR4 and EmiMIC3-MAR5 protein polyclonal antibodies against challenge infection with *E. mitis*.

Groups	Average body weight gains(g)	Oocyst output (lg)	Oocyst decrease ratio (%)
Unchallenged control	67.35 ± 7.16^{c}	0.00 ± 0.00^{a}	100
pET-32a protein polyclonal antibody control	23.73 ± 4.83^{a}	3.97 ± 1.26^{b}	3.40
Recombinant EmiMIC3 protein polyclonal antibody	63.84 ± 6.33^{bc}	1.04 ± 0.23^{a}	74.45
Recombinant EmiMIC3-MAR4 protein polyclonal antibody	53.28 ± 5.96^{bc}	1.73 ± 0.55^{a}	58.04
Recombinant EmiMIC3-MAR5 protein polyclonal antibody	45.77 ± 5.16^{b}	1.74 ± 0.46^{a}	57.6
Challenged control	20.81 ± 6.11^{a}	4.11 ± 0.78^{b}	0.00

The difference ($p < 0.05$) between groups is shown in each column with different letters.

Type I like repeats (TSR-like) domain, and MAR domain, which were responsible for the entry of parasites into host cells (9). Of note, the MAR domain that governs interaction with host ligands has been shown to be restricted to coccidial parasites. As a result, for *Eimeria* spp., sequence and structural variations of MAR domains lead to variant capacities for sialyl ligand binding, which account for the divergence in host and site specificities of apicomplexan parasites. There are seven MAR domains for EaMIC3, five MAR domains for EmMIC3, and nine MAR domains for EmiMIC3. Multiple sequence alignment revealed that each of EaMIC3-MARs, EmMIC3-MARs, and EmiMIC3-MARs contains seven cysteine residues, with the exception of an incomplete repeating sequence. These cysteine residues might play a role in forming the disulfide bond in *E. acervulina*, *E. maxima*, and *E. mitis*, respectively. The presence of multiple disulfide bonds stabilizes the core structure and enhances the stability of the protein molecule against external influences. By conducting a comparative analysis of the amino acid sequences of the MAR domains of three *Eimeria* species, we discovered that each complete MAR domain possesses a relatively conserved type I MAR structure, characterized by the presence of the HxT/HxS and LxxY motifs. The LxxY motif, which takes the form of an α1 helix/loop structure, plays a crucial role in facilitating interactions between the MAR domain and sialyl saccharides, while simultaneously preventing contact with N-hydroxylacetyl sialic acid. As a result, this motif contributes significantly to the specificity of the EaMIC3-MAR, EmMIC3-MAR, and EmiMIC3-MAR domains in their binding. The HxT/HxS motif, on the other hand, operates through hydrogen bonding and π-stacking with conserved histidine and threonine residues, modulating binding to sialic acid polysaccharides. This recognition pattern of sialic acids is similar to that observed in other pathogen lectins, suggesting that the HxT/HxS motif also contributes to the binding properties of EaMIC3-MARs, EmMIC3-MARs, and EmiMIC-MARs. In this study, we further compared the binding capabilities of these EaMIC3-MARs, EmMIC3-MARs, and EmiMIC3-MARs to host intestinal tissues. Of all EaMIC3-MARs, EaMIC3-MAR3 showed significant binding to the upper intestines, and EmMIC3-MAR2 gave the most robust binding to the mid intestines among the five EmMIC3-MARs. Besides, EmiMIC3-MAR4 had a more robust binding to the lower intestines than other EmiMIC3-MARs. All these binding patterns suggested the predominant roles of EaMIC3-MAR3, EmMIC3-MAR2, and EmiMIC3-MAR4 in the tissue binding mediated by EaMIC3, EmMIC3-MAR2, and EmiMIC3, respectively. With the aim to confirm this, we next carried out cell-based binding ELISA assays. The results showed that all EaMIC3-MARs, EmMIC3-MARs, or EmiMIC3-MARs could interact with intestinal epithelial cells, but the binding capacity of each MAR domain varied. Consistent with the observation from the IFA assays, among these different MAR domains, EaMIC3-MAR3 of *E. acervulina*, EmMIC3-MAR2 of *E. maxima*, and EmiMIC3-MAR4 of *E. mitis* also exerted the highest binding capacity.

In this study, to further understand the restricted binding properties of EaMIC3-MAR3, EmMIC3-MAR2, and EmiMIC3-MAR4, chimeric EaMIC3-EtMIC3 or EtMIC3-EaMIC3 proteins were constructed by substituting the EtMIC3-MAR1b or EaMIC3-MAR3 domains in EaMIC3 or EtMIC3, respectively. Results from the intestinal tissue binding experiment with the chimeric proteins showed that EtMIC3-EaMIC3 with an EaMIC3-MAR3 domain was able to bind to the upper intestine of a chicken but not to the cecum. Conversely, EaMIC3-EtMIC3 with an EtMIC3-MAR1b domain exhibited robust binding to the cecum but lost its ability to interact with the host's upper intestine. These findings demonstrate the crucial role of the MAR domains in governing interaction with host cells and indicate that, in *E. acervuline*, the specificity of the EaMIC3 function is largely determined by the EaMIC3-MAR3 domain. In addition to domain substitution tests, we also evaluated the efficacy of MIC and MAR antibodies in blocking sporozoite invasion mediated by MICs or MARs. Our findings showed that *E. acervulina* sporozoites that invade the upper intestine of chickens could be effectively blocked with EaMIC3 antiserum. While EaMIC2 and EaMIC5 antisera also exhibit some inhibitory effects, they are not as potent as EaMIC3. The pathogenicity of *E. maxima* sporozoites was found to be effectively inhibited by EmMIC3 antiserum when compared with EmMIC2 and EmAMA1 antisera. Similarly, EmiMIC3 antiserum showed promising efficacy in restricting the invasion of *E. mitis* sporozoites to the lower intestine compared to EmiMIC2, EmiEtmic2/7h, and EmiAMA1 antisera. A similar trend was observed with the use of anti-MAR antibodies, with EaMIC3-MAR3, EmMIC3-MAR2, and EmiMIC3-MAR4 antisera exhibiting the highest inhibitory effects. In particular, rat anti-EmMIC3-MAR2 was found to be the most effective in blocking the invasion of *E. maxima* sporozoites, thus indicating that EmMIC3-MAR2 may play a crucial role in the entire invasion process. The ability of *E. acervuline* or *E. mitis* sporozoites to invade was significantly impaired when they were treated with rat anti-EaMIC3-MAR3 or anti-EmiMIC3-MAR4 antibodies, making EaMIC3-MAR3 or EmiMIC3-MAR4 the most active of the seven EaMIC3-MARs or nine EmiMIC3-MARs.

Animal experiments have demonstrated the significant role of MICs and MARs in conferring immunity. The EaMIC3 protein was found to be present in the sporozoite stage and located at the apical tip of the sporozoite. Immunization with recombinant EaMIC3 was shown to stimulate strong Th1 immune responses against *E. acervuline* infection and significantly improve weight gain while reducing mortality (25). Similarly, vaccination with recombinant EmiMIC3 protein resulted in reduced weight loss and decreased oocyst output in chickens infected with *E. mitis* (32). The use of *Salmonella typhimurium* X4550 carrying two EtMIC3-C-MAR domains as a live attenuated vaccine showed promising results in terms of improving immunogenic protection in the host (39). The current study investigated the protective efficacies of the EmiMIC3, EmiMIC3-MAR4, and EmiMIC3-MAR5 proteins and their polyclonal antibodies. The results indicated that chickens immunized with EmiMIC3-MAR5 and EmiMIC3-MAR4 elicited comparatively better protection. The protective effects of EaMIC3-MAR3 and EaMIC3-MAR6 from *E. acervulina* were also demonstrated, with EaMIC3-MAR3 exhibiting the best binding capacity to the upper section of the intestine and providing improved immunoprotective efficacy (40).

To conclude, our findings suggested that EaMIC3, EmMIC3, and EmiMIC3 play crucial roles in the site specificity of *E. acervulina*, *E. maxima*, and *E. mitis*, respectively, and EaMIC3-MAR3, EmMIC3-MAR2, and EmiMIC3-MAR4 are the underlying factors behind their

variable tissue tropisms. The results provided valuable insights into the modes of action of *Eimeria* MICs on a molecular basis, thus offering a rational explanation for the distinct tissue tropisms observed across *E. acervuline*, *E. maxima*, and *E. mitis*.

Materials and methods

Ethics statement

Animal experiments were conducted in strict accordance with the guidelines of the Animal Welfare and Ethical Review Board of Nanjing Agricultural University, China. All animal studies and protocols were evaluated and approved by the Institutional Animal Care and Use Committee of Nanjing Agricultural University (Approval number: 2012CB120750).

Parasites and animals

E. acervulina Nanjing strain, *E. maxima* Nanjing strain, and *E. mitis* Nanjing strain were obtained and propagated in conditions as previously described (25, 30, 32). New-born Hy-Line layer chickens were raised under coccidia-free conditions. The chickens were provided with anticoccidial drug-free feed and water. SD rats of 30 days old were purchased from the Comparative Medicine Center of Yangzhou University (Yangzhou, China) and kept in specific-pathogen-free conditions for antiserum collection.

Sequence alignment and three-dimensional structure analysis of MIC3-MARs of *Eimeria acervulina*, *Eimeria maxima*, and *Eimeria mitis*

The full sequence of the *EmMIC3* gene was obtained using the rapid-amplification of cDNA ends (RACE) method with the forward gene-specific primers (Table S1) as previously described (24). The complete open reading frame (ORF) of EmMIC3 was submitted to GenBank under Accession No. KU93609. All the MARs identified in EaMIC3 (AMN15064.1), EmMIC3 (AOY42085.1), and EmiMIC3 (AXC32915.1) were analyzed using NCBI (https://www.ncbi.nlm.nih.gov/nuccore). Clustal X and ESPript 3 (http://espript.ibcp.fr/ESPript/ESPript/) were used to align the sequences of MARs of *E. acervulina*, *E. maxima*, and *E. mitis*. The pyMOL software (Version 2.5.4) was employed to construct the three-dimensional structures of the MAR3 of EaMIC3 (EaMIC3-MAR3), MAR2 of EmMIC3 (EmMIC3-MAR2) and MAR4 of EmiMIC3 (EmiMIC3-MAR4).

Productions of recombinant proteins of MICs and MARs

The ORFs of *EaMIC2*, *EaMIC3*, *EaMIC5*, *EmMIC2*, *EmMIC3*, *EmAMA1*, *EmiMIC2*, *EmiMIC3*, *EmiAMA1*, and *EmiEtmic-2/7* genes were amplified by PCR using specific primers designed according to available mRNA sequences of EaMIC2 (KR063282), EaMIC3 (KU359773), EaMIC5 (KF922373), EmMIC2 (FR718971.1), EmMIC3 (KU93609), EmAMA1 (FN813221.1), EmiMIC2 (XM013494084.1), EmiMIC3 (MG888670.1), EmiAMA1 (XM013496458.1) and EmiEtmic-2/7 (CDJ36057.1). The primers are listed in Table S2. Corresponding MAR domains of EaMIC3 (EaMIC3-MARs), EmMIC3 (EmMIC3-MARs), and EmiMIC3 (EmiMIC3-MARs) were then amplified by PCR using specific primers (Table S3). The ORFs of EaMIC2, EaMIC3, EaMIC5, EmMIC2, EmMIC3, EmAMA1, EmiMIC2, EmiMIC3, EmiAMA, EmiEtmic-2/7, EaMIC3-MARs, EmMIC3-MARs, EmiMIC3-MARs and were each ligated into the pET-32a plasmid (Sigma-Aldrich, St. Louis, MO) and expressed in *Escherichia coli* BL21 (DE3) (Sigma-Aldrich). Subsequently, the expressed recombinant proteins were purified by His-Trap columns (GE Healthcare, Piscataway, NJ) using previously described strategies (29). Purified proteins were then stored at -80°C until further analysis. Meanwhile, the fusion proteins of pET-32a used as mock control were also prepared with the same procedure.

Productions of chimeric proteins EaMIC3-EtMIC3 and EtMIC3-EaMIC3

To specify tissue tropism characteristics of *E. acervulina*, two chimeric proteins, namely EaMIC3-EtMIC3 and EtMIC3-EaMIC3, were generated. EaMIC3-EtMIC3 protein was produced by the replacement of EaMIC3-MAR3 fragments with the EtMIC3-MAR1b domain. As a result, EaMIC3-EtMIC3 comprised sequences encompassing EaMIC3-MAR1, EaMIC3-MAR2, EtMIC3-MAR1b, EaMIC3-MAR4, EaMIC3-MAR5, EaMIC3-MAR6, and EaMIC3-MAR7. Likewise, the chimeric EtMIC3-EaMIC3 was constructed by replacing the EtMIC3-MAR1b domain with EaMIC3-MAR3 residues; therefore, it consisted of the sequences of EaMIC3-MAR3, EtMIC3-MAR1c, EtMIC3-MAR1d, and EtMIC3-MAR1e. Specific primers used to construct the chimeric MICs are listed in Table S4. Chimeric EaMIC3-EtMIC3 and EtMIC3-EaMIC3 constructs were cloned into the pET-32a expression vector, and recombinant EaMIC3-EtMIC3 and EtMIC3-EaMIC3 proteins were then obtained as stated above.

Generations of polyclonal antibodies against recombinant proteins

Rat pAbs against rEaMIC2, rEaMIC3, rEaMIC5, rEmMIC2, rEmMIC3, rEmAMA1, rEmiMIC2, rEmiMIC3, rEmiAMA1, rEmiEtmic-2/7, rEaMIC3-MARs, rEmMIC3-MARs, rEmiMIC3-MARs, rEtMIC3-MARs, and pET-32a tag protein were each prepared as previously described (41). Briefly, purified recombinant proteins (200 μg) were emulsified with complete Freund's adjuvant (Sigma-Aldrich) thoroughly, and the first injection was administered to SD rats. Two weeks later, proteins (200 μg) emulsified with incomplete Freund's adjuvant (Sigma-Aldrich) were given as the second immunization. Later on, the third and fourth administrations were given at a 7-day interval as above.

The rats were bled for serum collection seven days after the last injection. Small aliquots of antiserum were stored at -20°C for further usage.

Binding profiles of MICs and MARs to small intestine and caecum

The binding abilities of recombinant MICs and MARs to the upper, mid, and lower intestine and caecum were evaluated by the immunofluorescence assay (IFA). Varying small intestine samples (3 cm in length), including upper intestine (5 cm from the stomach), mid intestine (revolving around yolk stalk), and lower intestine (5 cm from recta), as well as caecum tissues, were removed immediately from 2-week-old Hy-Line layer chickens post-mortem. They were fixed in 4% paraformaldehyde and subsequently subjected to dehydration, paraffin embedding, and sectioning (10 μm). To minimize non-specific staining, sections were blocked overnight with 5% bovine serum albumin (BSA, Sigma-Aldrich) in tris-buffered saline with Tween 20 (TBST). The recombinant proteins of MICs and MARs (5μg/mL for each) were incubated with the sections of the upper, mid, and lower intestines and caecum for 30 min at room temperature, respectively. Sections were washed 3 times with TBST and then incubated with rat sera against MICs and MARs of *E. acervulina*, *E. maxima*, and *E. mitis* (1:100 in dilution) for 1 h, respectively. After washing 3 times, sections were incubated with goat anti-rat Alexa Fluor 568 second antibody (red) and later incubated with 4,6-diamidino-2-phenylin-dole (DAPI; blue). After three washes, the slides were mounted with coverslips and analyzed under a laser confocal microscope (Zeiss LSM 710, Germany). The comparison of the binding capability to the upper, mid, and lower small intestines was carried out among different MICs of *E. acervulina* (EaMIC2, EaMIC5, and EaMIC3), *E. maxima* (EmMIC3, EmMIC2, and EmAMA1), and *E. mitis* (EmiMIC3, EmiMIC2, EmiAMA1, and EmiEtmic-2/7), respectively. Meanwhile, the differences in the binding capability of seven MARs of *E. acervulina*, five MARs of *E. maxima*, and nine MARs of *E. mitis* were also investigated.

Cell binding assay

Cell ELISA was carried out to determine the interaction between MARs and host intestinal epithelial cells. The samples (10 cm in length) of the upper, mid, and lower intestines were collected from 2-week-old chickens. The isolation and cultivation of intestinal epithelial cells of chickens were conducted using a standard procedure as described elsewhere (42, 43). Purified intestinal epithelial cells were seeded in 96-well high-binding culture plates and then incubated with recombinant MARs (0 μg/ml to 100 μg/ml) for 1 h at 41°C with 5% CO_2. After the centrifuge, cell culture fluid was discarded, and the cells were washed three times with phosphate buffer saline (PBS). Cells were fixed in 4% paraformaldehyde for 10 min at room temperature. After three washes in TBST, cells were blocked with 4% BSA in TBST for 1 h. Subsequently, cells were incubated with rat anti-EaMIC3, -EmMIC3, or -EmiMIC3 serum (1:500 in dilution) for 1 h, respectively. After three washes with TBST, cells were incubated with Horseradish Peroxidase (HRP)-conjugated goat anti-rat IgG (Bioworld, Nanjing, Jiangsu, China) for 1 h. After washing, 3,3',5,5'-Tetramethylbenzidine (TMB; Sigma-Aldrich) were added in the dark at room temperature for 5min. The reaction was stopped with 2 mol/L H_2SO_4, and the values were measured at 450nm (OD_{450}) with an automated ELISA reader (Thermo Multiskan™ FC, USA).

Binding profiles of chimeric proteins to small intestine and caecum

The effects of MAR substitutions on the abilities of chimeric EaMIC3-EtMIC3 and EtMIC3-EaMIC3 proteins to bind to the intestine were also analyzed by IFA assays as above. Recombinant proteins of EaMIC3-EtMIC3, EtMIC3-EaMIC3, and EtMIC3-MAR1b were incubated with the sections of the upper, mid, and lower intestines and caecum, respectively. For EtMIC3-EaMIC3 and EtMIC3-MAR1b, rat anti-EtMIC3 (1:100 in dilution) was used for the determination of binding, whereas for EaMIC3-EtMIC3, rat anti-EaMIC3 (1:100 in dilution) was used for IFA assays.

Inhibition experiments

The effects of antiserum against MICs and MARs on the invasion of sporozoites into the intestinal epithelial cells were determined using an *in vitro* inhibition assay. The collection and purification of sporozoites were carried out as previously described (44). Purified sporozoites were blocked by varying pAbs with a final antibody titer of 2^{10} in 10mL PBS for 30 min at 4°C by gently rotating. For *E. acervulina* sporozoites, they were treated with rat anti-EaMIC2, -EaMIC3, -EaMIC5, and -EaMIC3-MARs pAbs, respectively. The sporozoites of *E. maxima* were treated with rat anti-EmMIC2, -EmMIC3, -EmAMA1, and -EmMIC3-MARs pAbs, respectively, while *E. mitis* sporozoites were blocked with rat anti-EmiMIC3, -EmiMIC2, -EmiEtmic2/7h, -EmiAMA1 or -EmiMIC3-MARs pAbs, respectively. Sporozoites blocked with control rat serum and PBS were set as controls. After three washes with PBS, sporozoites were resuspended in 2mL PBS. The upper, mid, and lower intestine segments (5 cm in length) were taken immediately from 2-week-old Hy-Line layer chickens post-mortem and soaked in preheated Hanks Balanced Salt Solution (HBSS; Gibco, Grand Island, NY) (41°C) with one end of each intestine segment ligatured. Pretreated sporozoites (1×10^7) of *E. acervulina*, *E. maxima*, and *E. mitis* in 2mL PBS were poured into the upper, mid, and lower intestine segments, respectively. After ligating another end of intestine segments, intestine samples were incubated in PBS with gentle shaking at 41°C for 15 min. The sporozoites within the intestinal lumen (not entered into the intestinal epithelial cells) were collected after PBS washing three times. The number of sporozoites collected from the intestine lumen was counted by McMaster's method (45).

Immunoprotective effect of the MIC3 and MARs vaccines of *Eimeria mitis* in chickens

The protective roles of EmiMIC3, EmiMIC3-MAR4 (the strongest binding capacity with lower intestine), and EmiMIC3-MAR5 (the weakest binding capacity with lower intestine) against *E. mitis* were evaluated using challenge infection models. Two-week-old coccidia-free chickens with similar weight were randomly divided into six groups (20 birds/group), as shown in Table 1. The chickens were immunized intramuscularly with 200 μg of rEmiMIC3, rEmiMIC3-MAR4, or rEmiMIC3-MAR5 proteins. Control birds were immunized with an equal volume of PBS or pET-32a tagged protein. One week after primary immunization, the chickens were given a booster immunization. Seven days after the booster immunization, chickens were orally challenged with 1×10^5 *E. mitis* oocysts per bird except for the unchallenged chicken. Seven days post-challenge, all the chickens were euthanized for the collection of intestine samples.

For passive immunization trials, twenty-eight-day-old coccidia-free chickens with similar weight were randomly divided into six groups (20/group), as presented in Table 2. The birds were orally challenged with 1×10^5 *E. mitis* oocysts, while unchallenged chickens were inoculated with sterile PBS. The chickens were immunized intravenously with anti-EmiMIC3, anti-EmiMIC3-MAR4, or anti-EmiMIC3-MAR5 pAbs for up to seven days. Each bird was injected with 0.5 mL of antiserum. All the chickens were euthanized by cervical dislocation on day 8 of immunization.

The immunoprotective roles of EaMIC3, EaMIC3-MAR3, and EaMIC3-MAR6 of *E. acervulina*, and EmMIC3, EmMIC3-MAR2, and EmMIC3-MAR5 of *E. maxima* were evaluated by the previous research in our lab (40, 46).

Statistics analysis

GraphPad Prism 6.0 (GraphPad Software, USA) and SPSS 19 (SPSS Software, IBM, USA) were used to calculate the *p*-Values. The comparison was performed using the one-way analysis of variance (ANOVA) corrected by Dunnett's tests. The expression levels were denoted as mean ± standard deviation (SD).

Data availability statement

The original contributions presented in the study are included in the article/Supplementary Material. Further inquiries can be directed to the corresponding author.

Ethics statement

The animal study was approved by Animal experiments were conducted in strict accordance with the guidelines of the Animal Welfare and Ethical Review Board of Nanjing Agricultural University, China. All animal studies and protocols were evaluated and approved by the Institutional Animal Care and Use Committee of Nanjing Agricultural University (Approval number: 2012CB120750). The study was conducted in accordance with the local legislation and institutional requirements.

Author contributions

YZ: Conceptualization, Data curation, Investigation, Writing – original draft. ML: Conceptualization, Writing – review & editing. ZZ: Investigation, Writing – review & editing. XH: Investigation, Writing – review & editing. JWH: Investigation, Writing – review & editing. JL: Investigation, Writing – review & editing. JMH: Software, Writing – review & editing. XS: Conceptualization, Writing – review & editing. LX: Conceptualization, Writing – review & editing. RY: Conceptualization, Writing – review & editing. XL: Conceptualization, Funding acquisition, Writing – review & editing.

Funding

The author(s) declare financial support was received for the research, authorship, and/or publication of this article. This work was supported by the National Natural Science Foundation of China (Grant No. 31372428), the Joint Research Project between National Natural Science Foundation of China and Pakistan Science Foundation (NSFC-PSF) (Grant No. 31661143017) and the Youth Science Fund of National Natural Science Foundation of China (Grant No. 32202837).

Conflict of interest

The authors declare that the research was conducted in the absence of any commercial or financial relationships that could be construed as a potential conflict of interest.

Publisher's note

Supplementary material

The Supplementary Material for this article can be found online at: https://www.frontiersin.org/articles/10.3389/fimmu.2023.1291379/full#supplementary-material

SUPPLEMENTARY FILE 1

Binding of EaMIC3-MARs to fixed upper intestinal epithelial cells determined by ELISA. The upper intestinal epithelial cells were isolated and cultivated from 2-week-old chickens. The chicken upper epithelial cells were co-cultured respectively with the recombinant EaMIC3-MARs. The final concentration of every protein were 12.5 μg/mL **(A)**, 25 μg/mL **(B)**, 50 μg/mL **(C)**, and 100 μg/mL **(D)**. Among different MARs, the significant difference within the group was shown by different letters ($p < 0.05$).

SUPPLEMENTARY FILE 2

Binding of EmMIC3-MARs to fixed mid intestinal epithelial cells determined by ELISA. The mid intestinal epithelial cells were isolated and cultivated from 2-week-old chickens. The chicken mid intestinal epithelial cells were co-cultured respectively with the recombinant EmMIC3-MARs. The final concentration of every protein were 12.5 μg/mL **(A)**, 25 μg/mL **(B)**, 50 μg/mL **(C)**, and 100 μg/mL **(D)**. Among different MARs, the significant difference within the group was shown by different letters ($p < 0.05$).

SUPPLEMENTARY FILE 3

Binding of EmiMIC3-MARs to fixed lower intestinal epithelial cells determined by ELISA. The lower intestinal epithelial cells were isolated and cultivated from 2-week-old chickens. The chicken lower intestinal epithelial cells were co-cultured respectively with the recombinant EmiMIC3-MARs. The final concentration of every protein were 12.5 μg/mL **(A)**, 25 μg/mL **(B)**, 50 μg/mL **(C)**, and 100 μg/mL **(D)**. Among different MARs, the significant difference within the group was shown by different letters ($p < 0.05$).

References

1. Blake DP, Tomley FM. Securing poultry production from the ever-present *Eimeria* challenge. *Trends Parasitol* (2014) 30(1):12–9. doi: 10.1016/j.pt.2013.10.003

2. Smith MK, Buhr DL, Dhlakama TA, Dupraw D, Fitz-Coy S, Francisco A, et al. Automated enumeration of *Eimeria* oocysts in feces for rapid coccidiosis monitoring. *Poult Sci* (2023) 102(1):102252. doi: 10.1016/j.psj.2022.102252

3. Blake DP, Knox J, Dehaeck B, Huntington B, Rathinam T, Ravipati V, et al. Re-calculating the cost of coccidiosis in chickens. *Vet Res* (2020) 51(1):115. doi: 10.1186/s13567-020-00837-2

4. El-Shall NA, Abd El-Hack ME, Albaqami NM, Khafaga AF, Taha AE, Swelum AA, et al. Phytochemical control of poultry coccidiosis: a review. *Poult Sci* (2022) 101(1):101542. doi: 10.1016/j.psj.2021.101542

5. Quiroz-Castañeda RE, Dantán-González E. Control of avian coccidiosis: future and present natural alternatives. *BioMed Res Int* (2015) 2015:430610. doi: 10.1155/2015/430610

6. Burrell A, Tomley FM, Vaughan S, Marugan-Hernandez V. Life cycle stages, specific organelles and invasion mechanisms of *Eimeria* species. *Parasitology* (2020) 147(3):263–78. doi: 10.1017/s0031182019001562

7. Jeurissen SH, Janse EM, Vermeulen AN, Vervelde L. *Eimeria tenella* infections in chickens: aspects of host-parasite: interaction. *Vet Immunol Immunopathol* (1996) 54(1-4):231–8. doi: 10.1016/s0165-2427(96)05689-9

8. Carruthers VB. Armed and dangerous: *Toxoplasma gondii* uses an arsenal of secretory proteins to infect host cells. *Parasitol Int* (1999) 48(1):1–10. doi: 10.1016/s1383-5769(98)00042-7

9. Cowper B, Matthews S, Tomley F. The molecular basis for the distinct host and tissue tropisms of coccidian parasites. *Mol Biochem Parasitol* (2012) 186(1):1–10. doi: 10.1016/j.molbiopara.2012.08.007

10. Chapman HD. Milestones in avian coccidiosis research: a review. *Poult Sci* (2014) 93(3):501–11. doi: 10.3382/ps.2013-03634

11. Sharma P, Chitnis CE. Key molecular events during host cell invasion by Apicomplexan pathogens. *Curr Opin Microbiol* (2013) 16(4):432–7. doi: 10.1016/j.mib.2013.07.004

12. López-Osorio S, Chaparro-Gutiérrez JJ, Gómez-Osorio LM. Overview of poultry *eimeria* life cycle and host-parasite interactions. *Front Vet Sci* (2020) 7:384. doi: 10.3389/fvets.2020.00384

13. Parker ML, Penarete-Vargas DM, Hamilton PT, Guérin A, Dubey JP, Perlman SJ, et al. Dissecting the interface between apicomplexan parasite and host cell: Insights from a divergent AMA-RON2 pair. *Proc Natl Acad Sci U.S.A.* (2016) 113(2):398–403. doi: 10.1073/pnas.1515898113

14. Wang Y, Zhou X, Wang H, Sun L, Wang B, Jiang Y, et al. The role of *Eimeria tenella* EtCab protein in the attachment and invasion of host cells. *Vet Parasitol* (2021) 292:109415. doi: 10.1016/j.vetpar.2021.109415

15. Tomley FM, Clarke LE, Kawazoe U, Dijkema R, Kok JJ. Sequence of the gene encoding an immunodominant microneme protein of Eimeria tenella. *Mol Biochem Parasitol* (1991) 49(2):277–88. doi: 10.1016/0166-6851(91)90071-d

16. Tomley FM, Bumstead JM, Billington KJ, Dunn PP. Molecular cloning and characterization of a novel acidic microneme protein (Etmic-2) from the apicomplexan protozoan parasite, Eimeria tenella. *Mol Biochem Parasitol* (1996) 79(2):195–206. doi: 10.1016/0166-6851(96)02662-x

17. Brown PJ, Billington KJ, Bumstead JM, Clark JD, Tomley FM. A microneme protein from *Eimeria tenella* with homology to the Apple domains of coagulation factor XI and plasma pre-kallikrein. *Mol Biochem Parasitol* (2000) 107(1):91–102. doi: 10.1016/s0166-6851(00)00179-1

18. Labbé M, de Venevelles P, Girard-Misguich F, Bourdieu C, Guillaume A, Péry P. *Eimeria tenella* microneme protein EtMIC3: identification, localisation and role in host cell infection. *Mol Biochem Parasitol* (2005) 140(1):43–53. doi: 10.1016/j.molbiopara.2004.12.002

19. Periz J, Ryan R, Blake DP, Tomley FM. *Eimeria tenella* microneme protein EtMIC4: capture of the full-length transcribed sequence and comparison with other microneme proteins. *Parasitol Res* (2009) 104(3):717–21. doi: 10.1007/s00436-008-1301-0

20. Jiang L, Lin J, Han H, Dong H, Zhao Q, Zhu S, et al. Identification and characterization of *Eimeria tenella* apical membrane antigen-1 (AMA1). *PloS One* (2012) 7(7):e41115. doi: 10.1371/journal.pone.0041115

21. Zhao N, Ming S, Lu Y, Wang F, Li H, Zhang X, et al. Identification and application of epitopes in etMIC1 of *eimeria tenella* recognized by the monoclonal antibodies 1-A1 and 1-H2. *Infect Immun* (2019) 87(11):e00596-19. doi: 10.1128/iai.00596-19

22. Wang Q, Zhu S, Zhao Q, Huang B, Yu S, Yu Y, et al. Identification and characterization of a novel apical membrane antigen 3 in eimeria tenella. *J Eukaryot Microbiol* (2021) 68(2):e12836. doi: 10.1111/jeu.12836

23. Zhang Z, Huang J, Li M, Sui Y, Wang S, Liu L, et al. Identification and molecular characterization of microneme 5 of Eimeria acervulina. *PloS One* (2014) 9(12):e115411. doi: 10.1371/journal.pone.0115411

24. Zhang Z, Liu L, Huang J, Wang S, Lu M, Song X, et al. The molecular characterization and immune protection of microneme 2 of Eimeria acervulina. *Vet Parasitol* (2016) 215:96–105. doi: 10.1016/j.vetpar.2015.10.028

25. Zhang Z, Liu X, Yang X, Liu L, Wang S, Lu M, et al. The molecular characterization and immunity identification of microneme 3 of eimeria acervulina. *J Eukaryot Microbiol* (2016) 63(6):709–21. doi: 10.1111/jeu.12318

26. Pasamontes L, Hug D, Hümbelin M, Weber G. Sequence of a major *Eimeria maxima* antigen homologous to the *Eimeria tenella* microneme protein Etp100. *Mol Biochem Parasitol* (1993) 57(1):171–4. doi: 10.1016/0166-6851(93)90255-v

27. Witcombe DM, Belli SI, Wallach MG, Smith NC. Molecular characterisation of EmTFP250: a novel member of the TRAP protein family in Eimeria maxima. *Int J Parasitol* (2003) 33(7):691–702. doi: 10.1016/s0020-7519(03)00086-9

28. Li WC, Zhang XK, Du L, Pan L, Gong PT, Li JH, et al. *Eimeria maxima*: efficacy of recombinant Mycobacterium bovis BCG expressing apical membrane antigen1 against homologous infection. *Parasitol Res* (2013) 112(11):3825–33. doi: 10.1007/s00436-013-3570-5

29. Huang J, Zhang Z, Li M, Song X, Yan R, Xu L, et al. *Eimeria maxima* microneme protein 2 delivered as DNA vaccine and recombinant protein induces immunity against experimental homogenous challenge. *Parasitol Int* (2015) 64(5):408–16. doi: 10.1016/j.parint.2015.06.002

30. Huang J, Zhang Z, Li M, Song X, Yan R, Xu L, et al. Immune protection of microneme 7 (EmMIC7) against *Eimeria maxima* challenge in chickens. *Avian Pathol* (2015) 44(5):392–400. doi: 10.1080/03079457.2015.1071780

31. Huang J, Liu T, Li K, Song X, Yan R, Xu L, et al. Proteomic analysis of protein interactions between *Eimeria maxima* sporozoites and chicken jejunal epithelial cells by shotgun LC-MS/MS. *Parasit Vectors* (2018) 11(1):226. doi: 10.1186/s13071-018-2818-4

32. Huang X, Liu J, Tian D, Li W, Zhou Z, Huang J, et al. The molecular characterization and protective efficacy of microneme 3 of *Eimeria mitis* in chickens. *Vet Parasitol* (2018) 258:114–23. doi: 10.1016/j.vetpar.2018.06.020

33. Hoan TD, Zhang Z, Huang J, Yan R, Song X, Xu L, et al. Identification and immunogenicity of microneme protein 2 (EbMIC2) of Eimeria brunetti. *Exp Parasitol* (2016) 162:7–17. doi: 10.1016/j.exppara.2015.12.015

34. Carruthers VB, Tomley FM. Microneme proteins in apicomplexans. *Subcell Biochem* (2008) 47:33–45. doi: 10.1007/978-0-387-78267-6_2

35. Aquilini E, Cova MM, Mageswaran SK, Dos Santos Pacheco N, Sparvoli D, Penarete-Vargas DM, et al. An Alveolata secretory machinery adapted to parasite host cell invasion. *Nat Microbiol* (2021) 6(4):425–34. doi: 10.1038/s41564-020-00854-z

36. Bumstead, Janene M. *Eimeria tenella microneme protein 3: localisation and function during invasion*. Staffordshire, UK: University of Keele (2008).

37. Lai L, Bumstead J, Liu Y, Garnett J, Campanero-Rhodes MA, Blake DP, et al. The role of sialyl glycan recognition in host tissue tropism of the avian parasite Eimeria tenella. *PloS Pathog* (2011) 7(10):e1002296. doi: 10.1371/journal.ppat.1002296

38. Chen W, Ma C, Li G, Jia Z, Yang X, Pan X, et al. Specific EtMIC3-binding peptides inhibit *Eimeria tenella* sporozoites entry into host cells. *Vet Res* (2021) 52 (1):24. doi: 10.1186/s13567-020-00873-y

39. Zhao N, Lv J, Lu Y, Jiang Y, Li H, Liu Y, et al. Prolonging and enhancing the protective efficacy of the EtMIC3-C-MAR against *eimeria tenella* through delivered by attenuated salmonella typhimurium. *Vet Parasitol* (2020) 279:109061. doi: 10.1016/j.vetpar.2020.109061

40. Liu J, Zhang Y, Wang M, Huang J, Jing C, Song X, et al. Evaluation of immunoprotective effective of Microneme protein 3 and Microneme adhesive region protein of Eimeria acervulina. *J Nanjing Agric Univ* (2022) 45(1):124–30.

41. Tian L, Li W, Huang X, Tian D, Liu J, Yang X, et al. Protective efficacy of coccidial common antigen glyceraldehyde 3-phosphate dehydrogenase (GAPDH) against challenge with three *eimeria* species. *Front Microbiol* (2017) 8:1245. doi: 10.3389/fmicb.2017.01245

42. Ali A, Reynolds DL. Primary cell culture of Turkey intestinal epithelial cells. *Avian Dis* (1996) 40(1):103–8. doi: 10.2307/1592378

43. Tao R, Han Y, Chai J, Li D, Sun T. Isolation, culture, and verification of human sweat gland epithelial cells. *Cytotechnology* (2010) 62(6):489–95. doi: 10.1007/s10616-010-9303-z

44. Jiang J, Jiang J. A improved method for purification eimeria tenella oocysts, sporozoites and second generation merozoites. *J China Agric Univ* (1996) (05):99–102.

45. Vadlejch J, Petrtýl M, Zaichenko I, Cadková Z, Jankovská I, Langrová I, et al. Which McMaster egg counting technique is the most reliable? *Parasitol Res* (2011) 109 (5):1387–94. doi: 10.1007/s00436-011-2385-5

46. Liu J, Zhang Y, Wang M, Huang J, Jing C, Song X, et al. Immunoprotective effect of micronme adhesive region of microneme protein 3 of Eimeria maxiam. *Chin J Vet Sci* (2021) 008:041. doi: 10.16303/j.cnki.1005-4545.2021.08.1

frontiers | Frontiers in Immunology

TYPE Original Research
PUBLISHED 07 December 2023
DOI 10.3389/fimmu.2023.1280949

OPEN ACCESS

EDITED BY
Xiang Wu,
Central South University, China

REVIEWED BY
Maria Armanda Rodrigues,
New University of Lisbon, Portugal
Greta Volpedo,
University of Genoa, Italy

*CORRESPONDENCE
Léa Cristina Castellucci
leacastel@hotmail.com

RECEIVED 21 August 2023
ACCEPTED 20 November 2023
PUBLISHED 07 December 2023

CITATION
Lago T, Medina L, Lago J, Santana N, Cardoso T, Rocha A, Leal-Calvo T, Carvalho EM and Castellucci LC (2023) MicroRNAs regulating macrophages infected with *Leishmania L.* (*V.*) *Braziliensis* isolated from different clinical forms of American tegumentary leishmaniasis. *Front. Immunol.* 14:1280949. doi: 10.3389/fimmu.2023.1280949

MicroRNAs regulating macrophages infected with *Leishmania L.* (*V.*) *Braziliensis* isolated from different clinical forms of American tegumentary leishmaniasis

Tainã Lago[1,2,3], Lilian Medina[1,2], Jamile Lago[1,2,3], Nadja Santana[1,2], Thiago Cardoso[3,4], Alan Rocha[4], Thyago Leal-Calvo[5], Edgar M. Carvalho[1,2,3,4] and Léa Cristina Castellucci[1,2,3]*

[1]Serviço de Imunologia da Universidade Federal da Bahia, Salvador, Brazil, [2]Programa de Pós-graduação em Ciências da Saúde da Universidade Federal da Bahia, Salvador, Brazil, [3]Instituto Nacional de Ciência e Tecnologia em Doenças Tropicais (INCT-DT), Ministério da Ciência, Tecnologia, Inovações e Comunicações, CNPq, Brasília, DF, Brazil, [4]Laboratório de Pesquisas Clínicas (LAPEC), Instituto Gonçalo Moniz-FIOCRUZ, Sakvador, Bahia, Brazil, [5]Fundação Oswaldo Cruz, Fiocruz, Rio de Janeiro, BA, Brazil

Background: Leishmaniasis is an infectious disease caused by protozoa of the genus *Leishmania*. There are still no vaccines, and therapeutic options are limited, indicating the constant need to understand the fine mechanisms of its pathophysiology. An approach that has been explored in leishmaniasis is the participation of microRNAs (miRNAs), a class of small non-coding RNAs that act, in most cases, to repress gene expression. miRNAs play a role in the complex and plastic interaction between the host and pathogens, either as part of the host's immune response to neutralize infection or as a molecular strategy employed by the pathogen to modulate host pathways to its own benefit.

Methods: Monocyte-derived macrophages from healthy subjects were infected with isolates of three clinical forms of *L. braziliensis*: cutaneous (CL), mucosal (ML), and disseminated (DL) leishmaniasis. We compared the expression of miRNAs that take part in the TLR/NFkB pathways. Correlations with parasite load as well as immune parameters were analyzed.

Results: miRNAs -103a-3p, -21-3p, 125a-3p -155-5p, -146a-5p, -132- 5p, and -147a were differentially expressed in the metastatic ML and DL forms, and there was a direct correlation between miRNAs -103a-3p, -21-3p, -155-5p, -146a-5p, -132-5p, and -9-3p and parasite load with ML and DL isolates. We also found a correlation between the expression of miR-21-3p and miR-146a-5p with the antiapoptotic gene *BCL2* and the increase of viable cells, whereas miR-147a was indirectly correlated with CXCL-9 levels.

10.3389/fimmu.2023.1280949

Conclusion: The expression of miRNAs is strongly correlated with the parasite load and the inflammatory response, suggesting the participation of these molecules in the pathogenesis of the different clinical forms of *L. braziliensis*.

KEYWORDS

leishmaniasis, macrophages, genes, miRNAs, parasite load

1 Introduction

According to the World Health Organization, there are three main forms of leishmaniasis: visceral (VL), the most serious form because it can be fatal if untreated; cutaneous (CL), the most common disease, usually causing skin ulcers; and mucocutaneous (ML), affecting mouth, nose, and throat (1). Given the complexity of CL presentation in South America, we will therefore use the term American tegumentary leishmaniasis (ATL) in order to describe these clinical forms. ATL extends from Mexico to Argentina (2) and is caused by various species of the *Leishmania (Viannia) braziliensis* and *Leishmania mexicana* complexes of parasites (3). *Leishmania* spp. mainly infect and survive in macrophages, but other cell types such as dendritic cells, lymphocytes, NK cells, and neutrophils participate in disease pathogenesis (4, 5). *Leishmania (Viannia) braziliensis* is the main species causing ATL in Brazil and can provoke cutaneous leishmaniasis (CL), characterized by one or more granulomatous ulcers, to the debilitating mucosal (ML) or disseminated (DL) forms of the disease (6–11). ML presents many distinct manifestations, from lesions limited to the nasal and oral cavity (mild stage), involvement of the epiglottis (moderate stage), to the involvement of the vocal cords, subglottic region, trachea, and even bronchi (severe stage) (12). DL is a severe and emerging form of ATL, defined by the presence of more than 10 polymorphic cutaneous lesions, distributed over more than two noncontiguous parts of the body. Nasal mucosal involvement is frequent, and the therapeutic failure rate is about 75%. DL development is related to a complex network involving environmental, host immune response, and parasite factors. It is important to distinguish DL from the anergic diffuse form—a very rare form of ATL caused by *L. amazonensis*, and from atypical manifestations, common in immunosuppressed patients who have multiple cutaneous lesions (13). Toll-like receptors (TLR) are used by several cell types in the recognition, internalization, and processing of antigens working as a link between the innate and adaptive immune response (14, 15). Data have demonstrated key interactions between macrophages and *Leishmania* through TLR2, TLR4, and TLR9 (16, 17). In CL, infection with *L. braziliensis* specifically increases the expression of TLR2 and TLR4 (18, 19), strengthening TLR signaling as an important layer of the host–pathogen interaction that will culminate in both inflammatory and healing responses. These fine mechanisms are regulated by the action of epigenetic factors, such as miRNAs, which represent a well-characterized class of non-coding RNA molecules of ~22 nucleotides. These molecules target messenger RNA (mRNA) by inhibiting its translation and, subsequently, protein synthesis (20, 21). In leishmaniasis, data showed alterations in the expression of miRNAs in macrophages infected by *L. major* after signaling of TLRs (22). Furthermore, there was a species-specific down-regulation in the expression of host cell miRNAs after infection with *L. major* and *L. donovani* (23). In another study, miR-193b, miR-671, and TREM1 were correlated with faster wound healing in patients infected with *L. braziliensis* (24). In addition, we documented that miR-361-3p was significantly more expressed in CL lesions caused by *L. braziliensis* than in normal skin and that this miR expression was also associated with failure of antimonial therapy and, consequently, prolonged healing time of cutaneous ulcers (25). In this work, we evaluated the expression of miRNAs acting on the TLR/NFKB pathway in macrophages infected with isolates of *L. braziliensis* derived from patients with different forms of ATL (CL, ML, and DL) from an endemic site of northeastern Brazil.

2 Material and methods

2.1 Culture of *L. braziliensis* isolates

Isolates of *L. braziliensis* (BR/18627, BR/30028, BR/30035) were obtained from skin and mucosal lesions of patients with CL, ML, and DL from the endemic area of Corte de Pedra, Bahia, Brazil. The parasites were initially cultured in biphasic medium NNN—Neal, Novy, and Nicolle (modified blood agar) and LIT (Liver Infusion Tryptose). Following isolation, the parasites were cryopreserved in frozen nitrogen. The isolates were expanded in Schneider medium supplemented with 10% fetal bovine serum (FCS) and 2% urine, and cultivated in a CO2 oven at 24°C. For seven days, the growth cycle of the parasite was monitored by counting viable promastigotes in order to assess the different stages of *L. braziliensis* growth until the stationary phase.

2.2 Obtaining macrophages from PBMC

Ten healthy volunteers of both sexes, aged between 25 and 50 years, were recruited from the staff of the Immunology Service at the Federal University of Bahia, where the study was conducted. As a non-endemic site, these people were not tested for present or previous history of the disease; however, all of them reported verbally that they

had never had leishmaniasis or had lived in an endemic site. Peripheral blood mononuclear cells (PBMCs) were obtained from heparinized blood using Ficoll Hypaque™ Plus density gradient (GE Healthcare, Biosciences AB Durham, NC, USA), as previously described (26, 27). Briefly, cells were incubated in Teflon flasks for 6 days at 37°C and 5% CO2 to differentiate monocytes into macrophages. After this incubation period, the cells were washed and adjusted to $1x10^6$ and distributed in duplicate Lab-Tek slide wells and in 12-well culture plates. Subsequently, the cells were incubated for 24 hours for the macrophages to adhere to the plate prior to saline wash. Cultured cells were identified as macrophages by microscopic observation. Due to the practice we used in this protocol, we chose not to add growth factors to the culture, as these could influence the expression of miRNAs. However, this component can be added to improve the performance of obtaining monocyte-derived macrophages (MDMs).

2.3 Infection of macrophages with isolates of *L. braziliensis*

Macrophage cultures ($1x10^6$ cells/well) were infected with *L. braziliensis* promastigotes in the stationary phase at a ratio of 5:1, in duplicate, for 48 hours, and uninfected macrophages were used as controls. The infection rate was evaluated by optical microscopy, counting the percentage of infected macrophages and the number of amastigotes per 200/cells in duplicate, for 4 hours only, which would be enough time to guarantee the entry of the parasites into the macrophages. We used the Panótico Rápido (Laborclin, Brasil) kit, a rapid staining set in hematology that contains dyes with chemical characteristics and affinities.

2.4 RNA extraction, cDNA synthesis, and evaluation of miRNA expression by quantitative RT-PCR

Based on previous work done with infected cells (22, 28), we evaluated the expression of miRNAs 4, 12, and 24 hours after parasite exposure, considering that their expression should be optimal in the first hours post-infection. The cell RNA was extracted using the TRIzol® Reagent method, according to the manufacturer's instructions. The isolated RNA was resuspended in 25µl of RNAse-free water, and the concentration was determined by optical density measurements (260 and 280 nm) using Nanodrop®. The miRNAs -146a-5p, -146b-5p, -147a, -155-5p, -9-3p, -125a-3p, -132-5p, 21-3p, hsa-let-7a-3p, -511-3p, -103a-3p, and the U6snComplementary DNA (cDNA) were chosen according to their contribution to the TLR activation pathway according to the literature and websites for TargetScanHuman (release 7.1; http://www.targetscan.org/) and miRBase (release 21; http://www.mirbase.org/). cDNA was obtained using the miRCURY LNA™ RT Kit (QIAGEN), following the manufacturer's guidelines. The gene expression was performed using qPCR, using the miRCURY LNA SYBR Kit. Samples were prepared in duplicates as follows: 5µl of 2x miRCURY LNA SYBR Green Master mix, 0.05µl of ROX Reference Dye, 1µl of PCR primer mix, and 1µl of RNase-free water. A final amount of 10µl was used for each reaction, containing 3µl of the diluted cDNA template (1:5) and 7µl of the reaction mix. The amplification conditions followed the following cycling: (I) 2 minutes at 95°C, (II) 10 seconds at 95°C, (III) 60 seconds at 56°C, and (IV) for 40 cycles following the melting curve. For normalization, the threshold cycle (Ct) values of the expression of each miRNA were used. The expression of the evaluated miRNAs was normalized by miR-146b-5p miRNAs and by corresponding U6 (nucleolar RNA) for each sample in order to control for variability between samples. After normalization, gene expression units were calculated from values of ΔCt.

2.5 cDNA synthesis and gene expression of BCL2, CFLAR, ATG12, GZMB, and TNFRSF10A

In order to choose genes related to cell death processes and which were regulated by miRNAs previously associated with the ML and DL forms in the study, we consulted the notes deposited in the TargetScan database. TaqMan™ assays containing specific primers and probes for the *BCL2* (Hs01048932_g1), *CFLAR* (Hs01048932_g1), *ATG12*, (Hs00269492_m1), *GZMB* (Hs00188051_m1), and *TNFRSF10A* (Hs00269492_m1) genes were purchased from Thermo Fisher Scientific as well as the normalizer for the *ACTB* gene (Hs99999903_m1). Reverse transcription reactions were performed using the commercially available High-Capacity cDNA Reverse Transcription Kit (Thermo Fisher Scientific), starting from 10µl of total RNA and using the MultiScribe Reverse Transcriptase enzyme, according to the manufacturer's instructions. Gene expression analysis was performed using the qPCR technique with the QuantStudio 3 (Applied Biosystems®). All samples were prepared in duplicate using the reagents recommended by the manufacturer. Data were analyzed using the Ct comparative method, according to the $2^{-\Delta\Delta CT}$ equation, where ΔCT is the Ct value of the target gene subtracted from the Ct of the endogenous gene, and the ΔΔCT is the ΔCT value of each individual, minus the median ΔCT of the control group.

2.6 Evaluation of cell death and oxidative burst

Flow cytometry was used to access apoptotic/necrotic cells and determine nitric oxide (NOS) and reactive oxygen species (ROS) expression. At 24 and 48 hours, cultured cells were labeled with 5 µL PE–anti-CD14 MAb (clone 61D3; BD Bioscience). Afterwards, 5 µL of annexin V (AnV) FITC in annexin binding buffer (BD Bioscience PharMingen) was added for 20 min. Samples were analyzed on a FACS Fortessa flow cytometer (BD Bioscience PharMingen, San Jose, CA). To access NOS and ROS intracellular species, cells were labeled with dihydrorhodamine 123, DAF-FM diacetate (Life Technologies), dihydroethidium (Life Technologies), and CM-H2DCFDA (Invitrogen—Thermo Fisher Scientific), diluted

10.3389/fimmu.2023.1280949

according to the manufacturer's instructions. Viable cells (AnV-/IP-) after 48 hours were counted. A minimum of 50,000 gated events from each sample were collected in a FACS Fortessa flow cytometer (BD Bioscience PharMingen, San Jose, CA) and analyzed using the FlowJo 7.6.5 program.

2.7 Cytokine and chemokine production in macrophage culture supernatants

Cytokine and chemokine were measured in the supernatant of macrophages infected with *L. braziliensis* isolates at 24 hours after infection by the sandwich ELISA immunoenzymatic technique, using the commercially available R&D Systems Kit (R&D Systems). The levels of chemokines/cytokines CXCL-9, CXCL-10, TNF, IFN-γ, IL-6, IL-1β, and IL-10 were measured using the protocol recommended by the manufacturer.

2.8 Statistical analysis

We used Refinder (https://www.heartcure.com.au/reffinder/?type=reference) to analyze the stability of miRNAs expression. Refinder integrates computer programs available for normalization (geNorm, Normfinder, BestKeeper) and the comparative delta-Ct method to rank candidate reference genes tested among the different samples. In our study, U6snRNA and miR-146b-5p were identified as normalizing genes. After normalizing the genes, the miRNA expression data were represented in relative expression units between the CL, ML, and DL. Then, within each time point, conditions were tested against each other through the mixed linear model with random effect for individuals, followed by Tukey's test for multiple comparisons. Correlation analysis with immune markers, parasite load, and gene expression was performed using the Spearman correlation test implemented by the GraphPad Prism 8 software. p-values < 0.05 were considered statistically significant.

2.9 Ethical statement

The study was approved by the institutional review board of the Federal University of Bahia (CAAE: 93214818.2.0000.0049) and according to the recommendations of Resolution 466/12 of the National Health Council for research with human beings and the Declaration of Helsinki.

3 Results

3.1 Infection of human macrophages with strains of *L. braziliensis*

Macrophages were infected at a ratio of 5:1 with the three isolates used, and the percentage of infected cells after 4 hours was similar for the three isolates of *L. braziliensis* (CL 70 ± 9, ML 75 ± 9, and DL 65 ± 8); Figure 1A. The percentage of infected cells and number of amastigotes/200 cells was similar for CL, ML, and DL at all time points (CL 410 ± 121, ML 472 ± 134, and DL 415 ± 151); Figure 1B, P>0.05. Figure 1C shows a microcopy image of macrophages with internalized parasites derived from patients with CL.

3.2 MiRNAs are differentially expressed among ATL isolates

We evaluated the expression of miRNAs infected with CL, ML, and DL isolates at 4, 12, and 24 hours; see Supplementary Figure 1. Only at 12 hours were there differences between isolates. Essentially, these differences occurred between ML and DL in relation to CL and uninfected cells (controls), so all observed associations were for metastatic and invasive forms of ATL. In fact, some of these associations were exclusive to the ML form, such as miRNAs -5103a-3p, -21-3p, and 125a-3p; Figure 2A. miRs -155-5p, -146a-5p, -132-5p, and -147a were differentially expressed in macrophages

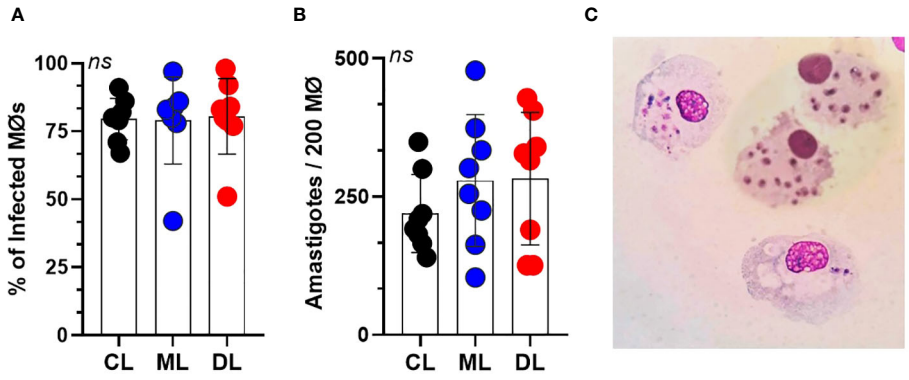

FIGURE 1
Parasite load of infected macrophages (Mϕ) for 4 hours, at a rate of five parasites per cell. **(A)** Mean percentage of macrophages from 10 healthy donors, infected with each *L. braziliensis* isolate (CL, ML, and DL). **(B)** Average number of amastigotes per Mϕ. There were no differences either in the percentage of infected Mϕ or in the number of amastigotes per 200 Mϕ. Data show mean ± SD. **(C)** Microscopic image of macrophages with internalized *L. braziliensis* parasites (BR/30035).

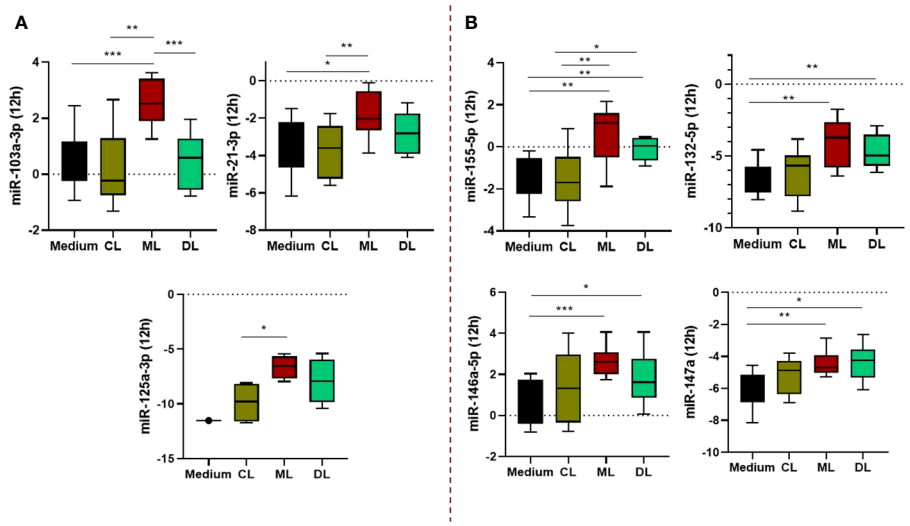

FIGURE 2
Expression profile of miRNAs regulating TLR/NFkB activation pathways in macrophages (Mϕ) infected with *L. braziliensis* isolates (CL, ML, and DL). The miRs -103a-3p, -21-3p, and 125a-3p were significantly higher in ML than other isolates and uninfected cells **(A)**, while miRs -155-5p, -146a-5p, -132-5p, and -147a, were differentially expressed in Mϕ infected with both ML and DL strains **(B)**. Samples from 10 subjects, in duplicate. After normalization, gene expression was calculated from values of ΔCt. *P<0,05; **P< 0,01; ***P< 0,001.

infected with both ML and DL isolates compared to either CL or uninfected, as shown in Figure 2B. In addition, we did not observe a correlation between miRNA expression and infection with the CL isolate (data not shown).

3.3 MiRNA expressions were correlated with the parasite load in ML

There was a positive correlation between parasitic load in macrophages infected with the ML isolate and miRNAs -103a-3p (r=0.8, p=0.006), -21-3p (r=0.7, p=0.012), -155-5p (r=0.7, p=0.014), -146a-5p (r=0.7, p=0.014), -132-5p (r=0.8, p=0.003), and -9-3p (r=0.8, p=0.034). Interestingly, these represent five of the seven miRNAs that were differentially expressed in this metastatic clinical form, as shown in Figure 3A-F. By adding DL, these associations were kept, except for miR132-3p and -9-3p, although the inclusion of this isolate slightly reduced the strength of these correlations, probably due to a greater dispersion of the samples (Supplementary Figure 2). We ran the same analysis for CL which returned no significant correlations. On the other hand, the miRs 125a-3 p, -511-3p, let-7a-3p, and 147a returned no significant results for this analysis.

3.4 miR-21-3p and miR-146a-5p correlate to antiapoptotic genes and influence cell viability in ML

Among miRNAs correlated with parasitic load in ML, we observed that miR-21-3p showed an inverse correlation with the antiapoptotic gene BLC2. In addition, this miR showed an increase in the number of viable cells (non-apoptotic), which was accompanied by an inverse correlation with apoptotic cells annexin-positive (AnV+); Figure 4A-C. On the other hand, miR146a-5p was inversely correlated with both BLC2 and CFLAR genes; Figure 4D, E. Consistent with this, there was a negative correlation with necrotic cells (IP+) and a positive association with the increase of viable cells; Figure 4F, G. Supplementary Figure 3 shows cell viability and oxidative burst data in the macrophages.

3.5 Expression of miRNAs and cytokine production

miR-147a showed an inverse correlation with the production of CXCL-9 and the frequency of viable cells in the first hours of infection for both ML and DL infected macrophages; Figure 5A-D. In addition, for DL we observed a correlation with a lower expression of DHR+, indicating a parallel impairment in the oxidative burst; Figure 5E. None of the other immune markers tested were correlated to the miRNAs tested.

4 Discussion

Our study showed expression profile changes in miRNAs from human macrophages infected by different isolates of *L. braziliensis*. Specifically, while isolates from CL did not modify miRNAs expression, isolates from the metastatic forms ML and DL enhanced miRNA expression. These miRNAs share the common feature of regulating TLR activation pathways, participating in events such as lymphocyte activation, cell migration, and cytokine production, in addition to cell death mechanisms. Macrophages, on the other hand, host *Leishmania*, act as antigen-presenting cells, and secrete molecules that induce the inflammatory response and

10.3389/fimmu.2023.1280949

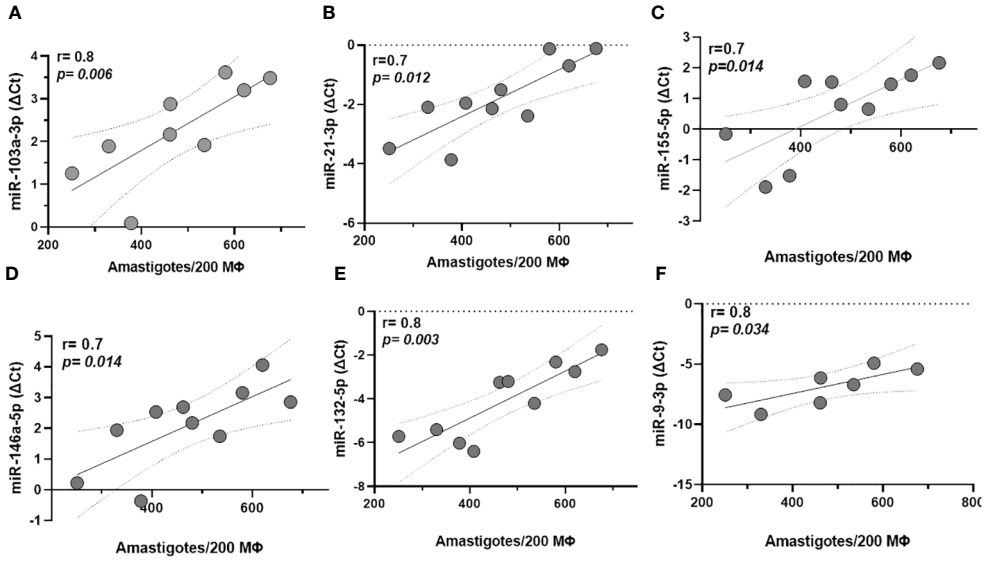

FIGURE 3
Correlation between miRNA expression and parasite load in macrophages (Mϕ) derived from monocytes infected with mucosal leishmaniasis isolates. MiRNAs -103a-3p, -21-3p, -155-5p, -146a-5p, -132-5p, and -9-3p **(A–F)**, respectively correlate with higher parasitic load in macrophages infected with the ML isolate. Data related 10 subjects with experiments performed in duplicate. Spearman correlation was implemented with GraphPad Prism 8 software. R values above 0.7 and *p*-values < 0.05 were considered significant.

parasite killing (26). MiRNAs -155-5p, -146a-5p, -147a, and -132-5p were significantly more expressed in both ML and DL than CL isolates. Parasites of *Leishmania* spp. are strong promoters of cell-mediated immunity, mainly by induction of pro-inflammatory cytokines after *in vivo* infection. However, during intracellular infection of macrophages, the parasite initially suppresses the signal transduction pathways that lead to these pro-inflammatory responses (27). This likely reflects the parasite's need to modulate immunity promptly, allowing it to multiply and survive in the host while avoiding excessive responses that could result in its elimination. Our findings strengthen the hypothesis that this modulation is influenced by miRNAs. Consistent with our findings, Lemaire et al. (2013) previously showed that miRNAs -132, -146a, -146b, and -155 were more expressed in macrophages infected by *L. major* (22). In addition, a recent study showed that miR-548d-3p has an important role in CL caused by *L. braziliensis*

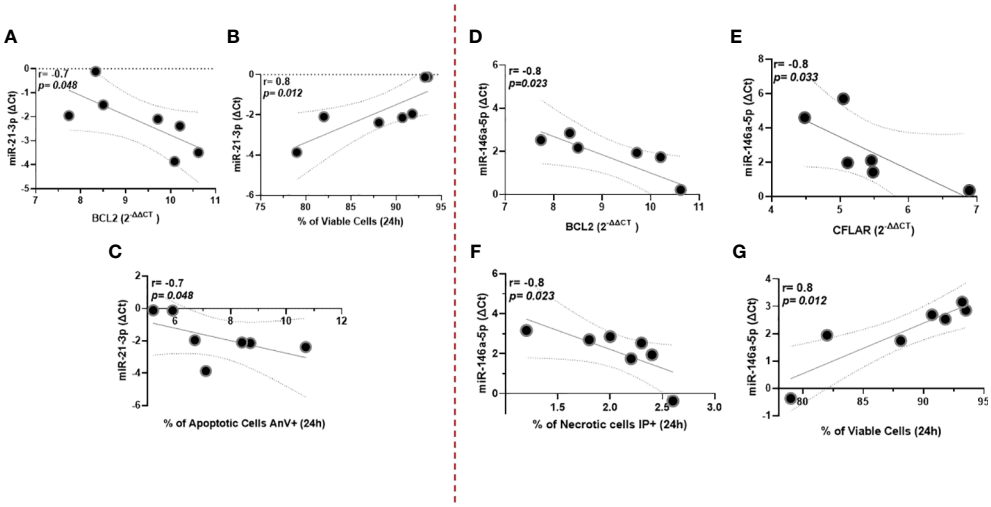

FIGURE 4
miR-21-3p showed an inverse correlation with the antiapoptotic gene *BLC2*, whereas miR146a-5p was with both *BLC2* and *CFLAR* genes **(A–C)**, respectively. Data related to 10 subjects with experiments performed in duplicate. Both miRNAs were also associated with increased numbers of viable (non-apoptotic) cells in culture for 24 hours **(D, E)**. Additionally, miR-146a-5p correlates negatively with necrotic cells (IP+), whereas for miR-21-3p there is an inverse correlation with apoptotic cells annexin-positive (AnV+) **(F, G)**. Data related to seven subjects with experiments performed in duplicate. Spearman correlation was implemented using GraphPad Prism 8 software. R values above 0.7 and *p*-values < 0.05 were considered significant.

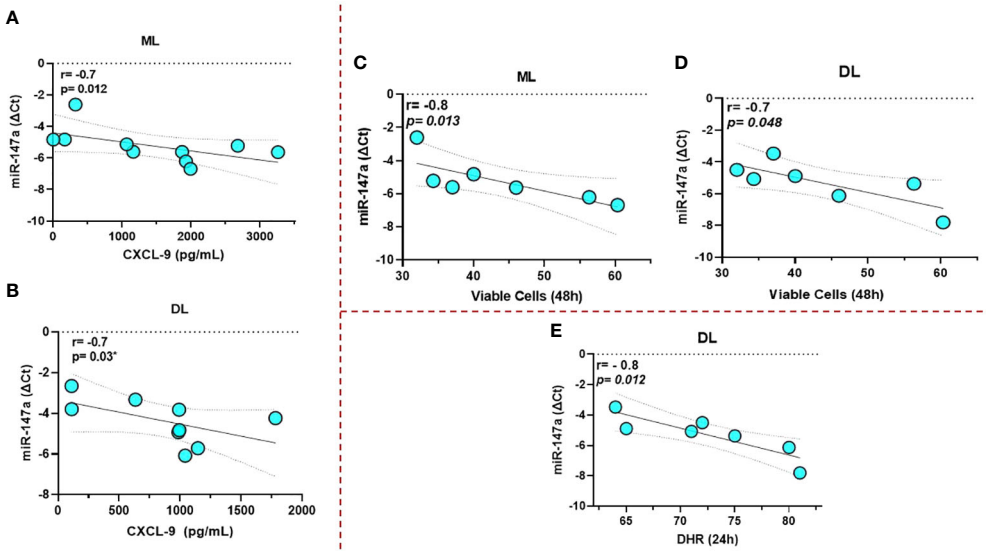

FIGURE 5
miR-147a showed an inverse correlation with the production of CXCL-9 and the frequency of viable cells for both ML and DL infected macrophages **(A–D)**, respectively. Data related to 10 subjects with experiments performed in duplicate. In addition, for DL, we also observed a correlation with a lower expression of 123 DHR+, indicating an impairment in the oxidative burst **(E)**. Data related to seven subjects with experiments performed in duplicate. Spearman correlation was implemented using GraphPad Prism 8 software. R values above 0.7 and *p*-values < 0.05 were considered significant.

since inhibition of this miR in infected THP-1 cells was associated with reduced parasite growth early after infection and increased the production of molecules such as MCP1/CCL2, RANTES/CCL5, and IP10/CXCL10, data corroborated in the plasma of individuals with active or cured disease compared to controls (28). Another study showed that during *Leishmania* infection, a signature composed of miR-147a, -146a, -146b, and -155, among others, might influence the inflammatory regulatory network of *L. major*-infected macrophages (29). We propose that once parasites enter the cell, these miRNAs are recruited, assisting the parasites' ability to multiply and, in some cases, escape from the original site and establish infection in other areas.

Most miRNAs that were associated with ML and DL were also correlated with the parasite load. In leishmaniasis, the activation of macrophages by IFN-γ induces the production of IL-12, TNF, reactive oxygen species (ROS), and nitric oxide (NO) to eliminate the parasite (30). Despite this strong response, enough *Leishmania* survive, and the parasites establish and cause disease. Consistent with this, *L. braziliensis* isolates from DL patients showed a greater ability to penetrate and multiply in monocytes than CL isolates, in spite of a greater respiratory burst induction and increased production of pro-inflammatory cytokines (31). Additionally, monocytes from DL patients were more permissive to parasite infection, with enhanced multiplication compared to cells from CL patients infected with a DL isolate (31). These data show that the combination of the strain, aligned to the host response, determines the parasite load. In lesions from CL patients, *Leishmania* is scarce due to the intense inflammatory response, but the parasite load is quite variable. As ML usually occur after a primary CL, it is expected that in the skin of patients who will develop ML, the parasite load is higher than in those who do not develop ML. We did not observe significant differences in percentages of macrophage infectivity between isolates, but miRNA expression was correlated with parasite load in ML, and this correlation was maintained when we added DL to the analysis. We suggest that the mechanistic details triggered by these parasites, especially in ML, induce a greater expression of micro RNAs that modulate pathways of initial host–pathogen interaction and that, finally, provide parasites with the ability to multiply and escape cells after infection by interfering mechanisms such as phagocytosis, secretion of chemokines and prostaglandins, and the inhibition of IFN-γ inducible pathways.

We observed a negative correlation between the expression of miRNAs 146a-5p and 21-3p and the antiapoptotic *BCL2* gene in macrophages infected with ML isolate, suggesting a correlation between increased expression of these miRNAs, increased *Leishmania* burden, and reduced *BLC2*, which may reflect changes in apoptotic mechanisms by the parasite. This is strengthened by the fact that both miRNAs are also correlated with an increase in viable cells in culture. In addition, miR-21-3p was inversely correlated with apoptotic cells (AnV+) and, similarly, miR-146a-5p with necrotic cells (IP+) after 24 hours. The BCL2 family express domains that are anti-apoptotic, such as BCL-2, MCL-1, and Bcl-xL, and pro-apoptotic proteins such as Bad and Bik. Data showed that functional inhibition of *BCL2* caused increased nitric oxide (NO) response and reduced parasite burden in monocytes after *L. major* infection, confirming the role of *BCL2* during infection (32). Another important apoptosis regulator is *CFLAR*, which inhibits the assembly of caspase-8 and the FADD complex. Increased *CFLAR* expression prevents the accidentally formed signaling complexes between TNFRSF1A/TRADD/RIPK1/FADD, leading to clustering and activation of caspases and

therefore apoptosis (33). Our data showed a negative correlation between miR-146a-5p and *CFLAR*, reinforcing a possible role of this miR as an inhibitor of apoptosis. To summarize, we suggest that by inhibiting cell death, the miRNAs help promote the escape and metastasization characteristic of these forms, which would be aligned with their correlation with the parasite load.

The chemokine genes CXCL-9 and CXCL-10 are direct targets of miRNA 147a. In the context of ML and DL, we consider the involvement of this axis in tumor growth and metastasis (34). The function of the CXCL9, -10, -11/CXCR3 axis in response to IFN-γ is mainly divided into two directions: paracrine signaling for immune activation and autocrine signaling for cancer cell proliferation and metastasis. With regard to the paracrine signal, this axis works mainly for the migration, differentiation, and activation of immune cells, including Th1 polarization. On the other hand, for the autocrine signal, cancer cells have a propensity to metastasize due to the activity of tumor-derived ligands mainly through CXCR3A (34). In context, Oliveira et al. (2021) showed that infection with DL isolates causes a different behavior than CL in terms of internalization and multiplication of parasites, as well as activation of monocytes in cells from endemic patients. Yet, according to Oliveira et al.'s study, DL induces more CXCL-9 than CL isolates (31). In addition to CXCL-9, because miR-147a was concurrently associated with lower frequency of viable cells and oxidative burst, we hypothesize that the initial expression of this miRNA may stimulate mechanisms of cell lysis, releasing amastigotes and, finally, favoring a process of dissemination of parasites at some point after infection. We can also assume that inhibition of CXCL-9 by this miR is transitory and restored after time.

As a key part of the regulatory layer of parasite–host interactions, a series of studies have demonstrated the potential of miRNAs as prognostic markers, as well as possible therapeutic targets in cancer and parasitic pathologies such as malaria (35–37), schistosomiasis (38, 39), and Chagas disease (40–42). To date, this is the first study that focuses on different isolates of *L. braziliensis* and compares variations in miRNA expression and some of the biological effects, which expands the field and may lead to the identification of new pathways and possible prognostic/therapeutic alternatives based on these molecules in ATL.

5 Conclusion

In conclusion, there is a differentiated expression of miRNAs in macrophages infected with isolates of the metastatic ML and DL forms of leishmaniasis. Some of these miRNAs were also correlated with parasite load, genes linked to apoptosis, CXCL-9, and cell viability. We propose that fine regulation by miRNAs in the early hours after infection is the mechanism that favors parasite entry and multiplication in the phagosome to then escape from the original site and establish infection in other areas. Since these miRNAs are involved in events mediated by the activation of TLRs, this regulation involves the modulation of key genes of immune response and cell death.

Data availability statement

The original contributions presented in the study are included in the article/Supplementary Material, further inquiries can be directed to the corresponding author/s.

Ethics statement

The studies involving humans were approved by Institutional review board of the Federal University of Bahia (CAAE: 93214818.2.0000.0049). The studies were conducted in accordance with the local legislation and institutional requirements. The participants provided their written informed consent to participate in this study.

Author contributions

LC: Conceptualization, Supervision, Writing – original draft. TL: Investigation, Methodology, Writing – original draft. LM: Methodology. JL: Methodology. NS: Methodology. TC: Formal analysis, Methodology. AR: Methodology. TL-C: Data curation, Formal analysis. EC: Writing – review & editing, Funding acquisition.

Funding

The author(s) declare financial support was received for the research, authorship, and/or publication of this article. This study was supported by National Institute of Science and Technology in Tropical Diseases, Brazil (N&z.ousco; 573839/2008-5) and publication costs supported by the Fundação Maria Emilia.

Conflict of interest

The authors declare that the research was conducted in the absence of any commercial or financial relationships that could be construed as a potential conflict of interest.

Publisher's note

Supplementary material

The Supplementary Material for this article can be found online at: https://www.frontiersin.org/articles/10.3389/fimmu.2023.1280949/full#supplementary-material

SUPPLEMENTARY FIGURE 1
Expression of miRNAs in macrophages infected with different isolates of *L. braziliensis* (CL, ML, DL) at different times of infection (4, 12, and 24 hours). Data is represented in log fold change.

SUPPLEMENTARY FIGURE 2
Direct correlation between miRNAs -103a-3p, -21-3p, -155-5p, and -146a-5p and infection with the ML and DL isolates in macrophages derived from monocytes.

SUPPLEMENTARY FIGURE 3
Expression of annexin-positive (AnV+), viable cells (AnV-/IP-), and ROS (123 DHR +) for 24 and 48 hours in macrophages uninfected (medium) and infected with CL, ML, and DL isolates of *L. braziliensis*. Data related to seven subjects, generated by flow cytometry, and analyzed using the FlowJo 7.6.5 program, with minimum of 50,000 gated events from each sample. Kruskal-Wallis test was implemented using GraphPad Prism 8 software.

References

1. World Health Organization. *Leishmaniasis* (2023). Available at: https://www.who.int/news-room/fact-sheets/detail/leishmaniasis (Accessed November 13, 2023).

2. Alvar J, Vélez ID, Bern C, Herrero M, Desjeux P, Cano J, et al. Leishmaniasis worldwide and global estimates of its incidence. *PloS One* (2012) 7:e35671. doi: 10.1371/journal.pone.0035671

3. Thomaz-Soccol V, Lanotte G, Rioux JA, Pratlong F, Martini-Dumas A, Serres E. Phylogenetic taxonomy of new world leishmania. *Ann Parasitol Hum Comp* (1993) 68:104–6. doi: 10.1051/parasite/1993682104

4. Ribeiro-Gomes FL, Sacks D. The influence of early neutrophil-Leishmania interactions on the host immune response to infection. *Front Cell Infect Microbiol* (2012) 2:59. doi: 10.3389/fcimb.2012.00059

5. Ribeiro-Gomes FL, Romano A, Lee S, Roffê E, Peters NC, Debrabant A, et al. Apoptotic cell clearance of Leishmania major-infected neutrophils by dendritic cells inhibits $CD8^+$ T-cell priming in *vitro* by Mer tyrosine kinase-dependent signaling. *Cell Death Dis* (2015) 6:e2018. doi: 10.1038/cddis.2015.351

6. Liu D, Uzonna JE. The early interaction of Leishmania with macrophages and dendritic cells and its influence on the host immune response. *Front Cell Infect Microbiol* (2012) 2:83. doi: 10.3389/fcimb.2012.00083

7. Marsden PD. Clinical presentations of Leishmania Braziliensis. *Parasitol Today* (1985) 1:129–33. doi: 10.1016/0169-4758(85)90057-2

8. Marsden PD. Mucosal leishmaniasis ("espundia" Escomel, 1911). *Trans R Soc Trop Med Hygiene* (1986) 80:859–76. doi: 10.1016/0035-9203(86)90243-9

9. Carvalho EM, Barral A, Costa JM, Bittencourt A, Marsden P. Clinical and immunopathological aspects of disseminated cutaneous leishmaniasis. *Acta Trop* (1994) 56:315–25. doi: 10.1016/0001-706x(94)90103-1

10. Carvalho EM. Parasite, vectors and reservoirs as determinants of tegumentary leishmaniasis. *Rev Soc Bras Med Trop* (2012) 45:423–4. doi: 10.1590/s0037-86822012000400001

11. Turetz ML, MaChado PR, Ko AI, Alves F, Bittencourt A, Almeida RP, et al. Disseminated leishmaniasis: a new and emerging form of leishmaniasis observed in northeastern Brazil. *J Infect Dis* (2002) 186:1829–34. doi: 10.1086/345772

12. Carvalho EM, Llanos-Cuentas A, Romero GAS. Mucosal leishmaniasis: urgent need for more research. *Rev Soc Bras Med Trop* (2018) 51:120–1. doi: 10.1590/0037-8682-0463-2017

13. MaChado GU, Prates FV, MaChado PRL. Disseminated leishmaniasis: clinical, pathogenic, and therapeutic aspects. *Bras Dermatol* (2019) 94:9–16. doi: 10.1590/abd1806-4841.20198775

14. Medzhitov R, Janeway C Jr. Innate immune recognition: mechanisms and pathways. *Immunol Ver* (2000) 173:89–97. doi: 10.1034/j.1600-065x.2000.917309.x

15. Kawasaki T, Kawai T. Toll-like receptor signaling pathways. *Front Immunol* (2014) 5:461. doi: 10.3389/fimmu.2014.00461

16. Becker I, Salaiza N, Aguirre M, Delgado J, Carrillo-Carrasco N, Kobeh LG, et al. Leishmania lipophosphoglycan (LPG) activates NK cells through toll-like receptor-2. *Mol Biochem Parasitol* (2003) 130:65–74. doi: 10.1016/s0166-6851(03)00160-9

17. de Veer MJ, Curtis JM, Baldwin TM, DiDonato JA, Sexton A, McConville MJ, et al. MyD88 is essential for clearance of Leishmania major: possible role for lipophosphoglycan and Toll-like receptor 2 signaling. *Eur J Immunol* (2003) 33:2822–31. doi: 10.1002/eji.200324128

18. Polari LP, Carneiro PP, Macedo M, MaChado PRL, Scott P, Carvalho EM, et al. Leishmania Braziliensis infection enhances toll-like receptors 2 and 4 expression and triggers TNF-α and IL-10 production in human cutaneous leishmaniasis. *Front Cell Infect Microbiol* (2019) 9:120. doi: 10.3389/fcimb.2019.00120

19. Carneiro PP, Dórea AS, Oliveira WN, Guimarães LH, Brodskyn C, Carvalho EM, et al. Blockade of TLR2 and TLR4 attenuates inflammatory response and parasite load in cutaneous leishmaniasis. *Front Immunol* (2021) 12:706510. doi: 10.3389/fimmu.2021.706510

20. Bartel DP. MicroRNAs: genomics, biogenesis, mechanism, and function. *Cell* (2004) 116:281–97. doi: 10.1016/s0092-8674(04)00045-5

21. Cloonan N. Re-thinking miRNA-mRNA interactions: intertwining issues confound target discovery. *Bioessays* (2015) 37:379–88. doi: 10.1002/bies.201400191

22. Lemaire J, Mkannez G, Guerfali FZ, Gustin C, Attia H, Sghaier RM, et al. MicroRNA expression profile in human macrophages in response to Leishmania major infection. *PloS Negl Trop Dis* (2013) 7:e2478. doi: 10.1371/journal.pntd.0002478

23. Geraci NS, Tan JC, McDowell MA. Characterization of microRNA expression profiles in Leishmania-infected human phagocytes. *Parasite Immunol* (2015) 37:43–51. doi: 10.1111/pim.12156

24. Nunes S, Silva IB, Ampuero MR, de Noronha ALL, de Souza LCL, Correia TC, et al. Integrated Analysis Reveals That miR-193b, miR-671, and TREM-1 Correlate With a Good Response to Treatment of Human Localized Cutaneous Leishmaniasis Caused by Leishmania Braziliensis. *Front Immunol* (2018) 9:640. doi: 10.3389/fimmu.2018.00640

25. Lago TS, Silva JA, Lago EL, Carvalho EM, Zanette DL, Castellucci LC. The miRNA 361-3p, a regulator of GZMB and TNF is associated with therapeutic failure and longer time healing of cutaneous leishmaniasis caused by L. *(viannia) Braziliensis Front Immunol* (2018) 9:2621. doi: 10.3389/fimmu.2018.02621

26. Giudice A, Vendrame C, Bezerra C, Carvalho LP, Delavechia T, Carvalho EM, et al. Macrophages participate in host protection and the disease pathology associated with Leishmania Braziliensis infection. *BMC Infect Dis* (2012) 12:75. doi: 10.1186/1471-2334-12-75

27. Sousa R, Andrade VM, Bair T, Ettinger NA, Guimarães L, Andrade L, et al. Early suppression of macrophage gene expression by leishmania Braziliensis. *Front Microbiol* (2018) 9:2464. doi: 10.3389/fmicb.2018.02464

28. Souza MA, Ramos-Sanchez EM, Muxel SM, Lagos D, Reis LC, Pereira VRA, et al. miR-548d-3p alters parasite growth and inflammation in leishmania (Viannia) Braziliensis infection. *Front Cell Infect Microbiol* (2021) 11:687647. doi: 10.3389/fcimb.2021.687647

29. Nimsarkar P, Ingale P, Singh S. Systems Studies Uncover miR-146a as a Target in Leishmania major Infection Model. *ACS Omega* (2020) 5:12516–26. doi: 10.1021/acsomega.0c01502

30. Scott P, Novais FO. Cutaneous leishmaniasis: immune responses in protection and pathogenesis. *Nat Rev Immunol* (2016) 16:581–92. doi: 10.1038/nri.2016.72

31. Oliveira WN, Dórea AS, Carneiro PP, Nascimento MT, Carvalho LP, MaChado PRL, et al. The influence of infection by different leishmania (Viannia) Braziliensis isolates on the pathogenesis of disseminated leishmaniasis. *Front Cell Infect Microbiol* (2021) 11:740278. doi: 10.3389/fcimb.2021.740278

32. Pandey RK, Mehrotra S, Sharma S, Gudde RS, Sundar S, Shaha C. Leishmania donovani-induced increase in macrophage bcl-2 favors parasite survival. *Front Immunol* (2016) 7:456. doi: 10.3389/fimmu.2016.00456

33. Lee HC, Goodman JL. Anaplasma phagocytophilum causes global induction of antiapoptosis in human neutrophils. *Genomics* (2006) 884:496–503. doi: 10.1016/j.ygeno.2006.06.002

34. Tokunaga R, Zhang W, Naseem M, Puccini A, Berger MD, Soni S, et al. CXCL9, CXCL10, CXCL11/CXCR3 axis for immune activation - A target for novel cancer therapy. *Cancer Treat Rev* (2018) 63:40–7. doi: 10.1016/j.ctrv.2017.11.007

35. Paroo Z, Ye X, Chen S, Liu Q. Phosphorylation of the human microRNA-generating complex mediates MAPK/Erk signaling. *Cell* (2009) 139:112–22. doi: 10.1016/j.cell.2009.06.044

36. Cai J, Guan H, Fang L, Yang Y, Zhu X, Yuan J, et al. MicroRNA-374a activates Wnt/β-catenin signaling to promote breast cancer metastasis. *J Clin Invest* (2013) 123:566–79. doi: 10.1172/JCI65871

37. Rangel G, Teerawattanapong N, Chamnanchanunt S, Umemura T, Pinyachat A, Wanram S. Candidate microRNAs as biomarkers in malaria infection: A systematic review. *Curr Mol Med* (2019) 20:36–43. doi: 10.2174/1566524019666190820124827

38. Zhu L, Liu J, Cheng G. Role of microRNAs in schistosomes and schistosomiasis. *Front Cell Infect Microbiol* (2014) 4:165. doi: 10.3389/fcimb.2014.00165

39. Chen Q, Zhang J, Zheng T, Chen H, Nie H, Zheng B, et al. The role of microRNAs in the pathogenesis, grading and treatment of hepatic fibrosis in schistosomiasis. *Parasit Vectors* (2019) 12:611. doi: 10.1186/s13071-019-3866-0

40. Ferreira LR, Frade AF, Santos RH, Teixeira PC, Baron MA, Navarro IC, et al. MicroRNAs miR-1, miR-133a, miR-133b, miR-208a and miR-208b are dysregulated in Chronic Chagas disease Cardiomyopathy. *Int J Cardiol* (2014) 175:409–17. doi: 10.1016/j.ijcard.2014.05.019

41. Monteiro CJ, Mota SL, Diniz Lde F, Bahia MT, Moraes KC. Mir-190b negatively contributes to the Trypanosoma cruzi-infected cell survival by repressing PTEN protein expression. *Mem Inst Oswaldo Cruz* (2015) 110:996–1002. doi: 10.1590/0074-02760150184

42. Navarro IC, Ferreira FM, Nakaya HI, Baron MA, Vilar-Pereira G, Pereira IR, et al. MicroRNA transcriptome profiling in heart of trypanosoma cruzi-infected mice: parasitological and cardiological outcomes. *PloS Negl Trop Dis* (2015) 9:e0003828. doi: 10.1371/journal.pntd.0003828

frontiers | Frontiers in Immunology

TYPE Review
PUBLISHED 22 January 2024
DOI 10.3389/fimmu.2024.1344941

OPEN ACCESS

EDITED BY
Xiang Wu,
Central South University, China

REVIEWED BY
Gaoqian Feng,
Nanjing Medical University, China
Daniel Fernández Ruiz,
University of New South Wales, Australia

*CORRESPONDENCE
Wenyue Xu
xuwenyue@tmmu.edu.cn

†These authors have contributed equally to this work

RECEIVED 27 November 2023
ACCEPTED 08 January 2024
PUBLISHED 22 January 2024

CITATION
Zhu C, Jiao S and Xu W (2024) CD8+ Trms against malaria liver-stage: prospects and challenges.
Front. Immunol. 15:1344941.
doi: 10.3389/fimmu.2024.1344941

CD8$^+$ Trms against malaria liver-stage: prospects and challenges

Chengyu Zhu[1,2†], Shiming Jiao[2†] and Wenyue Xu[1,2*]

[1]The School of Medicine, Chongqing University, Chongqing, China, [2]Department of Pathogenic Biology, Army Medical University (Third Military Medical University), Chongqing, China

Attenuated sporozoites provide a valuable model for exploring protective immunity against the malarial liver stage, guiding the design of highly efficient vaccines to prevent malaria infection. Liver tissue-resident CD8$^+$ T cells (CD8$^+$ Trm cells) are considered the host front-line defense against malaria and are crucial to developing prime-trap/target strategies for pre-erythrocytic stage vaccine immunization. However, the spatiotemporal regulatory mechanism of the generation of liver CD8$^+$ Trm cells and their responses to sporozoite challenge, as well as the protective antigens they recognize remain largely unknown. Here, we discuss the knowledge gap regarding liver CD8$^+$ Trm cell formation and the potential strategies to identify predominant protective antigens expressed in the exoerythrocytic stage, which is essential for high-efficacy malaria subunit pre-erythrocytic vaccine designation.

KEYWORDS

malaria, attenuated sporozoite vaccine, liver tissue-resident CD8$^+$ T cells, protective antigens, prime-trap/target

1 Introduction

Malaria is one of the most devastating diseases worldwide. In 2022, 249 million cases and 608,000 deaths were recorded, most of which were children (1). Malarial infections are caused by the genus *Plasmodium*, including *Plasmodium falciparum* (*P. falciparum*), *Plasmodium vivax* (*P. vivax*), *Plasmodium malariae*, *Plasmodium knowlesi*, and *Plasmodium ovale*, with *P. falciparum* being the most common parasite responsible for malaria-related deaths.

Malarial infections are initiated by the bite of an infected *Anopheles* mosquito. The sporozoites are inoculated into the dermis of the host during a mosquito bite and subsequently enter the bloodstream and circulate into the liver sinusoids, where sporozoites pass through the sinusoidal cell layer and invade hepatocytes. Sporozoites in hepatocytes sequentially transform into trophozoites and schizonts, producing thousands of hepatic merozoites. One *P. falciparum* sporozoite produces ~40,000 merozoites (2). The pre-erythrocytic stage is approximately 2 days for rodent malaria and approximately 1 week for human malaria. The blood stage begins when the released hepatic merozoites invade red blood cells, leading to fever, weakness, headache, anemia, and even death, owing to malarial parasites replicating in the blood. In contrast to the blood stage, patients with malaria are

clinically asymptomatic at the pre-erythrocytic stage (including sporozoite and liver stages). Moreover, the pre-erythrocytic stage is a key bottleneck in the life cycle of malarial parasites because mosquito bites deposit about tens to hundreds of sporozoites, and only a fraction reaches the liver (3). Vaccines targeting the pre-erythrocytic stage abrogate blood-stage infection, thus averting disease and disrupting transmission to the mosquito vector (4). Therefore, the pre-erythrocytic stage is an ideal target for malaria-preventative vaccines.

2 Whole sporozoite vaccine: a valuable model to dissect protective immunity against the pre-erythrocytic stage

Three approaches have been pursued to develop efficient pre-erythrocytic malaria vaccines: subunit vaccines, whole sporozoite vaccines (WSVs), and viral/bacterial vector-delivered vaccines (5). RTS, S/AS01E, the leading subunit vaccine, has been recently approved by the World Health Organization for use in moderate to high malaria endemic regions (6). However, the protective efficacy of RTS, S/AS01E is only approximately 30% for infants and 50% for children, and protection wanes after 18 months (7–9). R21/Matrix-M™ vaccine, which is regarded as the next-generation RTS, S-like vaccine, showed more than 70% protective efficacy in phase 2b trial (10), but its protective efficacy in phase III remains to be defined. In contrast, WSVs can induce high levels (> 90%) of sustained protection against malarial parasite infection (11–13). In whole sporozoite vaccination, subjects are immunized with sporozoites through mosquito bites or intradermal (i.d.)/intravenous (i.v.) injection, wherein sporozoite development in hepatocytes is arrested at the early or late stage due to attenuation, leading to persistent stimulation of the host immune system. To date, three WSVs, namely radiation-attenuated sporozoites (RAS) (14), genetically attenuated sporozoites (GAS) (15), and chemoprophylaxis vaccination (CVac) (16), have been developed using different attenuation approaches.

RAS were the first reported WSVs in which mosquitoes harboring infectious sporozoites were attenuated by X-ray irradiation. With a sufficient dose of irradiation for mosquito carrying sporozoites to prevent the completion of liver-stage infection but not over-irradiated to lose the immunogenicity required to induce immune-mediated protection (14). RAS development in the liver is arrested at an early stage and thus requires bites of more than 1,000 irradiated infected mosquitoes to induce sterile protection in human subjects (13). Unlike RAS production, the genetic attenuation of parasites is more precise and efficient since GAS are generated by deleting the specific gene responsible for parasite development in hepatocytes (15). Late liver stage-arresting GAS, generated by gene knockout, e.g., of the *P. falciparum* fabB/F gene, at the late liver stage, could develop into liver schizonts but fail to produce merozoites. The immunogenicity of late liver stage-arresting GAS is much higher than that of RAS or GAS arrested at the early stage because there are more antigens for the immune system to recognize (17). The safety issue for GAS is related to infection breakthrough. Clinical evaluation of p52/p36 GAP in humanized mouse models showed severe early liver-stage growth defects (18); nonetheless, infection breakthroughs have been achieved in human trials (19). After increasing the number of knockout genes, Pf GAP3KO (*Pf* p52/p36/SAP1) was demonstrated to be fully attenuated (20, 21), inducing relatively high protective immunity in controlled human malaria infection (CHMI) (22).

CVac involves vaccination with live sporozoites under anti-malarial drug prophylaxis, efficiently killing emerging blood-stage parasites but not liver-stage parasites (23). Under these circumstances, parasites can complete the entire liver-stage development, allowing a greater antigen repertoire to stimulate the host immune system. The negative effect of the blood stage on anti-liver-stage immune responses is also limited. Therefore, CVac immunogenicity is much higher than that of RAS, and 20-fold fewer infected mosquito bites are required for CVac to induce sterile protective immunity in controlling human malaria infection (16, 24). Initially, chloroquine was used to kill emerging blood-stage parasites after immunization with live sporozoites. However, the emergence and spread of chloroquine-resistant *P. falciparum* strains have raised safety concerns regarding chloroquine use in this vaccination approach; therefore, other anti-malarial drugs, such as mefloquine (24), artesunate (25), and pyrimethamine (12), have been used instead. Recently, primaquine and antibiotics (clindamycin and azithromycin) (26, 27), which arrest liver-stage parasite development, have been used as causal prophylaxis, eliciting high protective immunity.

Although attenuated sporozoites have proven to be the most efficient vaccines for preventing malaria infection, their wide application has been hampered by a requirement for mass production and safety limitations. Sporozoites must be aseptic, provided in large numbers, and transported via a cold chain (28). Sanaria (Rockville, MD, USA) established a facility for aseptic sporozoite production and has successfully produced infective *P. falciparum* sporozoites *in vitro* (29). Nevertheless, knowledge about the mechanism of protective immunity induced by attenuated sporozoites will help in designing high-efficacy next-generation subunit malaria vaccines.

3 Liver $CD8^+$ Trm cells: correlation with WSV-induced protection

Determining the correlation between attenuated sporozoite-induced protection and immune effectors could guide the design of efficient subunit malaria vaccines. Immunization with RAS swiftly activates $CD8^+$ T cells, which play a central role in the protective immunity induced by inoculating mice with RAS, as the sterile protection induced by RAS is abolished after $CD8^+$ T cell depletion (30, 31). Adoptive transfer experiments have also shown that activated effector $CD8^+$ T cells significantly resist sporozoite challenge (32). However, prolonged protection after vaccination is not dependent on these short-lived activated effector $CD8^+$ T cells.

Therefore, researchers have focused on memory $CD8^+$ T cell subsets, which provide long-term protection when induced by vaccines. In fact, both effector memory $CD8^+$ T (Tem) cells and central memory $CD8^+$ T (Tcm) cells have been detected in protected mice immunized with RAS (33, 34); however, only a high frequency of $CD8^+$ Tem cells can confer long-term protection induced after RAS immunization (35, 36).

$CD8^+$ Tem cells patrol the blood and non-lymphoid tissues (NLTs) due to a lack of the expression of the secondary lymphoid organ (SLO)-homing receptors, such as L-selectin (CD62L), and exert effector functions during recall responses. Tcm cells are $CD62L^+$ cells and are enriched in SLOs. They proliferate and differentiate into effector cells during recall responses (37, 38). Notably, apart from circulating memory $CD8^+$ T cells ($CD8^+$ Tem and Tcm cells), two pioneering studies discovered a new memory T cell subset—tissue-resident $CD8^+$ memory T (Trm) cells—which enhances regional immunity in the host (39, 40). Like $CD8^+$ Tem, $CD8^+$ Trm cells do not express CD62L but highly express CD69, which contributes to their retention in tissues by forming a complex with sphingosine-1-phosphate receptor (S1PR1) and inhibiting S1PR1-induced tissue egress (41, 42). Liver $CD8^+$ Trm cells were characterized by the upregulation of tissue retention molecules CD11a, CXCR3, and CXCR6 and the downregulation of tissue egress molecules CD62L and CCR7 (43). Although $CD8^+$ Tem cells have also been implicated in protective immunity after RAS immunization (36), liver $CD8^+$ Trm cells were found to patrol the hepatic sinuses and form the front-line defense against malarial liver-stage infection (43). The depletion of liver $CD8^+$ Trm cells by anti-CXCR3 antibody abrogates RAS protection and demonstrates their essential roles in the protection induced by RAS (43).

As the liver $CD8^+$ Trm cells cannot be detected in peripheral blood, the inability to obtain human liver samples greatly limited our knowledge about human liver $CD8^+$ Trm against the malaria liver stage. The existence of human liver $CD8^+$ Trm was demonstrated through a study of transplantation, in which T cells were detected in the donor liver transplanted for more than a decade (44). However, unlike liver $CD8^+$ Trm cells in mice, 5–30% of human liver $CD8^+$ Trm cells express CD103 (44–46). $CD103^+$ liver Trm cells were specific for hepatotropic infections, but $CD103^-$ Trm cells were specific for both hepatotropic and non-hepatotropic infections (45). Human liver Trm cells have been associated with protective immunity against HBV infection (46). In malaria, intravenous RAS vaccination of non-human primates resulted in the generation of parasite-specific memory $CD8^+$ T cells in the liver, but not in the blood. In contrast, parasite-specific memory $CD8^+$T cells were not detected after subcutaneous RAS vaccination, which is markedly less protective (47). This indicated that liver $CD8^+$ Trm cells are also essential for protection against liver-stage infection in non-human primates and humans.

Considering only 20% T cells in liver could be detected by flow cytometry (48), it is estimated that approximately 2.5 million liver $CD8^+$ Trm cells are required to screen 99% of the whole liver for parasite infection during a 2-day window in mouse liver-stage malaria (43).This indicated that a large amount of liver $CD8^+$ Trm cells are required to prevent progression to the blood stage, and the optimal generation of $CD8^+$ Trm cells in the liver could guide the design of highly effective malaria vaccines.

4 Prospects for pre-erythrocytic stage vaccine designed to induce liver $CD8^+$ Trm cells

Epithelial $CD8^+$ Trm cells are thought to be derived from circulating effector $CD8^+$ T cells wherein the Trm cell lineage is committed (49). Consistently, liver $CD8^+$ Trm cells were also generated from circulating effector $CD8^+$ T cells, as only the *in vitro* activated $CD8^+$ T cells, but not naïve $CD8^+$ T cells, intravenously adoptive transferred, were found to be seeded in sinusoids and transformed into liver $CD8^+$ Trm cells (50). Therefore, the magnitude of $CD8^+$ T cell responses during priming would affect the number of liver Trm cells that are finally generated.

Sporozoite injected intravenously could be detected in the spleen, lung, and liver, but only develop in the liver (51). Splenectomy prior to RAS immunization by i.v. greatly reduced the protection of the vaccinated mice, indicating the essential role of the spleen in the priming of parasite-specific $CD8^+$ T cell responses (52). Further study showed that splenic $CD11c^+$ DCs were responsible for the cross-priming of sporozoite circumsporozoite protein (CSP)-specific $CD8^+$ T cells (53). During this process, $CD4^+$ T cells are essential for activating and maintaining CSP-specific $CD8^+$ T cells via the secretion of interleukin (IL)-4 (54, 55). However, parasite-infected hepatocytes are captured by monocyte-derived $CD11c^+$ cells, and $CD8^+$ T cells are primed in the liver-draining lymphoid nodes, after RAS successfully invade hepatocytes and develop into EEFs (56). Notwithstanding, there was much more pronounced $CD8^+$T cell expansion in the spleen than in the liver draining lymphoid nodes following intravenous RAS vaccination (57). Moreover, γδ T cells are required to prime parasite-specific $CD8^+$ T cells possibly through promoting $CD8\alpha^+$ DC influx into the liver (58). In contrast, malaria blood-stage infections significantly suppress protective $CD8^+$ T cells against the liver stage by inhibiting splenic DC maturation (59). After priming, the activated $CD8^+$ T cells either generated in the liver or circulated from the spleen, would convert into $CD8^+$ Trm cells. The turnover of the circulating effector $CD8^+$ T cells into liver $CD8^+$ Trm cells was significantly affected by the local inflammatory status or antigen expression (50), which was consistent with the formation of resident memory $CD8^+$ T cells in other tissues (60, 61) (Figure 1).

Based on the knowledge of liver Trm formation, a prime-trap/target strategy has been developed to generate high-frequency, parasite-specific $CD8^+$ Trm cells in the liver. As the cross-priming by DGNR-1^+ ($CLEC9A^+$) DCs was essential for lung Trm precursor commitment (62), anti-Clec9A was fused to a malaria-specific epitope to increase the priming efficiency of Trm precursors (43, 62). After priming, parasite-specific Trm precursors would convert into Trm cells under the effect of the local inflammatory status or antigen expression in the liver. This goal was achieved by liver-targeting nanoparticles or intravenous infection with the

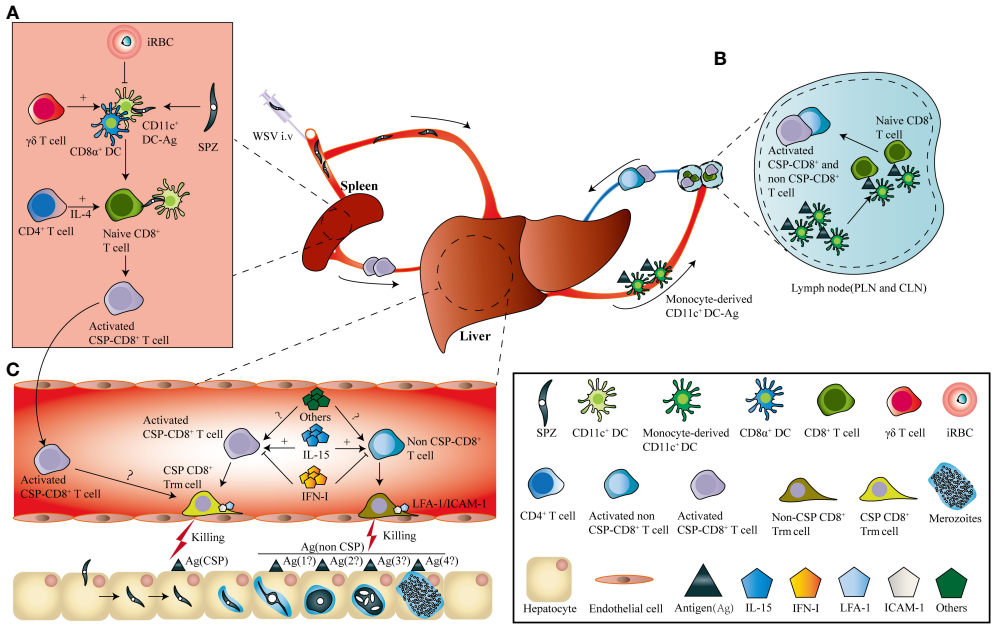

FIGURE 1
I.v immunization of WSV induces the generation of parasite-specific liver CD8+ Trm. **(A)**. After i.v. immunization, sporozoites (SPZs) enter the spleen and are captured by conventional dendritic cells, and circumsporozoite protein (CSP)-specific $CD8^+$ T cells are cross-primed. During this process, γδ T cells were required to prime the effector $CD8^+$ T cells by inhibiting the influx of $CD11c^+$ dendritic cells into the liver, and $CD4^+$ T cells promote $CD8^+$ T cell activation through interleukin (IL)-4 secretion. In contrast, malaria blood-stage infections suppress protective $CD8^+$ T cells against the liver stage by inhibiting splenic DC maturation **(B)**. Sporozoites invading the liver develop into exo-erythrocytic forms (EEFs), which are captured by monocyte-derived $CD11c^+$ cells and prime both CSP- and non-CSP-specific $CD8^+$ T cells in the liver-draining lymph nodes. **(C)**. Both CSP-and non-CSP-specific $CD8^+$ T cells primed in liver-draining lymph nodes, as well as CSP-specific $CD8^+$ T cells activated in the spleen, circulate into the liver sinusoids and transform into CSP-and non-CSP-$CD8^+$ Trm cells. The location of $CD8^+$ Trm cells in liver sinusoids depends on the interaction between LFA-1 on $CD8^+$ Trm cells and ICAM-1 on endothelial cells. The transformation of $CD8^+$ Trm cells is positively and negatively regulated by IL-15 and type I interferon, as well as by other factors, respectively.

recombinant adeno-associated virus vector or attenuated sporozoites (43, 63–65). Clinical trials have also shown that the delivery of recombinant chimpanzee adenovirus (ChAd) and modified vaccinia Ankara (MVA) viral vectors expressing protective liver-stage epitopes intramuscularly (i.m.) through a prime-boost strategy significantly induced circulating $CD8^+$ T cell responses, but with low levels of protection in malaria-naïve humans. In contrast, the recombinant viral vector vaccine boosted with MVA i.v. generated higher protection through the induction of high frequency of liver $CD8^+$ Trm cells (63) (Figure 2). It seems that the different protective immunity of RAS vaccinated by i.v. and i.d. might be closely associated with their ability to generate liver Trm. As compared to RAS immunized i.v, RAS injected by i.d. seldom enters into the liver and develops into EEFs in hepatocytes (66). Under this circumstance, fewer Trm precursors primed in the draining lymph nodes would convert into liver Trm, as i.d. injection of RAS does not lead to inflammatory response and parasite antigen expression in the liver.

Strikingly, a single immunization with a self-adjuvating glycolipid-peptide conjugate vaccine, designed to simultaneously activate natural killer T cell (NKT) and DCs, has been reported to generate large numbers of liver $CD8^+$ Trm cells and protect against malaria infection (67). As liposome nanoparticles (LNPs) have been suggested as the most promising platform for designing vaccines against a variety of infectious diseases (68), and mRNA in LNP delivered i.v efficiently targets and expresses in the liver (69). Thereby, a messenger RNA (mRNA)-based vaccine containing an NKT cell agonist has been designed and successfully induced sterile protection against sporozoite challenge, which was unaffected by previous exposure to blood-stage infection (70) (Figure 2). This indicated that the local inflammatory response induced by NKT cell agonist and targeted expression of malaria antigen in liver by i.v delivery of mRNA vaccine could efficiently promote the generation of liver $CD8^+$ Trm.

5 Challenges with the research of liver $CD8^+$ Trm cells against malaria liver stage

Great progress has been made in understanding the essential role of $CD8^+$ Trm cells in the protection induced by RAS vaccination. Nonetheless, several knowledge gaps, including the mechanism of liver $CD8^+$ Trm commitment, formation, and maintenance, and secondary responses to sporozoite challenge, as well as the protective antigens they recognized, warrant further investigation.

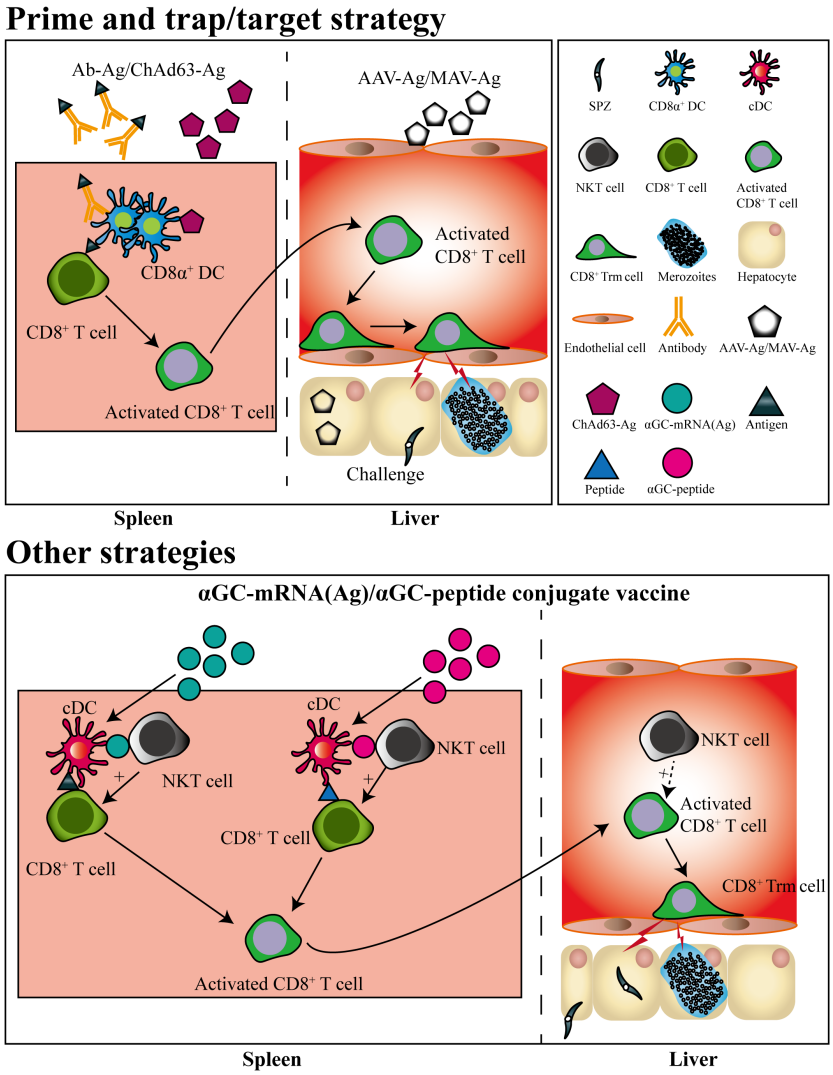

FIGURE 2
Pre-erythrocytic subunit vaccine designed by prime-and-trap/target strategies. $CD8^+$ T cells are primed by antigens conjugated with a dendritic cell-targeted antibody or antigen-expressed chimpanzee Adenovirus (ChAd) 63 vector, after which the primed $CD8^+$ T cells are trapped or targeted by delivering adeno-associated virus (AAV) or modified vaccinia Ankara (MVA) viral vector expressing the same antigen. The primed $CD8^+$ T cells trapped or targeted in liver would convert into $CD8^+$ Trm cells. Liver $CD8^+$ Trm cells could also be generated by a single immunization of mRNA vaccine or self-adjuvating glycolipid-peptide conjugate vaccine both containing the natural killer T cell agonist αGC.

5.1 The regulatory mechanism of liver $CD8^+$ Trm cells generation and maintenance

Two models have been proposed for the formation of $CD8^+$ Trm cells. One is the "local divergent" model, in which the lineage of Trm was determined by the local tissue microenvironment. The other is the "systematic divergent" model, in which the lineage decision of Trm has been made during activation, and the local tissue micro-environment promotes the generation of $CD8^+$ Trm. Most current studies focused on $CD69^+CD103^+$ Trm cells in epithelial tissues and supported the "systematic divergent" model for $CD8^+$ Trm generation (49). In this model, epithelial $CD8^+$ Trm precursors were poised in naïve $CD8^+$ T cells (62, 71), and the activated $CD8^+$ T cells were more prone to circulate into nonlymphoid tissues (NLTs), and differentiated into mature $CD8^+$ Trm in the local tissue microenvironment (72, 73). Parasite-specific $CD8^+$ T cells were cross-primed in different SLOs with the different immunization routes of RAS. For instance, $CD8^+$ T cells were primed by DCs in skin-draining lymph nodes when RAS was i.d. or s.c. immunization, but sporozoite-specific $CD8^+$ T cells and EEF-specific $CD8^+$ T cells were primed in the spleen by $CD8\alpha^+$ DCs (57) and liver-draining lymph nodes by monocyte-derived $CD11c^+$ cells (56, 66) after RAS vaccination i.v, respectively (Figure 1). It is well known that i.v. immunization of RAS is more prone to induce sterile protection than RAS vaccinated i.d. or s.c. in humans (47, 74). However, whether RAS immunized by different routes leads to their distinct abilities to commit liver $CD8^+$ Trm cells is largely unknown. Although a vaccine designed to target DNGR-1^+ DCs for cross-

priming parasite-specific CD8$^+$ T cells successfully induced the generation of liver CD8$^+$ Trm (43), whether this approach well poised liver CD8$^+$ Trm precursors also remains to be defined.

Liver and epithelial Trm cells share a common gene expression signature that is regulated by the transcription factors Hobit and Blimp1 (75); however, the regulatory mechanism underlying the formation of CD8$^+$ Trm located in distinct tissues is different (76). For example, chemokines, such as CXCL9 and CXCL10, recruit - Trm precursors by acting on CXCR3 on their surface to the inflamed tissues, promoting Trm cell formation in the skin (73). In contrast, liver Trm cells also express CXCR3 (77), but this chemokine receptor is not necessary for the formation and maintenance of liver Trm (78). However, CXCR6, which is highly expressed by liver Trm cells, is required for their long-term maintenance (78). Transforming growth factor (TGF)-β signaling is essential for the maintaining of Trm cells in the intestine and salivary glands, but not for those in the fat, kidney, and liver (76). As compared to Trm in other tissues, an extreme difference was found between skin and liver CD8$^+$ Trm (76, 79). Several inflammatory cytokines, such as IL-7, IL-15, IL-33, and TNF-α, have been reported to modulate epithelial CD8$^+$ Trm formation (80, 81); only IL-15, but not TNF and IFN-γ, has a significant effect on the generation of liver Trm cells (50). Strikingly, type I IFN signaling, which is activated by EEFs in hepatocytes (82), even inhibits liver CD8$^+$ Trm cell generation (83) (Figure 1). Recently, a system analysis of immune responses to the vaccination of the attenuated *P. falciparum* sporozoite showed that protection was associated with the inflammatory status of the human volunteers (84, 85). Although the formation of both hepatic and epithelial Trm did not always require antigen presentation (50, 61, 86, 87), local antigen presentation promoted liver CD8$^+$ Trm formation (50). Liver Trm cells are located in the sinusoids, a part of the bloodstream, but epithelial Trm cells are found in the parenchyma of peripheral tissues. Integrin CD103, which is highly expressed in epithelial Trm cells of the skin and the gut, is required for T cell residence in the skin (39, 73, 88). However, differentiated liver CD8$^+$ Trm cells do not express CD103 but upregulate the expression of the integrin LFA-1(CD11a/CD18). The interaction between LFA-1 and ICAM-1 allows liver CD8$^+$ Trm cells to patrol and remain in the hepatic sinusoids (77) (Figure 1). Therefore, the regulation of liver CD8$^+$ Trm cell generation and maintenance by tissue microenvironment is distinct from that of epithelial CD8$^+$ Trm cell, and the regulatory mechanism of liver CD8$^+$ Trm cell formation is required to be elucidated in the future.

5.2 Secondary responses of liver CD8$^+$ Trm cells to sporozoite challenge

Upon reinfection, skin CD8$^+$ Trm cells were found to expand locally, and the secondary Trm cells formed from pre-existing Trm cells, as well as from precursors recruited from the circulation (89). However, further study showed that the expansion of CD103$^+$ Trm cells *in situ* was limited after secondary infection (90). Upon secondary challenge, Trm cells were mainly derived from CD103$^-$ Trm cells, with limited contribution from the circulating Tcm (90). As compared to skin CD8$^+$ Trm cells, the adoptive transfer of liver CD8$^+$ Trm cells exhibited a higher potential to trans-differentiate into circulating memory T cells and other tissue Trm cells in response to secondary challenge (79). In addition, skin CD8$^+$ Trm cells could sense the invading pathogens (91) and activate both innate and adaptive immune responses upon secondary infection (92). Although liver CD8$^+$ Trm cells expressed IFN-γ, TNF, granzyme B and CD107a (43), the protective mechanism of liver CD8$^+$ Trm cells of the RAS-immunized mice against sporozoite challenge remains to be defined. Therefore, the dynamic response and protective mechanism of liver CD8$^+$ Trm cells upon sporozoite challenge also needs to be clarified in the future researches.

5.3 Identification of protective antigens recognized by liver CD8$^+$ Trm cells

CSP is the predominant protective antigen of RAS (93), but non-CSP antigens expressed by EEFs are also required for the full protection induced by attenuated sporozoites (93). This is confirmed by the finding that the immunogenicity of attenuated sporozoites arrested at an early stage was much lower than that of sporozoites arrested at a late stage (17). Thus, identifying antigens presented by MHC-I molecules in infected hepatocytes may uncover the unidentified antigens required for full protection of WSV.

In the pre-genomic era, a few protective antigens, such as CSP, thrombospondin-related anonymous protein (TRAP, also called SSP2), and liver-stage antigen-1, were primarily identified using immunized sera or oligonucleotide probe screening of sporozoites or *P. falciparum* genomic DNA expression libraries (94–96). In 2002, the genomes of *P. falciparum* and rodent malarial parasites were sequenced (97, 98), beginning the post-genomic era. With the availability of transcriptomic and proteomic data on the rodent malaria liver stage (99), two liver-stage antigens, ribosomal L3 protein and TRAP, were identified through using protective CD8$^+$ T cells to screen H2^b-restricted peptides predicted by genome-wide analysis (100, 101). Recently, ribosomal protein L6 (RPL6) of *Plasmodium berghei*, a novel protective liver-stage antigen, was identified by the approach of combinational peptide library scan and protein Blast within PlasmoDB (57, 65). Based on *P. falciparum* genomic and proteomic data and a combination of bioinformatics predictions and human leukocyte antigen analysis, 16 pre-erythrocytic antigenic proteins were identified in volunteers immunized with *P. falciparum* RAS (102).

With the development of T-cell receptor (TCR) repertoire sequencing techniques, a functional TCR-guided antigen discovery strategy, T-scan, has been developed (103). This strategy enabled genome-wide antigen library screening using a given T-cell clone with an orphan TCR of interest. Upon TCR-pMHC engagement, granzyme B (GzB) is delivered to target cells and cleaves the fluorescent protein (IFP)-based GzB reporter (IFP^{GZB}) and activates the IFP^{GZB} reporter. The target cells are then sorted by IFP, and the encoding antigen is identified by secondary generation sequencing. Similar strategies have been adopted to identify both MHC-I- and MHC-II-derived peptides

of the malaria blood-stage (104, 105), but only the peptides in CSP recognized by the follicular helper T cell clones expanded in volunteers immunized with WSVs have been recently reported (106). Identifying peptides presented by MHC-I molecules against the malarial liver stage is greatly hampered by the difficulty of obtaining sufficient parasites to construct a cDNA library for screening. Since an extremely low rate of hepatocytes was often infected with rodent (< 5%) and human malaria parasites (< 2.5%) *in vitro* (107, 108), enough infected hepatocytes of sufficient purity could not be obtained for transcriptomic and proteomic analyses.

Protective antigens should not only be immunogenic to induce $CD8^+$ T cell responses but also be presented to MHC-I on the surface of the infected cells for $CD8^+$ T cells to recognize and kill the pathogens (109). For the malaria liver stage, protective antigens should be proteins with the ability to translocate from the parasitophorous vacuole into the cytosol of the infected hepatocyte and subsequently be presented to MHC-I molecules (110, 111). This was exemplified by the predominant protective antigen CSP, which can access hepatocyte cytoplasm and presented to MHC-I on hepatocytes (112–114). Therefore, the combination of *in silico* prediction of the candidate peptides of malaria liver-stage antigens presented by MHC-I molecules and TCR repertoire sequencing would be an alternative approach to identify the protective antigens recognized by $CD8^+$ Trm after WSV immunization.

6 Concluding remarks

Recent scientific findings have demonstrated that liver $CD8^+$ Trm cells are the predominant immune effectors of WSVs. With priming regulatory mechanisms and liver $CD8^+$ Trm cell maintenance beginning to be elucidated, a prime-trap strategy has been developed for pre-erythrocytic vaccines to optimally generate liver $CD8^+$ Trm cells. However, many knowledge gaps are still to be elucidated. Firstly, the environmental cues and cellular mechanisms promoting the optimal generation and maintenance of liver $CD8^+$ Trm cells, as well as the dynamic secondary response to the sporozoite challenge, have not been completely defined. Secondly, non-CSP antigens are also important for the protective immunity induced by attenuated sporozoite vaccines, but only a few parasite antigens at the liver stage have been identified, limiting the designation of highly efficient subunit malaria vaccines. Finally, our understanding of the correlation between liver $CD8^+$ Trm cells and the protection induced by WSVs stems mainly from studies in mouse models, and verification in human subjects is warranted for translational research.

Author contributions

CZ: Writing – original draft. SJ: Writing – original draft. WX: Writing – review & editing.

Funding

The author(s) declare financial support was received for the research, authorship, and/or publication of this article. This work was supported by the State Key Program of the National Natural Science Foundation of China (No. 81830067) and the National Natural Science Foundation of China (Nos. 82072299).

Acknowledgments

We would like to thank Editage (www.editage.cn) for English language editing.

Conflict of interest

The authors declare that the research was conducted in the absence of any commercial or financial relationships that could be construed as a potential conflict of interest.

Publisher's note

References

1. World Health Organization. *World malaria report* (2023). Available at: https://www.who.int/teams/global-malaria-programme/reports/world-malaria-report-2023 (Accessed December 26, 2023).

2. Miller LH, Ackerman HC, Su XZ, Wellems TE. Malaria biology and disease pathogenesis: insights for new treatments. *Nat Med* (2013) 19:156–67. doi: 10.1038/nm.3073

3. Amino R, Thiberge S, Martin B, Celli S, Shorte S, Frischknecht F, et al. Quantitative imaging of Plasmodium transmission from mosquito to mammal. *Nat Med* (2006) 12:220–4. doi: 10.1038/nm1350

4. Draper SJ, Sack BK, King CR, Nielsen CM, Rayner JC, Higgins MK, et al. Malaria vaccines: Recent advances and new horizons. *Cell Host Microbe* (2018) 24:43–56. doi: 10.1016/j.chom.2018.06.008

5. Duffy PE, Patrick Gorres J. Malaria vaccines since 2000: progress, priorities, products. *NPJ Vaccines* (2020) 5:48. doi: 10.1038/s41541-020-0196-3

6. World Health Organization. *Approves Historic Rts, S Malaria Vaccine* (2021). Available at: https://lenstapesmed.com/who-approves-historic-rtss-malaria-vaccine/ (Accessed August 15, 2023).

7. Agnandji ST, Lell B, Soulanoudjingar SS, Fernandes JF, Abossolo BP, Conzelmann C, et al. First results of phase 3 trial of RTS, S/AS01 malaria vaccine in African children. *N Engl J Med* (2011) 365:1863–75. doi: 10.1056/NEJMoa1102287

8. Agnandji ST, Lell B, Fernandes JF, Abossolo BP, Methogo BG, Kabwende AL, et al. A phase 3 trial of RTS, S/AS01 malaria vaccine in African infants. *N Engl J Med* (2012) 367:2284–95. doi: 10.1056/NEJMoa1208394

9. Rts SCTP. Efficacy and safety of RTS, S/AS01 malaria vaccine with or without a booster dose in infants and children in Africa: final results of a phase 3, individually randomised, controlled trial. *Lancet* (2015) 386:31–45. doi: 10.1016/S0140-6736(15)60721-8

10. Datoo MS, Natama MH, Somé A, Traoré O, Rouamba T, Bellamy D, et al. Efficacy of a low-dose candidate malaria vaccine, R21 in adjuvant Matrix-M, with seasonal administration to children in Burkina Faso: a randomised controlled trial. *Lancet* (2021) 397:1809–18. doi: 10.1016/S0140-6736(21)00943-0

11. Mordmuller B, Surat G, Lagler H, Chakravarty S, Ishizuka AS, Lalremruata A, et al. Sterile protection against human malaria by chemoattenuated PfSPZ vaccine. *Nature* (2017) 542:445–9. doi: 10.1038/nature21060

12. Mwakingwe-Omari A, Healy SA, Lane J, Cook DM, Kalhori S, Wyatt C, et al. Two chemoattenuated PfSPZ malaria vaccines induce sterile hepatic immunity. *Nature* (2021) 595:289–94. doi: 10.1038/s41586-021-03684-z

13. Hoffman SL, Goh LM, Luke TC, Schneider I, Le TP, Doolan DL, et al. Protection of humans against malaria by immunization with radiation-attenuated *Plasmodium falciparum* sporozoites. *J Infect Dis* (2002) 185:1155–64. doi: 10.1086/339409

14. Nussenzweig RS, Vanderberg J, Most H, Orton C. Protective immunity produced by the injection of x-irradiated sporozoites of Plasmodium berghei. *Nature* (1967) 216:160–2. doi: 10.1038/216160a0

15. Mueller AK, Labaied M, Kappe SHI, Matuschewski K. Genetically modified Plasmodium parasites as a protective experimental malaria vaccine. *Nature* (2005) 433:164–7. doi: 10.1038/nature03188

16. Roestenberg M, McCall M, Hopman J, Wiersma J, Luty AJF, Jan van Gemert G, et al. Protection against a malaria challenge by sporozoite inoculation. *N Engl J Med* (2009) 361:468–77. doi: 10.1056/NEJMoa0805832

17. Butler NS, Schmidt NW, Vaughan AM, Aly AS, Kappe SHI, Harty JT. Superior antimalarial immunity after vaccination with late liver stage-arresting genetically attenuated parasites. *Cell Host Microbe* (2011) 9:451–62. doi: 10.1016/j.chom.2011.05.008

18. VanBuskirk KM, O'Neill MT, de la Vega P, Maier AG, Krzych U, Williams J, et al. Preerythrocytic, live-attenuated *Plasmodium falciparum* vaccine candidates by design. *Proc Natl Acad Sci U.S.A.* (2009) 106:13004–9. doi: 10.1073/pnas.0906387106

19. Spring M, Murphy J, Nielsen R, Dowler M, Bennett JW, Zarling S, et al. First-in-human evaluation of genetically attenuated *Plasmodium falciparum* sporozoites administered by bite of Anopheles mosquitoes to adult volunteers. *Vaccine* (2013) 31:4975–83. doi: 10.1016/j.vaccine.2013.08.007

20. Kublin JG, Mikolajczak SA, Sack BK, Fishbaugher ME, Seilie A, Shelton L, et al. Complete attenuation of genetically engineered *Plasmodium falciparum* sporozoites in human subjects. *Sci Transl Med* (2017) 9:eaad9099. doi: 10.1126/scitranslmed.aad9099

21. Mikolajczak SA, Lakshmanan V, Fishbaugher M, Camargo N, Harupa A, Kaushansk A, et al. A next-generation genetically attenuated *Plasmodium falciparum* parasite created by triple gene deletion. *Mol Ther* (2014) 22:1707–15. doi: 10.1038/mt.2014.85

22. Murphy SC, Vaughan AM, Kublin JG, Fishbauger M, Seilie AM, Cruz KP, et al. A genetically engineered *Plasmodium falciparum* parasite vaccine provides protection from controlled human malaria infection. *Sci Transl Med* (2022) 14:eabn9709. doi: 10.1126/scitranslmed.abn9709

23. Belnoue E, Costa FTM, Frankenberg T, Vigário AM, Voza T, Leroy N, et al. Protective T cell immunity against malaria liver stage after vaccination with live sporozoites under chloroquine treatment. *J Immunol* (2004) 172:2487–95. doi: 10.4049/jimmunol.172.4.2487

24. Bijker EM, Schats R, Obiero JM, Behet MC, van Gemert G-J, van de Vegte-Bolmer M, et al. Sporozoite immunization of human volunteers under mefloquine prophylaxis is safe, immunogenic and protective: a double-blind randomized controlled clinical trial. *PloS One* (2014) 9:e112910. doi: 10.1371/journal.pone.0112910

25. Peng X, Keitany GJ, Vignali M, Chen L, Gibson C, Choi K, et al. Artesunate versus chloroquine infection-treatment-vaccination defines stage-specific immune responses associated with prolonged sterile protection against both pre-erythrocytic and erythrocytic *Plasmodium yoelii* infection. *J Immunol* (2014) 193:1268–77. doi: 10.4049/jimmunol.1400296

26. Friesen J, Silvie O, Putrianti ED, Hafalla JCR, Matuschewski K, Borrmann S. Natural immunization against malaria: causal prophylaxis with antibiotics. *Sci Transl Med* (2010) 2:40ra49. doi: 10.1126/scitranslmed.3001058

27. Putrianti ED, Silvie O, Kordes M, Borrmann S, Matuschewski K. Vaccine-like immunity against malaria by repeated causal-prophylactic treatment of liver-stage Plasmodium parasites. *J Infect Dis* (2009) 199:899–903. doi: 10.1086/597121

28. Luke TC, Hoffman SL. Rationale and plans for developing a non-replicating, metabolically active, radiation-attenuated *Plasmodium falciparum* sporozoite vaccine. *J Exp Biol* (2003) 206:3803–8. doi: 10.1242/jeb.00644

29. Eappen AG, Li T, Marquette M, Chakravarty S, Kc N, Zanghi G, et al. *In vitro* production of infectious *Plasmodium falciparum* sporozoites. *Nature* (2022) 612:534–9. doi: 10.1038/s41586-022-05466-7

30. Weiss WR, Sedegah M, Beaudoin RL, Miller LH, Good MF. $CD8^+$ T cells (cytotoxic/suppressors) are required for protection in mice immunized with malaria sporozoites. *Proc Natl Acad Sci U.S.A.* (1988) 85:573–6. doi: 10.1073/pnas.85.2.573

31. Sano G, Hafalla JC, Morrot A, Abe R, Lafaille JJ, Zavala F. Swift development of protective effector functions in naive CD8(+) T cells against malaria liver stages. *J Exp Med* (2001) 194:173–80. doi: 10.1084/jem.194.2.173

32. Krzych U, Schwenk R, Guebre-Xabier M, Sun P, Palmer D, White K, et al. The role of intrahepatic lymphocytes in mediating protective immunity induced by attenuated *Plasmodium berghei* sporozoites. *Immunol Rev* (2000) 174:123–34. doi: 10.1034/j.1600-0528.2002.00013h.x

33. Guebre-Xabier M, Schwenk R, Krzych U. Memory phenotype CD8(+) T cells persist in livers of mice protected against malaria by immunization with attenuated *Plasmodium berghei* sporozoites. *Eur J Immunol* (1999) 29:3978–86. doi: 10.1002/(SICI)1521-4141(199912)29:12<3978::AID-IMMU3978>3.0.CO;2-0

34. Berenzon D, Schwenk RJ, Letellier L, Guebre-Xabier M, Williams J, Krzych U. Protracted protection to *Plasmodium berghei* malaria is linked to functionally and phenotypically heterogeneous liver memory $CD8^+$ T cells. *J Immunol* (2003) 171:2024–34. doi: 10.4049/jimmunol.171.4.2024

35. Schmidt NW, Butler NS, Badovinac VP, Harty JT. Extreme CD8 T cell requirements for anti-malarial liver-stage immunity following immunization with radiation attenuated sporozoites. *PloS Pathog* (2010) 6:e1000998. doi: 10.1371/journal.ppat.1000998

36. Lefebvre MN, Surette FA, Anthony SM, Vijay R, Jensen IJ, Pewe LL, et al. Expeditious recruitment of circulating memory CD8 T cells to the liver facilitates control of malaria. *Cell Rep* (2021) 37:109956. doi: 10.1016/j.celrep.2021.109956

37. Sallusto F, Lenig D, Förster R, Lipp M, Lanzavecchia A. Two subsets of memory T lymphocytes with distinct homing potentials and effector functions. *Nature* (1999) 401:708–12. doi: 10.1038/44385

38. Masopust D, Vezys V, Marzo AL, Lefrançois L. Preferential localization of effector memory cells in nonlymphoid tissue. *Science* (2001) 291:2413–7. doi: 10.1126/science.1058867

39. Gebhardt T, Wakim LM, Eidsmo L, Reading PC, Heath WR, Carbone FR. Memory T cells in nonlymphoid tissue that provide enhanced local immunity during infection with herpes simplex virus. *Nat Immunol* (2009) 10:524–30. doi: 10.1038/ni.1718

40. Wakim LM, Waithman J, van Rooijen N, Heath WR, Carbone FR. Dendritic cell-induced memory T cell activation in nonlymphoid tissues. *Science* (2008) 319:198–202. doi: 10.1126/science.1151869

41. Walsh DA, Borges da Silva H, Beura LK, Peng C, Hamilton SE, Masopust D, et al. The functional requirement for CD69 in establishment of resident memory CD8 (+) T cells varies with tissue location. *J Immunol* (2019) 203:946–55. doi: 10.4049/jimmunol.1900052

42. Mackay LK, Braun A, Macleod BL, Collins N, Tebartz C, Bedoui S, et al. Cutting edge: CD69 interference with sphingosine-1-phosphate receptor function regulates peripheral T cell retention. *J Immunol* (2015) 194:2059–63. doi: 10.4049/jimmunol.1402256

43. Fernandez-Ruiz D, Ng WY, Holz LE, Ma JZ, Zaid A, Wong YC, et al. Liver-resident memory $CD8^+$ T cells form a front-line defense against malaria liver-stage infection. *Immunity* (2016) 45:889–902. doi: 10.1016/j.immuni.2016.08.011

44. Pallett LJ, Burton AR, Amin OE, Rodriguez-Tajes S, Patel AA, Zakeri N, et al. Longevity and replenishment of human liver-resident memory T cells and mononuclear phagocytes. *J Exp Med* (2020) 217:e20200050. doi: 10.1084/jem.20200050

45. Kim JH, Han JW, Choi YJ, Rha M-S, Koh JY, Kim KH, et al. Functions of human liver $CD69^+CD103\text{-}CD8^+$ T cells depend on HIF-2α activity in healthy and pathologic livers. *J Hepatol* (2020) 72:1170–81. doi: 10.1016/j.jhep.2020.01.010

46. Pallett LJ, Davies J, Colbeck EJ, Robertson F, Hansi N, Easom NJW, et al. IL-2^{high} tissue-resident T cells in the human liver: Sentinels for hepatotropic infection. *J Exp Med* (2017) 214:1567–80. doi: 10.1084/jem.20162115

47. Epstein JE, Tewari K, Lyke KE, Sim BK, Billingsley PF, Laurens MB, et al. Live attenuated malaria vaccine designed to protect through hepatic CD8 T cell immunity. *Science* (2011) 334:475–80. doi: 10.1126/science.1211548

48. Steinert EM, Schenkel JM, Fraser KA, Beura LK, Manlove LS, Igyártó BZ, et al. Quantifying memory CD8 T cells reveals regionalization of immunosurveillance. *Cell* (2015) 161:737–49. doi: 10.1016/j.cell.2015.03.031

49. Kok L, Masopust D, Schumacher TN. The precursors of CD8(+) tissue resident memory T cells: from lymphoid organs to infected tissues. *Nat Rev Immunol* (2022) 22:283–93. doi: 10.1038/s41577-021-00590-3

50. Holz LE, Prier JE, Freestone D, Steiner TM, English K, Johnson DN, et al. CD8 (+) T cell activation leads to constitutive formation of liver tissue-resident memory T cells that seed a large and flexible niche in the liver. *Cell Rep* (2018) 25:68–79 e4. doi: 10.1016/j.celrep.2018.08.094

51. Wen-yue X, Xing-xiang W, Jie Q, Jian-hua D, Fu-sheng H. *Plasmodium yoelii*: influence of immune modulators on the development of the liver stage. *Exp Parasitol* (2010) 126:254–8. doi: 10.1016/j.exppara.2010.05.005

52. Spitalny GL, Rivera-Ortiz CI, Nussenzweig RS. *Plasmodium berghei*: the spleen in sporozoite-induced immunity to mouse malaria. *Exp Parasitol* (1976) 40:179–88. doi: 10.1016/0014-4894(76)90080-1

53. Jung S, Unutmaz D, Wong P, Sano G, De los Santos K, Sparwasser T, et al. *In vivo* depletion of $CD11c^+$ dendritic cells abrogates priming of $CD8^+$ T cells by exogenous cell-associated antigens. *Immunity* (2002) 17:211–20. doi: 10.1016/S1074-7613(02)00365-5

54. Carvalho LH, Sano G, Hafalla JC, Morrot A, Curotto de Lafaille MA, Zavala F. IL-4-secreting $CD4^+$ T cells are crucial to the development of $CD8^+$ T-cell responses against malaria liver stages. *Nat Med* (2002) 8:166–70. doi: 10.1038/nm0202-166

55. Overstreet MG, Chen YC, Cockburn IA, Tse SW, Zavala F. CD4$^+$ T cells modulate expansion and survival but not functional properties of effector and memory CD8$^+$ T cells induced by malaria sporozoites. *PloS One* (2011) 6:e15948. doi: 10.1371/journal.pone.0015948

56. Kurup SP, Anthony SM, Hancox LS, Vijay R, Pewe LL, Moioffer SJ, et al. Monocyte-derived CD11c (+) cells acquire plasmodium from hepatocytes to prime CD8 T cell immunity to liver-stage malaria. *Cell Host Microbe* (2019) 25:565–77.e6. doi: 10.1016/j.chom.2019.02.014

57. Lau LS, Fernandez-Ruiz D, Mollard V, Sturm A, Neller MA, Cozijnsen A, et al. CD8+ T cells from a novel T cell receptor transgenic mouse induce liver-stage immunity that can be boosted by blood-stage infection in rodent malaria. *PloS Pathog* (2014) 10:e1004135. doi: 10.1371/journal.ppat.1004135

58. Zaidi I, Diallo H, Conteh S, Robbins Y, Kolasny J, Orr-Gonzalez S, et al. gammadelta T cells are required for the induction of sterile immunity during irradiated sporozoite vaccinations. *J Immunol* (2017) 199:3781–8. doi: 10.4049/jimmunol.1700314

59. Ocana-Morgner C, Mota MM, Rodriguez A. Malaria blood stage suppression of liver stage immunity by dendritic cells. *J Exp Med* (2003) 197:143–51. doi: 10.1084/jem.20021072

60. Linda M, Wakim AWD, Bevan MJ. Memory T cells persisting within the brain after local infection show functional adaptations to their tissue of residence. *Proc Natl Acad Sci U.S.A.* (2010) 107:17872–9. doi: 10.1073/pnas.1010201107

61. Mackay LK, Stock AT, Ma JZ, Jones CM, Kent SJ, Mueller SN, et al. Long-lived epithelial immunity by tissue-resident memory T (TRM) cells in the absence of persisting local antigen presentation. *Proc Natl Acad Sci U.S.A.* (2012) 109:7037–42. doi: 10.1073/pnas.1202288109

62. Iborra S, Martínez-López M, Khouili Sofia C, Enamorado M, Cueto Francisco J, Conde-Garrosa R, et al. Optimal generation of tissue-resident but not circulating memory T cells during viral infection requires crosspriming by DNGR-1$^+$ dendritic cells. *Immunity* (2016) 45:847–60. doi: 10.1016/j.immuni.2016.08.019

63. Gola A, Silman D, Walters AA, Sridhar S, Uderhardt S, Salman AM, et al. Prime and target immunization protects against liver-stage malaria in mice. *Sci Transl Med* (2018) 10:eaap9128. doi: 10.1126/scitranslmed.aap9128

64. Olsen TM, Stone BC, Chuenchob V, Murphy SC. Prime-and-trap malaria vaccination to generate protective CD8(+) liver-resident memory T cells. *J Immunol* (2018) 201:1984–93. doi: 10.4049/jimmunol.1800740

65. Valencia-Hernandez AM, Ng WY, Ghazanfari N, Ghilas S, de Menezes MN, Holz LE, et al. A natural peptide antigen within the plasmodium ribosomal protein RPL6 confers liver TRM cell-mediated immunity against malaria in mice. *Cell Host Microbe* (2020) 27:950–62 e7. doi: 10.1016/j.chom.2020.04.010

66. Obeid M, Franetich JF, Lorthiois A, Gego A, Gruner AC, Tefit M, et al. Skin-draining lymph node priming is sufficient to induce sterile immunity against pre-erythrocytic malaria. *EMBO Mol Med* (2013) 5:250–63. doi: 10.1002/emmm.201201677

67. Holz LE, Chua YC, de Menezes MN, Anderson RJ, Draper SL, Compton BJ, et al. Glycolipid-peptide vaccination induces liver-resident memory CD8(+) T cells that protect against rodent malaria. *Sci Immunol* (2020) 5:eaaz8035. doi: 10.1126/sciimmunol.aaz8035

68. Chaudhary N, Weissman D, Whitehead KA. mRNA vaccines for infectious diseases: principles, delivery and clinical translation. *Nat Rev Drug Discovery* (2021) 20:817–38. doi: 10.1038/s41573-021-00283-5

69. Rizvi F, Everton E, Smith AR, Liu H, Osota E, Beattie M, et al. Murine liver repair via transient activation of regenerative pathways in hepatocytes using lipid nanoparticle-complexed nucleoside-modified mRNA. *Nat Commun* (2021) 12:613. doi: 10.1038/s41467-021-20903-3

70. Ganley M, Holz LE, Minnell JJ, de Menezes MN, Burn OK, Poa KCY, et al. mRNA vaccine against malaria tailored for liver-resident memory T cells. *Nat Immunol* (2023) 24:1487–98. doi: 10.1038/s41590-023-01562-6

71. Mani V, Bromley SK, Äijö T, Mora-Buch R, Carrizosa E, Warner RD, et al. Migratory DCs activate TGF-b to precondition naïve CD8$^+$ T cells for tissue-resident memory fate. *Science* (2019) 366:eaav5728. doi: 10.1126/science.aav5728

72. Hirai T, Zenke Y, Yang Y, Bartholin L, Beura LK, Masopust D, et al. Keratinocyte-mediated activation of the cytokine TGF-β maintains skin recirculating memory CD8$^+$ T cells. *Immunity* (2019) 50:1249–61.e5. doi: 10.1016/j.immuni.2019.03.002

73. Mackay LK, Rahimpour A, Ma JZ, Collins N, Stock AT, Hafon M-L, et al. The developmental pathway for CD103$^+$CD8$^+$ tissue-resident memory T cells of skin. *Nat Immunol* (2013) 14:1294–301. doi: 10.1038/ni.2744

74. Seder RA, Chang LJ, Enama ME, Zephir KL, Sarwar UN, Gordon IJ, et al. Protection against malaria by intravenous immunization with a nonreplicating sporozoite vaccine. *Science* (2013) 341:1359–65. doi: 10.1126/science.1241800

75. Mackay LK, Minnich M, Kragten NA, Liao Y, Nota B, Seillet C, et al. Hobit and Blimp1 instruct a universal transcriptional program of tissue residency in lymphocytes. *Science* (2016) 352:459–63. doi: 10.1126/science.aad2035

76. Crowl JT, Heeg M, Ferry A, Milner JJ, Omilusik KD, Toma C, et al. Tissue-resident memory CD8(+) T cells possess unique transcriptional, epigenetic and functional adaptations to different tissue environments. *Nat Immunol* (2022) 23:1121–31. doi: 10.1038/s41590-022-01229-8

77. McNamara HA, Cai Y, Wagle MV, Sontani Y, Roots CM, Miosge LA, et al. Up-regulation of LFA-1 allows liver-resident memory T cells to patrol and remain in the hepatic sinusoids. *Sci Immunol* (2017) 2:eaaj1996. doi: 10.1126/sciimmunol.aaj1996

78. Tse SW, Radtke AJ, Espinosa DA, Cockburn IA, Zavala F. The chemokine receptor CXCR6 is required for the maintenance of liver memory CD8(+) T cells specific for infectious pathogens. *J Infect Dis* (2014) 210:1508–16. doi: 10.1093/infdis/jiu281

79. Christo SN, Evrard M, Park SL, Gandolfo LC, Burn TN, Fonseca R, et al. Discrete tissue microenvironments instruct diversity in resident memory T cell function and plasticity. *Nat Immunol* (2021) 22:1140–51. doi: 10.1038/s41590-021-01004-1

80. Adachi T, Kobayashi T, Sugihara E, Yamada T, Ikuta K, Pittaluga S, et al. Hair follicle–derived IL-7 and IL-15 mediate skin-resident memory T cell homeostasis and lymphoma. *Nat Med* (2015) 21:1272–9. doi: 10.1038/nm.3962

81. Skon CN, Lee J-Y, Anderson KG, Masopust D, Hogquist KA, Jameson SC. Transcriptional downregulation of S1pr1 is required for the establishment of resident memory CD8$^+$ T cells. *Nat Immunol* (2013) 14:1285–93. doi: 10.1038/ni.2745

82. Liehl P, Zuzarte-Luis V, Chan J, Zillinger T, Baptista F, Carapau D, et al. Host-cell sensors for *Plasmodium* activate innate immunity against liver-stage infection. *Nat Med* (2014) 20:47–53. doi: 10.1038/nm.3424

83. Minkah NK, Wilder BK, Sheikh AA, Martinson T, Wegmair L, Vaughan AM, et al. Innate immunity limits protective adaptive immune responses against pre-erythrocytic malaria parasites. *Nat Commun* (2019) 10:3950. doi: 10.1038/s41467-019-11819-0

84. Du Y, Hertoghs N, Duffy FJ, Carnes J, McDermott SM, Neal ML, et al. Systems analysis of immune responses to attenuated *P. falciparum* malaria sporozoite vaccination reveals excessive inflammatory signatures correlating with impaired immunity. *PloS Pathog* (2022) 18:e1010282. doi: 10.1371/journal.ppat.1010282

85. Oyong DA, Duffy FJ, Neal ML, Du Y, Carnes J, Schwedhelm KV, et al. Distinct immune responses associated with vaccination status and protection outcomes after malaria challenge. *PloS Pathog* (2023) 19:e1011051. doi: 10.1371/journal.ppat.1011051

86. Valencia-Hernandez AM, Zillinger T, Ge Z, Tan PS, Cozijnsen A, IM G, et al. Complexing CpG adjuvants with cationic liposomes enhances vaccine-induced formation of liver T(RM) cells. *Vaccine* (2023) 41:1094–107. doi: 10.1016/j.vaccine.2022.12.047

87. Casey KA, Fraser KA, Schenkel JM, Moran A, Abt MC, Beura LK, et al. Antigen-independent differentiation and maintenance of effector-like resident memory T cells in tissues. *J Immunol* (2012) 188:4866–75. doi: 10.4049/jimmunol.1200402

88. Masopust D, Choo D, Vezys V, Wherry EJ, Duraiswamy J, Akondy R, et al. Dynamic T cell migration program provides resident memory within intestinal epithelium. *J Exp Med* (2010) 207:553–64. doi: 10.1084/jem.20090858

89. Park SL, Zaid A, Hor JL, Christo SN, Prier JE, Davies B, et al. Local proliferation maintains a stable pool of tissue-resident memory T cells after antiviral recall responses. *Nat Immunol* (2018) 19:183–91. doi: 10.1038/s41590-017-0027-5

90. Fung HY, Teryek M, Lemenze AD, Bergsbaken T. CD103 fate mapping reveals that intestinal CD103$^-$tissue-resident memory T cells are the primary responders to secondary infection. *Sci Immunol* (2022) 7:eabl9925. doi: 10.1126/sciimmunol.abl9925

91. Ariotti S, Hogenbirk MA, Dijkgraaf FE, Visser LL, Hoekstra ME, Song JY. T cell memory. Skin-resident memory CD8$^+$ T cells trigger a state of tissue-wide pathogen alert. *Science* (2014) 346:101–5. doi: 10.1126/science.1254803

92. Schenkel JM, Fraser KA, Beura LK, Pauken KE, Vezys V, Masopust D. T cell memory. Resident memory CD8 T cells trigger protective innate and adaptive immune responses. *Science* (2014) 346:98–101. doi: 10.1126/science.1254536

93. Kumar KA, Sano G, Boscardin S, Nussenzweig RS, Nussenzweig MC, Zavala F, et al. The circumsporozoite protein is an immunodominant protective antigen in irradiated sporozoites. *Nature* (2006) 444:937–40. doi: 10.1038/nature05361

94. Guerin-Marchand C, Druilhe P, Galey B, Londono A, Patarapotikul J, Beaudoin RL, et al. A liver-stage-specific antigen of *Plasmodium falciparum* characterized by gene cloning. *Nature* (1987) 329:164–7. doi: 10.1038/329164a0

95. Yoshida N, Nussenzweig RS, Potocnjak P, Nussenzweig V, Aikawa M. Hybridoma produces protective antibodies directed against the sporozoite stage of malaria parasite. *Science* (1980) 207:71–3. doi: 10.1126/science.6985745

96. Rogers WO, Rogers MD, Hedstrom RC, Hoffman SL. Characterization of the gene encoding sporozoite surface protein 2, a protective *Plasmodium yoelii* sporozoite antigen. *Mol Biochem Parasitol* (1992) 53:45–51. doi: 10.1016/0166-6851(92)90005-5

97. Gardner MJ, Hall N, Fung E, White O, Berriman M, Hyman RW, et al. Genome sequence of the human malaria parasite *Plasmodium falciparum*. *Nature* (2002) 419:498–511. doi: 10.1038/nature01097

98. Carlton JM, Angiuoli SV, Suh BB, Kooij TW, Pertea M, Silva JC, et al. Genome sequence and comparative analysis of the model rodent malaria parasite Plasmodium yoelii yoelii. *Nature* (2002) 419:512–9. doi: 10.1038/nature01099

99. Mauduit M, Gruner AC, Tewari R, Depinay N, Kayibanda M, Chavatte JM, et al. A role for immune responses against non-CS components in the cross-species protection induced by immunization with irradiated malaria sporozoites. *PloS One* (2009) 4:e7717. doi: 10.1371/journal.pone.0007717

100. Hafalla JC, Bauza K, Friesen J, Gonzalez-Aseguinolaza G, Hill AV, Matuschewski K. Identification of targets of CD8(+) T cell responses to malaria liver stages by genome-wide epitope profiling. *PloS Pathog* (2013) 9:e1003303. doi: 10.1371/journal.ppat.1003303

101. Murphy SC, Kas A, Stone BC, Bevan MJ. A T-cell response to a liver-stage Plasmodium antigen is not boosted by repeated sporozoite immunizations. *Proc Natl Acad Sci U.S.A.* (2013) 110:6055–60. doi: 10.1073/pnas.1303834110

102. Doolan DL, Southwood S, Freilich DA, Sidney J, Graber NL, Shatney L, et al. Identification of *Plasmodium falciparum* antigens by antigenic analysis of genomic and proteomic data. *Proc Natl Acad Sci U.S.A.* (2003) 100:9952–7. doi: 10.1073/pnas.1633254100

103. Kula T, Dezfulian MH, Wang CI, Abdelfattah NS, Hartman ZC, Wucherpfennig KW, et al. T-Scan: A genome-wide method for the systematic discovery of T cell epitopes. *Cell* (2019) 178:1016–28 e13. doi: 10.1016/j.cell.2019.07.009

104. Draheim M, Wlodarczyk MF, Crozat K, Saliou JM, Alayi TD, Tomavo S, et al. Profiling MHC II immunopeptidome of blood-stage malaria reveals that cDC1 control the functionality of parasite-specific CD4 T cells. *EMBO Mol Med* (2017) 9:1605–21. doi: 10.15252/emmm.201708123

105. Howland SW, Poh CM, Gun SY, Claser C, Malleret B, Shastri N, et al. Brain microvessel cross-presentation is a hallmark of experimental cerebral malaria. *EMBO Mol Med* (2013) 5:984–99. doi: 10.1002/emmm.201202273

106. Wahl I, Obraztsova AS, Puchan J, Hundsdorfer R, Chakravarty S, Sim BKL, et al. Clonal evolution and TCR specificity of the human TFH cell response to *Plasmodium falciparum* CSP. *Sci Immunol* (2022) 7:eabm9644. doi: 10.1126/sciimmunol.abm9644

107. Sattabongkot J, Yimamnuaychoke N, Leelaudomlipi S, Rasameesoraj M, Jenwithisuk R, Coleman RE, et al. Establishment of a human hepatocyte line that supports *in vitro* development of the exo-erythrocytic stages of the malaria parasites *Plasmodium falciparum* and *P. vivax*. *Am J Trop Med Hyg* (2006) 74:708–15. doi: 10.4269/ajtmh.2006.74.708

108. Prudencio M, Rodrigues CD, Ataide R, Mota MM. Dissecting *in vitro* host cell infection by Plasmodium sporozoites using flow cytometry. *Cell Microbiol* (2008) 10:218–24. doi: 10.1111/j.1462-5822.2007.01032.x

109. Doll KL, Pewe LL, Kurup SP, Harty JT. Discriminating protective from nonprotective plasmodium-specific CD8+ T cell responses. *J Immunol* (2016) 196:4253–62. doi: 10.4049/jimmunol.1600155

110. Montagna GN, Beigier-Bompadre M, Becker M, Kroczek RA, Kaufmann SH, Matuschewski K. Antigen export during liver infection of the malaria parasite augments protective immunity. *MBio* (2014) 5(4):e01321–14. doi: 10.1128/mBio.01321-14

111. Muller K, Gibbins MP, Roberts M, Reyes-Sandoval A, Hill AVS, Draper SJ, et al. Low immunogenicity of malaria pre-erythrocytic stages can be overcome by vaccination. *EMBO Mol Med* (2021) 13:e13390. doi: 10.15252/emmm.202013390

112. Singh AP, Buscaglia CA, Wang Q, Levay A, Nussenzweig DR, Walker JR, et al. Plasmodium circumsporozoite protein promotes the development of the liver stages of the parasite. *Cell* (2007) 131:492–504. doi: 10.1016/j.cell.2007.09.013

113. Bongfen SE, Torgler R, Romero JF, Renia L, Corradin G. *Plasmodium berghei*-infected primary hepatocytes process and present the circumsporozoite protein to specific $CD8^+$ T cells *in vitro*. *J Immunol* (2007) 178:7054–63. doi: 10.4049/jimmunol.178.11.7054

114. Cockburn IA, Tse SW, Radtke AJ, Srinivasan P, Chen YC, Sinnis P, et al. Dendritic cells and hepatocytes use distinct pathways to process protective antigen from plasmodium in vivo. *PloS Pathog* (2011) 7:e1001318. doi: 10.1371/journal.ppat.1001318

frontiers | Frontiers in Immunology

TYPE Original Research
PUBLISHED 20 February 2024
DOI 10.3389/fimmu.2024.1344878

OPEN ACCESS

EDITED BY
Xuexian Yang,
University of New Mexico, United States

REVIEWED BY
Daniela More,
Agricultural Research Service (USDA), United States
Pedro Augusto Carvalho Costa,
Federal University of Minas Gerais, Brazil

*CORRESPONDENCE
Kutty Selva Nandakumar
nandakumar@smu.edu.cn
Michail Kotsyfakis
kotsyfakis@paru.cas.cz

†These authors have contributed equally to this work

RECEIVED 26 November 2023
ACCEPTED 31 January 2024
PUBLISHED 20 February 2024

CITATION
Wu H, Jmel MA, Chai J, Tian M, Xu X, Hui Y, Nandakumar KS and Kotsyfakis M (2024) Tick cysteine protease inhibitors suppress immune responses in mannan-induced psoriasis-like inflammation. *Front. Immunol.* 15:1344878. doi: 10.3389/fimmu.2024.1344878

Tick cysteine protease inhibitors suppress immune responses in mannan-induced psoriasis-like inflammation

Huimei Wu[1,2], Mohamed Amine Jmel[3], Jinwei Chai[4], Maolin Tian[4], Xueqing Xu[4,5], Yuan Hui[6], Kutty Selva Nandakumar[2,7*†] and Michail Kotsyfakis[3,8*†]

[1]Department of Pharmacy, The Eighth Affiliated City Hospital of Guangzhou Medical University, The Eighth People's Hospital of Guangzhou, Guangzhou, China, [2]Karolinska Institute United Medical Inflammation Center, School of Pharmaceutical Sciences, Southern Medical University, Guangzhou, China, [3]Institute of Parasitology, Biology Centre, Czech Academy of Sciences, České Budějovice, Czechia, [4]Guangdong Provincial Key Laboratory of New Drug Screening, School of Pharmaceutical Sciences, Southern Medical University, Guangzhou, China, [5]Department of Pulmonary and Critical Care Medicine, Zhujiang Hospital, Southern Medical University, Guangzhou, China, [6]Department of Endocrinology, Fifth Affiliated Hospital, Southern Medical University, Guangzhou, China, [7]Department of Environmental and Biosciences, School of Business, Innovation and Sustainability, Halmstad University, Halmstad, Sweden, [8]Institute of Molecular Biology and Biotechnology, Foundation for Research and Technology-Hellas, Heraklion, Crete, Greece

Protease inhibitors regulate various biological processes and prevent host tissue/organ damage. Specific inhibition/regulation of proteases is clinically valuable for treating several diseases. Psoriasis affects the skin in the limbs and scalp of the body, and the contribution of cysteine and serine proteases to the development of skin inflammation is well documented. Cysteine protease inhibitors from ticks have high specificity, selectivity, and affinity to their target proteases and are efficient immunomodulators. However, their potential therapeutic effect on psoriasis pathogenesis remains to be determined. Therefore, we tested four tick cystatins (Sialostatin L, Sialostatin L2, Iristatin, and Mialostatin) in the recently developed, innate immunity-dependent mannan-induced psoriasis model. We explored the effects of protease inhibitors on clinical symptoms and histological features. In addition, the number and percentage of immune cells (dendritic cells, neutrophils, macrophages, and γδT cells) by flow cytometry, immunofluorescence/immunohistochemistry and, the expression of pro-inflammatory cytokines (TNF-a, IL-6, IL-22, IL-23, and IL-17 family) by qPCR were analyzed using skin, spleen, and lymph node samples. Tick protease inhibitors have significantly decreased psoriasis symptoms and disease manifestations but had differential effects on inflammatory responses and immune cell populations, suggesting different modes of action of these inhibitors on psoriasis-like inflammation. Thus, our study demonstrates, for the first time, the usefulness of tick-derived protease inhibitors for treating skin inflammation in patients.

KEYWORDS

autoimmune disease, psoriasis, tick, protease inhibitors, immune responses

Introduction

Autoimmune diseases are comprised of a group of 70 different chronic diseases (1) characterized by inflammatory autoimmune responses to self-antigens and reported as a third leading cause of morbidity in the world (2). Psoriasis, one of the autoimmune diseases, is a chronic inflammatory skin disease with a complicated pathogenesis (3). Traditional drugs for treating psoriasis mainly include methotrexate, cyclosporine, retinoic acid, and glucocorticoids (4), but the disadvantages of slow action, limited efficacy, and adverse reactions limited their use. Biologics have drastically improved our ability to treat psoriasis and psoriatic arthritis over the last 20 years, which include inhibitors of cytokines or their receptors and enzyme inhibitors. Cytokine inhibitors are mostly recombinant monoclonal antibodies or receptor fusion proteins specific to inflammatory mediators, like TNF-α, IL-17, IL-12/IL-23 p40, and IL-23p19 (5). As an enzyme inhibitor, Apremilast inhibits phosphodiesterase 4 (PDE4), which in turn decreases the expression of pro-inflammatory cytokines TNF-α and IL-23, shows therapeutic efficacy in psoriasis, psoriatic arthropathies, and Behçet's syndrome (6). Other enzyme inhibitors targeting Janus Kinase (JAK) (7) and tyrosine kinase 2 (TYK2) (8) show a significant therapeutic effect in the clinical and preclinical evaluations of psoriasis.

Tick saliva affects coagulation, complement activation, and immune response in terms of recruiting the immune cells, cytokine production, and cell maturation (9). It comprises a complex mixture of proteins and peptides (10, 11). Transcriptomic analysis of tick saliva shows the expression of various protease inhibitors (12, 13), including Kunitz-type inhibitors, cystatins, and serpins based on their structures and target proteases (10, 14). Several type 1 and 2 cystatins from tick saliva were described earlier. Sialostatin L, a type 1 cystatin identified in the saliva of hard tick *Ixodes scapularis*, modulates the cytokine production by lymphocytes, dendritic cells, and mast cells, causing impairment of T-cell expansion by inhibiting various (cathepsin C, L, S, V, X, and papain) enzymes (15). Another type 1 cystatin from the saliva of hard tick *Ixodes scapularis*, Sialostatin L2, suppresses the activities of cathepsins C, L, S, and V but not X (16), reduces the production of cytokines from the macrophages and inhibits caspase-1 maturation (17). As a type 2 cystatin, Iristatin inhibits proteolytic activities of cathepsins L and C, leading to decreased cytokine production from different T cells, mast cells, and nitric oxide production by macrophages. In addition, Iristatin inhibited OVA-induced $CD4^+$ T-cell proliferation and leukocyte recruitment *in vivo*, indicating its versatility (18). Mialostatin, a cystatin from the midgut of *Ixodes ricinus*, inhibits several digestive cysteine-cathepsins, with a high-level potency observed against cathepsin L isoforms. Mialostatin has also effectively blocked *in vitro* proteolysis of blood proteins by midgut cysteine cathepsins (19).

Herein, we explored the effects of four cysteine protease inhibitors (Sialostatin L, Sialostatin L2, Iristatin, and Mialostatin) on mannan-induced psoriasis-like inflammation and evaluated the disease in terms of clinical and histological symptoms, infiltration of immune cells and expression of several pro-inflammatory cytokines.

Abbreviations: BMDM, bone marrow-derived macrophages; IFA, incomplete Freund's adjuvant; IMQ, Imiquimod; MISI, mannan-induced skin inflammation; PASI, psoriasis area and severity index; RORγt, Retinoid-related orphan receptor gamma-t; VEGF, vascular endothelial growth factor.

Materials and methods

Mice

Eight to twelve-weeks-old BALB/c female mice purchased from Southern Medical University Animal Center were used and maintained in a pathogen-free animal house. Mice were placed in polystyrene cages in a climate-controlled environment with 12-h light/dark cycles and given food and water *ad libitum*. The animal studies were approved by the institutional review board of Southern Medical University (l2018183), Guangzhou, China, and performed according to the guidelines of the National Institutes of Health (NIH Publication No. 8023).

Cloning, expression, and purification of the recombinant protease inhibitors

Sialostatin L, Sialostatin L2, Iristatin, and Mialostatin were expressed, purified and tested in presence of various proteases as described in detail elsewhere (16, 18–21). Briefly, the genes coding for the studied cystatins without a signal peptide but with an inserted ATG codon were cloned into a pET-17b vector and then transformed into *E.coli* strain BL21(DE3)pLysS. LB medium containing ampicillin (100 μg/ml) and chloramphenicol (34 μg/ml) was used for bacterial cultures until the optical density reached 0.8 at 600 nm. Protein expression was induced by adding 1 mM isopropyl 1-thio-β-D-galactopyranoside (IPTG). After 5 h, the cultures were harvested, and the inclusion bodies were recovered, washed, and dissolved in a solution containing 6 M guanidine hydrochloride, 20 mM Tris, and 10 mM DTT, pH 8. The refolded proteins were purified by HiLoad Superdex 200 26/60 gel filtration and ion exchange chromatographic methods. Endotoxin was removed by ARVYS proteins (Trumbull, Connecticut) using the Triton X-14 partitioning method (22) from all the recombinant protease inhibitors before using them in various *in vitro* and *in vivo* assays. Initial and final endotoxin concentrations were tested using Cambrex (Lonza) PyroGene Recombinant Factor C endotoxin detection system (Lonza Biologics) following manufacturer recommendations and the results are summarized in Supplementary Table 1. The toxicity of the tested cystatins was evaluated as reported in (23).

Therapeutic effects of protease inhibitors on mannan-induced skin inflammation

To establish the mannan-induced skin inflammation (MISI) model, mice were shaved on the back skin one day before the treatment. Mannan (100 μl of 100 mg/ml stock solution, Sigma-Aldrich, USA) was mixed with incomplete Freund's adjuvant (IFA,

Sigma-Aldrich) at a 1:1 ratio and applied daily for three consecutive days, as described earlier (24). Induction of psoriasis in the inbred strains of mice than the classically used Imiquimod was reported to be relatively simple in inducing skin inflammation and found to be robust, economically more viable, and less harmful to the mice (25). The severity of the disease was assessed daily with a scoring system based on the development of scales, erythema, and skin thickness, like the human Psoriasis Area and Severity Index measurements with a scoring system having 0 to 4 scores (0, none; 1, mild; 2, moderate; 3, severe; 4, very severe) and a total score of 12. An increase in skin thickness was detected using an Ozaki digital caliper (Neill-Lavielle, Kentucky, USA). A detailed protocol was described elsewhere (26).

To investigate the effects of protease inhibitors on psoriasis-like inflammation, mice were randomly assigned to eight groups with at least six mice in each group as follows: PBS, mannan, negative control, Sialostatin L, Sialostatin L2, Iristatin or Mialostatin treated groups. Alpha-lactalbumin (Sigma-Aldrich) was used as a negative control. Different protease inhibitors were subcutaneously injected (4 mg/kg) individually from days 0 to 7. Skin, spleen, and the draining lymph node samples harvested on days 4 and 7 were used to evaluate the disease pathology, infiltrating immune cells, and the expression of cytokine genes.

Histological, Immunohistochemical, and Immunofluorescent analysis

For hematoxylin and eosin (H&E) staining, skin samples were fixed in 4% formaldehyde and embedded in paraffin, and 6-8 μm sections were cut before the staining was performed. Histological sections were analyzed using LAS software version 4.9 (Leica, Germany) and a light microscope. Epidermal thickness was measured from the photomicrographs of skin sections after H&E staining by randomly selecting five regions using the Image Pro Plus software (Leeds Precision Instruments, USA). Baker's scores were used to analyze the pathological severity of the skin (27), which has lesions in the stratum corneum, epidermis, and dermis. Neutrophils and macrophages were stained with biotin-rat anti-mouse Ly6G (1:200, BioLegend, USA) and F4/80 (1:100, BioLegend) antibodies, respectively, at 4°C overnight, followed by incubation with streptavidin-HRP antibodies (Yeasen, China) for 40 min. Before visualization, sections were developed with DAB (Vector Laboratories, California, USA) and counter-stained with hematoxylin (Phygene, China). For immunofluorescence staining, frozen samples were cut into 8 μm sections (Leica). At first, slices were permeabilized by acetone (Aladdin, China) and then incubated with the biotin-rat anti-mouse CD11c antibodies (1:100, BioLegend) overnight. Sections were treated with Alexa Fluor® 488 conjugated streptavidin (1:800, Biyotimes, China) secondary antibodies at RT for 1 h. After washing with PBST (0.2% Tween-20 in PBS), the tissue slices were fixed with Vectashield® containing DAPI and used for visualization. Fluorescence pictures were acquired and analyzed using Nikon Laser Confocal Microscope and NIS Elements Viewer Imaging Software (Nikon).

Flow cytometry

Each mouse lymph nodes and spleen were minced separately and passed through a 70 μm cell strainer to obtain single-cell suspensions. Single cells from the draining lymph nodes were used for the detection of innate immune cells and were stained with the following monoclonal antibodies: F4/80-PerCP-Cy 5.5, CD11c-PE, CD11b-APC, and Ly6G-FITC (BD Biosciences, USA). The γδT and Th17 cells from the spleen samples were detected with the following fluorescent antibodies: CD45-PerCP-Cy 5.5, γδT-PE, CD4-APC, and IL-17A-PE (BD Biosciences, USA). For the surface antigen staining, cells were incubated with the antibodies for 30 min at room temperature (RT) after washing the cells with PBS. To stain the intracellular cytokines, the cells were stimulated with a cell stimulation cocktail (eBiosicence) for 4 h. After that, the cells were stained for surface antigens and then fixed with BD Cytofix buffer, permeabilized by using Perm/Wash reagent (BD Biosciences) and then stained with anti-IL-17A antibodies. The cells were acquired using an LSR II Flow Cytometer (BD Biosciences), and the data were analyzed using the Flow Jo software version 7.0 (Tree Star, California, USA).

RNA isolation and qRT-PCR

Total RNA was extracted from the skin using a Trizol reagent kit (Invitrogen, California, USA). Reverse transcription (RT) reactions were carried out with PrimeScript RT reagent Kit (ThermoFisher, USA), and a quantitative real-time polymerase chain reaction was performed using the SYBR Premix Ex Taq II (Takara biotech, Japan) in a LightCycler 96 thermocycler (Roche, Switzerland). The amplification program consists of 1 cycle of 95°C for 3 min followed by 45 cycles of 95°C for 5 s, 55°C for 5 s, and 72°C for 10 s and at the end, one cycle at 72°C for 5 min. VEGF, TGF-β, TNF-α, IL-6, IL-22, IL-23(P19), IL-17A, IL-17E, and IL-17F primers were purchased from Jierui (Shanghai, China), and β-actin was used as the internal control. The primers used to detect the expression of different genes are listed below *β-actin*, forward, 5'-ACCGTGAAAAGATGACCCAG-3', and reverse 5'-GTACGACCAGAGGCATACAG-3'; *VEGF*, forward, 5'-GTCCTCTCCTTACCCCACCTCCT, and reverse 5'-CTCACACACACAGCCAAGTCTCCT-3'; *TGF-β*, forward, 5'-AGTGGAAGTGGTGCCTTTCAA-3', and reverse, 5'-GTGAGACACCTCATCAG. GGTA-3'; *TNF-α*, forward, 5'-ACGCTCTTCTGTCTACTGAACT-3', and reverse, 5'-ATCTGAGTGTGAGGGTCTGG-3'; *IL-6*, forward, 5'-GAGAAAAGAGTTGTGC AATGGC-3', and reverse, 5'-CCAGTTTGGTAGCATCCATCAT-3'; *IL-22*, forward, 5'-CATGCAGGAGGTGGTACCTT-3', and reverse, 5'-CAGACGCAAGCATTTCTC AG-3'; *IL-23-P19*, forward, 5'-AGCAACTTCACACCTCCCTAC-3', and reverse, 5'-ACTGCTGACTAGAACTCAGGC-3'; *IL-17A*, forward, 5'-CCCCTAAGAAACCC CCACG-3', and reverse, 5'-TAAAGTCCACAGAAAAACAAACACG-3'; *IL-17E*, forward, 5'-ACAGGGACTTGAATCGGGTC-3', and reverse, 5'-TGGTAAAGTGGGACGGAGTTG-3'; *IL-17F*, forward, 5'-GTCAGGAAGACAGCACCA-3', and reverse 5'-AGCCAACTTTTAGGAGCA-3';*IL-10*,

forward,5′-GGCCTTCCCTACTTCACAA G-3′,and reverse 5′-GGCCTTCCCTACTTCACAAG-3′; *IL-4*,5′-GTCATCCTGCTC TTCTTTCTCG-3′, and reverse 5′-TTGGCACATCC ATCTCCGT-3′.

Statistical analysis

Data were analyzed using GraphPad Prism software version 5.0. For standard data sets, data were shown as mean ± SEM, and an unpaired two-tailed Student's t-test was used for statistical analyses. For multiple groups, a one-way analysis of variance was applied. In the qPCR analysis, an average value for the expression of a particular gene from the mannan-treated group (Man) was given the value "1" (standard) and used for comparison with other groups. Probability values < 0.05 were considered significant at a 95% confidence interval.

Results

Tick protease inhibitors and their structures

This study explores the therapeutic effects of four tick cystatins previously reported for their various immunomodulatory activities and specificity towards key cysteine proteases involved in different pathways related to immunity, inflammation, and homeostasis. Sialostatin L and Sialostatin L2, two cystatins isolated from the salivary glands of *Ixodes scapularis* (15–17, 23, 28–31), Iristatin, a salivary gland cystatin and Mialostatin, a midgut cystatin were isolated from *Ixodes ricinus* (18, 19, 21). Table 1 and Supplementary Figure 1 show the protease inhibitors, their primary targets, and published structures.

In addition to their structure and functions, we report the inhibitory potency of the studied cystatins on various proteases involved in key immune pathways such as cathepsins L, S, and C (Supplementary Table 2). Amino acid sequences of the cystatins used in this study are given in Supplementary Table 3.

TABLE 1 Summary of the tested tick protease inhibitors.

Protease inhibitor	Sources	Inhibited proteases	Effects on immune systems
Sialostatin L	Salivary glands of *Ixodes scapularis*	Cathepsins L, S, C, and X, Papain	Modulates cytokine production by immune cells and impairs T-cell proliferation (31)
Sialostatin L2	Salivary glands of *Ixodes scapularis*	Cathepsins L, S and C Papain (20)	Reduces cytokine(s) production from macrophages and inhibits caspase-1 maturation (20)
Iristatin	Salivary glands of *Ixodes ricinus*	Cathepsins L and C	Decreases cytokine(s) and nitric oxide production from immune cells, inhibits T-cell proliferation and leukocyte recruitment (18).
Mialostatin	Midgut of *Ixodes ricinus*	Human cathepsins L, C, S, B, K and H	Blocks proteolysis of blood proteins (19)

Tick protease inhibitors ameliorate mannan-induced skin inflammation

Toxicity analysis of the used tick protease inhibitors on BMDMs did not show any toxic effects (Supplementary Figure 2). To explore the effects of these inhibitors on the pathogenesis of psoriasis-like inflammation, we treated psoriatic mice by injecting an individual inhibitor. We monitored disease severity, epidermal thickness, and pathological manifestations at the microscopic level and also evaluated the expression of specific growth factors, like VEGF and TGF-β.

Cysteine protease inhibitors treatment significantly decreased psoriasis area and severity index (PASI) compared to the untreated group (Figures 1A, B), with a more prominent effect observed from day 3 onwards in the case of Sialostatin L and Sialostatin L2. In contrast, the effect of Iristatin and Mialostatin was observed a day later as they significantly improved PASI from day 4 onwards. On the other hand, a significant decrease in the epidermal thickness and histological scores was observed on day 4 (Figures 1C, D). The highest reduction in the epidermal thickness was observed for Sialostatin L (26.6 μm), Iristatin (24.5 μm), and Mialostatin (27.1 μm). Sialostatin L2 had a lower yet significant effect (36.4 μm), as shown in Figures 1C, E.

Based on the crucial role of TGF-β1 in inducing angiogenesis in the skin through the VEGF-mediated apoptosis (32), we analyzed the expression patterns of VEGF and TGF-β in the inflamed areas of the treated and untreated skin. We found a significantly lower level of VEGF mRNA expression at the peak of psoriasis after treatment with the tick cystatins, with a more significant effect observed with Iristatin treatment (Figure 1F). On the other hand, all the salivary protease inhibitors, except Mialostatin, down-regulated TGF-β mRNA expression in the inflamed skin. The midgut protease inhibitor, Mialostatin, significantly increased its expression (Figure 1G), showing that the inhibitory effects of the protease inhibitors on TGF-β expression were dependent on the origin of inhibitors in the ticks.

Modulation of innate immune cells contributes to the improvement of PASI

The infiltration of immune cells to the skin inflammation area was evaluated by measuring the percentage of innate immune cells. $CD11b^+CD11c^+$ (Dendritic cells), $CD11b^+F4/80^+$ (Macrophages), and $CD11b^+Ly6G^+$ (Neutrophils) cells were detected in the different groups to assess the effect of the tick salivary cystatins on these cells at the skin lesional area. We observed variable effects depending on the studied immune cell and the injected protease inhibitor (Figures 2A–C). The most significant effect on dendritic cell percentage in the lesional area was observed with Mialostatin, followed by a similar effect after Iristatin or Sialostatin L

10.3389/fimmu.2024.1344878

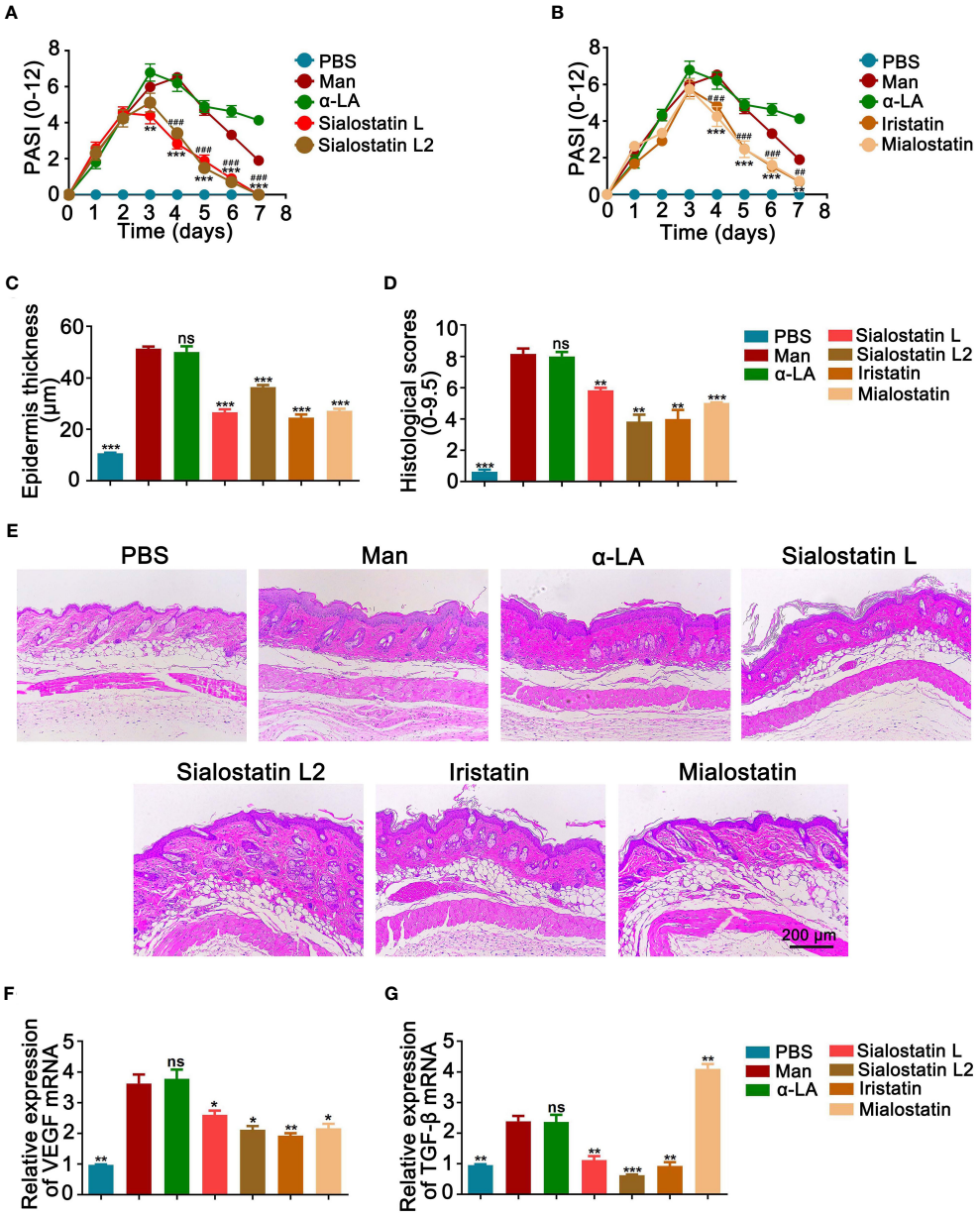

FIGURE 1
Tick protease inhibitors decreased psoriasis severity and microscopical disease manifestations. Effect of Sialostatin L, L2 **(A)** Iristatin or Mialostatin **(B)** treatment in MISI. **(C, D)** Statistical results showing the epidermal thickness and histological scores of psoriatic skins from sialostatin L, Sialostatin L2, Iristatin, or Mialostatin-treated mice (n = 12/group). **(E)** Representative pictures of H&E-stained skin sections (n = 5/group). The scale bar is 200 μm. **(F, G)** Expression of VEGF and TGF-β in psoriatic skin (n = 5/group). Man, Mannan; α-LA, alpha-lactalbumin, negative control. Results are shown from a representative experiment. All mice developed psoriasis-like inflammation. Statistical analysis was performed using an unpaired t-test; ns, not significant; *, $p < 0.05$; **, $p < 0.01$; ***, $p < 0.001$. #, $p < 0.05$; ##, $p < 0.01$; ###, $p < 0.001$. *** in Panel A was used to show the difference between mannan and Sialostatin L group. ### in Panel A showed significance between mannan and Sialostatin L2 group, and indicates $p < 0.001$.

treatments. However, sialostatin L2 didn't affect the percentage of DCs present in the skin lesions (Figure 2A). On the other hand, macrophage infiltration to the inflammation site was most prominently impaired by Mialostatin, followed by Iristatin and Sialostatin L2. Meanwhile, Sialostatin L didn't significantly inhibit macrophage migration (Figure 2B). Finally, neutrophil infiltration in the skin lesions was altered by all four tested protease inhibitors, with the most distinct effect observed with Mialostatin (Figure 2C).

As tick-derived cystatins were repeatedly reported for their immunomodulatory and immunosuppressive activities, we analyzed the effects of all four protease inhibitors on the expression of innate immune cells in the secondary lymphoid organs, and we detected their expression in the spleen at days 4 and 7 using flow cytometry (Figures 3A–I).

Dendritic cells significantly contribute to psoriasis development during the initiation and maintenance phases (33). The tested

10.3389/fimmu.2024.1344878

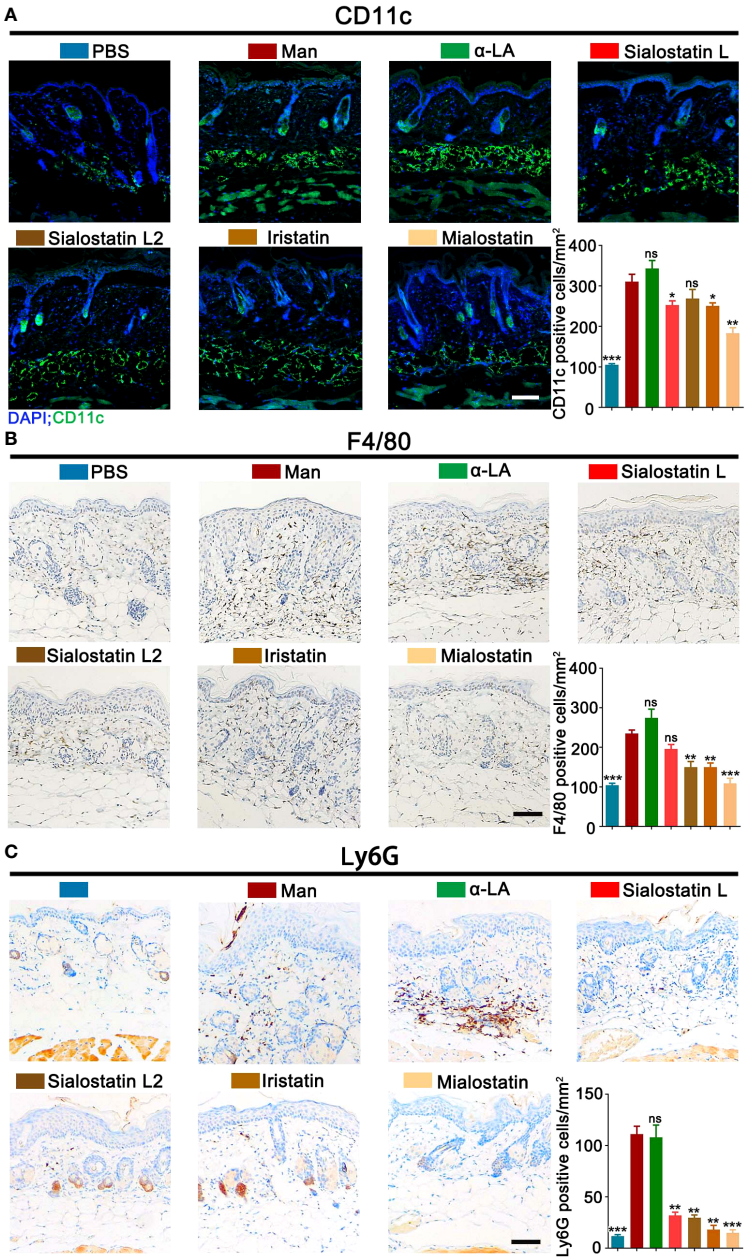

FIGURE 2
Tick protease inhibitors improved mannan-induced skin inflammation by modulating infiltrated immune cells in the skin lesions. **(A)** Representative pictures of immunofluorescence staining and statistical results show $CD11c^+$ cells (green) expression in MISI after Sialostatin L, Sialostatin L2, Iristatin, or Mialostatin treatment (n = 3/group). Nuclei were counterstained with DAPI (blue). **(B, C)** Immunohistochemistry staining and statistical results show $F4/80^+$ and $Ly6G^+$ cell expression in the tick protease inhibitors treated mice (n = 3/group). The scale bar is 100 µm. Positive cells in each mm^2 were calculated under optical and confocal microscopy. Man, mannan; α-LA, alpha-lactalbumin, negative control. Results are from a representative experiment. All mice developed psoriasis-like inflammation. Statistical analysis was performed using an unpaired t-test; ns, not significant; *, $p < 0.05$; **, $p < 0.01$; ***, $p < 0.001$.

cystatins affected $CD11b^+CD11c^+$ cells differently (Figures 3A–C). On day 4, we observed a significant inhibitory effect of Sialostatin L and a moderate effect with Mialostatin while Sialostatin L2 and Iristatin had no effects (Figure 3A). At the declining phase of psoriasis (Day 7), Sialostatin L still had a significant effect on $CD11b^+CD11c^+$ cells, albeit at a lower level. At the same time, Mialostatin lost its immunomodulatory effects on these cells (Figure 3B). On the other hand, dendritic cell overexpression was observed in the presence of Sialostatin L2, while Iristatin was still ineffective from days 4 to 7. The observed inhibition of dendritic cells suggests that the proteases secreted by these cells could be a primary target for the protease inhibitors Sialostatin L and Mialostatin.

The indispensable role of skin macrophages in developing psoriasis-like inflammation of K14-Cre-$IKK2^{fl/fl}$ mice was documented earlier (34). Similarly, depletion of monocytes/macrophages using clodronate liposomes reduced mannan-induced

10.3389/fimmu.2024.1344878

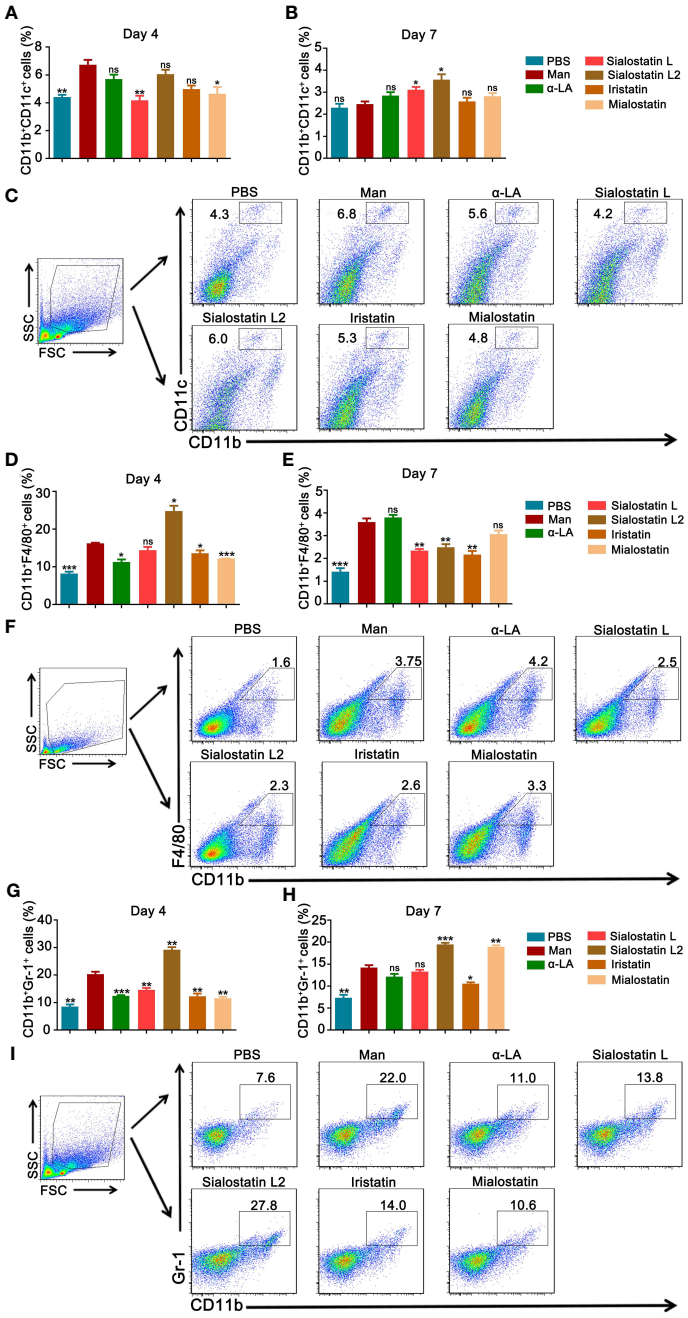

FIGURE 3
Inhibiting innate immune cells from the spleen improves MISI by tick protease inhibitors. **(A, B)** Statistical results showing the effects of Sialostatin L, Sialostatin L2, Iristatin, and Mialostatin on dendritic cells ($CD11b^+CD11c^+$) at days 4 and 7 (n = 5/group). **(C)** Gating strategy and representative pictures showing $CD11b^+CD11c^+$ cells in the spleen at day 4 in the tick protease inhibitors treated mice (n = 5/group). **(D, E)** Effects of Sialostatin L, Sialostatin L2, Iristatin or Mialostatin on macrophages ($CD11b^+F4/80^+$) expression at day 4 and 7 (n = 5/group). **(F)** Representative plots of spleen cells from mice in MISI at day 7 that were treated with Sialostatin L, Sialostatin L2, Iristatin, or Mialostatin (n = 5/group). **(G, H)** Effects of Sialostatin L, Sialostatin L2, Iristatin, or Mialostatin on neutrophils ($CD11b^+Ly6G^+$ cells) expression in the spleen cells at day 4 and 7 were analyzed by flow cytometry (n = 5/group). **(I)** Representative pictures showing macrophage staining ($CD11b^+$ cells) within the spleen cells from protease inhibitors treated mice (n = 5/group). Man, mannan; α-LA, alpha-lactalbumin, negative control. Results are shown from a representative experiment. All mice developed psoriasis-like inflammation. Statistical analysis was performed using an unpaired t-test; ns, not significant; *, $p < 0.05$; **, $p < 0.01$; ***, $p < 0.001$.

joint and skin inflammation in B10Q.*Ncf1*$^{m1j/m1j}$ mice (35). In this study, $CD11b^+F4/80^+$ cells (Figures 3D–F) were mainly inhibited by Mialostatin and Iristatin at day 4, while Sialostatin L2 significantly increased their expression (Figure 3D). At the end of psoriasis (Day 7), we observed a decrease in the number of macrophages after treatment with Sialostatin L, Sialostatin L2, and Iristatin. At the same time, Mialostatin had no effect (Figure 3E).

The contribution of neutrophils in mannan-induced joint and skin inflammation in B10Q.*Ncf1*$^{m1j/m1j}$ mice was documented earlier by depleting them using anti-Ly6G antibodies (35). Here, we

observed a significant inhibition of the percentage of neutrophils in the spleen on day 4 (Figures 3G–I) by Sialostatin L, Mialostatin and Iristatin. However, on day 7, only Iristatin had a significant inhibitory effect. The percentage of neutrophils increased in the Mialostatin-treated mice on day 7, and there was no significant difference between untreated and Silaostatin L-treated mice, suggesting a requirement for a higher concentration of these inhibitors for treatment. In contrast, Sialostatin L2 had a significant activating effect on neutrophil expression both on days 4 and 7, which warrants further experiments to decipher this anomaly.

The γδT and Th17 cells contribute to the therapeutic effect

Psoriasis development highly depends on the γδT and Th17 cell axis (36, 37). Thus, we evaluated the effect of the protease inhibitors on these cells to understand their implication and effects on the development of Psoriasis. Only Sialostatin L and Iristatin decreased $CD45^{+}\gamma\delta T^{+}$ cells in the draining lymph nodes at day 4 (Figures 4A, C). However, none of the protease inhibitors significantly affected these cells on day 7 (Figure 4B).

On the other hand, in the draining lymph nodes, only Mialostatin and Sialostatin L2 significantly inhibited the percentage of Th17 cells on day 4 (Figures 4D, F); however, we observed an increase in the presence of Sialostatin L. On day 7 (Figure 4E), Mialostatin inhibited the percentage of Th17 cells in addition to Sialostatin L, while Iristatin remained ineffective. An increase in Th17 cells was also observed in the case of Sialostatin L2.

Tick protease inhibitors ameliorate mannan induced skin inflammation by altering the expression of pro- and anti-inflammatory cytokine genes

The abnormal proliferation of epidermal keratinocytes during psoriasis is mainly due to the pro-inflammatory cytokines secreted by keratinocytes and resident immune cells such as dendritic cells, T cells, and other innate immune cells (38, 39). Here, we investigated the expression of psoriasis-related cytokines (TNF-α, IL-6, IL-22, IL-23, IL-17A, IL-17E, IL-17F, IL-4 and IL-10) in the inflamed skin after mannan exposure at the peak (day 4) and the end (day 7) of psoriasis with/without inhibitor(s) treatment. Although IL-1β and TNF-α significantly induced IL-17A production from mannan-activated skin cells, only TNF-α but not IL-1β neutralization had a significant effect on joint and skin inflammation induced by an intraperitoneal injection of mannan in B10Q.*Ncf1*$^{m1j/m1j}$ mice (35). In this study, all the inhibitors, mainly Iristatin, significantly decreased TNF-α expression during psoriasis development (Figure 5A).

IL-6, a key cytokine secreted by macrophages that promotes keratinocyte proliferation, showed an unusual expression pattern. Except for Iristatin, all the other tested cystatins increased the expression of IL-6 at the peak of psoriasis (Day 4). At the end of psoriasis (Day 7), IL-6 expression increased with the Sialostatin L treatment, while Sialostatin L2, Iristatin, and Mialostatin significantly decreased its expression (Figure 5B).

We also analyzed the expression of IL-22, a cytokine produced in response to IL-6 and TNF-α, which has a crucial function in developing dermal inflammation and epidermal acanthosis (40). At the peak of MISI (day 4), Sialostatin L2, Iristatin, and Mialostatin decreased IL-22 mRNA expression, while Sialostatin L showed no significant inhibition (Figure 5C). On day 7, IL-22 was inhibited by all the cystatins except Mialostatin, suggesting different inhibitory time kinetics for various cystatins.

Among the IL-17 family upstream cytokines, IL-23 is expressed by the activated macrophages and dendritic cells and acts as a critical cytokine in psoriasis pathogenesis. IL-23 mRNA level in the inflamed skin was significantly reduced after subcutaneous injection of Sialostatin L, Sialostatin L2, Iristatin, or Mialostatin at the peak of psoriasis (Figure 5D), suggesting a direct connection between the action of tick protease inhibitors on the proteases secreted by the antigen-presenting cells. At the end of psoriasis (Day 7), only Iristatin kept its inhibitory effect on IL-23 expression, while Mialostatin significantly increased it, while sialostatin L and Sialostatin L2 didn't show any effect.

A previous report showed that the Th17 family of cytokines (IL-17A and IL-17F) secreted by skin contained infiltrating γδT cells and $ROR\gamma t^{+}$ innate lymphocytes, which promoted the initiation of IMQ-induced psoriasis (41). Subcutaneous injection of Sialostatin L, Sialostatin L2, Iristatin, or Mialostatin in the psoriatic mice decreased IL-17A and IL-17F mRNA expression at days 4 and 7 (Figures 5E, G).

On the other hand, when we evaluated the expression of IL-17E (IL-25) cytokine that contributes to the Th2 type of immune responses (42), the cystatin(s) effect was unclear and needed further clarification. Only Iristatin inhibited IL-17E expression at the peak of psoriasis. By day 7, we observed an inhibition after the injection of Sialostatin L and Sialostatin L2, while an increase in the expression was observed in the case of Iristatin and Mialostatin. (Figure 5F).

Interleukin-10 (IL-10) is a member of cytokine family produced by monocytes, Th2 cells and keratinocytes (43). Earlier studies documented the low-level expression of IL-10 in psoriasis and its reversal after the conventional anti-psoriatic therapies (44). The therapeutic response of IL-10 in psoriasis is associated with suppression of cutaneous inflammation, downregulation of the IL-8/CXCR2 pathway, and normalization of keratinocyte maturation (45). Th2 cells, basophils, mast cells, NK T cells, and type II innate lymphoid cells produce IL-4 (46) and IL-4 therapy in psoriasis patients induced Th2 responses and improved psoriasis (47). Our results show that there is a significant decrease in the expression of IL-10 in MISI, whereas Sialostatin L, Sialostatin L2, Iristatin, and Mialostatin reversed their expression during the inflammatory and declining phase of psoriasis on days 4 and 7. Except for Mialostatin, which has a significant effect on the expression of IL-4 at day 4, other inhibitors significantly reversed the IL-4 expression on days 4 and 7 (Figures 5H, I).

Of note, alpha-lactalbumin (α-LA) was used as a protein control in all the experiments. Hence, this protein could have its

10.3389/fimmu.2024.1344878

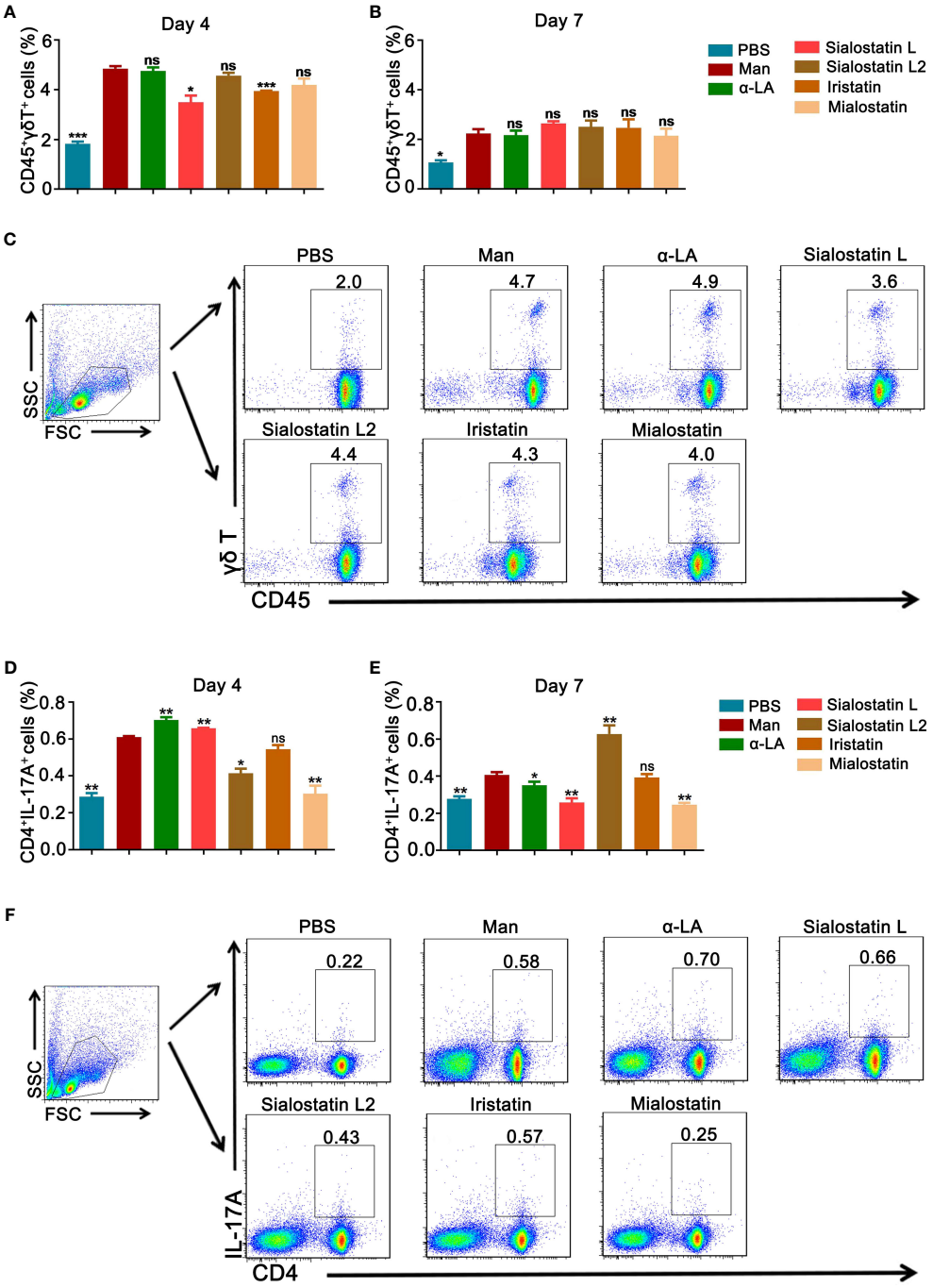

FIGURE 4
Effect of tick protease inhibitors on γδ T and Th17 cells at the peak and end of psoriasis. **(A, B)** Statistical analysis on the effect of Sialostatin L, Sialostatin L2, Iristatin, or Mialostatin on γδ T cells from draining lymph nodes at the peak (day 4) as well as the end (day 7) of psoriasis (n = 5/group). **(C)** Gating strategy and representative blots showing γδ T cells ($CD45^+\gamma\delta\ T^+$) expression at day 4 in the tick protease inhibitors treated mice (n = 5/group). **(D, E)** The spleen cells' frequency is depicted as a fraction of total Th17 cells at days 4 and 7 after Sialostatin L, Sialostatin L2, Iristatin, or Mialostatin treatment in MISI (n = 5/group). **(F)** Representative pictures show $CD4^+$ $IL\text{-}17A^+$ positive cells from the spleen at day 4 in MISI after tick protease inhibitor treatment (n = 5/group). Man, mannan; α-LA, alpha-lactalbumin, negative control. Results are shown from a representative experiment. All mice developed psoriasis-like inflammation. Statistical analysis was performed using an unpaired t-test; n ns, not significant; *, $p < 0.05$; **, $p < 0.01$; ***, $p < 0.001$.

own effects in the animals on the expression of cytokine genes, activation of immune cells in the skin, and immune cells derived from the spleen, which explains the variations between the untreated and the α-LA treated groups.

Discussion

Cysteine proteases are indispensable in various physiological processes and contribute to the development of several diseases.

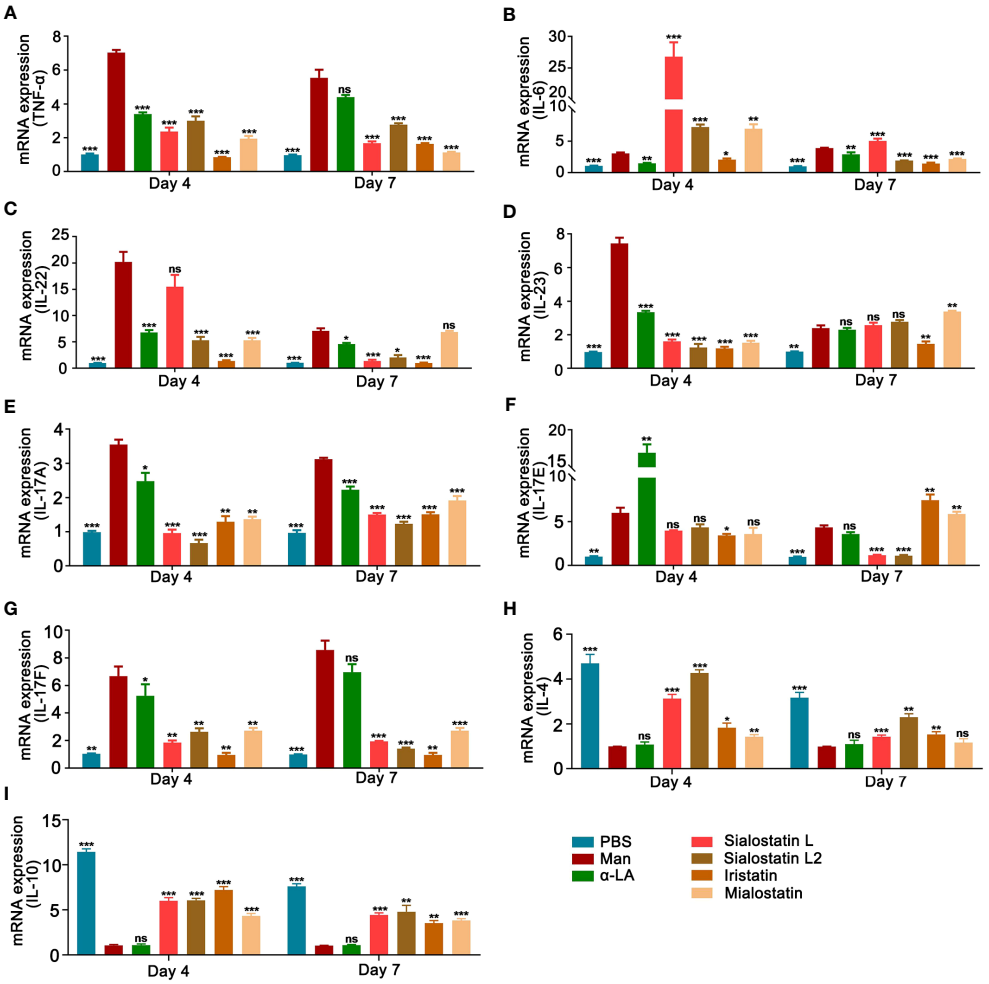

FIGURE 5
Tick protease inhibitors decreased mannan-induced skin inflammation by modulating the expression of pro-inflammatory cytokines. Statistical analysis showing the effects of Sialostatin L, Sialostatin L2, Iristatin, or Mialostatin on the mRNA expression of **(A)** TNF-α, **(B)** IL-6, **(C)** IL-22, **(D)** IL-23 **(E)** IL-17A, **(F)** IL-17E, **(G)** IL-17F, **(H)** IL-4 and **(I)** IL-10 in the skin lesions at the peak (day 4) as well as the end (day 7) of mannan induced skin inflammation after Sialostatin L, Sialostatin L2, Iristatin or Mialostatin treatment (n = 5/group). **(A–G)** PBS group was normalized to 1, and **(H, I)** mannan group was normalized to 1 for showing the differences between each group. Man, mannan; α-LA, alpha-lactalbumin, negative control. All mice developed psoriasis-like inflammation. Statistical analysis was performed using an unpaired t-test; ns, not significant; *, $p < 0.05$; **, $p < 0.01$; ***, $p < 0.001$.

The role of these proteases in the processing of antigens for presentation, maturation of MHC class II molecules, apoptosis, autophagy, extracellular matrix remodeling, activation of granzymes in T cells, coagulation, cytokines and pro-hormones maturation, breakdown of intracellular proteins, cell growth, and differentiation are well known (48, 49). Therefore, cysteine proteases are potential drug targets in treating the underlying pathological processes in tissue degeneration and inflammation. Therapeutic targeting of these proteases could alter specific changes in cell functions. In this context, the relevance of tick protease inhibitors as therapeutics is increasingly highlighted as more and more proteins target host hemostasis, inflammation, and immunity with a unique and precise mechanism of action (50). In this work, we investigated the effect of a panel of tick cysteine protease inhibitors on the previously established psoriasis model in mice (24) to demonstrate their potential for developing pharmacological applications.

Psoriasis, an inflammatory skin disease affecting over 60 million people worldwide with an enormous negative effect on their psychosocial well-being (5), remains one of the significant challenges for modern medicine as no cure has yet been discovered to treat this disease. Only a few treatments aim to minimize the patients' physical burden, which usually reaches extreme conditions such as depression (51) or suicide (52, 53).

The biologics used for the treatment of moderate and severe psoriasis are mainly receptor fusion proteins or monoclonal antibodies, and they can be divided into four classes, namely anti-TNFα, anti-IL17, anti-IL-23p40 (also known as anti-IL-12p40), and anti-IL-23p19 (5, 7, 38). Except for Infliximab, an anti-TNFα biologic administrated by an intravenous infusion, all the biologics targeting psoriasis are delivered by subcutaneous injections (5) as proceeded similarly in this work using the tick protease inhibitors. As the number of FDA-approved biologics

keeps increasing, a permanent need for new therapeutics with increased specificity and lower side effects is demanded in parallel with the increasing knowledge about disease pathogenesis.

Since the biologics used for psoriasis treatments are mainly immunomodulators (54), tick-derived protease inhibitors can play a pivotal role by targeting the central cytokines involved in the inflammatory pathogenesis of the disease (42, 55, 56). Changes in the balance between the proteolytic function of proteases and their regulators (natural inhibitors) present in the skin can result in inflammation, leading to clinical signs of redness, scaling, and itching. Previously, cathepsins and cysteine proteases were reported to have an essential function in the development of psoriasis (49, 57, 58). Here, we tested four cysteine protease inhibitors (cystatins) that showed promising immunomodulatory activities and pluripotent effects on immune cells and targets. The tested inhibitors are Sialostatin L and Sialostatin L2, two cystatins from the salivary glands of *Ixodes scapularis* (15–17, 23, 28–31), Iristatin, a cystatin from the salivary glands of *Ixodes ricinus* (18, 21) and finally Mialostatin, a midgut cystatin from *Ixodes ricinus* (19).

Following the subcutaneous injection of the protease inhibitors, we observed a significant decrease in the macroscopical and microscopical inflammation induced by mannan in the skin. However, the immune responses targeted were different for each protease inhibitor. Both Sialostatin L and Iristatin showed an overall therapeutic capacity by decreasing the percentage of innate immune cells, T cells, and pro-inflammatory cytokine expression in the skin lesions and secondary lymphoid organs. On the other hand, Sialostatin L2 mainly affected the immune cells and cytokines from the inflamed skin but not the draining lymph node. Mialostatin modulated the immune responses by reducing the percentage of macrophages, dendritic cells, neutrophils, Th17 cells and cytokines.

Tick salivary glands and midguts are recognized as a rich source of pharmaco-active molecules (50), which contains a rich cocktail of proteins with a remarkable binding affinity, avidity, and selectivity for their targets in various host defense systems (10). Sialostatin L, a cysteine protease inhibitor from tick saliva, shows multifunctional effects on the immune system, which not only inhibits the percentage of $CD4^+$ cells (31) but also reduces the production of IL-9 from Th9 cells in an OVA-induced experimental asthma (28). In this work, Sialostatin L decreased mannan-induced experimental psoriasis via a unique immunomodulatory effect by inhibiting the proliferation of γδ T cells and Th17 cells. In a previous study, Sialostatin L inhibited LPS-induced maturation of dendritic cells by affecting cathepsin S activity *in vivo* (15). Indeed, our result confirmed that Sialostatin L inhibits the proliferation of dendritic cells and other innate immune cells (macrophages and neutrophils) expression in MISI. In another study on Sialostatin L, the authors showed that this cystatin restrained IL-9, IL-1β, and IRF4 secretion from mast cells, whereas degranulation and IL-6 expression were unaffected (23). Effectively, Sialostatin L didn't show any significant inhibition of IL-6, although psoriasis-related pro-inflammatory cytokines (TNF-α, IL-22, IL-23/IL-17) expression was reduced.

Sialostatin L2, the second salivary cystatin from *Ixodes scapularis*, binds to Annexin A2 and impairs NLRC4 inflammasome formation following macrophage infection (30). It affects IFN-β mediated immune reactions and tick-borne encephalitis (TBE) virus replications in mouse dendritic cells (29). When Sialostatin L2 was subcutaneously injected, it reduced mannan-induced psoriasis by affecting the number of macrophages in lesional skin and spleen and dendritic cells in the skin. Interestingly, it also decreased neutrophils and the expression of IL-23/IL-17 axis cytokines in the skin lesions and Th17 cells expression in the lymph nodes. This immunomodulation pattern allowed Sialostatin L2 to extenuate psoriasis by reducing the number of innate immune and Th17 cells, and the expression of pro-inflammatory cytokines.

Compared to Sialostatin L and Sialostatin L2, fewer reports dealt with the other tested protease inhibitors, namely Mialostatin and Iristatin. The latter is also a pluripotential cystatin, mainly affecting the adaptive immune system by diminishing IL-2, IL-4, IL-9, and IFN-γ production by different T-cell populations. At the same time, it also affects cytokines and nitric oxide secretion from the activated macrophages (18). Following the mannan application, Iristatin didn't affect the Th17 cells, which aligns with the previous reports of Kotal et al. (18). Also, in accordance with the latter reference, Iristatin inhibited macrophages and neutrophils in the lesional skin and spleen. In addition, the decrease in psoriasis severity after applying Iristatin is mainly explained by the critical inhibition of the IL-6/IL-23/IL-17 axis cytokines, which are the main contributors to the disease pathogenesis (38).

The only midgut protein from *Ixodes ricinus* tested in this work, Mialostatin, was reported to inhibit some of the hard tick digestive cysteine cathepsins, with the greatest potency observed against cathepsin L isoforms. Although the effect of Mialostatin on various immune responses remained unexplored, this cystatin effectively blocked *in vitro* proteolysis of blood proteins (19). It reduced erythema (data not shown) and mRNA expression of VEGF in the lesional skin after mannan stimulation, which can be correlated with its inhibition on proteolysis of blood proteins. Mialostatin also showed interesting anti-inflammatory and immunosuppressive effects in MISI by reducing the percentage of innate immune cells and pro-inflammatory cytokines in the psoriasis skin, and the Th17 cells in draining lymph nodes. The subcutaneous injection of Mialostatin showed promising therapeutic effects in MISI. It was the most effective among the tested cystatins in decreasing the number of macrophages, dendritic cells, and neutrophils to the skin lesions.

Neutralizing the different cytokines involved in psoriasis remains a prominent approach of high clinical relevance in treating the disease (56). At the same time, drugs targeting several IL-17 are highly in demand, with several drugs being tested in advanced clinical stages (59). Bimekizumab represents a good example, targeting IL-17A and IL-17F (55). Here, we report tick cysteine protease inhibitors with similar activities to these commercial drugs but with additional targets belonging to the psoriasis-related cytokines. However, more profound studies should be conducted about other cytokines as some tested inhibitors promoted their expression.

In summary, the tested tick protease inhibitors, Sialostatin L, Sialostatin L2, Iristatin, and Mialostatin, showed potential therapeutic effects on mannan-induced psoriasis-like skin inflammation through different immune effectors. They are promising candidates for drug

development to treat vertebrate immune and inflammatory diseases. While this work proves the potential applicability of tick-derived immunomodulatory proteins in treating psoriasis, further studies are needed to address the specificity of various tick proteins to the central cytokines involved in psoriasis pathogenesis. Importantly, targeting cysteine proteases with specific inhibitors by applying them through the skin might be a good strategy for treating psoriasis with less risk of systemic adverse reactions. In addition, the MISI described herein offers a unique model to study the effect of various inhibitors *in vivo* for future studies with the perspective of understanding/resolving the intriguing pathological cascades of psoriasis.

Data availability statement

The original contributions presented in the study are included in the article/Supplementary Materials, further inquiries can be directed to the corresponding authors.

Ethics statement

The animal study was approved by the institutional review board of Southern Medical University (l2018183), Guangzhou, China, and performed according to the guidelines of the National Institutes of Health (NIH Publication No. 8023). The study was conducted in accordance with the local legislation and institutional requirements.

Author contributions

HW: Investigation, Methodology, Writing – original draft, Writing – review & editing. MAJ: Data curation, Formal analysis, Investigation, Methodology, Writing – original draft, Writing – review & editing. JC: Investigation, Writing – original draft. MT: Investigation, Writing – original draft. XX: Data curation, Funding acquisition, Investigation, Supervision, Writing – review & editing. YH: Investigation, Writing – review & editing. KSN: Conceptualization, Formal analysis, Funding acquisition, Investigation, Methodology, Project administration, Supervision, Writing – review & editing. MK: Conceptualization, Data curation, Formal analysis, Funding acquisition, Supervision, Validation, Writing – review & editing.

Funding

The author(s) declare financial support was received for the research, authorship, and/or publication of this article. This project was supported by "High-level talent introduction plan" project grants from Southern Medical University, Guangzhou, China (Grant numbers C1034211, C1051004) given to KN, the Project of Innovative Talent Exchange Foreign Experts under "The Belt and Road" (DL2023030011L) and Guangdong Basic and Applied Basic Research Foundation (2023A1515010914) given to XX. MK received funding received from the Grant Agency of the Czech Republic (grant 19-38207247S) and ERD Funds, project CePaVip OPVVV (No. 384 CZ.02.1.01/0.0/0.0/16_019/0000759). MJ received the European Union funding (MSCA fellowship CZ) within the Operational program Jan Amos Komensky (OP JAK), Priority Research and development (Project No. CZ.02.01.01/00/22_010/0003414).

Conflict of interest

The authors declare that the research was conducted in the absence of any commercial or financial relationships that could be construed as a potential conflict of interest.

The author(s) declared that they were editorial board members of Frontiers, at the time of submission. This had no impact on the peer review process and the final decision.

Publisher's note

Supplementary material

The Supplementary Material for this article can be found online at: https://www.frontiersin.org/articles/10.3389/fimmu.2024.1344878/full#supplementary-material

References

1. Dragin N, Bismuth J, Cizeron-Clairac G, Biferi MG, Berthault C, Serraf A, et al. Estrogen-mediated downregulation of AIRE influences sexual dimorphism in autoimmune diseases. *J Clin Invest* (2016) 126(4):1525–37. doi: 10.1172/JCI81894.

2. Hayter SM, Cook MC. Updated assessment of the prevalence, spectrum and case definition of autoimmune disease. *Autoimmun Rev* (2012) 11:754–65. doi: 10.1016/j.autrev.2012.02.001.

3. Knight J, Spain SL, Capon F, Hayday A, Nestle FO, Clop A, et al. Conditional analysis identifies three novel major histocompatibility complex loci associated with psoriasis. *Hum Mol Genet* (2012) 21(23):5185–92. doi: 10.1093/hmg/dds344.

4. Armstrong AW, Read C. Pathophysiology, clinical presentation, and treatment of psoriasis: A review. *JAMA* (2020) 323:1945–60. doi: 10.1001/jama.2020.4006.

5. Griffiths CEM, Armstrong AW, Gudjonsson JE, Barker JNWN. Psoriasis. *Lancet* (2021) 397(10281):1301–15. doi: 10.1016/S0140-6736(20)32549-6.

6. Schafer PH, Parton A, Capone L, Cedzik D, Brady H, Evans JF, et al. Apremilast is a selective PDE4 inhibitor with regulatory effects on innate immunity. *Cell Signalling* (2014) 26(9):2016–29. doi: 10.1016/j.cellsig.2014.05.014.

7. Mayba JN, Gooderham MJ. Real-world experience with apremilast in treating psoriasis. *J Cutan Med Surg* (2017) 21:145–51. doi: 10.1177/1203475416676030.

8. Papp K, Gordon K, Thaci D, Morita A, Gooderham M, Foley P, et al. Phase 2 trial of selective tyrosine kinase 2 inhibition in psoriasis. *N Engl J Med* (2018) 379(14):1313–21. doi: 10.1056/NEJMoa1806382.

9. Kotal J, Langhansova H, Lieskovska J, Andersen JF, Francischetti IM, Chavakis T, et al. Modulation of host immunity by tick saliva. *J Proteomics* (2015) 128:58–68. doi: 10.1016/j.jprot.2015.07.005.

10. Francischetti IM, Sa-Nunes A, Mans BJ, Santos IM, Ribeiro JM. The role of saliva in tick feeding. *Front Biosci (Landmark Ed)* (2009) 14(6):2051–88. doi: 10.2741/3363.

11. Jmel MA, Aounallah H, Bensaoud C, Mekki I, Chmelar J, Faria F, et al. Insights into the Role of Tick Salivary Protease Inhibitors during Ectoparasite-Host Crosstalk. *Int J Mol Sci* (2021) 22(2). doi: 10.3390/ijms22020892.

12. Valenzuela JG, Francischetti IM, Pham VM, Garfield MK, Mather TN, Ribeiro JM. Exploring the sialome of the tick Ixodes scapularis. *J Exp Biol* (2002) 205(Pt 18):2843–64. doi: 10.1242/jeb.205.18.2843.

13. Medina JM, Jmel MA, Cuveele B, Gomez-Martin C, Aparicio-Puerta E, Mekki I, et al. Transcriptomic analysis of the tick midgut and salivary gland responses upon repeated blood-feeding on a vertebrate host. *Front Cell Infection Microbiol* (2022) 12. doi: 10.3389/fcimb.2022.919786.

14. Jmel MA, Voet H, Araujo RN, Tirloni L, Sa-Nunes A, Kotsyfakis M. Tick salivary kunitz-type inhibitors: targeting host hemostasis and immunity to mediate successful blood feeding. *Int J Mol Sci* (2023) 24(2). doi: 10.3390/ijms24021556.

15. Sa-Nunes A, Bafica A, Antonelli LR, Choi EY, Francischetti IM, Andersen JF, et al. The immunomodulatory action of sialostatin L on dendritic cells reveals its potential to interfere with autoimmunity. *J Immunol* (2009) 182(12):7422–9. doi: 10.4049/jimmunol.0900075.

16. Kotsyfakis M, Karim S, Andersen JF, Mather TN, Ribeiro JM. Selective cysteine protease inhibition contributes to blood-feeding success of the tick Ixodes scapularis. *J Biol Chem* (2007) 282(40):29256–63. doi: 10.1074/jbc.M703143200.

17. Chen G, Wang X, Severo MS, Sakhon OS, Sohail M, Brown LJ, et al. The tick salivary protein sialostatin L2 inhibits caspase-1-mediated inflammation during Anaplasma phagocytophilum infection. *Infect Immun* (2014) 82(6):2553–64. doi: 10.1128/IAI.01679-14.

18. Kotal J, Stergiou N, Busa M, Chlastakova A, Berankova Z, Rezacova P, et al. The structure and function of Iristatin, a novel immunosuppressive tick salivary cystatin. *Cell Mol Life Sci* (2019) 76(10):2003–13. doi: 10.1007/s00018-019-03034-3.

19. Kotal J, Busa M, Urbanova V, Rezacova P, Chmelar J, Langhansova H, et al. Mialostatin, a novel midgut cystatin from ixodes ricinus ticks: crystal structure and regulation of host blood digestion. *Int J Mol Sci* (2021) 22(10). doi: 10.3390/ijms22105371.

20. Kotsyfakis M, Horka H, Salat J, Andersen JF. The crystal structures of two salivary cystatins from the tick Ixodes scapularis and the effect of these inhibitors on the establishment of Borrelia burgdorferi infection in a murine model. *Mol Microbiol* (2010) 77:456–70. doi: 10.1111/j.1365-2958.2010.07220.x.

21. Chlastakova A, Kotal J, Berankova Z, Kascakova B, Martins LA, Langhansova H, et al. Iripin-3, a new salivary protein isolated from ixodes ricinus ticks, displays immunomodulatory and anti-hemostatic properties in vitro. *Front Immunol* (2021) 12:626200. doi: 10.3389/fimmu.2021.626200.

22. Bordier C. Phase separation of integral membrane proteins in Triton X-114 solution. *J Biol Chem* (1981) 256:1604–7. doi: 10.1016/S0021-9258(19)69848-0.

23. Klein M, Bruhl TJ, Staudt V, Reuter S, Grebe N, Gerlitzki B, et al. Tick salivary sialostatin L represses the initiation of immune responses by targeting IRF4-dependent transcription in murine mast cells. *J Immunol* (2015) 195(2):621–31. doi: 10.4049/jimmunol.1401823.

24. Wu HM, Zeng LH, Ou JX, Wang TT, Chen Y, Nandakumar KS. Estrogen acts through estrogen receptor-beta to promote mannan-induced psoriasis-like skin inflammation. *Front Immunol* (2022) 13. doi: 10.3389/fimmu.2022.818173.

25. Wu H, Ou J, Li K, Wang T, Nandakumar KS. Comparative studies on mannan and imiquimod induced experimental plaque psoriasis inflammation in inbred mice. *Clin Exp Immunol* (2023) 211(3):288–300. doi: 10.1093/cei/uxad004.

26. Wu H, Nandakumar KS. Epicutaneous application of mannan induces psoriasis-like inflammation in an inbred mouse strain. *Bio Protoc* (2023) 13:e4845. doi: 10.21769/BioProtoc.4845.

27. Baker BS, Brent L, Valdimarsson H, Powles AV, Alimara L, Walker M, et al. Is epidermal-cell proliferation in psoriatic skin-grafts on nude-mice driven by T-cell derived cytokines. *Br J Dermatol* (1992) 126(2):105–10. doi: 10.1111/j.1365-2133.1992.tb07805.x.

28. Horka H, Staudt V, Klein M, Taube C, Reuter S, Dehzad N, et al. The tick salivary protein sialostatin L inhibits the th9-derived production of the asthma-promoting cytokine IL-9 and is effective in the prevention of experimental asthma. *J Immunol* (2012) 188(6):2669–76. doi: 10.4049/jimmunol.1100529.

29. Lieskovska J, Palenikova J, Sirmarova J, Elsterova J, Kotsyfakis M, Campos Chagas A, et al. Tick salivary cystatin sialostatin L2 suppresses IFN responses in mouse dendritic cells. *Parasite Immunol* (2015) 37(2):70–8. doi: 10.1111/pim.12162

30. Wang X, Shaw DK, Sakhon OS, Snyder GA, Sundberg EJ, Santambrogio L, et al. The tick protein sialostatin L2 binds to annexin A2 and inhibits NLRC4-mediated inflammasome activation. *Infect Immun* (2016) 84:1796–805. doi: 10.1128/IAI.01526-15.

31. Kotsyfakis M, Sa-Nunes A, Francischetti IM, Mather TN, Andersen JF, Ribeiro JM. Antiinflammatory and immunosuppressive activity of sialostatin L, a salivary cystatin from the tick Ixodes scapularis. *J Biol Chem* (2006) 281(36):26298–307. doi: 10.1074/jbc.M513010200.

32. Ferrari G, Cook BD, Terushkin V, Pintucci G, Mignatti P. Transforming growth factor-beta 1 (TGF-beta 1) induces angiogenesis through vascular endothelial growth factor (VEGF)-mediated apoptosis. *J Cell Physiol* (2009) 219(2):449–58. doi: 10.1002/jcp.21706.

33. Kamata M, Tada Y. Dendritic cells and macrophages in the pathogenesis of psoriasis. *Front Immunol* (2022) 13:941071. doi: 10.3389/fimmu.2022.941071.

34. Stratis A, Pasparakis M, Rupec RA, Markur D, Hartmann K, Scharffetter-Kochanek K, et al. Pathogenic role for skin macrophages in a mouse model of keratinocyte-induced psoriasis-like skin inflammation. *J Clin Invest* (2006) 116:2094–104. doi: 10.1172/JCI27179.

35. Khmaladze I, Kelkka T, Guerard S, Wing K, Pizzolla A, Saxena A, et al. Mannan induces ROS-regulated, IL-17A-dependent psoriasis arthritis-like disease in mice. *Proc Natl Acad Sci U.S.A* (2014) 111:E3669–78. doi: 10.1073/pnas.1405798111.

36. Cai Y, Shen X, Ding C, Qi C, Li K, Li X, et al. Pivotal role of dermal IL-17-producing gammadelta T cells in skin inflammation. *Immunity* (2011) 35:596–610. doi: 10.1016/j.immuni.2011.08.001.

37. Li B, Huang L, Lv P, Li X, Liu G, Chen Y, et al. The role of Th17 cells in psoriasis. *Immunol Res* (2020) 68(5):296–309. doi: 10.1007/s12026-020-09149-1.

38. Lowes MA, Bowcock AM, Krueger JG. Pathogenesis and therapy of psoriasis. *Nature* (2007) 445:866–73. doi: 10.1038/nature05663.

39. Li H, Yao Q, Mariscal AG, Wu XD, Hulse J, Pedersen E, et al. Epigenetic control of IL-23 expression in keratinocytes is important for chronic skin inflammation. *Nat Commun* (2018) 9. doi: 10.1038/s41467-018-03704-z.

40. Ma HL, Liang S, Li J, Napierata L, Brown T, Benoit S, et al. IL-22 is required for Th17 cell-mediated pathology in a mouse model of psoriasis-like skin inflammation. *J Clin Invest* (2008) 118(2):597–607. doi: 10.1172/JCI33263.

41. Pantelyushin S, Haak S, Ingold B, Kulig P, Heppner FL, Navarini AA, et al. Rorgammat+ innate lymphocytes and gammadelta T cells initiate psoriasiform plaque formation in mice. *J Clin Invest* (2012) 122(6):2252–6. doi: 10.1172/JCI61862.

42. Borowczyk J, Shutova M, Brembilla NC, Boehncke WH. IL-25 (IL-17E) in epithelial immunology and pathophysiology. *J Allergy Clin Immunol* (2021) 148(1):40–52. doi: 10.1016/j.jaci.2020.12.628.

43. Glowacka E, Lewkowicz P, Rotsztejn H, Zalewska A. IL-8, IL-12 and IL-10 cytokines generation by neutrophils, fibroblasts and neutrophils- fibroblasts interaction in psoriasis. *Adv Med Sci* (2010) 55(2):254–60. doi: 10.2478/v10039-010-0037-0.

44. Al-Robaee AA, Al-Zolibani AA, Al-Shobili HA, Kazamel A, Settin A. IL-10 implications in psoriasis. *Int J Health Sci (Qassim)* (2008) 2(1):53–8.

45. Reich K. Response of psoriasis to interleukin-10 is associated with suppression of cutaneous type 1 inflammation, downregulation of the epidermal interleukin-8/CXCR2 pathway and normalization of keratinocyte maturation. *J Invest Dermatol* (2001) 116:829–9. doi: 10.1046/j.1523-1747.2001.01248.x.

46. Hahn M, Ghoreschi K. The role of IL-4 in psoriasis. *Expert Rev Clin Immunol* (2017) 13:171–3. doi: 10.1080/1744666X.2017.1279054.

47. Ghoreschi K, Thomas P, Breit S, Dugas M, Mailhammer R, van Eden W, et al. Interleukin-4 therapy of psoriasis induces Th2 responses and improves human autoimmune disease. *Nat Med* (2003) 9(1):40–6. doi: 10.1038/nm804.

48. Yang N, Matthew MA, Yao C. Roles of cysteine proteases in biology and pathogenesis of parasites. *Microorganisms* (2023) 11. doi: 10.3390/microorganisms11061397.

49. Schonefuss A, Wendt W, Schattling B, Schulten R, Hoffmann K, Stuecker M, et al. Upregulation of cathepsin S in psoriatic keratinocytes. *Exp Dermatol* (2010) 19(8):e80–8. doi: 10.1111/j.1600-0625.2009.00990.x.

50. Chmelar J, Kotal J, Kovarikova A, Kotsyfakis M. The use of tick salivary proteins as novel therapeutics. *Front Physiol* (2019) 10. doi: 10.3389/fphys.2019.00812.

51. Ryan C, Sadlier M, De Vol E, Patel M, Lloyd AA, Day A, et al. Genital psoriasis is associated with significant impairment in quality of life and sexual functioning. *J Am Acad Dermatol* (2015) 72(6):978–83. doi: 10.1016/j.jaad.2015.02.1127.

52. Singh S, Taylor C, Kornmehl H, Armstrong AW. Psoriasis and suicidality: A systematic review and meta-analysis. *J Am Acad Dermatol* (2017) 77(3):425–+. doi: 10.1016/j.jaad.2017.05.019.

53. Hung WK, Tung TH, Wang TY, Liao SC, Chi CC. Risk for incident suicidality among psoriasis patients: a systematic review and meta-analysis. *Arch Dermatol Res* (2022) 315(3):455–65. doi: 10.1007/s00403-022-02377-5.

54. Singh R, Koppu S, Perche PO, Feldman SR. The cytokine mediated molecular pathophysiology of psoriasis and its clinical implications. *Int J Mol Sci* (2021) 22(23). doi: 10.3390/ijms222312793.

55. Glatt S, Baeten D, Baker T, Griffiths M, Ionescu L, Lawson ADG, et al. Dual IL-17A and IL-17F neutralisation by bimekizumab in psoriatic arthritis: evidence from preclinical experiments and a randomised placebo-controlled clinical trial that IL-17F contributes to human chronic tissue inflammation. *Ann Rheum Dis* (2018) 77(4):523–32. doi: 10.1136/annrheumdis-2017-212127.

56. Brembilla NC, Senra L, Boehncke WH. The IL-17 family of cytokines in psoriasis: IL-17A and beyond. *Front Immunol* (2018) 9:1682. doi: 10.3389/fimmu.2018.01682.

57. Hirai T, Kanda T, Sato K, Takaishi M, Nakajima K, Yamamoto M, et al. Cathepsin K is involved in development of psoriasis-like skin lesions through TLR-dependent Th17 activation. *J Immunol* (2013) 190(9):4805–11. doi: 10.4049/jimmunol.1200901.

58. Ainscough JS, Macleod T, McGonagle D, Brakefield R, Baron JM, Alase A, et al. Cathepsin S is the major activator of the psoriasis-associated proinflammatory cytokine IL-36gamma. *Proc Natl Acad Sci U.S.A* (2017) 114:E2748–57. doi: 10.1073/pnas.1620954114.

59. Conrad C, Gilliet M. Psoriasis: from pathogenesis to targeted therapies. *Clin Rev Allergy Immunol* (2018) 54:102–13. doi: 10.1007/s12016-018-8668-1.

frontiers | Frontiers in Immunology

TYPE Original Research
PUBLISHED 12 March 2024
DOI 10.3389/fimmu.2024.1280877

OPEN ACCESS

EDITED BY
William Harold Witola,
University of Illinois at Urbana–Champaign, United States

REVIEWED BY
Shahbaz Manzoor Khan,
Johns Hopkins University, United States
Daniel A. Abugri,
Alabama State University, United States

*CORRESPONDENCE
Virginia Maria Barros de Lorena
virginia.lorena@fiocruz.br

RECEIVED 21 August 2023
ACCEPTED 27 February 2024
PUBLISHED 12 March 2024

CITATION
Moreira LR, Silva AC, Costa-Oliveira CN, Silva-Júnior CDd, Oliveira KKdS, Torres DJL, Barros MdS, Rabello MCdS and de Lorena VMB (2024) Interaction between peripheral blood mononuclear cells and *Trypanosoma cruzi*-infected adipocytes: implications for treatment failure and induction of immunomodulatory mechanisms in adipose tissue.
Front. Immunol. 15:1280877.
doi: 10.3389/fimmu.2024.1280877

Interaction between peripheral blood mononuclear cells and *Trypanosoma cruzi*-infected adipocytes: implications for treatment failure and induction of immunomodulatory mechanisms in adipose tissue

Leyllane Rafael Moreira[1,2], Ana Carla Silva[2], Cíntia Nascimento da Costa-Oliveira[2], Claudeir Dias da Silva-Júnior[1,2], Kamila Kássia dos Santos Oliveira[2], Diego José Lira Torres[1,2], Michelle D. Barros[2], Michelle Christiane d. S. Rabello[2] and Virginia Maria Barros de Lorena[2]*

[1]Department of Tropical Medicine, Federal University of Pernambuco, Recife, Brazil, [2]Department of Immunology, Aggeu Magalhães Institute, Recife, Brazil

Background/Introduction: Adipose tissue (AT) has been highlighted as a promising reservoir of infection for viruses, bacteria and parasites. Among them is *Trypanosoma cruzi*, which causes Chagas disease. The recommended treatment for the disease in Brazil is Benznidazole (BZ). However, its efficacy may vary according to the stage of the disease, geographical origin, age, immune background of the host and sensitivity of the strains to the drug. In this context, AT may act as an ally for the parasite survival and persistence in the host and a barrier for BZ action. Therefore, we investigated the immunomodulation of T. cruzi-infected human AT in the presence of peripheral blood mononuclear cells (PBMC) where BZ treatment was added.

Methods: We performed indirect cultivation between T. cruzi-infected adipocytes, PBMC and the addition of BZ. After 72h of treatment, the supernatant was collected for cytokine, chemokine and adipokine assay. Infected adipocytes were removed to quantify T. cruzi DNA, and PBMC were removed for immunophenotyping.

Results: Our findings showed elevated secretion of interleukin (IL)-6, IL-2 and monocyte chemoattractant protein-1 (MCP-1/CCL2) in the AT+PBMC condition compared to the other controls. In contrast, there was a decrease in tumor necrosis factor (TNF) and IL-8/CXCL-8 in the groups with AT. We also found high adipsin secretion in PBMC+AT+T compared to the treated condition (PBMC+AT +T+BZ). Likewise, the expression of CD80+ and HLA-DR+ in CD14+ cells decreased in the presence of T. cruzi.

10.3389/fimmu.2024.1280877

Discussion: Thus, our findings indicate that AT promotes up-regulation of inflammatory products such as IL-6, IL-2, and MCP-1/CCL2. However, adipogenic inducers may have triggered the downregulation of TNF and IL-8/CXCL8 through the peroxisome proliferator agonist gamma (PPAR-g) or receptor expression. On the other hand, the administration of BZ only managed to reduce inflammation in the microenvironment by decreasing adipsin in the infected culture conditions. Therefore, given the findings, we can see that AT is an ally of the parasite in evading the host's immune response and the pharmacological action of BZ.

KEYWORDS

adipose tissue, immunomodulation, *Trypanosoma cruzi*, cytokine, chemokine, adipokine, benznidazole

Introduction

Chagas disease, caused by the hemoflagellate protozoan *Trypanosoma cruzi*, persists as a significant public health challenge (1). About 6–7 million people worldwide are estimated to be infected with *T. cruzi*, mainly in Latin America, where Chagas disease is considered endemic (2). On the other hand, due to migratory flows, Chagas disease has now spread more widely, and non-endemic areas, such as North America and European countries, have also reported several cases in the recent past (1).

The classic form of Chagas disease transmission is via the vector route, wherein the individual's damaged skin comes into contact with the contaminated feces of triatomine insects. The lesion allows the entry of trypomastigotes, which differentiate and thus infect and multiply inside the cells. However, other transmission routes also play an important role, such as congenital, transfusion/organ transplant, and oral and laboratory accidents. The onset of infection, which represents the acute phase of Chagas disease, is characterized by high parasitemia and nonspecific symptoms such as fever, malaise, and apathy, often making early diagnosis difficult. Around 2 to 4 months after infection, infected individuals can enter the chronic phase of the disease, which can generate more severe symptomatic manifestations, such as the cardiac, digestive, or mixed form. However, around 70% of patients present an asymptomatic condition called the indeterminate form (3).

Faced with such heterogeneous clinical forms, the immune response associated with each form is quite complex. Patients with the indeterminate form show a more regulatory immune response, with a predominance of anti-inflammatory cytokines such as IL-10. In contrast, the symptomatic clinical forms promote robust inflammation, increasing pro-inflammatory cytokines such as interferon-gamma (IFN-γ) and TNF. Nevertheless, the immunological mechanisms associated with disease progression to asymptomatic or symptomatic forms are not fully elucidated (4). In addition, factors such as comorbidities, the host's immunological background, or the strain of *T. cruzi* can alter the expected immune response pattern (4, 5).

T. cruzi is a versatile parasite with mechanisms for evading the immune response, allowing it to survive and multiply in the infected host (5, 6). Among the evasion strategies, infection of the AT by *T. cruzi* has stood out as a promising reservoir of infection/latency and metabolic modulation of the parasite (7) . The AT is an endocrine organ responsible for the body's energy reserve. However, it also has immunological properties, such as the secretion of bioactive factors known as adipokines. AT is divided into three types of tissue: white adipose tissue (WAT), associated with energy storage and secretion of adipokines; brown adipose tissue (BAT), which is associated with thermogenic activity and beige/brite adipose tissue, which comes from WAT, but has thermogenic functions (8, 9).

The visceral AT of mice infected with the Brazil strain of *T. cruzi* shows elevated levels of TNF, IFN-γ and IL-1, as well as reduced adiponectin and leptin, as a reflection of the inflammatory profile of the infection (10). In addition, adipocytes differentiated from murine fibroblasts, upon *in vitro* infection with the Tulahuen strain of *T. cruzi*, demonstrated an inflammatory phenotype, with increased expression of the cytokines IFN-γ, TNF and IL-1β and the chemokines CCL2, CCL5 and CXCL10 (11).

In contrast, administration of murine AT-derived mesenchymal cells in untreated *T. cruzi* Brazil strain-infected mice three days post-infection reduced parasitaemia and inflammation, with increased IL-10 expression through modulation of the immune response (12). However, the immunological mechanisms of differentiated human adipose cells infected with *T. cruzi* and treated with BZ were not verified in such studies. In humans, little is known about the role of this reservoir of infection in Chagas disease; however, the presence of *T. cruzi* kDNA in the AT of patients with the disease has been detected (13). However, the impact of the immune response of this reservoir of infection against the parasite has not yet been explored.

Currently, the drugs available to treat Chagas disease are two nitro heterocyclic compounds: BZ and Nifurtimox. Both drugs have a trypanocidal effect on all evolutionary forms of the parasite (amastigotes, epimastigotes, and trypomastigotes). It is believed

that the drugs act on the formation of free radicals and electrophilic metabolites, affecting the parasite's macromolecules. However, from the 1980s onwards, Nifurtimox was discontinued in Brazil and other South American countries due to its high toxicity compared to BZ and the reduction in its trypanocidal effect in some endemic regions (14–16). Therefore, BZ is the recommended drug in Brazil. However, its efficacy is controversial in the chronic phase of the disease, and some variables such as age, geographical origin and susceptibility of the strains to the drug significantly alter the efficacy of the drug (17, 18).

In this context, once the AT acts as a reservoir of infection, it may represent a barrier to the drug's action, thus reducing its effectiveness. In addition, immune response cells such as PBMCs also participate in the immune modulation generated by infection and/or treatment with BZ, which may be an important factor to be evaluated. Therefore, we evaluated the modulation of the immune response induced by human mesenchymal stem cells differentiated into adipocytes infected with *T. cruzi* under indirect contact with PBMC and the addition of BZ treatment to mimic what happens in this microenvironment.

Materials and methods

Parasites

Vero cells (ATCC – CCL-81™) cultured in 75 cm^2 flasks containing RPMI 1640 medium (Sigma™) supplemented with 10% fetal bovine serum (FBS) (GIBCO®) and 1% penicillin/streptomycin (Lonza) (complete medium) were used to maintain the parasites. After 70-80% confluence of the cells, trypomastigote forms of *T. cruzi* strain Y (DTU II), kept frozen in liquid nitrogen, were thawed and used to infect the cells. Approximately $1x10^6$ parasites/mL were added to the cell culture for infection in complete medium for 24 hours in an incubator with 5% CO_2 in a humidified atmosphere. At the end of incubation, the supernatant was discarded to remove the parasites that were unable to infect cells. Complete RPMI 1640 medium (Sigma™) was added, and the cultures were incubated for 5 to 8 days. Vero cells were observed daily under an inverted microscope. After the rupture of the Vero cells, the free trypomastigotes in the culture medium were collected, centrifuged (2555 x g for 10 min at 20°C), and the pellet was stained with Trypan blue (Sigma™) to observe the cell viability of the trypomastigotes that were used in the culture.

Cultivation of human adipose tissue stem cells (ADSC)

ADSC (PT-5006, LONZA™) were grown in 75 cm^3 culture flasks in Dulbecco's Modified Eagle Medium (DMEM) supplemented with 20% FBS and 1% penicillin-streptomycin. When they reached full confluence, the cells were detached using 2% trypsin/EDTA solution (GIBCO™), washed with complete medium, and seeded in new flasks for further propagation of the cells. All ADSC experiments were performed between the third and sixth cell passages.

Adipogenic differentiation

When they reached confluence, ADSC were harvested using 2% trypsin/EDTA solution (GIBCO™) and plated at a concentration of 5 x 10^5 cells/well in individual 35 mm × 10 mm culture plates (CORNING®). When they reached about 90% confluence (24/48 hours post-plating), the differentiation wells were cultured with DMEM supplemented with 10% FBS and 1% gentamicin-amphotericin (PT-8205, LONZA™) with the adipogenic inducers (insulin, dexamethasone, 3-isobutyl-methyl-xanthine and indomethacin), according to the recommendations of the adipogenic differentiation kit (PT-9502, LONZA™) for 12 days. A control group of wells, which included cells cultured in DMEM supplemented with 10% FBS and 1% gentamicin-amphotericin, was also included. After the culture time recommended by the manufacturer, the cells were stained with the AdipoRed™ reagent (PT-7009, LONZA™), which uses Nile red dye to highlight lipid vesicles. After adding AdipoRed™ in the wells, the fluorescence of the lipid vesicles was visualized in the 485nm filter under 572nm emission in the confocal microscope.

Study population

Five volunteer subjects were included, three females and two males, with a mean age of 26.6 ± 4.03. From each participant, 30 mL of blood was collected in vacuum tubes (Vacutainer®) containing sodium heparin to obtain PBMC. In addition, 5 mL of blood were collected in dry tubes to obtain serology confirmation of *T. cruzi*. Exclusion criteria for our study were residing in an endemic area for Chagas disease, having received a blood transfusion, being under 18 years of age and presenting reactive serology for Chagas disease or being a carrier of any other chronic inflammatory or autoimmune disease. All study participants answered a research form and signed the Free and Informed Consent Form voluntarily.

Isolation of peripheral blood mononuclear cells

Blood was dispensed into polypropylene tubes (BD Falcon™) and diluted 1:2 in sterile filtered phosphate-buffered saline (PBS). This solution was added to polypropylene tubes (BD Falcon™) containing Ficoll-Hypaque PLUS™ (Amersham Biosciences) (1:3). Cells were separated by centrifugation for 30 min at 900 x g 20°C, and the PBMC ring formed between the Ficoll interface and plasma was collected. Cells were washed twice by centrifugation and resuspended in DMEM medium (SIGMA™) supplemented with 10% FBS and 1% gentamicin-amphotericin (GIBCO®). Cells were counted in a Neubauer chamber using Trypan Blue dye (Sigma™).

Indirect culture between *T. cruzi* infected adipocytes, PBMC and addition of BZ treatment

Initially, we plated ADSC in 24-well cell culture plates (KASVI) at a concentration of 0.2 x 10^4 cells/well and performed adipogenic differentiation. After the end of differentiation, we infected these adipocytes with trypomastigote forms of *T. cruzi* strain Y for approximately 3 hours at a ratio of 5:1 parasites per cell as described by Nagajyothi et al. (11). After the infection period, we renewed the culture medium with DMEM supplemented with 10% FBS and 1% gentamicin-amphotericin to remove parasites that had not internalized into the cells. Then, above each cultured well, we added an indirect culture insert with a pore size of 0.4µm (Thincert® - n° 662640 – GREINER) and deposited the PBMC at a concentration of 2 x 10^6 cells/mL directly on the membrane in DMEM supplemented with 10% FBS and 1% gentamicin-amphotericin and were incubated at 37°C at 5% CO_2 for 48 h. After this period, we carried out the treatmentwith BZ at a 1µg/mL concentration, according to Romanha et al. (19), and returned the plates to the incubator (Figure 1). About 72 h after treatment, according to Moreira et al. (20) we collected the culture supernatant for cytokine and chemokine dosage, removed the PBMC from the inserts for immunophenotyping, and the infected adipocytes for *T. cruzi* DNA quantification.

Quantification of *T. cruzi*-DNA

After the indirect culture time, cells from each culture condition were removed from the culture plates by washing with ice-cold Phosphate-buffered saline (PBS) and promptly deposited in polypropylene tubes (BD Falcon™ – 15 mL) for washing with PBS (500 x g, 10 min, brake 1). Then, the final pellet was transferred to 1.5 mL microtubes, and extraction was performed with the QIAamp DNA Mini Kit – QIAGEN according to the manufacturer's recommendations. The primers TcSAT1 – F (5′AAATTCCTCCA AGCAGCGGA3′) and TcSAT2 – R (5′ ATGAATGGCGGG AGTCAGAG3′) were used to amplify the *T. cruzi* satellite DNA (SAT-DNA), as described previously (21). *T. cruzi* genomic DNA (strain Y) was used to generate a standard curve to quantify the parasite load in samples by quantitative PCR (qPCR). Quantification of parasite load was performed with the QuantStudio 5 Real-Time PCR System (Thermo Fisher Scientific) using the TcSAT-IAM system (21). Samples were tested in duplicate at all stages. The results were analyzed, interpreted, and recorded using the QuantStudio Design and Analysis Software, as described by Moreira et al. (20).

Cytokine and chemokine assay

After collection of culture supernatants from indirect cultivation, cytokines (IL-2, IL-4, IL-6, IL-10, TNF and IFN-γ) and chemokines (IP-10/CXCL-10, MCP-1/CCL2, MIG/CXCL9, RANTES/CCL5 and IL-8/CXCL8) using CBA (Cytometric Bead Array-BD Biosciences, USA), according to the manufacturer's recommendations. Samples were acquired at the Flow Cytometry Technology Platform, located at the Nucleus of Technological Platforms (NPT)/IAM/Fiocruz, through the FACScalibur flow cytometer (Becton Dickson Immunocytometry Systems), with the CellQuestPro software (Beckton Dickson) and analyzed in the FCAP Array 3.1 software.

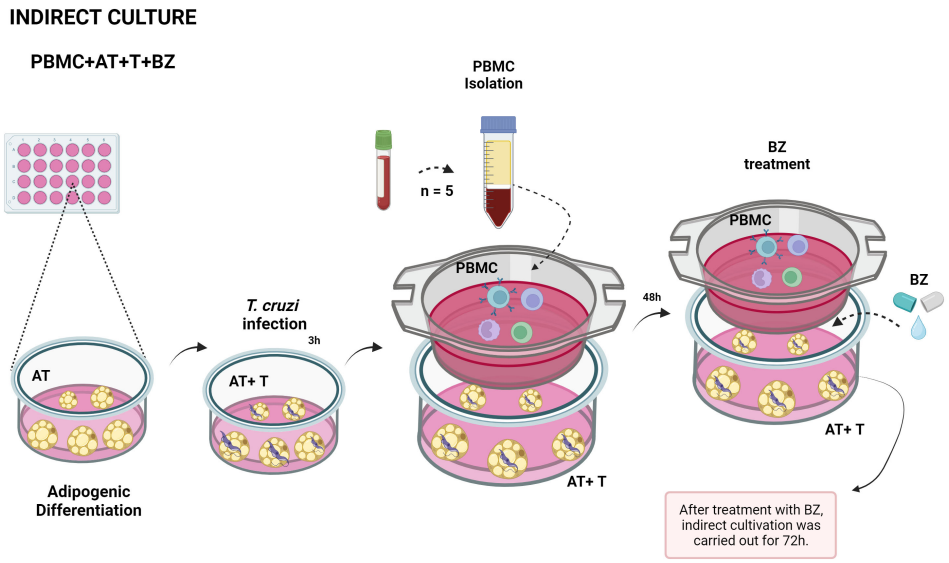

FIGURE 1
Schematic representation of indirect culture between *Trypanosoma cruzi*-infected AT, PBMC and benznidazole treatment. PBMC, Peripheral blood mononuclear cells (PBMC); AT, Adipose tissue from adipogenic differentiation of ADSC (AT); *Trypanosoma cruzi* (T); Benz nidazole (BZ). Design created with the aid of Biorender®.

Adipokines dosage and acquisition strategy

Adipokines (adiponectin, adipsin, leptin and resistin) were measured using the LEGENDplex™ Human Metabolic Panel 1 kit (Biolegend®), according to the manufacturer's recommendations. Samples were acquired from the Flow Cytometry Technology Platform, located at NPT/IAM/Fiocruz, using the FACScalibur flow cytometer (Becton Dickson Immunocytometry Systems), with BD CellQuestPro software (Beckton Dickson) and analyzed using LEGENDplex™ Data Analysis software (Biolegend®). The adipokine population was selected using pseudocolor density (FSC) versus side scatter (SSC) plots. Eight hundred beads were acquired within window A (Beads A – Adiponectin and Adipsin) and 800 beads from window B (Beads B – Leptin and Resistin). The classification of the beads was performed using the FL4 channel. After selecting the window of interest (A) and (B), the adipokines were analyzed by obtaining two-dimensional plots of the spot fluorescence distribution using LEGENDplex™ Data Analysis (Biolegend®) (Supplementary Figure 1).

Immunophenotyping of lymphocytes and monocytes from an indirect culture between *T. cruzi* infected adipocytes, PBMC and addition of BZ treatment

PBMC adhered to the insert were removed using ice-cold PBS-Wash (PBS containing 0.5% bovine serum albumin and 1% sodium azide) and centrifuged at 400 x g for 5 minutes. The supernatant was discarded, and the pellet containing the cells was distributed into cytometry tubes and incubated with monoclonal antibodies anti-CD4/PerCP (BD™), CD8/FITC (BD™), CD28/PE (BD™) and CTLA-4/APC (BD™) for lymphocytes, and anti-CD14/FITC (BD™), CD80/PE (BD™), HLA-DR/PerCP (BD™) for CD14+ cells, for 30 min at room temperature protected from light. After incubation, the cells were washed by centrifugation (400 x g for 5 min at room temperature). Then, the cells were fixed with BD Cytofix™ (BD Biosciences®) for 15 min at 4°C. Furthermore, after washing (400 x g for 5 min at room temperature), the cells were resuspended with 300 µL of PBS-Wash/tube and stored at 4°C until the time of acquisition on the FACScalibur flow cytometer (Beckton Dickson). The lymphocyte population was selected FSC versus SSC plots, with 20,000 events acquired within the R1 lymphocyte window, and CD14+ cells were selected via FCS versus FL1, with 1,000 events acquired within the R2 window. After selecting the window of interest (R1) and (R2), CD4+ and CD8+ T lymphocytes and CD14+ cells and molecules were analyzed by obtaining two-dimensional plots of the spot fluorescence distribution using FlowJo® software version 10.8.1.

Statistical analysis

The results were analyzed using GraphPad PRISM 8.0 Windows® software (USA) and submitted to the Shapiro-Wilk normality test. When the samples showed normal distribution, the One-Way ANOVA test was applied, followed by Tukey's post-test. However, when they did not follow the normal distribution, we used the Friedman test and Dunn's post-test to assess the differences between the groups. All conclusions were made at the 5% significance level.

Ethical considerations

The approaches that were used in the study were approved by the Research Ethics Committee (CEP) of IAM/Fiocruz (C.A.A.E 97930918.3.0000.5190).

Results

Adipogenic differentiation of ADSCs and assessment of parasite load of *T. cruzi*-infected adipocytes in indirect culture between AT and PBMC after BZ treatment

Twelve days after the induction of adipogenic differentiation, we observed the presence of small lipid vesicles (multilocular) within the adipocytes (Figure 2). In general, there was a high parasite load in the culture conditions where the cells were infected with *T. cruzi* (Figure 3). However, we found that the average parasite load quantification of the PBMC+AT+T+BZ group was lower than the PBMC+AT+T, although it did not represent a statistically significant difference (p= 0.2337) (Figure 3).

AT induces upregulation of IL-2, IL-6 and MCP-1 but promotes downregulation of TNF and Il-8 in the presence of PBMC and *T. cruzi*

Regarding cytokines, it was possible to observe that the presence of AT (PBMC+AT), even if indirectly, promotes an increase in IL-2 production that is statistically significant (p=0.0014) compared to the PBMC condition (Figure 4A). On the other hand, the presence of *T. cruzi* in PBMC+AT+T and PBMC+AT+T+BZ culture conditions considerably decreased the production of this cytokine compared to the PBMC + AT condition (Figure 4A). The production of IL-4 and IL-10 was similar in all culture conditions evaluated (Figures 4B, C).

In the production of IL-6, we observed that AT promoted an increase in the inflammatory cytokine in all groups with AT when compared to the PBMC condition, thus being statistically significant in the PBMC+AT group (p=0.0172) (Figure 4D). We detected that TNF production decreased in all groups in which AT was present, being statistically significant (p=0.0332) between PBMC+AT when compared to the PBMC group (Figure 4E). However, in the presence of *T. cruzi* (PBMC+AT+T and PBMC+AT+T+BZ), there was a decrease in IFN-γ compared to the other culture conditions studied (Figure 4F). Yet, the production

10.3389/fimmu.2024.1280877

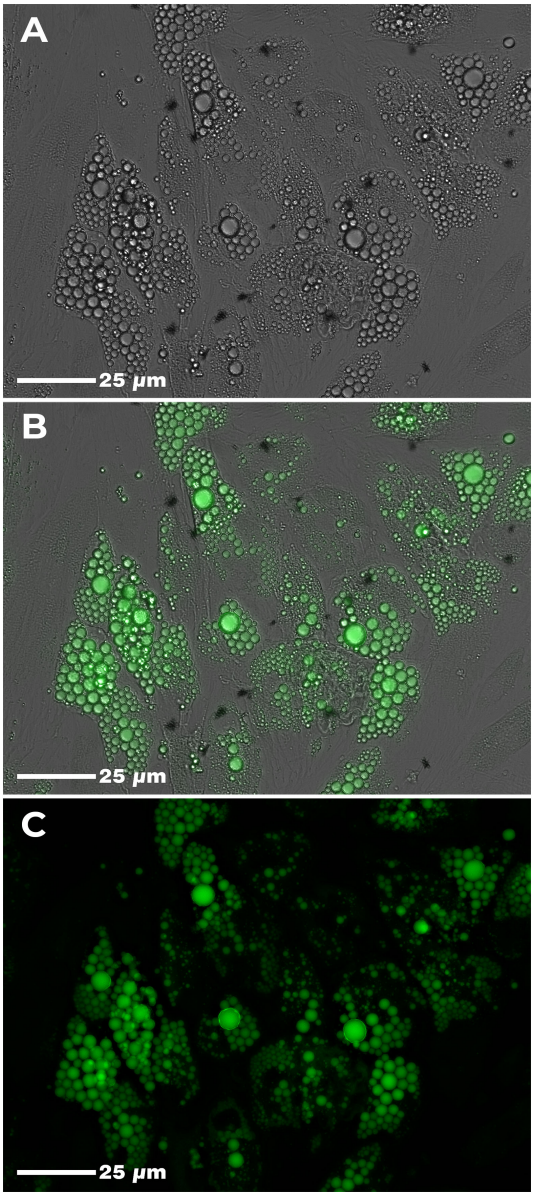

FIGURE 2
Adipogenic differentiation of human adipose-derived stem cells (ADSC). Legend: Human adipose tissue-derived stem cells (ADSC) after adipogenic differentiation. Lipid vesicles were highlighted by green color after staining with AdipoRed™ and visualized in confocal microscopy. **(A)** Adipogenic differentiation of ADSC (phase-contrast); **(B)** Adipogenic differentiation of ADSC (phase-contrast + fluorescence); **(C)** Adipogenic differentiation of ADSC (fluorescence).

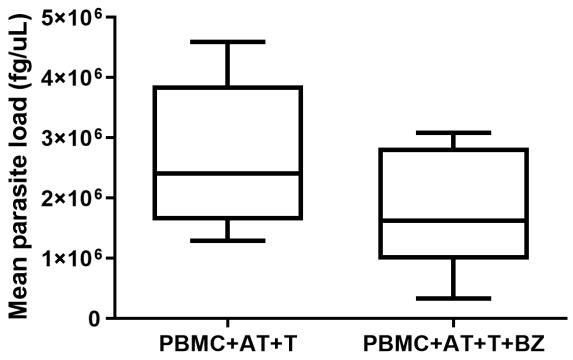

FIGURE 3
Quantification of parasite load of *Trypanosoma cruzi* infected adipocytes in indirect culture between adipose tissue, peripheral blood mononuclear cells and Benznidazole treatment. PBMC, Peripheral blood mononuclear cells (PBMC); AT, Adipose tissue from adipogenic differentiation of ADSC (AT); *Trypanosoma cruzi* (T); Benznidazole (BZ). Horizontal bars represent the median and vertical bars the lower and upper limit. Symbols (*) above the bars indicate statistical difference with $p \leq 0.05$.

of cytokines between the infected and BZ-treated culture condition (PBMC+AT+T+BZ) was similar when compared to the only infected one (PBMC+AT+T) (Figure 4F).

As for chemokines, we found that there was a decrease in IP-10/CXCL10 and MIG/CXCL-9 in the culture conditions infected by *T. cruzi* (PBMC+AT+T and PBMC+AT+T+BZ) in comparison to uninfected controls (PBMC, PBMC+AT and PBMC+AT+BZ) (Figures 5A, B). Another chemokine that followed the same behavior was MCP-1/CCL2, where there is a decrease of this chemokine in conditions where *T. cruzi* is present, compared to the PBMC+AT condition, and therefore being statistically significant in the PBMC+AT+T group (p=0.0106) (Figure 5C).

For RANTES/CCL-5, we found that the averages of the culture conditions studied were similar to each other, except in the culture conditions infected by *T. cruzi* (PBMC+AT+T and PBMC+AT+T+BZ), where there was a higher production of this chemokine (Figure 5D). In contrast, for IL-8/CXCL-8, we observed that AT promotes an inhibition/decrease in all culture conditions compared to PBMC and is statistically significant for the PBMC+AT condition (p=0.0208) (Figure 5E). It is worth noting that this same phenomenon occurred with the cytokine TNF (Figure 4D).

BZ decreases adipsin in AT infected with *T. cruzi* in the presence of PBMC

Regarding adipokines, there was high production of adiponectin, leptin and resistin, which is similarly distributed among the culture conditions studied (Figures 6A, C, D). However, although adipsin is widely secreted in the culture conditions studied, we observed that there was a greater increase in the PBMC+AT+T condition in contrast with the treated culture condition (PBMC+AT+T+BZ), then being statistically significant (p=0.0207) (Figure 6B).

AT infected by *T. cruzi* promotes decreased expression of $CD80^+$ and HLA-DR^+ molecules in $CD14^+$ cells

Regarding the frequency of the lymphocyte population present in the indirect culture, we found that there was a higher frequency of $CD4^+$ T lymphocytes in the culture conditions in which there is

10.3389/fimmu.2024.1280877

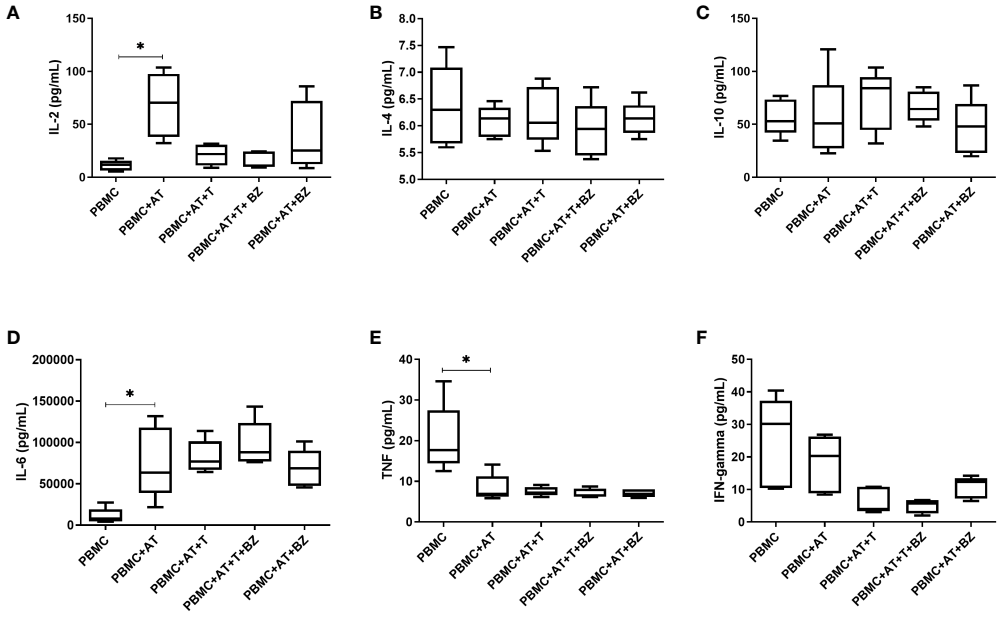

FIGURE 4
Measurement of cytokines in the culture supernatant of indirect culture between Trypanosoma cruzi-infected adipose tissue, peripheral blood mononuclear cells and benznidazole treatment. PBMC, Peripheral blood mononuclear cells (PBMC); AT, Adipose tissue from adipogenic differentiation of ADSC (AT); Trypanosoma cruzi (T); Benznidazole (BZ). **(A)** IL-2 cytokine measurement; **(B)** IL-4 cytokine measurement; **(C)** IL-10 cytokine measurement; **(D)** IL-6 cytokine measurement; **(E)** TNF cytokine measurement; **(F)** IFN-gamma cytokine measurement. Horizontal bars represent the median and vertical bars the lower and upper limit. Symbols (*) above the bars indicate statistical difference with $p \leq 0.05$.

the presence of AT, being statistically significant in the PBMC+AT condition (p=0.0025) when compared to PBMC (Figure 7A). In contrast, the opposite behavior in $CD8^+$ T lymphocytes was noticed, in which the presence of AT decreases the frequency of these cells, also having statistical significance in the PBMC+AT condition (p=0.0037) compared to PBMC (Figure 7B).

When evaluating the surface molecules responsible for cell activation and inhibition, we observed that the frequency of

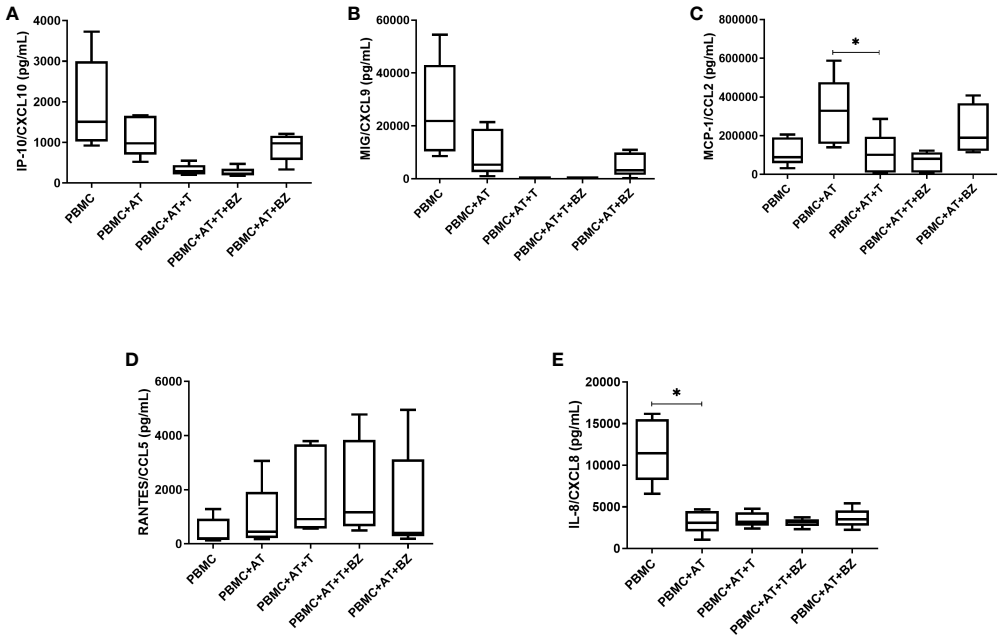

FIGURE 5
Measurement of chemokines in the culture supernatant of indirect culture between adipose tissue infected by *Trypanosoma cruzi*, peripheral blood mononuclear cells and treatment with benznidazole. PBMC, Peripheral blood mononuclear cells (PBMC); AT, Adipose tissue from adipogenic differentiation of ADSC (AT); *Trypanosoma cruzi* (T); Benznidazole (BZ). **(A)** IP-10/CXCL10 chemokine measurement; **(B)** MIG/CXCL9 chemokine measurement; **(C)** MCP-1/CCL2 chemokine measurement; **(D)** RANTES/CCL5 chemokine measurement; **(E)** IL-8/CXCL8 chemokine measurement. Horizontal bars represent the median and vertical bars the lower and upper limit. Symbols (*) above the bars indicate statistical difference with $p \leq 0.05$.

10.3389/fimmu.2024.1280877

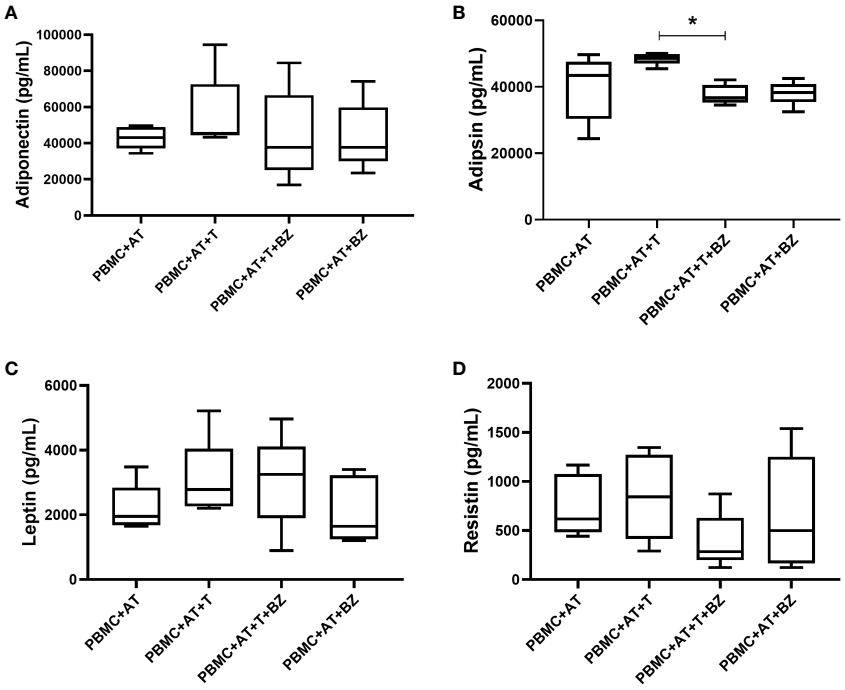

FIGURE 6
Measurement of adipokines in the culture supernatant of indirect culture between adipose tissue infected by *Trypanosoma cruzi*, peripheral blood mononuclear cells and treatment with benznidazole. PBMC, Peripheral blood mononuclear cells (PBMC); AT, Adipose tissue from adipogenic differentiation of ADSC (AT); *Trypanosoma cruzi* (T); Benznidazole (BZ). **(A)** Adiponectin adipokine measurement; **(B)** Adipsin adipokine measurement; **(C)** Leptin adipokine measurement; **(D)** Resistin adipokine measurement. Horizontal bars represent the median and vertical bars the lower and upper limit. Symbols (*) above the bars indicate statistical difference with $p \leq 0.05$.

$CD28^+$ molecules in $CD4^+$ T lymphocytes was similar in all culture conditions studied (Figure 7C). Still, in $CD8^+$ T lymphocytes, there was a higher frequency of $CD28^+$ in culture conditions where there is the presence of AT, which was found in PBMC+AT in contrast with the PBMC group (p=0.0141), as well as in PBMC+AT+T+BZ when compared to PBMC+AT+BZ (p=0.0222) (Figure 7D).

Moreover, the research concluded that the frequency of CTLA-4 in $CD4^+$ T lymphocytes was similar between culture conditions, except for the PBMC+AT and PBMC+AT+BZ groups that showed higher medians regarding the frequency of this molecule in comparison with the other culture conditions (Figure 7E). However, in $CD8^+$ T lymphocytes, according to the average of each group, we observed that in the conditions in which the cells were infected (PBMC+AT+T and PBMC+AT+T+BZ), they demonstrated a higher frequency of CTLA-4 than the other culture conditions (Figure 7F).

Regarding $CD14^+$ cells, it was ascertained that the frequency of $CD80^+$ was higher in the PBMC+AT group compared to PBMC+AT+T (p=0.0114), as well as in the PBMC+AT+BZ group compared to PBMC+AT+T+BZ (0.0008) (Figure 8A). However, in $CD14^+HLA\text{-}DR^+$ cells, there was a decrease in the frequency of this cell population in the culture conditions infected by *T. cruzi* (PBMC+AT+T and PBMC+AT+T+BZ), when compared to the other groups (Figure 8B).

Discussion

AT has, for many years, been considered only an energy backup (22). Regardless, this endocrine organ plays a crucial role in the immune response, such as secreting adipokines and cytokines and acting in the host's energy homeostasis (9, 23). Also, the AT has been seen as a "sanctuary" for several microorganisms – such as viruses, bacteria and parasites – that use this mechanism to try to escape the host's immune response (24, 25). Therefore, our object of study was the AT as a reservoir for *T. cruzi* (7). However, as the human host is complex and the AT is a very heterogeneous organ, composed of several cell types (26), we mimicked an *in vitro* microenvironment in which there is indirect contact of the AT infected by *T. cruzi* and the PBMC in addition to verifying if there is any repercussion in the face of treatment with BZ. As a result, we found that indirect contact between PBMC and infected AT is sufficient to promote immunomodulatory changes that can stimulate the production of cytokines such as IL-6 and IL-2 and reduce the production of TNF and IL-8/CXCL8.

During our study, we used ADSC to perform adipogenic differentiation, which, although possessing AT as its source, can differentiate other cell types according to the stimulus to which it is applied (27). Thus, we observed that after the differentiation induction, the differentiated cells' lipid droplets were multilocular,

10.3389/fimmu.2024.1280877

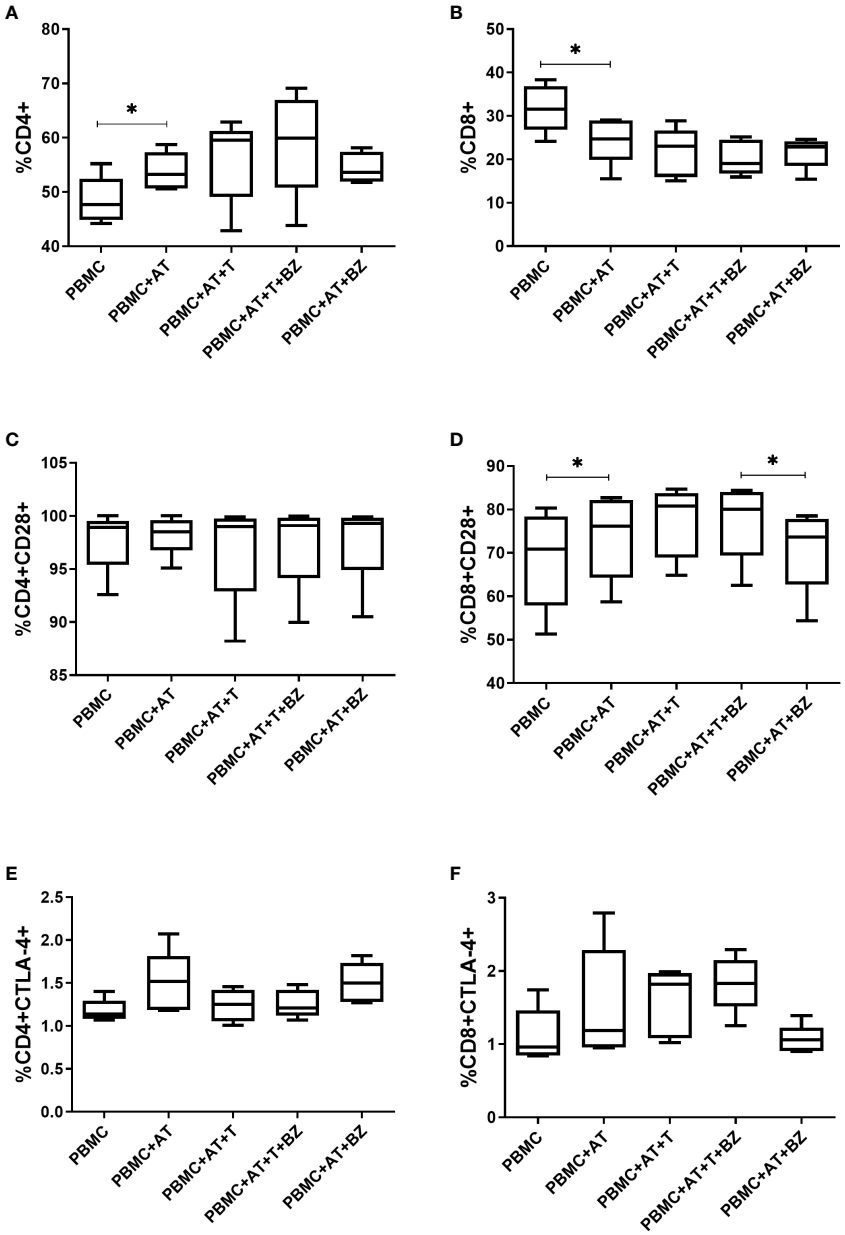

FIGURE 7
Evaluation of the expression of activation/inhibition molecules in CD4+ and CD8+ T lymphocytes from indirect culture between Trypanosoma cruzi-infected adipose tissue, peripheral blood mononuclear cells and benznidazole treatment. PBMC, Peripheral blood mononuclear cells (PBMC); AT, Adipose tissue from adipogenic differentiation of ADSC (AT); Trypanosoma cruzi (T); Benznidazole (BZ). **(A)** CD4+ expression on lymphocytes; **(B)** CD8+ expression on lymphocytes; **(C)** CD28+ expression on CD4+ T lymphocytes; **(D)** CD28+ expression on CD8+ T lymphocytes; **(E)** CTLA-4+ expression in CD4+ T lymphocytes; **(F)** CTLA-4+ expression in CD8+ T lymphocytes. Horizontal bars represent the median and vertical bars the lower and upper limit. Symbols (*) above the bars indicate statistical difference with $p \leq 0.05$.

which may be associated with BAT or beige adipocytes. Although our differentiation kit does not define which type of AT will be differentiated, we believe that adipogenic inducers have a determining role in cell type specialization because, depending on the concentration of the compounds, the AT can differentiate into distinct subtypes (28).

BAT and beige adipocytes are associated with thermogenesis processes. However, they have different origins (29). Beige adipocytes derive from white adipocyte precursors and are found in scattered clusters within WAT (30). On the other hand, BAT occurs separately in deposits more associated with the cervical, axillary and interscapular regions (8). In agreement with our study, Rashnonejad et al. (31) have already found that ADSC and umbilical cord-derived stem cells present adipocytes with unilocular lipid droplets – when differentiated into WAT – and multilocular lipid droplets – when differentiated into BAT. Although this was not the aim of this study, phenotypic markers could assist in this classification of AT type.

In vitro treatment with BZ did not statistically alter the production of cytokines, chemokines and the quantification of *T.*

10.3389/fimmu.2024.1280877

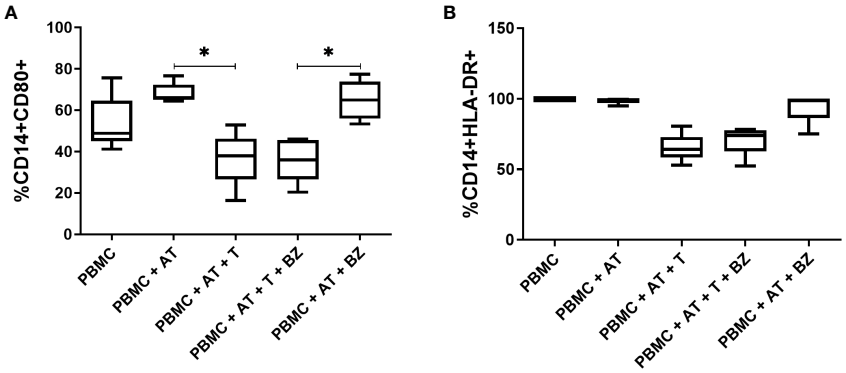

FIGURE 8
Evaluation of the expression of activation/inhibition molecules in CD14$^+$ cells from indirect culture between *Trypanosoma cruzi*-infected adipose tissue, peripheral blood mononuclear cells and benznidazole treatment. PBMC, Peripheral blood mononuclear cells (PBMC); AT, Adipose tissue from adipogenic differentiation of ADSC (AT); *Trypanosoma cruzi* (T); Benznidazole (BZ). **(A)** CD80+ expression on CD14+ monocytes; **(B)** HLA-DR+ expression on CD14+ monocytes Horizontal bars represent the median and vertical bars the lower and upper limit. Symbols (*) above the bars indicate statistical difference with $p \leq 0.05$.

cruzi DNA under the culture conditions in which the cells were infected in a significant way. Even so, *in vitro* studies using PBMC from chronic patients with Chagas disease or volunteers who were infected with *T. cruzi* were able to reduce the exacerbated inflammation generated by the infection through the administration of BZ (32, 33). In addition, our research group – also using an *in vitro* model – found that AT infected with *T. cruzi* and treated with BZ showed a reduction in parasite load and inflammation through a decrease in IL-6, when compared to the AT that was only infected (20). However, according to the results derived from our study, the use of AT as an escape from the immune response may be an alternative to the parasite infection since the efficiency of the drug may be reduced. Furthermore, interaction with PBMC significantly altered immune modulation and the effect of BZ on infected AT, strengthening the hypothesis that these cells can affect the immunometabolic balance even when acting indirectly.

Regarding immunomodulation, it could be concluded that the interaction between AT and PBMC promotes the production of the cytokine IL-2 when compared to the other groups. IL-2 plays a central role in regulating immune cells' proliferation, activation and homeostasis (34–36). This cytokine is mainly secreted into the circulation by activated CD4$^+$ and CD8$^+$ T cells and, to a lesser extent, by dendritic cells and macrophages (36). In the study by Kochumon et al. (37), it was observed that IL-2 expression was upregulated in obese subjects compared to lean subjects. Furthermore, this elevation of IL-2 is associated with insulin resistance and several inflammatory markers. Thus, the results of Kochumon et al. (37) corroborate our study since adipogenic differentiation promotes fat accumulation within cells, which leads to an inflammatory state.

Similarly, we found that, in culture conditions where AT is present, IL-6 production occurs regardless of *T. cruzi* infection. Our data corroborates the literature since IL-6 belongs to the group of adipokines. These bioactive factors are secreted by WAT but can also be produced by cells that infiltrate AT, such as macrophages (38). Yet, curiously enough, *T. cruzi* infection did not promote a significant increase in IL-6 compared to the PBMC+AT condition. In contrast, Moreira et al. (20) noticed that treatment with BZ in *T. cruzi*-infected AT led to a decrease in IL-6 compared to untreated AT. Nonetheless, in this case, there was no influence of PBMCs in the microenvironment.

In the study held by Gonzaléz et al. (39) investigating the cytokine profile, an increase in IL-6 and TNF was observed in chronic chagasic patients. However, compared to healthy individuals, these patients had metabolic imbalances such as high body mass index (BMI) and high blood glucose and insulin resistance. Moreover, Wueest and Konrad (40) have already highlighted that IL-6 signaling in adipocytes is involved in the development of insulin resistance associated with obesity and hepatic steatosis by inducing the release of free fatty acids and leptin from adipocytes, thus affecting hepatic metabolism and pancreatic β-cell function. Therefore, not only does the infection promote inflammatory microenvironment – fatty acid synthesis *in vitro* model – but also obesity and metabolic dysfunctions act on IL-6 elevation (41–44).

In opposition, TNF secretion remained at basal levels in the presence of AT. TNF, like IL-6, is also considered an adipokine since it is well-established that isolated adipocytes and those differentiated from other cell populations can produce TNF (45). In spite of that, adipose tissue also contains a stromal vascular fraction (SVF), possessing several metabolically relevant cell types. These include preadipocytes, endothelial cells, smooth muscle cells, fibroblasts, leukocytes and macrophages. More recent studies have even shown that SVF can produce substantially more TNF than adipocytes (46–49).

Combs et al. (10) previously observed that visceral AT from mice infected with the Brazil strain of *T. cruzi* showed elevated TNF, IFN-γ and IL-1 and reduced adiponectin and leptin. Elevation of the pro-inflammatory cytokines TNF, IFN-γ and IL-1β has also been demonstrated in adipocytes differentiated from the murine fibroblasts infected by *T. cruzi* (11). Yet, some factors may have contributed to the decreased TNF levels in our indirect culture. These include adipogenic inducers, most notably indomethacin, a

PPAR-γ associated with decreased TNF when administered to human monocytes (50). PPAR-γ is an essential regulator for adipogenesis and is highly necessary for maintaining the mature adipocyte phenotype (51). Even the decrease of PPAR-γ in mature adipocytes compromises their viability and fat storage because there is a loss of expression of key metabolic enzymes (52, 53). Several agents that promote the differentiation of fibroblast lineages into adipocytes are PPAR-γ agonists, including prostaglandins, oral antiglycemics and various non-steroidal anti-inflammatory drugs (50).

Additionally, in the study held by González et al. (54), it was shown that adipocytes and SVF collected from mice show decreased PPAR-γ in infected mice when compared to uninfected controls and that this decrease is correlated with TNF elevation. In studies with no *T. cruzi* infection, we can also verify a decrease in TNF in obese individuals after bariatric surgery correlated with the loss of fat and weight (55, 56).

In correspondence with our findings, Fain et al. (46) found that TNF production by human visceral and subcutaneous adipose tissue explants occurs between 4 and 48 hours of culture incubation, suggesting that TNF is a short-lived cytokine in primary culture. Also, more than 95% of the cytokine secretion was related to non-adipose cells. During another study from our group, we observed that *T. cruzi* infection in PBMC already induces TNF production within 24 hours after culture initiation and significantly decays between 5 and 10 days (32). Therefore, as our culture was performed 72 hours after BZ treatment, the peak of TNF production may have already decayed to basal levels.

Regarding IL-10, although cytokine production occurs, it does so similarly between culture conditions. Both myeloid and lymphoid cells can secrete IL-10 depending on the stimulus applied. These cells include macrophages, monocytes, dendritic cells, neutrophils, mast cells, eosinophils, natural killer cells, CD4+, CD8+ T cells, and B cells (57). In addition, some non-hematopoietic cells, including epithelial cells, are also capable of producing IL-10 (58). So, we believe IL-10 secretion among culture conditions is associated with cultured PBMC.

On another note, *T. cruzi* infection promotes a decrease in the chemokines IP-10/CXCL10 and MIG/CXCL9 in the supernatant content of the culture. The chemokine IP-10/CXCL10 is activated by binding to the CXCR3 receptor, typically expressed on T, B, natural killer (NK) cells, dendritic cells and macrophages. Abnormal levels of IP-10/CXCL10 have been identified in the body fluids of individuals infected with viruses, bacteria, fungi and parasites (59–62). Similarly, MIG/CXCL9 binds to the CXCR3 receptor (63).

In the study done by Kiran et al. (64), $CD8^+$ T cells and AT from the epididymis of mice subjected to a high-fat diet showed elevation of IP-10/CXCL-10 and MCP-1/CCL2. Moreover, there is an increased expression of CXCR3 receptors on CD8+ T cells in contact with AT. However, AT also expresses CXCR3 receptors and modulates obesity-induced inflammation (65). For that reason, we suggest that in addition to the high expression of receptors caused by contact between AT and PBMC the infection enhances this increase, which may escalate the consumption of these chemokines in this microenvironment.

The chemokine MCP-1/CCL2 was widely secreted in all culture conditions, but the PBMC+AT interaction obtained the highest amount. The primary sources of MCP-1 are epithelial cells, endothelial cells, smooth muscle cells, monocytes/macrophages, fibroblasts, astrocytes and microglial cells regulated by several other cytokines and factors (66). Still, MCP-1 is associated with several metabolic issues, such as insulin resistance and obesity (67–70). In accordance with our study, Cabalén et al. (71) found that *T. cruzi*-infected mice fed an obesity-inducing diet showed elevated MCP-1/CCL2 levels. Additionally, it has already been reported that saturated fatty acids can induce the secretion of MCP-1/CCL2 and other inflammatory adipokines in murine 3T3-L1 adipocytes (72). Therefore, as AT and PBMC secrete MCP-1/CCL2, we believe that the decreased levels of this chemokine in culture conditions in which the parasite is present are attributed to the metabolism of *T. cruzi* itself, which, when multiplying and infecting new cells, promotes a reduction in lipid content and thus reduces the production of the chemokine.

Similar to what was observed with TNF, the chemokine IL-8/CXCL8 had the same behavior in the presence of TA. IL-8/CXCL8 is a chemokine produced by nucleated cells, mainly macrophages, which are actively involved in inflammation by promoting the recruitment of monocytes and neutrophils (73). Furthermore, macrophage-derived foam cells and adipocytes have been found to express and secrete this chemokine extensively (70).

In this regard, Ballesteros et al. (74) found that AT-derived stem cells supplemented with platelet lysate showed increased IL-8 and decreased CXCR2 receptor expression. Also, the authors point out that any changes in the expression of chemokine receptors may also result from factors secreted during the culture of AT-derived stem cells. However, increased CXCR2 expression on monocytes/macrophages has already been associated with atherosclerosis and found on PBMC and within atherosclerotic plaques in humans and murine (75–77).

The interaction of adipocytes and macrophages modulates the maintenance of metabolic and immune homeostasis (78). When cultured with RAW264.7 macrophages in a Transwell system, bone marrow mesenchymal stem cells can induce macrophages to polarize to M2 phenotype and secrete anti-inflammatory and immunomodulatory cytokines (79). Macrophages residing in lean AT tissues exhibit characteristics of anti-inflammatory M2-like macrophages and have a positive role in maintaining AT homeostasis, preventing obesity-induced inflammation and thus promoting insulin sensitivity. In contrast, infiltrated macrophages, mainly M1-like macrophages, are more commonly associated with AT inflammation and insulin resistance (80). Consequently, we suggest that the interaction of AT+PBMC may promote increased expression of CXCR1/CXCR2 receptors or modulation of macrophage phenotype that contribute to the decay of the chemokine IL8/CXCL8 and other cytokines, such as TNF, which should be investigated in the future.

There was high secretion of these molecules in all culture conditions studied regarding adipokines. Yet, for adipsin, an interesting phenomenon occurred: the treatment with BZ promoted a decrease in the secretion of this adipokine in the infected AT. Adipsin, also known as complement factor D, is a

serine protease secreted by adipocytes associated with forming C3 convertase by the complement system, but it also involves triacylglycerol synthesis in human adipocytes (81). Studies have emphasized that high levels of adipsin are associated with overweight/obese individuals and related to an increased cardiovascular risk in women with polycystic ovary syndrome (82, 83). In another study by Prugger et al. (84), higher plasma levels of adipsin were associated with an increased 10-year risk of ischemic stroke in a cohort of healthy middle-aged men. Although data regarding parasites and adipsin is still scarce, our findings comply with the literature since this adipokine was associated with inflammatory conditions. Also, BZ exerted a beneficial effect by reducing adipsin in infected AT.

Other adipokines, such as leptin and adiponectin, are intrinsically related to host metabolism. Leptin is mainly produced by the AT, associated with the amount of body fat stored. It is also involved in regulating food intake, neuroendocrine function, reproduction, angiogenesis and blood pressure (85). Circulating leptin levels correlate mainly with total body fat and are thus increased in obese individuals (86). Through *in vitro* experiments, the effects of leptin are associated with decreased lipogenesis, increased triglyceride hydrolysis and fatty acid oxidation (87).

Adiponectin is also secreted almost exclusively by the AT. It has cardioprotective functions, protecting against insulin resistance and excessive hepatic lipid accumulation and exerts anti-inflammatory effects (88). Circulating levels of this adipokine in obese patients are also decreased (89). Through *in vitro* experiments, adiponectin overexpression in 3T3-L1 cells increases lipid storage and adipogenesis (90).

González et al. (54) found that leptin and adiponectin expression decrease upon *T. cruzi* infection in 3T3-L1 adipocytes and AT of mice compared to uninfected mice. However, Lizardo et al. (91) observed the presence of disintegrated adipocytes with multilocular lipid droplets and infiltrated immune cells in AT 90 days post-infection. Even so, fat loss increased adiponectin and PPARγ levels, indicating that apoptotic cell death of adipocytes induces pro-adipogenic signaling (91). Therefore, leptin/adiponectin levels may vary according to the type of infection/phase of Chagas disease and metabolic imbalance (92). Given these findings, we believe that in our study, PBMC modulated adipokine secretion in infected AT.

Regarding cell activation and inhibition molecules, we noticed that the presence of AT promoted an increase in the frequency of $CD4^+$ T cells. Still, the same was not observed when the frequency of activated $CD4^+$ T lymphocytes was measured. In humans, $CD4^+$ T lymphocytes represent the main population of lymphocytes in adipose tissue. In general, $CD4^+$ T cells depending on cytokine stimulation may develop other activation states (93, 94).

On the other hand, in $CD8^+$ T lymphocytes, there was a decrease in the frequency of these cells in the presence of AT. Nevertheless, a higher frequency of activated CD8+ T cells in the presence of AT or *T. cruzi* infection was also verified. Similar to our findings, in the study by Nishimura et al. (95), a higher frequency of effector CD8+ T cells infiltrating the epididymal adipose tissue of mice ingesting a high-fat diet (HFD) was observed compared to the frequency of effector $CD4^+$ T cells. Furthermore, the study suggests that obese AT activates $CD8^+$ T cells, promoting macrophage recruitment and activation in this tissue.

In another study, by culturing $CD8^+$ T cells and adipocytes from epididymal tissue of mice subjected to HFD, it was found that monocyte-to-macrophage differentiation and phenotypic polarization was mediated by HFD-induced $CD8^+$ T cell interaction with adipocytes (64). These findings were confirmed because both $CD8^+$ T cells and adipocytes that did not undergo HFD when cultured alone did not induce sufficient macrophage amount for differentiation, which strengthens the hypothesis of the relationship between $CD8^+$ T cells, adipocytes and inflammation (64).

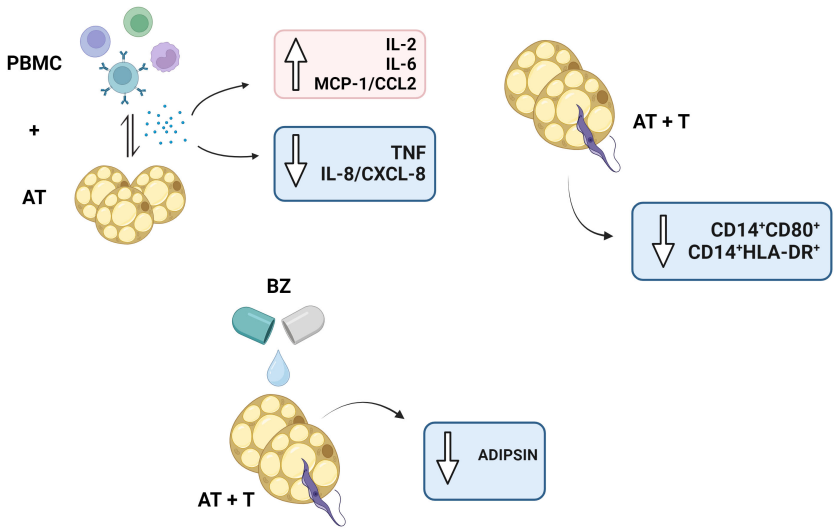

FIGURE 9
Schematic representation of the study's main findings. PBMC, Peripheral blood mononuclear cells (PBMC); AT, Adipose tissue from adipogenic differentiation of ADSC (AT); *Trypanosoma cruzi* (T); Benznidazole (BZ). Design created with the aid of Biorender®.

Interestingly, in $CD14^+$ cells, we found a decreased frequency of $CD80^+$ in *T. cruzi*-infected cell culture conditions. However, in PBMC infected by *T. cruzi*, an increase in the frequency of this molecule has already been observed in culture conditions infected by the parasite (32). Accordingly, this decrease may function as a defense mechanism for *T. cruzi* to remain in the AT and escape the host immune response.

In conclusion, our data indicates that BZ failed to promote and induce important immunomodulatory mechanisms in the infected AT, which is beneficial for *T. cruzi* and may use the AT as an ally in escaping the host immune response. Moreover, the interaction between PBMC and AT promotes mechanisms that may affect AT immunometabolism (Figure 9). Besides, as this is an *in vitro* study, a drug that has not undergone enzymatic metabolization to its active form or the long-term cultivation of infected AT should be considered. As a result, studies *in vivo* models may provide more evidence of how the parasite can use AT as a defense. Withal, our indirect *in vitro* culture model may be interesting for drug studies that evaluate the efficiency of drugs in this microenvironment.

Data availability statement

The raw data supporting the conclusions of this article will be made available by the authors, without undue reservation.

Ethics statement

The studies involving humans were approved by Research Ethics Committee - IAM/Fiocruz (C.A.A.E 97930918.3.0000.5190). The studies were conducted in accordance with the local legislation and institutional requirements. The participants provided their written informed consent to participate in this study.

Author contributions

LM: Conceptualization, Data curation, Formal analysis, Investigation, Methodology, Software, Visualization, Writing – original draft, Writing – review & editing. AS: Formal analysis, Investigation, Methodology, Visualization, Writing – review & editing. CC: Methodology, Writing – review & editing. CS: Methodology, Writing – review & editing. KO: Methodology, Writing – review & editing. DT: Methodology, Writing – review & editing. MB: Methodology, Writing – review & editing. MR: Formal analysis, Funding acquisition, Resources, Writing – review & editing. VL: Conceptualization, Formal analysis, Funding acquisition, Project administration, Resources, Supervision, Validation, Writing – review & editing.

Funding

The author(s) declare financial support was received for the research, authorship, and/or publication of this article. This study had the support and financial backing of the National Council for Scientific and Technological Development (CNPq) (Grant number 427039/2018-5-Universal).

Conflict of interest

The authors declare that the research was conducted in the absence of any commercial or financial relationships that could be construed as a potential conflict of interest.

Publisher's note

Supplementary material

The Supplementary Material for this article can be found online at: https://www.frontiersin.org/articles/10.3389/fimmu.2024.1280877/full#supplementary-material

SUPPLEMENTARY FIGURE 1
Acquisition strategy of adipokines dosage in the culture supernatant of the indirect culture between adipose tissue infected by *Trypanosoma cruzi*, peripheral blood mononuclear cells and benznidazole treatment.

References

1. Echeverria LE, Morillo CA. American trypanosomiasis (Chagas disease). *Infect Dis Clin North Am*. (2019) 33:119–34. doi: 10.1016/j.idc.2018.10.015

2. World Health Organization. World Chagas Disease Day 2022 - Finding and reporting every case to defeat Chagas disease (2022). Available online at: https://www.who.int/news-room/events/detail/2022/04/14/default-calendar/world-chagas-disease-day-2022—finding-and-reporting-every-case-to-defeat-chagas-disease (Accessed November 18, 2023).

3. Hochberg NS, Montgomery SP. Chagas disease. *Ann Intern Med*. (2023) 176: ITC17–32. doi: 10.7326/AITC202302210

4. Cristovão-Silva AC, Brelaz-de-Castro MCA, Hernandes MZ, Pereira VRA. Chagas disease: Immunology of the disease at a glance. *Cytokine Growth Factor Rev*. (2021) 62:15–22. doi: 10.1016/j.cytogfr.2021.10.001

5. Acevedo GR, Girard MC, Gómez KA. The unsolved jigsaw puzzle of the immune response in chagas disease. *Front Immunol*. (2018) 9:1929. doi: 10.3389/fimmu.2018.01929

6. Ferri G, Edreira MM. All roads lead to cytosol: *trypanosoma cruzi* multi-strategic approach to invasion. *Front Cell Infect Microbiol*. (2021) 11:634793. doi: 10.3389/fcimb.2021.634793

7. Tanowitz HB, Scherer PE, Mota MM, Figueiredo LM. Adipose tissue: A safe haven for parasites? *Trends Parasitol*. (2017) 33:276–84. doi: 10.1016/j.pt.2016.11.008

8. Frigolet ME, Gutiérrez-Aguilar R. The colors of adipose tissue. Los colores del tejido adiposo. *Gac Med Mex*. (2020) 156:142–9. doi: 10.24875/GMM.M20000356

9. Kumari M, Heeren J, Scheja L. Regulation of immunometabolism in adipose tissue. *Semin Immunopathol*. (2018) 40:189–202. doi: 10.1007/s00281-017-0668-3

10. Combs TP, Nagajyothi, Mukherjee S, de Almeida CJ, Jelicks LA, Schubert W, et al. The adipocyte as an important target cell for Trypanosoma cruzi infection. *J Biol Chem*. (2005) 280:24085–94. doi: 10.1074/jbc.M412802200

11. Nagajyothi F, Desruisseaux MS, Thiruvur N, Weiss LM, Braunstein VL, Albanese C, et al. Trypanosoma cruzi infection of cultured adipocytes results in an inflammatory phenotype. *Obes (Silver Spring)*. (2008) 16:1992–7. doi: 10.1038/oby.2008.331

12. Mello DB, Ramos IP, Mesquita FC, Brasil GV, Rocha NN, Takiya CM, et al. Adipose Tissue-Derived Mesenchymal Stromal Cells Protect Mice Infected with Trypanosoma cruzi from Cardiac Damage through Modulation of Anti-parasite Immunity. *PloS Negl Trop Dis*. (2015) 9:e0003945. doi: 10.1371/journal.pntd.0003945

13. Ferreira AV, Segatto M, Menezes Z, Macedo AM, Gelape C, de Oliveira Andrade L, et al. Evidence for Trypanosoma cruzi in adipose tissue in human chronic Chagas disease. *Microbes Infect*. (2011) 13:1002–5. doi: 10.1016/j.micinf.2011.06.002

14. Pérez-Molina JA, Crespillo-Andújar C, Bosch-Nicolau P, Molina I. Trypanocidal treatment of Chagas disease. *Enferm Infecc Microbiol Clin (Engl Ed)* 9:S0213-005X(20) 30193-2. doi: 10.1016/j.eimc.2020.04.011

15. Kratz JM, Garcia Bournissen F, Forsyth CJ, Sosa-Estani S. Clinical and pharmacological profile of benznidazole for treatment of Chagas disease. *Expert Rev Clin Pharmacol*. (2018) 11:943–57. doi: 10.1080/17512433.2018.1509704

16. Losada Galván I, Alonso-Padilla J, Cortés-Serra N, Alonso-Vega C, Gascón J, Pinazo MJ. Benznidazole for the treatment of Chagas disease. *Expert Rev Anti Infect Ther*. (2021) 19:547–56. doi: 10.1080/14787210.2021.1834849

17. Urbina JA. Specific chemotherapy of Chagas disease: relevance, current limitations and new approaches. *Acta Trop*. (2010) 115:55–68. doi: 10.1016/j.actatropica.2009.10.023

18. Revollo S, Oury B, Vela A, Tibayrenc M, Sereno D. *In vitro* benznidazole and nifurtimox susceptibility profile of trypanosoma cruzi strains belonging to discrete typing units tcI, tcII, and tcV. *Pathogens*. (2019) 8:197. doi: 10.3390/pathogens8040197

19. Romanha AJ, Castro SL, Soeiro Mde N, Lannes-Vieira J, Ribeiro I, Talvani A, et al. *In vitro* and in *vivo* experimental models for drug screening and development for Chagas disease. *Mem Inst Oswaldo Cruz*. (2010) 105:233–8. doi: 10.1590/s0074-02762010000200022

20. Moreira LR, Silva AC, Costa Oliveira CND, Silva Júnior CDD, Nascimento AV, Oliveira KKDS, et al. Benznidazole treatment decreases IL-6 levels in *Trypanosoma cruzi*-infected human adipocytes differentiated from adipose tissue-derived stem cells. *Mem Inst Oswaldo Cruz*. (2023) 118:e220295. doi: 10.1590/0074-02760220295

21. Costa-Oliveira CND, Paiva-Cavalcanti M, Barros MDS, Nakazawa M, Melo MGN, Pessoa-E-Silva R, et al. Outbreak of Chagas disease in Brazil: Validation of a molecular diagnostic method. *Exp Parasitol*. (2023) 247:108478. doi: 10.1016/j.exppara.2023.108478

22. Zwick RK, Guerrero-Juarez CF, Horsley V, Plikus MV. Anatomical, physiological, and functional diversity of adipose tissue. *Cell Metab*. (2018) 27:68–83. doi: 10.1016/j.cmet.2017.12.002

23. Vadde R, Gupta MK, Nagaraju GP. Is adipose tissue an immunological organ? *Crit Rev Immunol*. (2019) 39:481–90. doi: 10.1615/CritRevImmunol.2020033457

24. Schwing A, Pisani DF, Pomares C, Majoor A, Lacas-Gervais S, Jager J, et al. Identification of adipocytes as target cells for *Leishmania infantum* parasites. *Sci Rep*. (2021) 11:21275. doi: 10.1038/s41598-021-00443-y

25. Barthelemy J, Bogard G, Wolowczuk I. Beyond energy balance regulation: The underestimated role of adipose tissues in host defense against pathogens. *Front Immunol*. (2023) 14:1083191. doi: 10.3389/fimmu.2023.1083191

26. Cleal L, Aldea T, Chau YY. Fifty shades of white: Understanding heterogeneity in white adipose stem cells. *Adipocyte*. (2017) 6:205–16. doi: 10.1080/21623945.2017.1372871

27. Rochette L, Mazini L, Malka G, Zeller M, Cottin Y, Vergely C. The crosstalk of adipose-derived stem cells (ADSC), oxidative stress, and inflammation in protective and adaptive responses. *Int J Mol Sci*. (2020) 21:9262. doi: 10.3390/ijms21239262

28. Kolodziej M, Strauss S, Lazaridis A, Bucan V, Kuhbier JW, Vogt PM, et al. Influence of glucose and insulin in human adipogenic differentiation models with adipose-derived stem cells. *Adipocyte*. (2019) 8:254–64. doi: 10.1080/21623945.2019.1636626

29. Chu DT, Gawronska-Kozak B. Brown and brite adipocytes: Same function, but different origin and response. *Biochimie*. (2017) 138:102–5. doi: 10.1016/j.biochi.2017.04.017

30. Kaisanlahti A, Glumoff T. Browning of white fat: agents and implications for beige adipose tissue to type 2 diabetes. *J Physiol Biochem*. (2019) 75:1–10. doi: 10.1007/s13105-018-0658-5

31. Rashnonejad A, Ercan G, Gunduz C, Akdemir A, Tiftikcioglu YO. Comparative analysis of human UCB and adipose tissue derived mesenchymal stem cells for their differentiation potential into brown and white adipocytes. *Mol Biol Rep*. (2018) 45:233–44. doi: 10.1007/s11033-018-4156-1

32. Rafael Moreira L, Dos Santos Oliveira KK, Torres DJL, da Silva Barros M, de Arruda TR, Nascimento AV, et al. Benzonidazole treatment has a beneficial effect on cells infected with the Colombian strain of Trypanosoma cruzi. *Parasite Immunol*. (2023) 45:e12983. doi: 10.1111/pim.12983

33. Soares AKA, Neves PAF, Nascimento AV, et al. Benznidazole: Hero or villain of cellular immune response in chronic Chagas disease patients? *Immunobiology*. (2021) 226:152046. doi: 10.1016/j.imbio.2020.152046

34. Abbas AK, Trotta E R, Simeonov D, Marson A, Bluestone JA. Revisiting IL-2: Biology and therapeutic prospects. *Sci Immunol*. (2018) 3(25):eaat1482. doi: 10.1126/sciimmunol.aat1482

35. Gaffen SL, Liu KD. Overview of interleukin-2 function, production and clinical applications. *Cytokine*. (2004) 28:109–23. doi: 10.1016/j.cyto.2004.06.010

36. Kalia V, Sarkar S. Regulation of effector and memory CD8 T cell differentiation by IL-2-A balancing act. *Front Immunol*. (2018) 9:2987. doi: 10.3389/fimmu.2018.02987

37. Kochumon S, Al Madhoun A, Al-Rashed F, Thomas R, Sindhu S, Al-Ozairi E, et al. Elevated adipose tissue associated IL-2 expression in obesity correlates with metabolic inflammation and insulin resistance. *Sci Rep*. (2020) 10:16364. doi: 10.1038/s41598-020-73347-y

38. Conde J, Scotece M, Gómez R, López V, Gómez-Reino JJ, Lago F, et al. Adipokines: biofactors from white adipose tissue. *A Complex hub among inflammation metabolism immunity. Biofactors*. (2011) 37:413–20. doi: 10.1002/biof.185

39. González F, Villar S, D'Attilio L, Leiva R, Marquez J, Lioi S, et al. Dysregulated network of immune, endocrine and metabolic markers is associated to more severe human chronic chagas cardiomyopathy. *Neuroimmunomodulation*. (2018) 25:119–28. doi: 10.1159/000491699

40. Wueest S, Konrad D. The role of adipocyte-specific IL-6-type cytokine signaling in FFA and leptin release. *Adipocyte*. (2018) 7:226–8. doi: 10.1080/21623945.2018.1493901

41. Cartier A, Lemieux I, Alméras N, Tremblay A, Bergeron J, Després JP. Visceral obesity and plasma glucose-insulin homeostasis: contributions of interleukin-6 and tumor necrosis factor-alpha in men. *J Clin Endocrinol Metab*. (2008) 93:1931–8. doi: 10.1210/jc.2007-2191

42. Madani R, Karastergiou K, Ogston NC, Miheisi N, Bhome R, Haloob N, et al. RANTES release by human adipose tissue in *vivo* and evidence for depot-specific differences. *Am J Physiol Endocrinol Metab*. (2009) 296:E1262–8. doi: 10.1152/ajpendo.90511.2008

43. Pou KM, Massaro JM, Hoffmann U, Vasan RS, Maurovich-Horvat P, Larson MG, et al. Visceral and subcutaneous adipose tissue volumes are cross-sectionally related to markers of inflammation and oxidative stress: the Framingham Heart Study. *Circulation*. (2007) 116:1234–41. doi: 10.1161/CIRCULATIONAHA.107.710509

44. Ziccardi P, Nappo F, Giugliano G, Esposito K, Marfella R, Cioffi M, et al. Reduction of inflammatory cytokine concentrations and improvement of endothelial functions in obese women after weight loss over one year. *Circulation*. (2002) 105:804–9. doi: 10.1161/hc0702.104279

45. Cawthorn WP, Sethi JK. TNF-alpha and adipocyte biology. *FEBS Lett*. (2008) 582:117–31. doi: 10.1016/j.febslet.2007.11.051

46. Fain JN, Bahouth SW, Madan AK. TNFalpha release by the nonfat cells of human adipose tissue. *Int J Obes Relat Metab Disord*. (2004) 28:616–22. doi: 10.1038/sj.ijo.0802594

47. Fain JN. Release of inflammatory mediators by human adipose tissue is enhanced in obesity and primarily by the nonfat cells: a review. *Mediators Inflamm*. (2010) 2010:513948. doi: 10.1155/2010/513948

48. Ross SE, Erickson RL, Gerin I, DeRose PM, Bajnok L, Longo KA, et al. Microarray analyses during adipogenesis: understanding the effects of Wnt signaling on adipogenesis and the roles of liver X receptor alpha in adipocyte metabolism. *Mol Cell Biol*. (2002) 22:5989–99. doi: 10.1128/MCB.22.16.5989-5999.2002

49. Weisberg SP, McCann D, Desai M, Rosenbaum M, Leibel RL, Ferrante AW Jr. Obesity is associated with macrophage accumulation in adipose tissue. *J Clin Invest*. (2003) 112:1796–808. doi: 10.1172/JCI19246

50. Jiang C, Ting AT, Seed B. PPAR-gamma agonists inhibit production of monocyte inflammatory cytokines. *Nature*. (1998) 391:82–6. doi: 10.1038/34184

51. Tontonoz P, Spiegelman BM. Fat and beyond: the diverse biology of PPARgamma. *Annu Rev Biochem*. (2008) 77:289–312. doi: 10.1146/annurev.biochem.77.061307.091829

52. Imai T, Takakuwa R, Marchand S, Dentz E, Bornert JM, Messaddeq N, et al. Peroxisome proliferator-activated receptor gamma is required in mature white and brown adipocytes for their survival in the mouse. *Proc Natl Acad Sci U S A*. (2004) 101:4543–7. doi: 10.1073/pnas.0400356101

53. Tamori Y, Masugi J, Nishino N, Kasuga M. Role of peroxisome proliferator-activated receptor-gamma in maintenance of the characteristics of mature 3T3-L1 adipocytes. *Diabetes*. (2002) 51:2045–55. doi: 10.2337/diabetes.51.7.2045

54. González FB, Villar SR, Toneatto J, Pacini MF, Márquez J, D'Attilio L, et al. Immune response triggered by Trypanosoma cruzi infection strikes adipose tissue homeostasis altering lipid storage, enzyme profile and adipokine expression. *Med Microbiol Immunol*. (2019) 208:651–66. doi: 10.1007/s00430-018-0572-z

55. Eslick S, Williams EJ, Berthon BS, Wright T, Karihaloo C, Gately M, et al. Weight loss and short-chain fatty acids reduce systemic inflammation in monocytes and adipose tissue macrophages from obese subjects. *Nutrients*. (2022) 14:765. doi: 10.3390/nu14040765

56. Moschen AR, Molnar C, Geiger S, Graziadei I, Ebenbichler CF, Weiss H, et al. Anti-inflammatory effects of excessive weight loss: potent suppression of adipose interleukin 6 and tumour necrosis factor alpha expression. *Gut*. (2010) 59:1259–64. doi: 10.1136/gut.2010.214577

57. Saraiva M, Vieira P, O'Garra A. Biology and therapeutic potential of interleukin-10. *J Exp Med*. (2020) 217:e20190418. doi: 10.1084/jem.20190418

58. Jarry A, Bossard C, Bou-Hanna C, Masson D, Espaze E, Denis MG, et al. Mucosal IL-10 and TGF-beta play crucial roles in preventing LPS-driven, IFN-gamma-mediated epithelial damage in human colon explants. *J Clin Invest*. (2008) 118:1132–42. doi: 10.1172/JCI32140

59. Azzurri A, Sow OY, Amedei A, Bah B, Diallo S, Peri G, et al. IFN-gamma-inducible protein 10 and pentraxin 3 plasma levels are tools for monitoring inflammation and disease activity in Mycobacterium tuberculosis infection. *Microbes Infect*. (2005) 7:1–8. doi: 10.1016/j.micinf.2004.09.004

60. Dyer KD, Percopo CM, Fischer ER, Gabryszewski SJ, Rosenberg HF. Pneumoviruses infect eosinophils and elicit MyD88-dependent release of chemoattractant cytokines and interleukin-6. *Blood*. (2009) 114:2649–56. doi: 10.1182/blood-2009-01-199497

61. Shiraki Y, Ishibashi Y, Hiruma M, Nishikawa A, Ikeda S. Candida albicans abrogates the expression of interferon-gamma-inducible protein-10 in human keratinocytes. *FEMS Immunol Med Microbiol*. (2008) 54:122–8. doi: 10.1111/fim.2008.54.issue-1

62. Wilson NO, Huang MB, Anderson W, Bond V, Powell M, Thompson WE, et al. Soluble factors from Plasmodium falciparum-infected erythrocytes induce apoptosis in human brain vascular endothelial and neuroglia cells. *Mol Biochem Parasitol*. (2008) 162:172–6. doi: 10.1016/j.molbiopara.2008.09.003

63. Rosenblum JM, Shimoda N, Schenk AD, Zhang H, Kish DD, Keslar K, et al. CXC chemokine ligand (CXCL) 9 and CXCL10 are antagonistic costimulation molecules during the priming of alloreactive T cell effectors. *J Immunol*. (2010) 184:3450–60. doi: 10.4049/jimmunol.0903831

64. Kiran S, Kumar V, Murphy EA, Enos RT, Singh UP. High fat diet-induced $CD8^+$ T cells in adipose tissue mediate macrophages to sustain low-grade chronic inflammation. *Front Immunol*. (2021) 12:680944. doi: 10.3389/fimmu.2021.680944

65. Deiuliis JA, Oghumu S, Duggineni D, Zhong J, Rutsky J, Banerjee A, et al. CXCR3 modulates obesity-induced visceral adipose inflammation and systemic insulin resistance. *Obes (Silver Spring)*. (2014) 22:1264–74. doi: 10.1002/oby.20642

66. Singh S, Anshita D, Ravichandiran V. MCP-1: Function, regulation, and involvement in disease. *Int Immunopharmacol*. (2021) 101:107598. doi: 10.1016/j.intimp.2021.107598

67. Kanda H, Tateya S, Tamori Y, Kotani K, Hiasa K, Kitazawa R, et al. MCP-1 contributes to macrophage infiltration into adipose tissue, insulin resistance, and hepatic steatosis in obesity. *J Clin Invest*. (2006) 116:1494–505. doi: 10.1172/JCI26498

68. Malavazos AE, Cereda E, Morricone L, Coman C, Corsi MM, Ambrosi B. Monocyte chemoattractant protein 1: a possible link between visceral adipose tissue-associated inflammation and subclinical echocardiographic abnormalities in uncomplicated obesity. *Eur J Endocrinol*. (2005) 153:871–7. doi: 10.1530/eje.1.02033

69. Weisberg SP, Hunter D, Huber R, Lemieux J, Slaymaker S, Vaddi K, et al. CCR2 modulates inflammatory and metabolic effects of high-fat feeding [published correction appears in J Clin Invest. *2006 May;116(5):1457]. J Clin Invest*. (2006) 116:115–24. doi: 10.1172/JCI24335

70. Xue W, Fan Z, Li L, Lu J, Zhai Y, Zhao J. The chemokine system and its role in obesity. *J Cell Physiol*. (2019) 234:3336–46. doi: 10.1002/jcp.27293

71. Cabalén ME, Cabral MF, Sanmarco LM, Andrada MC, Onofrio LI, Ponce NE, et al. Chronic Trypanosoma cruzi infection potentiates adipose tissue macrophage polarization toward an anti-inflammatory M2 phenotype and contributes to diabetes progression in a diet-induced obesity model. *Oncotarget*. (2016) 7:13400–15. doi: 10.18632/oncotarget.7630

72. Schaeffler A, Gross P, Buettner R, Bollheimer C, Buechler C, Neumeier M, et al. Fatty acid-induced induction of Toll-like receptor-4/nuclear factor-kappaB pathway in adipocytes links nutritional signalling with innate immunity. *Immunology*. (2009) 126:233–45. doi: 10.1111/j.1365-2567.2008.02892.x

73. Apostolakis S, Vogiatzi K, Amanatidou V, Spandidos DA. Interleukin 8 and cardiovascular disease. *Cardiovasc Res*. (2009) 84:353–60. doi: 10.1093/cvr/cvp241

74. Ballesteros OR, Brooks PT, Haastrup EK, Fischer-Nielsen A, Munthe-Fog L, Svalgaard JD. Adipose-derived stromal/stem cell culture: effects of different concentrations of human platelet lysate in media. *Cells Tissues Organs*. (2020) 209:257–65. doi: 10.1159/000513604

75. Breland UM, Halvorsen B, Hol J, Øie E, Paulsson-Berne G, Yndestad A, et al. A potential role of the CXC chemokine GROalpha in atherosclerosis and plaque destabilization: downregulatory effects of statins. *Arterioscler Thromb Vasc Biol*. (2008) 28:1005–11. doi: 10.1161/ATVBAHA.108.162305

76. Satterthwaite G, Francis SE, Suvarna K, Blakemore S, Ward C, Wallace D, et al. Differential gene expression in coronary arteries from patients presenting with ischemic heart disease: further evidence for the inflammatory basis of atherosclerosis. *Am Heart J*. (2005) 150:488–99. doi: 10.1016/j.ahj.2004.10.025

77. Soehnlein O, Drechsler M, Doring Y, Lievens D, Hartwig H, Kemmerich K, et al. Distinct functions of chemokine receptor axes in the atherogenic mobilization and recruitment of classical monocytes. *EMBO Mol Med*. (2013) 5:471–81. doi: 10.1002/emmm.201201717

78. Cao D, Ma F, Ouyang S, Liu Z, Li Y, Wu J. Effects of macrophages and CXCR2 on adipogenic differentiation of bone marrow mesenchymal stem cells. *J Cell Physiol*. (2019) 234:9475–85. doi: 10.1002/jcp.27634

79. Yin Y, Wu RX, He XT, Xu XY, Wang J, Chen FM. Influences of age-related changes in mesenchymal stem cells on macrophages during *in-vitro* culture. *Stem Cell Res Ther*. (2017) 8:153. doi: 10.1186/s13287-017-0608-0

80. Castoldi A, Naffah de Souza C, Câmara NO, Moraes-Vieira PM. The macrophage switch in obesity development. *Front Immunol*. (2016) 6:637. doi: 10.3389/fimmu.2015.00637

81. Song NJ, Kim S, Jang BH, Chang SH, Yun UJ, Park KM, et al. Small molecule-induced complement factor D (Adipsin) promotes lipid accumulation and adipocyte differentiation. *PloS One*. (2016) 11:e0162228. doi: 10.1371/journal.pone.0162228

82. Derosa G, Fogari E, D'Angelo A, Bianchi L, Bonaventura A, Romano D, et al. Adipocytokine levels in obese and non-obese subjects: an observational study. *Inflammation*. (2013) 36:914–20. doi: 10.1007/s10753-013-9620-4

83. Gursoy Calan O, Calan M, Yesil Senses P, Unal Kocabas G, Ozden E, Sari KR, et al. Increased adipsin is associated with carotid intima media thickness and metabolic disturbances in polycystic ovary syndrome. *Clin Endocrinol (Oxf)*. (2016) 85:910–7. doi: 10.1111/cen.13157

84. Prugger C, Luc G, Haas B, Arveiler D, Machez E, Ferrieres J, et al. Adipocytokines and the risk of ischemic stroke: the PRIME Study. *Ann Neurol*. (2012) 71:478–86. doi: 10.1002/ana.22669

85. Blüher M, Mantzoros CS. From leptin to other adipokines in health and disease: facts and expectations at the beginning of the 21st century. *Metabolism*. (2015) 64:131–45. doi: 10.1016/j.metabol.2014.10.016

86. Gómez-Ambrosi J, Salvador J, Silva C, Pastor C, Rotellar F, Gil MJ, et al. Increased cardiovascular risk markers in obesity are associated with body adiposity: role of leptin. *Thromb Haemost*. (2006) 95:991–6. doi: 10.1160/TH06-02-0079

87. William WN Jr, Ceddia RB, Curi R. Leptin controls the fate of fatty acids in isolated rat white adipocytes. *J Endocrinol*. (2002) 175:735–44. doi: 10.1677/joe.0.1750735

88. Stern JH, Rutkowski JM, Scherer PE. Adiponectin, leptin, and fatty acids in the maintenance of metabolic homeostasis through adipose tissue crosstalk. *Cell Metab*. (2016) 23:770–84. doi: 10.1016/j.cmet.2016.04.011

89. Kadowaki T, Yamauchi T, Kubota N, Hara K, Ueki K, Tobe K. Adiponectin and adiponectin receptors in insulin resistance, diabetes, and the metabolic syndrome. *J Clin Invest*. (2006) 116:1784–92. doi: 10.1172/JCI29126

90. Fu Y, Luo N, Klein RL, Garvey WT. Adiponectin promotes adipocyte differentiation, insulin sensitivity, and lipid accumulation. *J Lipid Res*. (2005) 46:1369–79. doi: 10.1194/jlr.M400373-JLR200

91. Lizardo K, Ayyappan JP, Oswal N, Weiss LM, Scherer PE, Nagajyothi JF. Fat tissue regulates the pathogenesis and severity of cardiomyopathy in murine chagas disease. *PloS Negl Trop Dis*. (2021) 15:e0008964. doi: 10.1371/journal.pntd.0008964

92. Fernandes F, Dantas S, Ianni BM, Ramires FJ, Buck P, Salemi VM, et al. Leptin levels in different forms of Chagas' disease. *Braz J Med Biol Res*. (2007) 40:1631–6. doi: 10.1590/s0100-879x2006005000152

93. Kintscher U, Hartge M, Hess K, Foryst-Ludwig A, Clemenz M, Wabitsch M, et al. T-lymphocyte infiltration in visceral adipose tissue: a primary event in adipose tissue inflammation and the development of obesity-mediated insulin resistance. *Arterioscler Thromb Vasc Biol*. (2008) 28:1304–10. doi: 10.1161/ATVBAHA.108.165100

94. Luckheeram RV, Zhou R, Verma AD, Xia B. $CD4^+$T cells: differentiation and functions. *Clin Dev Immunol*. (2012) 2012:925135. doi: 10.1155/2012/925135

95. Nishimura S, Manabe I, Nagasaki M, Eto K, Yamashita H, Ohsugi M, et al. CD8+ effector T cells contribute to macrophage recruitment and adipose tissue inflammation in obesity. *Nat Med*. (2009) 15:914–20. doi: 10.1038/nm.1964

frontiers | Frontiers in Immunology

TYPE Original Research
PUBLISHED 14 March 2024
DOI 10.3389/fimmu.2024.1343567

OPEN ACCESS

EDITED BY
Hua Cong,
Shandong University, China

REVIEWED BY
Jonadab Efrain Olguin Hernandez,
National Autonomous University of Mexico, Mexico
Celio Geraldo Freire-de-Lima,
Federal University of Rio de Janeiro, Brazil

*CORRESPONDENCE
Renyong Lin
renyonglin@xjmu.edu.cn
Tuerganaili Aji
tuergan78@sina.com

RECEIVED 23 November 2023
ACCEPTED 29 February 2024
PUBLISHED 14 March 2024

CITATION
Li J, Zhao H, Lv G, Aimulajiang K, Li L, Lin R and Aji T (2024) Phenotype and function of MAIT cells in patients with alveolar echinococcosis.
Front. Immunol. 15:1343567.
doi: 10.3389/fimmu.2024.1343567

Phenotype and function of MAIT cells in patients with alveolar echinococcosis

Jintian Li[1,2], Hanyue Zhao[2,3], Guodong Lv[2], Kalibixiati Aimulajiang[2], Liang Li[2], Renyong Lin[2,3]* and Tuerganaili Aji[1,2,3]*

[1]School of Public Healthy, Xinjiang Medical University, Urumqi, China, [2]State Key Laboratory of Pathogenesis, Prevention, and Treatment of Central Asian High Incidence Diseases, Clinical Medical Research Institute, First Affiliated Hospital of Xinjiang Medical University, Urumqi, China, [3]Department of Hepatobiliary & Hydatid Disease, The First Affiliated Hospital of Xinjiang Medical University, Urumqi, China

Mucosal-associated invariant T (MAIT) cells are a subpopulation of unconventional T cells widely involved in chronic liver diseases. However, the potential role and regulating factors of MAIT cells in alveolar echinococcosis (AE), a zoonotic parasitic disease by *Echinococcus multilocularis* (*E. multilocularis*) larvae chronically parasitizing liver organs, has not yet been studied. Blood samples (n=29) and liver specimens (n=10) from AE patients were enrolled. The frequency, phenotype, and function of MAIT cells in peripheral blood and liver tissues of AE patients were detected by flow cytometry. The morphology and fibrosis of liver tissue were examined by histopathology and immunohistochemistry. The correlation between peripheral MAIT cell frequency and serologic markers was assessed by collecting clinicopathologic characteristics of AE patients. And the effect of *in vitro* stimulation with *E. multilocularis* antigen (Emp) on MAIT cells. In this study, MAIT cells are decreased in peripheral blood and increased in the close-to-lesion liver tissues, especially in areas of fibrosis. Circulating MAIT exhibited activation and exhaustion phenotypes, and intrahepatic MAIT cells showed increased activation phenotypes with increased IFN-γ and IL-17A, and high expression of CXCR5 chemokine receptor. Furthermore, the frequency of circulating MAIT cells was correlated with the size of the lesions and liver function in patients with AE. After excision of the lesion site, circulating MAIT cells returned to normal levels, and the serum cytokines IL-8, IL-12, and IL-18, associated with MAIT cell activation and apoptosis, were altered. Our results demonstrate the status of MAIT cell distribution, functional phenotype, and migration in peripheral blood and tissues of AE patients, highlighting their potential as biomarkers and therapeutic targets.

KEYWORDS

mucosa-associated invariant T cells, alveolar echinococcosis, parasitic lesion, pro-fibrogenic, serum cytokine

1 Introduction

Alveolar echinococcosis (AE) is a neglected zoonotic parasitic disease caused by tapeworms *E. multilocularis*, which is mainly parasitic in the liver (1). It is estimated that 91% of the 18,235 new cases of AE annually worldwide occur in China (2, 3), and the pastoral areas of northwestern China are a highly endemic region for *E. multilocularis* (4). The therapeutic approaches of surgical resection and pharmacotherapy remained notable limitations (5): Patients with lesions invading essential blood vessels, serious complications, hepatotoxicity, and adverse drug reactions with long-term medication who urgently need other treatment options to promote a curative prognosis (6).

The regulatory network of immune cells in the liver plays a vital role in maintaining tissue integrity and defending against infection. The *E. multilocularis* infection process stimulates both adaptive and innate immune responses in the host, where macrophages (7), NK cells (8), and T cells (9) regulate the immune response through different mechanisms for host defense (10). It has been shown that treatment based on immune checkpoints PD-1 (11), PD-L1 (12), and TIGIT (13, 14) immunotherapy has potential for the treatment of AE disease but is still not practiced in the clinic. One of the reasons for this is the limited understanding of the composition of the immune system in AE disease.

Mucosal-associated invariant T cells (MAIT) are a distinct population of T cells that express a semi-invariant T cell receptor containing the Vα7.2 segment. These cells are dependent on the non-classical major histocompatibility complex (MHC) related class 1-like molecule, MR1, for the presentation of antigens (15). MAIT are enriched in mucosal sites and comprise 45% of hepatic T cells (16). Capable of producing perforin and granzyme B (GzmB) that directly kill target cells, they secrete interferon γ (IFN-γ), TNF, and IL-17 cytokines to perform rapid effector functions (17). In addition, MAIT cells have been extensively studied in bacterial (18, 19), viral infections (20–22), and tumor diseases (23–25), especially in chronic liver diseases. The collective body of research supports the protective and anti-microbial role of MAIT cells (26–28). Moreover, in malaria-infected parasitic diseases, the frequency of activated MAIT cells increased significantly in a plasmodium falciparum sporozoites pathogens infection dose-dependent manner (29). Our previous study revealed that MAIT cells with the T-cell receptor (TCR) clone TRAV1-2_TRAJ33_TRAC were expanded in AE patients' peripheral blood and liver tissues and enriched in the liver tissues by single-cell RNA and TCR sequencing (30). However, the phenotype and function of MAIT cells and the correlation with clinicopathologic features are unknown.

In this study, we indicated that reduced MAIT cells in the peripheral blood of AE patients correlate with liver injury and lesion size due to *E. multilocularis* infection. Furthermore, the MAIT cell frequency in the peripheral blood return to control values after surgery. In addition, we revealed that MAIT cells aggregated in liver tissue close to lesions exerted potential anti-AE effects through pro-inflammatory and pro-fibrotic functions. These results extend our insights into the frequency and functional status of MAIT cells in *E. multilocularis* infection and suggest therapeutic targets based on MAIT cells for patients with AE.

2 Materials and methods

2.1 Human blood samples

Blood samples of 29 patients with *E. multilocularis* infection and 25 healthy donors (HDs) age- and sex-matched were collected at the First Affiliated Hospital of Xinjiang Medical University from 2022 to 2023. Fibrosis stratification was predicted using the aspartate transaminase (AST) -to-platelet ratio index (APRI) and fibrosis-4 interferon-gamma (FIB-4) indexes (22). Patients' characteristics are listed in Table 1. Specimens were collected from AE patients with no co-infections of other types of parasitic diseases, and preoperative (PreOp) blood was collected from AE patients within 0-3 days after admission, and postoperative (PostOp) blood was collected within 7 days when patients were free from other PostOp infections. The study protocol was approved by the ethics committee of the First Affiliated Hospital of Xinjiang Medical University (20211015–53), and written informed consent was obtained from each subject by the Declaration of Helsinki (1975) of the World Medical Association.

2.2 AE patient's liver samples

Liver specimens were collected during hepatic resection or liver transplantation from 10 AE patients. Specimens were divided into two parts: one part of the liver tissue is close to the parasite lesion by

TABLE 1 Baseline characteristics of the patients.

Samples	HDs	AE	*p*
No.	25	29	–
Sex (F/M)	13/12	14/15	0.790
Age (Year)	43.52 ± 13.20	44.72 ± 11.42	0.724
lymphocyte (%)	32.79 ± 5.62	21.60 ± 7.71	**1.06E-07**
Monocyte (%)	7.12 ± 1.66	7.39 ± 2.38	0.624
AST (U/L)	26.07 (23.89, 27.33)	38.75 (27.83, 83.07)	**9.80E-05**
ALT (U/L)	20.00 (17.50, 27.00)	38.00 (18.50, 74.00)	**0.007**
ALP (U/L)	70.02 ± 19.49	188.20 (124.42, 475.27)	**4.87E-08**
TBIL (μM)	13.94 ± 3.64	14.00 (8.70, 34.09)	**0.028**
IBIL (μM)	4.70 (2.94, 9.86)	6.64 (2.50, 20.03)	0.109
GGT(U/L)	20.59 (16.00, 29.12)	90.77 (45.70, 222.49)	**6.52E-08**
Total protein (g/L)	77.87 ± 4.36	83.04 ± 10.52	**0.001**
Globulin (g/L)	34.14 ± 3.35	46.64 ± 9.92	**3.21E-08**

Dashed line indicates not available. Normal distribution data are shown as mean ± SEM, non-normally distributed data are shown as median (IQR). The bold values is $p < 0.05$.

about 0.5 cm, named close liver tissue (CLT), and another part is distant from the parasite lesion by at least 2 cm, named distant liver tissue (DLT), which were frozen and formalin-fixed rapidly after resection, and fresh liver tissues extracted and separated tissue mononuclear cells. For all cases, patients' characteristics are listed in Supplementary Table 1. All patients signed an informed consent form, and the study was approved by the First Affiliated Hospital ethics committee of Xinjiang Medical University (20211015–53).

2.3 Flow cytometry

As previously described, fresh liver tissue specimens were dissociated into single-cell suspensions for flow cytometry analysis (13). The fresh single-cell suspension and peripheral blood mononuclear cells (PBMCs) used for the analysis of the surface phenotype of MAIT cells and were stimulated with phorbol myristate acetate (PMA; 25ng/mL) for 4h at 37°C in RPMI-1640 medium supplemented with 10% fetal bovine serum (Gibco), followed by surface staining, fixation/permeabilization for detecting IFN-γ, GzmB, and IL-17A cytokine production, and a minimum of 150,000 cells per sample were acquired using the Beckman DXflex (Beckman, USA) flow cytometer and analyzed by FlowJo software (version 10, USA).

The fluorescent-linked antibodies were as follows: CD3 (HIT3a), CD161 (HP-3G10), Vα7.2 (3C10), and CXCR5 (J252D4) antibodies were obtained from BioLegend, France. The CD4 (SK3), CD8 (SK1 and RPA-T8), CD69 (FN50), CD28 (CD28.2), PD-1 (EH12.1), CCR6 (11A9), IL-17A (SCPL1362), GzmB (GB11) and IFN-γ (B27) antibodies were obtained from BD Biosciences, California. The lymphocytes were gated on a population of $CD3^+CD161^+V\alpha7.2^+$ T cells (Supplementary Figure 1), defined as MAIT cells as previously reported (31). The PE-conjugated 5-OP-RU-loaded MR1 tetramers were used to analyze the surface expression of MR1 by flow cytometry as per the manufacturer's instructions (31) (Supplementary Figure 1). For the MAIT cell frequency and cell surface receptor assays in peripheral blood and liver tissue from AE patients, at least 100,000 cells per sample were collected for analysis using a Beckman DXflex (Beckman, USA) flow cytometer and analyzed using FlowJo software (version 10, USA). Due to the limited availability of collected peripheral blood and tissue samples, the extracted mononuclear lymphocytes were limited, and the MAIT cell frequency was preferentially detected. The gating strategies of surface receptor and cytokine are shown in Supplementary Figure 2.

2.4 Assessment of short-term *E. multilocularis* protein stimuli *in vitro*

Peripheral blood was collected from 3 HDs per experiment, and PBMC were isolated by the Ficoll-Paque (Solarbio, china), as previously described (13). The anti-CD3 (1 μg/mL) and anti-CD28 (0.5 μg/mL) antibodies diluted in RPMI-1640 medium (Gibco, USA) and supplement 10% fetal calf serum (Gibco, USA) and co-culture with $1*10^5$ PBMCs per well to activate before the co-cultures were exposed to 5 μg/μL and 10 μg/μL Emp for 24h at 37°C, 5% CO2, followed by flow cytometric analysis. DMSO group without Emp were used as controls.

2.5 Immunohistochemical and histomorphological staining

The hematoxylin and eosin (HE), Sirius red, and Masson stains were performed on 4 μm-thick serial tissue sections of the DLT and CLT from patients with AE, and immunohistochemical staining with a-SMA antibody (1:500, Abcam, Britain). Whole sections were scanned by KF-PRO-400-HI (KFBIO, China). The positive areas of each tissue section were quantified using Image J by three random fields.

OCT-embedded tissue specimens were incubated overnight at 4°C with anti-CD161 (1:40, Abcam, Britain) and anti-PD-1 (1:50, Abcam, Britain) antibodies in PBS containing 1% BSA and 0.2% Triton X-100. The slides were incubated at room temperature for 1h before adding a secondary antibody, followed by Alexa Fluor® 647 and Alexa Fluor® 488. Nuclear was counterstained by DAPI (1:20, KeyGEN BioTECH, China), and images were obtained by Olympus VS200 confocal microscopy (Leica, Germany).

2.6 Serum cytokine assay

The blood samples of pre- and postoperative AE patients, HDs were collected, and centrifuged at 4°C, 3500 rpm, for 15 min to obtain serum. The level of serum cytokines (IL-6, IL-8, IL-12p70, IL-17A, IL-18, IL-33, and IFN-γ) detected by LEGENDplex™ Human Inflammation Panel 1 kit (BioLegend, USA) on flow cytometers, according to manufacturer's instructions.

2.7 Statistical analyses

Statistical calculations were analyzed by GraphPad Prism software (version 8, USA) and SPSS software (version 26, USA). Data with normal distribution and equal variance were analyzed by the student t-test or Analysis of variance (ANOVA) for comparisons of groups. The Mann-Whitney U test or Wilcoxon's matched-pairs signed-rank test was performed for non-normally distributed variables. The Spearman test was employed for correlation analysis.

3 Results

3.1 Characteristics of patients

The clinical characteristics of the subjects are summarized in Table 1. The age, sex, percentage of monocyte, total bilirubin (TBIL), and globulin between patients with AE and HDs are not significantly different. The alanine aminotransferase (ALT), AST, Indirect Bilirubin (IBIL), γ-glutamyl transferase (GGT), and alkaline phosphatase (ALP) in patients with AE have significantly different ($p<0.05$).

3.2 Circulating MAIT cells are exhausted and decreased cytotoxic efficacy in AE patients

In peripheral blood, the percentage of MAIT cells was lower in AE patients than in HDs, and the relative frequency of MAIT cells in the AE patients is mainly clustered around 1% (Figure 1). Circulating MAIT cells from AE patients displayed an activated phenotype, characterized by higher percentage of $CD69^{+}$MAIT cells as compared to HDs (Figure 1). The $IL\text{-}17^{+}$ MAIT cells from AE patients were higher than HDs. In contrast, the $IFN\text{-}\gamma^{+}$ MAIT cells from AE patients were lower than HDs. The GzmB was no different between the two groups (Figure 1). Furthermore, the mean fluorescence intensity (MFI) of cell surface receptors and cytokines was consistent with the percentage statistics (Supplementary Figure 1). Altogether, the percentage of circulating MAIT cells is reduced in AE patients, which may be related to activation-induced exhaustion due to persistently high expression of the activation receptor CD69 and the immunosuppressive receptor PD-1 on the surface of MAIT cells in the peripheral blood of AE patients.

3.3 Intrahepatic MAIT cells maintain cytotoxic efficacy and are associated with the degree of fibrosis in AE patients

To investigate the phenotype and function of MAIT cells in the livers of patients infected with *E. multilocularis*, we collected close and distal liver tissues from lesions in patients undergoing hepatectomy. The percentage of MAIT cells was higher in the CLT than that DLT, and the relative frequency of MAIT cells in the CLT is mainly clustered around 4% (Figure 2). The CLT of AE patients had more inflammatory cell infiltration and higher degree of fibrosis than the DLT (Figure 2), moreover, the IOD value of α-SMA in CLT was higher than that of DLT, and notably, the number of MAIT cells was positively correlated with a-SMA (Figure 2). In contrast, fibrosis stage, predicted by APRI and FIB-4 index, increasing with decreasing frequency of MAIT cells in the blood (Supplementary Figure 2). CD28, T-cell co-stimulatory signal, was fewer in CLT than in DLT, suggesting that MAIT cells in CLT had a diminished stress response to antigens, and surface receptors CD69 and PD-1 were not significantly different between the two groups (Figure 2). Co-expression of PD-1 and CD161 was

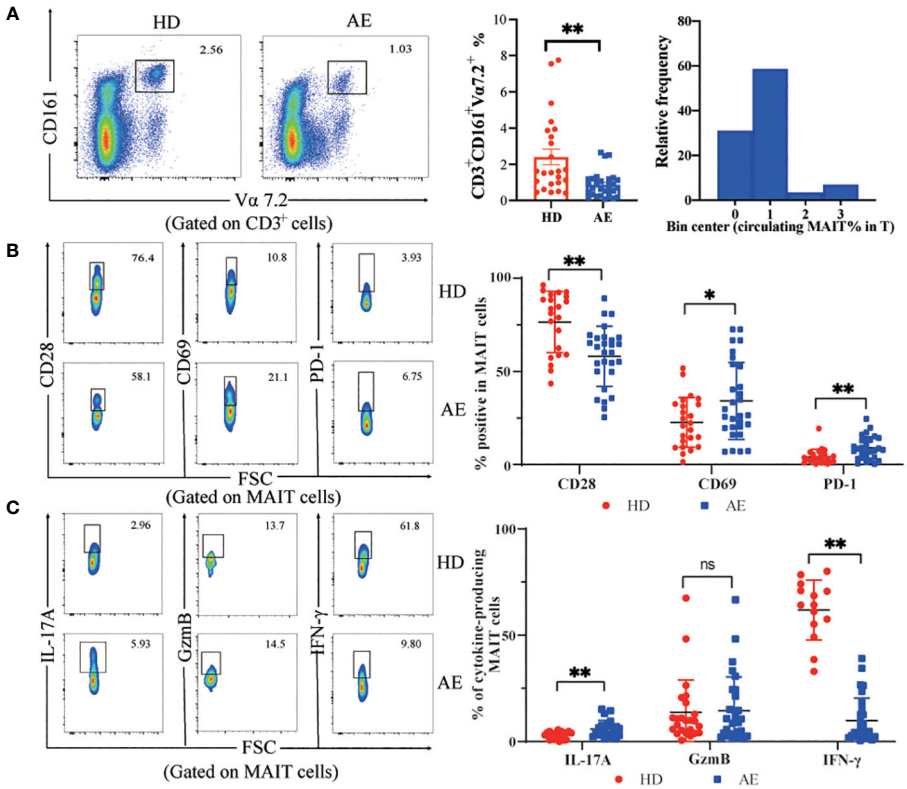

FIGURE 1
Frequency and functions of circulating MAIT cells are impaired in AE. **(A)** Representative dot plot showing reduction of $CD161^{+}V\alpha7.2^{+}$ double positive (MAIT) cell population in peripheral blood and summary data from AE patients (n = 29), as compared to that in HDs (n = 25), and frequency distribution of $CD3^{+}CD161^{+}V\alpha7.2^{+}$ MAIT cell within peripheral blood T cells in AE patients. **(B)** Representative dot plots and data of increased expression of the MAIT cell surface activating receptors CD28 and CD69 with the inhibitory receptor PD-1 from HDs (n = 22-24) and AE patients (n = 28-29). **(C)** Representative dot plots and cumulative data of cytokine profiles of MAIT cells in PBMCs from AE patients (n = 23-29) and HDs (n = 14-24). Statistical analysis was performed using Mann-Whitney or Kruskal-Wallis. ns $p > 0.05$; *$p < 0.01$; **$p < 0.05$.

10.3389/fimmu.2024.1343567

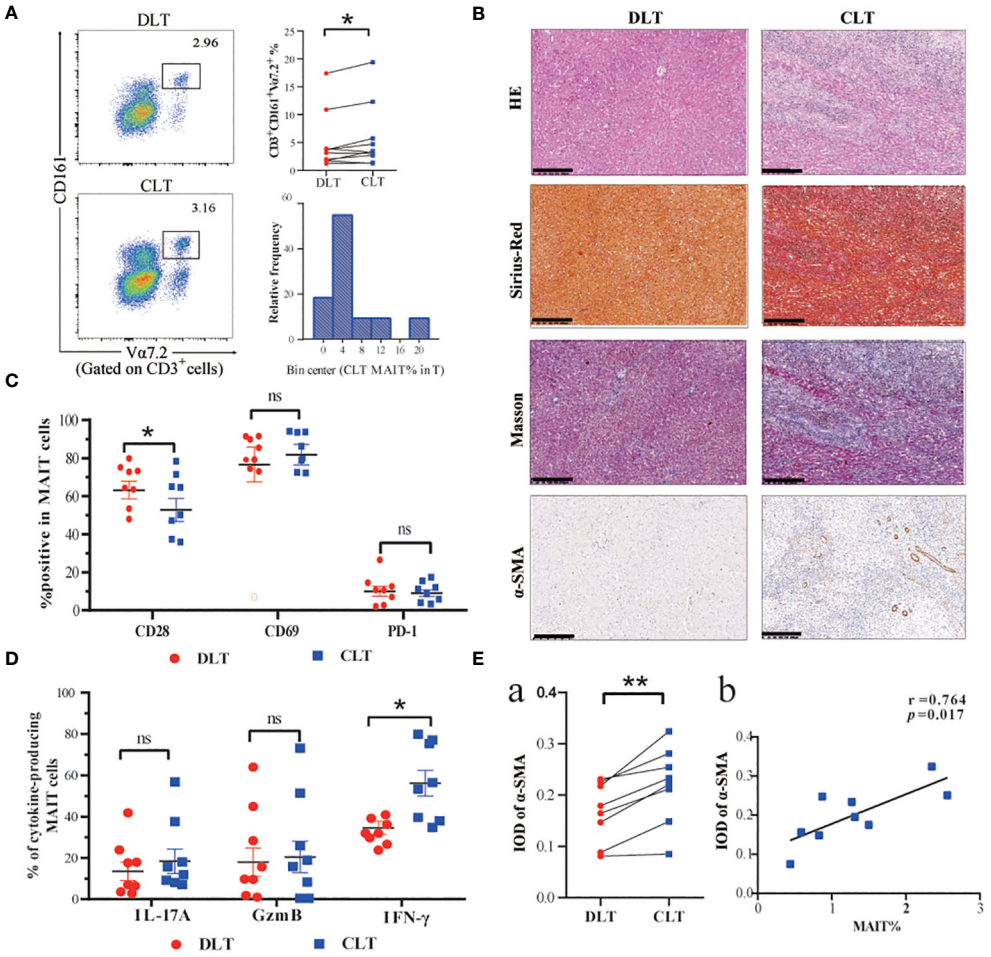

FIGURE 2
Frequency and functions of hepatic MAIT cells are impaired in AE patients. **(A)** Representative dot plots and cumulative data of MAIT cells in mononuclear cells isolated from CLT and DLT (n=10), and frequency distribution of $CD3^+CD161^+V\alpha7.2^+$ MAIT cell within CLT T cells in AE patients. **(B)** Pathologic section staining of CLT and DLT in AE patients (Scale bar = 200 μm). **(C)** Comparison of CD28, CD69, and PD-1 expression in hepatic MAIT cells in CLT and DLT (n = 8). **(D)** Cumulative data of cytokine profiles of hepatic MAIT cells in CLT and DLT (n = 8). **(E)** Statistical and correlation plots of Integral optical density (IOD) values of a-SMA in CLT and DLT. Statistical analyses were performed using paired Wilcoxon tests (a, c, d). ns $p > 0.05$; *$p < 0.01$; **$p < 0.05$.

higher in CLT than DLT of AE patients (Supplementary Figure 3). Furthermore, in terms of the ability of hepatic MAIT cells to secrete cytotoxic factors, the ability of MAIT cells to secrete IFN-γ was enhanced in the CLT with statistical significance. The levels of secreted IL-17 and GzmB were higher than those of DLT, but not statistically significant (Figure 2). The mean fluorescence intensity (MFI) of cell surface receptors and cytokines was consistent with the percentage statistics (Supplementary Figure 3).

3.4 Intrahepatic MAIT cell frequency correlates with CXCR5 expression and shows greater effector potency than circulating counterparts

To better understand the role of MAIT cells in peripheral blood and liver tissue, we first described the frequency and phenotype of MAIT cells in peripheral blood and liver tissues of AE patients and related their frequency changes to chemokine receptor expression. The percentage of MAIT cells in the CLT was higher in AE patients than in peripheral blood (Figure 3). Moreover, the MAIT cells highly expressed CXCR5 and CCR6 chemokine receptors in CLT compared to the DLT, suggesting that MAIT cells may have the tissue-homing ability during *E. multilocularis* infections. Notably, the expression of CXCR5 in CLT and DLT was significantly different (Figure 3-b, d). In addition, there was a significant positive correlation between intrahepatic MAIT cell frequency and their expression of CXCR5 and a tendency for CCR6 (Figure 3-c, e). The ability of MAIT cells to secrete IFN-γ and IL-17A cytokines in CLT was higher than in peripheral blood, but GzmB had no significant difference between two groups (Figure 3). Next, we investigated the phenotype of circulating and CLT MAIT cells in AE patients. CD28 was decreased in the CLT, and the proliferation and differentiation capacity of naive T cells in AE patients may be weakened. The MAIT cells in CLT highly expressing CD69 receptors, demonstrated that MAIT cells were

10.3389/fimmu.2024.1343567

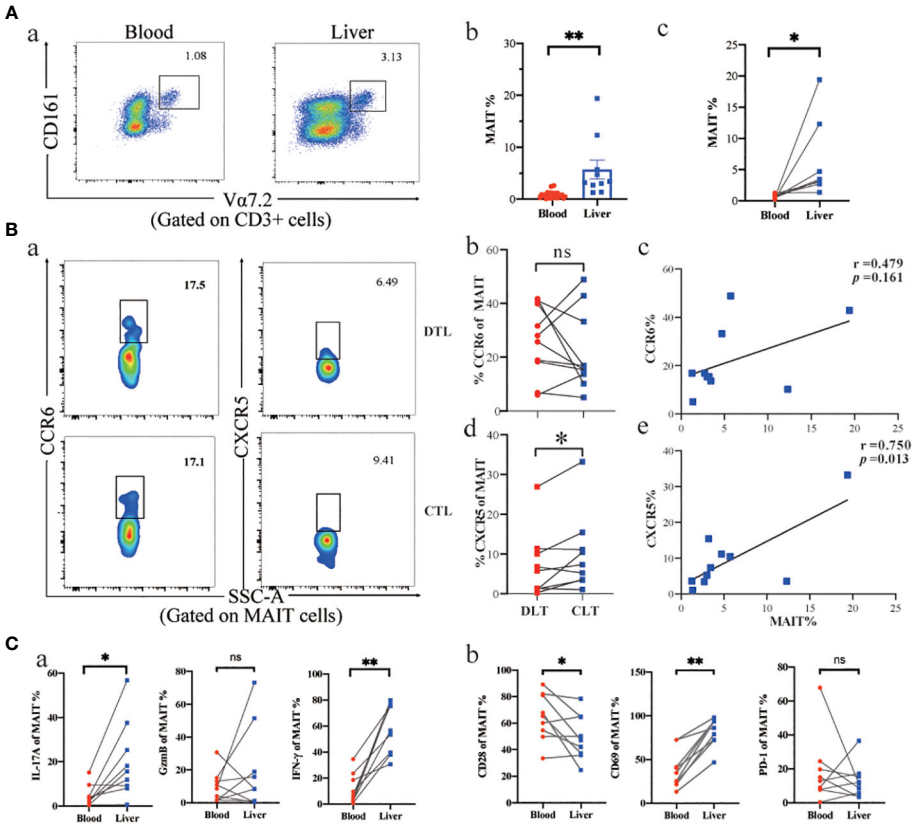

FIGURE 3
Phenotype and function of MAIT cells in AE patients' peripheral blood and liver tissue. **(A)** Representative dot plots and cumulative data of peripheral blood versus intrahepatic MAIT cells in AE patients (unpair: blood n = 29, liver n= 9; pair: n = 8). **(B)** Intrahepatic MAIT cells expressing CCR6 and CXCR5 chemokine receptors in CLT and DLT, and correlation between intrahepatic MAIT frequency and the percentage of MAIT cells for CCR6 (n = 10) and CXCR5 (n = 10) in AE patients. **(C)** Cytokine and cell surface receptor of MAIT cells in peripheral blood versus liver tissue in AE patients (n = 8). ns $p > 0.05$; *$p < 0.01$; **$p < 0.05$.

activated by the parasitic pathogens in liver tissue during infection. However, the PD-1 receptor, which indicates T-cell exhaustion, was not significantly different between the two groups. The results indicated that MAIT cells may be recruited in the CLT by elevated levels of CXCR5 and showed more active phenotype and pro-inflammatory function than circulating MAIT cells.

3.5 Decreased frequency of circulating MAIT cells correlates with liver injury caused by long-term *E.multilocularis* parasitism

To assess the clinical significance of circulating MAIT cells in AE patients, we performed Spearman's correlation analysis. Based on changes in clinical parameters presented in Table 1, we gained further insights regarding age, monocytes, lesion size, globulin, total protein and AST/ALT, and the correlation of MAIT cell frequency with the percentage of lymphocyte, TBIL, IBIL, GGT, AST, and ALT in Supplementary Figure 4. Notably, MAIT cell frequency has no correlation with age in patients with AE, showed a significant positive correlation with monocytes, and a significant negative correlation with the size of liver parasitic lesions, globulin, total protein, and AST/ALT (Figure 4). To assess the diagnostic ability of circulating MAIT cell frequency as it relates to validated markers of liver function, we constructed a receiver operating characteristic curve (ROC). We evaluated the diagnostic value of MAIT cells for AE and determined the area under the curve, sensitivity, specificity, and Youden's J statistic to be 0.742, 60.00%, 84.62%, and 0.4462, respectively (Figure 4). Taken together, our data reveal a negative correlation between circulating MAIT cell frequency and liver function, and support the notion that MAIT can be a biomarker to evaluate parasite infection of liver injury.

3.6 Changes in cytokine profiles and MAIT cytotoxic capacity after surgery in AE patients

We investigated the phenotype and effector function of circulating MAIT cells in patients with AE after surgical removal of parasitic lesions. The percentage of circulating MAIT cells in PostOp blood was increased after surgical removal of parasitic lesions compared to PerOp (Figure 5). Enhanced activation of circulating MAIT cells in PostOp AE patients was indicated by increased numbers of $CD69^{+}$MAIT (dot plot in Supplementary Figure 5).

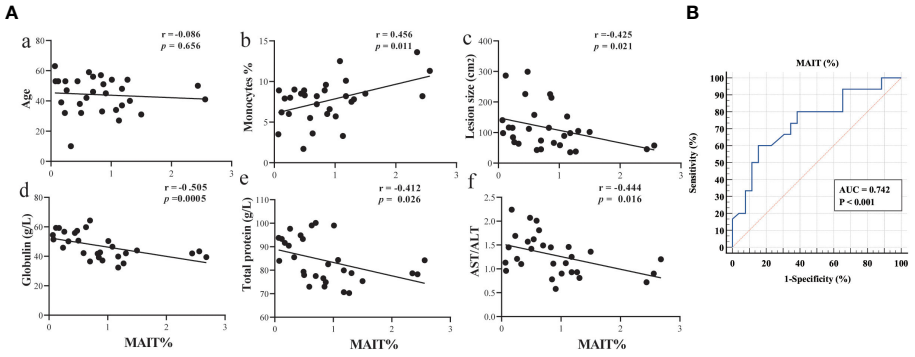

FIGURE 4
Circulating MAIT cell frequency correlated with liver function in AE patients. **(A)** Spearman correlation between circulating MAIT cell frequency in AE patients and levels of age, percent of monocytes, lesion size, globulin, total protein, and AST/ALT (n = 29); **(B)** ROC curve analysis of the diagnostic value of MAIT cell frequency in AE patients.

Moreover, the PD-1^{+}MAIT and CD28^{+}MAIT cells between PostOp and PreOp AE patients have no significantly different (Figure 5B). As T cell activation is associated with a change in effector function, compared with PreOp AE patients, IL-17A production was decreased in MAIT cells of PostOp AE patients. The MAIT cells produced IFN-γ and GzmB not significantly different between PostOp and PreOp AE patients (Figure 5A).

While the role of MAIT cells in infections has been widely focused, MAIT cells are also regulated by inflammatory cytokines in non-microbial diseases as well (15), we further explored the Preop and Postop changes of inflammatory cytokines in the serum of AE patients. The pro-inflammatory factors IFN-γ, and IL-17A of PostOp serum of AE patients were reduced with the PreOp and were not significantly different with HDs (p>0.05). Moreover, the pro-inflammatory factor IL-6 was increased in PostOp patients (Figure 5). IL-33, which is involved in the regulation of Th2-type immune and inflammatory responses, was reduced in the serum of PreOp patients compared with HDs, and was not significantly

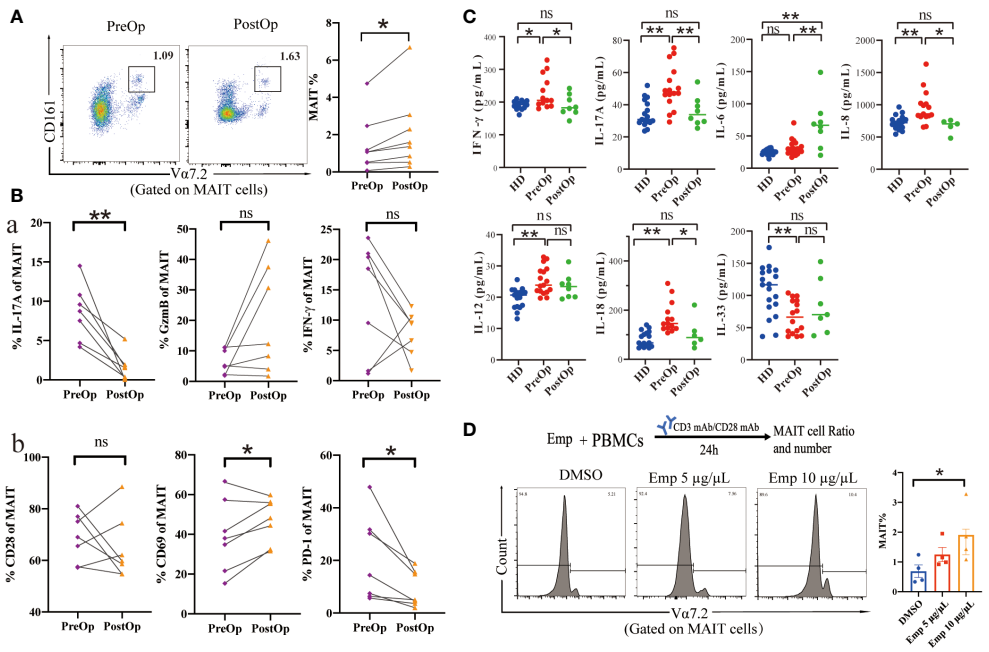

FIGURE 5
Phenotype and function of circulating MAIT cells in pre- and postoperative AE patients. **(A)** Representative dot plots of pre-and postoperative MAIT cells (n=8). **(B)** Percentage of receptors expression and intracellular cytokine staining of MAIT cells from pre-and postoperative AE patients (n=7). **(C)** Cytokine concentrations in pre-and postoperative AE patients (HDs: n =14-19; PreOp: n =14-19; PostOp: n=5-8). **(D)** Co-culture system of PBMC from HDs incubated with anti-CD3 and anti-CD28 antibodies and the frequency of MAIT cells stimulated by Emp for 24 hours, all data are representative of four independent experiments. Statistical analyses were performed using paired Wilcoxon tests **(A, B)**, ANOVA tests, and a two-sample t-test **(C, D)**. ns $p > 0.05$; *$p < 0.01$; **$p < 0.05$.

different with PostOp patients. Levels of IL-8, IL-12, and IL-18 cytokines associated with MAIT cell activation and apoptosis were significantly increased in PreOp patients compared with HDs ($p<0.01$), decreased PostOp compared with PreOp patients, and were not significantly different between PostOp patients and HDs ($p>0.05$). In addition, we found that the percentage of MAIT cell significantly increased with Emp concentration in a dose-dependent compared with the DMSO group, implying that MAIT cells are capable of responding in an early phase of infection.

4 Discussion

By escaping the host's immune defenses, *E. multilocularis* proliferated asexually in the liver for long periods triggering an intense immune infiltration around the parasitic lesion, causing changes in the AE patient's immune environment (32). This study is the first comprehensive analysis of the phenotype, cytokine secretion, and cytotoxicity of MAIT cells during chronic *E. multilocularis* infection from peripheral blood and liver tissue in AE patients.

We initially determined that the frequency of MAIT cells was severely reduced in the circulation of AE patients and displayed an exhausted phenotype. Various factors may contribute to MAIT cell depletion, including age (33), gender (34), redistribution (16), and activation-induced cell death (35). Our results showed that the frequency of MAIT cells in the peripheral blood of AE patients did not correlate with gender and age. Moreover, cellular exhaustion due to high expression of PD-1 and CD69 in circulating MAIT cells of AE patients may contribute to the loss of MAIT cells. In addition, both IL-12 and IL-18 can induce MAIT cell activation and death *in vitro* (36), and they were significantly increased in PreOp but not significantly different in PostOp AE patients compared with HDs, suggesting a possible mechanism for the severe loss of MAIT cells in AE patients. Notably, the reduced peripheral circulating MAIT cells in AE patients may be accumulated into the CLT, and the MAIT cells in the CLT showed enhanced activation capacity and cytotoxicity.

As previously reported MAIT cells proliferation *in situ* in infected organs (37). Tissue-resident molecules CXCR5 and CCR6 are expressed on the surface of MAIT cells, and stimulation by *E. multilocularis* infection causes MAIT cells migrate from the bloods to the site of infection. In particular, CXCR5 expression was positively correlated with the frequency of MAIT cells in CLT. The CXCR5 is a characteristic marker of T cells and mediates T-B cell interactions through CXCL13 chemokines (38, 39). During chronic HBV infection, high intrahepatic expression of CXCL13 promotes $CXCR5^{+}CD8^{+}$ T cell aggregation, exerting an immune control effect against HBV infection (40). MAIT cells migrate to the site of infection under chemokine guidance, where they contribute to pathogen clearance and immunoregulation.

Aggregation of MAIT cells in the CLT may be involved in the pathology of hepatic fibrosis caused by *E. multilocularis* infection. The liver fibrosis of AE patients is due to the stimulation of immune cells by *E. multilocularis* to form granulomas around parasitic vesicles, which are pathologically damaged by highly cross-linked collagen (41, 42). MAIT cells were found to accumulate in hepatic fibrotic septa in patients with alcoholic or nonalcoholic fatty liver-associated cirrhosis, and they have the ability to alter the fibrotic properties of hepatic myofibroblasts and exert a pro-fibrotic effect (31, 43). Also, the MAIT cells contribute to the development of hepatic stellate cell-mediated hepatic fibrosis may be a cellular and molecular pathway for fibrosis development in patients with autoimmune liver disease (44). Our results show that the circulating MAIT cells frequency in AE patients tended to decrease with the fibrosis stage, whereas the intrahepatic MAIT cells frequency was positively correlated with the expression of fibrosis indicator α-SMA. As speculated by previous studies, it is possible that MAIT cells accumulate in the liver tissue around the parasite lesion before they are depleted in peripheral blood, and exhibit pro-fibrogenic role to limit *E. multilocularis* larval growth.

MAIT cells are a key component of the immune system and are considered an important bridge between innate and adaptive immunity (15). Activation of innate and adaptive immunity plays a vital role in the parasitic process of *E. multilocularis* (12). The development of the MR1 tetramer tool loaded with 5-OP-RU promotes the previous studies of MAIT cells that relied on specific cell surface markers such as CD3, Va7.2, and CD161 (15). Here, the CD3, CD161, and Vα7.2 containing and the MR 1 tetramer labeling MAIT cells displayed similar percentages in the PBMCs of AE patients (Supplementary Figure 1). MAIT cells recognize vitamin B-based metabolite antigens presented by the MHC Class I related-1 protein, MR1, and MR1-deficient mice model lacking MAIT cells affects disease susceptibility (45). MR1-deficient mice showed impaired ability to response to infection with *E. coli* or *M. abscessus* (46), and to T cell respond to infection with bovis bacillus Calmette-Guérin before the full induction of adaptive immunity (47). Moreover, adoptive transfer of MAIT cells into hosts rescues immunodeficient mice lacking of T cells or NK cells from lethal *Legionella* infection (18). Additionally, the frequency of MAIT cells in the blood of patients correlates with the severity of ICU-acquired infections (48), and the frequency of intrahepatic MAIT cells in patients with hepatocellular carcinoma (24) and cholangiocarcinoma (23) was associated with overall survival. Thus, MAIT cells have the potential to be used as therapeutic targets and prognostic markers in immunological studies and clinical applications.

MAIT cells respond to a wide array of pathogens through diverse activation mechanisms, including both TCR-dependent and independent pathways, and play a crucial role in the body's anti-infection defense. Due to the plasticity of the antigen-binding cleft, non-riboflavin antigens such as microbial molecules (49) and tumor cell-derived molecules (50) can bind to MR1, adding to the diversity of MR1 ligands. In bacterial and fungal infectious diseases, vitamin B2 metabolites produced are presented by MR1 to MAIT cells, which rapidly produce the pro-inflammatory factors IFN-γ, TNF, IL-17, and IL-22 (51). MAIT cells are activated by viral infections in an MR1-independent manner through innate cytokines and TCR receptors (52). In parasite research, MAIT cell activation correlates with parasite antigen concentration in human Malaria Infection (29). *Leishmania* does not encode riboflavin biosynthesis, but MAIT cells respond to *Leishmania* in a dose- and MR1-dependent manner and produce TNF, IFN-γ, and IL-17A to exert protection from *Leishmania* parasites (53).

The 5μg/mL Emp stimulates high expression of CD155, a ligand for the TIGIT immunosuppressive receptor, in the HL-7702 hepatocyte cell line, mimicking T cell dysfunction due to TIGIT-CD155 interaction after *E.multilocularis* infection in an *in vitro* assay (13). Our results initially verified *in vitro* that MAIT cells have a tendency to increase in frequency after Emp stimulation. However, MAIT cells are constantly exposed to antigens (54) secreted from *E. multilocularis* or inflammatory signals produced by cytokines during *E. multilocularis* infections and further studies are needed to investigate the response and regulatory role of MAIT cells.

5 Conclusion

This study revealed differences in MAIT cell phenotype and function in the blood and liver of patients infected with *E. multilocularis*. The MAIT cells aggregated in liver tissue close to lesions exerted potential anti-AE effects through pro-inflammatory and pro-fibrotic functions. In addition, given the MAIT cells correlation with lesion size and response to surgical treatment, they have the potential to be biomarkers of disease progression. The present study expands our understanding of MAIT cells in parasitic infection diseases, and future studies should aim to further elucidate the mechanism of action of MAIT cells in AE diseases.

Data availability statement

The data and material in the study are available from the corresponding author on reasonable request.

Ethics statement

The studies involving humans were approved by the ethics committee of the First Affiliated Hospital of Xinjiang Medical University. The studies were conducted in accordance with the local legislation and institutional requirements. The participants provided their written informed consent to participate in this study.

Author contributions

JL: Writing – review & editing, Writing – original draft, Visualization. HZ: Writing – review & editing, Resources. GL: Writing – review & editing, Validation, Supervision, Project administration, Methodology, Investigation. KA: Writing – review & editing, Supervision, Methodology, Investigation, Data curation. LL: Writing – review & editing, Validation, Software, Investigation, Formal analysis, Data curation. RL: Writing – review & editing, Supervision, Resources, Project administration. TA: Writing – review & editing, Supervision, Resources, Project administration, Funding acquisition.

Funding

The author(s) declare financial support was received for the research, authorship, and/or publication of this article. This research was funded by the Key Project of the Natural Science Foundation of Xinjiang Uygur Autonomous Region, China (no. 2022D01D17) and Open Topics of State Key Laboratory of Pathogenesis, Prevention, and Treatment of Central Asian High Incidence Diseases (SKL-HIDCA-2021-4).

Acknowledgments

We thank the Department of Hepatobiliary Hydatid Surgery medical staff of the First Affiliated Hospital of Xinjiang Medical University for their assistance and support in collecting specimens and case information.

Conflict of interest

The authors declare that the research was conducted in the absence of any commercial or financial relationships that could be construed as a potential conflict of interest.

Publisher's note

All claims expressed in this article are solely those of the authors and do not necessarily represent those of their affiliated organizations, or those of the publisher, the editors and the reviewers. Any product that may be evaluated in this article, or claim that may be made by its manufacturer, is not guaranteed or endorsed by the publisher.

Supplementary material

The Supplementary Material for this article can be found online at: https://www.frontiersin.org/articles/10.3389/fimmu.2024.1343567/full#supplementary-material

SUPPLEMENTARY FIGURE 1
(A) Gating strategy of MAIT cells. Representative dot plots describing the percentage of MAIT cell among of T cells from AE patient. MAIT cells are defined as $CD3^+CD161^+V\alpha7.2^+$ cells in the lymphocyte gate. **(B)** Representative dot plot showing $CD161^+V\alpha7.2^+$ cells and positive to 5-OP-RU loaded MR1 from AE patient's PBMC. The quantities of $CD3^+CD161^+V\alpha7.2^+$ and positive to 5-OP-RU loaded MR1 is no significant different between three different AE patients ($p>0.05$). **(C)** The MFI of CD28, CD69 and PD-1 (HD n=23-25; AE n=27-29) of MAIT cells. **(D)** The mean fluorescence intensity (MFI) of GzmB, IL-17A and IFN-γ (HD n=23-25; AE n=27-29) of MAIT cells. ns $p>0.05$; *$p<0.05$; **$p<0.01$.

SUPPLEMENTARY FIGURE 2
Representative dot plots showing gating of surface receptor$^+$ and cytokine$^+$ MAIT cells.

SUPPLEMENTARY FIGURE 3
(A) Representative image of CD161$^+$PD-1$^+$ double positive cells in liver tissue sections from AE patients (n = 3), showing the presence of CD161$^+$ PD-1$^+$ cells in CLT more than DLT (Scale bar = 50 μm). **(B)** The MFI of cell surface receptors and secreted cytokines (n=8) of MAIT cells in AE patient liver tissues. **(C)** The degrees of fibrosis of AE patient's circulating MAIT cell proportion predicted by APRI/FIB-4 evaluation (n = 6-12 per group). ns $p>0.05$; *$p<0.05$; **$p<0.01$.

SUPPLEMENTARY FIGURE 4
Correlation of MAIT cell frequency with the percentage of lymphocyte, TBIL, IBIL, GGT, AST and ALT (n=28-29).

SUPPLEMENTARY FIGURE 5
Representative dot plots and data of the MAIT cell surface receptors and cytokines from PreOp and PostOp AE patients.

SUPPLEMENTARY TABLE 1
Specimens used for these studies. FCM, flow cytometry; IHC, immunohistochemistry; IF, immunofluorescence; α-SMA, alpha smooth muscle actin.

References

1. Wen H, Vuitton L, Tuxun T, Li J, Vuitton DA, Zhang W, et al. Echinococcosis: advances in the 21st century. *Clin Microbiol Rev*. (2019) 32:e00075–18. doi: 10.1128/cmr.00075-18

2. Torgerson PR, Keller K, Magnotta M and Ragland N. The global burden of alveolar echinococcosis. *PloS Negl Trop Dis*. (2010) 4:e722. doi: 10.1371/journal.pntd.0000722

3. Deplazes P, Rinaldi L, Alvarez Rojas CA, Torgerson PR, Harandi MF, Romig T, et al. Global distribution of alveolar and cystic echinococcosis. *Adv Parasitol*. (2017) 95:315–493. doi: 10.1016/bs.apar.2016.11.001

4. Guo B, Zhang Z, Guo Y, Guo G, Wang H, Ma J, et al. High endemicity of alveolar echinococcosis in Yili Prefecture, Xinjiang Autonomous Region, the People's Republic of China: Infection status in different ethnic communities and in small mammals. *PloS Negl Trop Dis*. (2021) 15:e0008891. doi: 10.1371/journal.pntd.0008891

5. Salm LA, Lachenmayer A, Perrodin SF, Candinas D and Beldi G. Surgical treatment strategies for hepatic alveolar echinococcosis. *Food Waterborne Parasitol*. (2019) 15:e00050. doi: 10.1016/j.fawpar.2019.e00050

6. Bhutani N, Kajal P. Hepatic echinococcosis: A review. *Ann Med Surg (Lond)*. (2018) 36:99–105. doi: 10.1016/j.amsu.2018.10.032

7. Wang H, Zhang CS, Fang BB, Hou J, Li WD, Li ZD, et al. Dual role of hepatic macrophages in the establishment of the *echinococcus multilocularis* metacestode in mice. *Front Immunol*. (2020) 11:600635. doi: 10.3389/fimmu.2020.600635

8. X B, Huang H, Gao S and Xu X. *Echinococcus multilocularis* induces surface high expression of inhibitory killer immunoglobulin-like receptor on natural killer cells. *Allergol Immunopathol (Madr)*. (2021) 49:78–86. doi: 10.15586/aei.v49i5.465

9. Wang J, Cardoso R, Marreros N, Müller N, Lundström-Stadelmann B, Siffert M, et al. Foxp3(+) T Regulatory Cells as a Potential Target for Immunotherapy against Primary Infection with *Echinococcus multilocularis* Eggs. *Infection Immunity*. (2018) 86:e00542-18. doi: 10.1128/iai.00542-18

10. Bakhtiar NM, Spotin A, Mahami-Oskouei M, Ahmadpour E and Rostami A. Recent advances on innate immune pathways related to host-parasite cross-talk in cystic and alveolar echinococcosis. *Parasit Vectors*. (2020) 13:232. doi: 10.1186/s13071-020-04103-4

11. Wang J, Jebbawi F, Bellanger AP, Beldi G, Millon L and Gottstein B. Immunotherapy of *alveolar echinococcosis* via PD-1/PD-L1 immune checkpoint blockade in mice. *Parasite Immunol*. (2018) 40:e12596. doi: 10.1111/pim.12596

12. Jebbawi F, Bellanger AP, Lunström-Stadelmann B, Rufener R, Dosch M, Goepfert C, et al. Innate and adaptive immune responses following PD-L1 blockade in treating chronic murine *alveolar echinococcosis*. *Parasite Immunol*. (2021) 43:e12834. doi: 10.1111/pim.12834

13. Zhang C, Lin R, Li Z, Yang S, Bi X, Wang H, et al. Immune exhaustion of T cells in *alveolar echinococcosis* patients and its reversal by blocking checkpoint receptor TIGIT in a murine model. *Hepatology*. (2020) 71:1297–315. doi: 10.1002/hep.30896

14. Zhang C, Wang H, Li J, Hou X, Li L, Wang W, et al. Involvement of TIGIT in natural killer cell exhaustion and immune escape in patients and mouse model with liver *echinococcus multilocularis* infection. *Hepatology*. (2021) 74:3376–93. doi: 10.1002/hep.32035

15. Godfrey DI, Koay HF, McCluskey J, Gherardin NA. The biology and functional importance of MAIT cells. *Nat Immunol*. (2019) 20:1110–28. doi: 10.1038/s41590-019-0444-8

16. Dusseaux M, Martin E, Serriari N, Péguillet I, Premel V, Louis D, et al. Human MAIT cells are xenobiotic-resistant, tissue-targeted, CD161hi IL-17-secreting T cells. *Blood*. (2011) 117:1250–9. doi: 10.1182/blood-2010-08-303339

17. Gao MG, Zhao XS. Mining the multifunction of mucosal-associated invariant T cells in hematological Malignancies and transplantation immunity: A promising hexagon soldier in immunomodulatory. *Front Immunol*. (2022) 13:931764. doi: 10.3389/fimmu.2022.931764

18. Wang H, D'Souza C, Lim XY, Kostenko L, Pediongco TJ, Eckle SBG, et al. MAIT cells protect against pulmonary *Legionella longbeachae* infection. *Nat Commun*. (2018) 9:3350. doi: 10.1038/s41467-018-05202-8

19. D'Souza C, Pediongco T, Wang H, Scheerlinck JY, Kostenko L, Esterbauer R, et al. Mucosal-associated invariant T cells augment immunopathology and gastritis in chronic *helicobacter pylori* infection. *J Immunol*. (2018) 200:1901–16. doi: 10.4049/jimmunol.1701512

20. Parrot T, Gorin JB, Ponzetta A, Maleki KT, Kammann T, Emgård J, et al. MAIT cell activation and dynamics associated with COVID-19 disease severity. *Sci Immunol*. (2020) 5:eabe1670. doi: 10.1126/sciimmunol.abe1670

21. Beudeker BJB, van Oord GW, Arends JE, Schulze Zur Wiesch J, van der Heide MS, de Knegt RJ, et al. Mucosal-associated invariant T-cell frequency and function in blood and liver of HCV mono- and HCV/HIV co-infected patients with advanced fibrosis. *Liver Int*. (2018) 38:458–68. doi: 10.1111/liv.13544

22. Liu Y, Zhu P, Wang W, Tan X, Liu C, Chen Y, et al. Mucosal-associated invariant T cell dysregulation correlates with conjugated bilirubin level in chronic HBV infection. *Hepatology*. (2021) 73:1671–87. doi: 10.1002/hep.31602

23. Zimmer CL, Filipovic I, Cornillet M, O'Rourke CJ, Berglin L, Jansson H, et al. Mucosal-associated invariant T-cell tumor infiltration predicts long-term survival in cholangiocarcinoma. *Hepatology*. (2022) 75:1154–68. doi: 10.1002/hep.32222

24. Duan M, Goswami S, Shi JY, Wu LJ, Wang XY, Ma JQ, et al. Activated and exhausted MAIT cells foster disease progression and indicate poor outcome in hepatocellular carcinoma. *Clin Cancer Res*. (2019) 25:3304–16. doi: 10.1158/1078-0432.Ccr-18-3040

25. Won EJ, Ju JK, Cho YN, Jin HM, Park KJ, Kim TJ, et al. Clinical relevance of circulating mucosal-associated invariant T cell levels and their anti-cancer activity in patients with mucosal-associated cancer. *Oncotarget*. (2016) 7:76274–90. doi: 10.18632/oncotarget.11187

26. von Seth E, Zimmer CL, Reuterwall-Hansson M, Barakat A, Arnelo U, Bergquist A, et al. Primary sclerosing cholangitis leads to dysfunction and loss of MAIT cells. *Eur J Immunol*. (2018) 48:1997–2004. doi: 10.1002/eji.201847608

27. Atif M, Warner S. and Oo YH Linking the gut and liver: crosstalk between regulatory T cells and mucosa-associated invariant T cells. *Hepatol Int*. (2018) 12:305–14. doi: 10.1007/s12072-018-9882-x

28. Bolte FJ, O'Keefe AC, Webb LM, Serti E, Rivera E, Liang TJ, et al. Intra-hepatic depletion of mucosal-associated invariant T cells in hepatitis C virus-induced liver inflammation. *Gastroenterology*. (2017) 153:1392–1403.e2. doi: 10.1053/j.gastro.2017.07.043

29. Mpina M, Maurice NJ, Yajima M, Slichter CK, Miller HW, Dutta M, et al. Controlled human malaria infection leads to long-lasting changes in innate and innate-like lymphocyte populations. *J Immunol*. (2017) 199:107–18. doi: 10.4049/jimmunol.1601989

30. Jiang T, Sun W, Aji T, Shao Y, Guo C, Zhang C, et al. Single-cell heterogeneity of the liver-infiltrating lymphocytes in individuals with chronic *echinococcus multilocularis* infection. *Infection Immunity*. (2022) 90:e0017722. doi: 10.1128/iai.00177-22

31. Hegde P, Weiss E, Paradis V, Wan J, Mabire M, Sukriti S, et al. Mucosal-associated invariant T cells are a profibrogenic immune cell population in the liver. *Nat Commun*. (2018) 9:2146. doi: 10.1038/s41467-018-04450-y

32. Gottstein B, Soboslay P, Ortona E, Wang J, Siracusano A. and vuitton D immunology of alveolar and cystic echinococcosis (AE and CE). *Adv Parasitol*. (2017) 96:1–54. doi: 10.1016/bs.apar.2016.09.005

33. Gherardin NA, Souter MN, Koay HF, Mangas KM, Seemann T, Stinear TP, et al. Human blood MAIT cell subsets defined using MR1 tetramers. *Immunol Cell Biol*. (2018) 96:507–25. doi: 10.1111/imcb.12021

34. Novak J, Dobrovolny J, Novakova L and Kozak T. The decrease in number and change in phenotype of mucosal-associated invariant T cells in the elderly and differences in men and women of reproductive age. *Scand J Immunol*. (2014) 80:271–5. doi: 10.1111/sji.12193

35. Huang W, He W, Shi X, Ye Q, He X, Dou L, et al. Mucosal-associated invariant T-cells are severely reduced and exhausted in humans with chronic HBV infection. *J Viral Hepat*. (2020) 27:1096–107. doi: 10.1111/jvh.13341

36. Dias J, Hengst J, Parrot T, Leeansyah E, Lunemann S, Malone DFG, et al. Chronic hepatitis delta virus infection leads to functional impairment and severe loss of MAIT cells. *J Hepatol*. (2019) 71:301–12. doi: 10.1016/j.jhep.2019.04.009

37. Yu H, Yang A, Liu L, Mak JYW, Fairlie DP and Cowley S. CXCL16 stimulates antigen-induced MAIT cell accumulation but trafficking during lung infection is CXCR6-independent. *Front Immunol*. (2020) 11:1773. doi: 10.3389/fimmu.2020.01773

38. Crotty S. T follicular helper cell biology: A decade of discovery and diseases. *Immunity*. (2019) 50:1132–48. doi: 10.1016/j.immuni.2019.04.011

39. Rao DA. T cells that help B cells in chronically inflamed tissues. *Front Immunol*. (2018) 9:1924. doi: 10.3389/fimmu.2018.01924

40. Li Y, Tang L, Guo L, Chen C, Gu S, Zhou Y, et al. CXCL13-mediated recruitment of intrahepatic CXCR5(+)CD8(+) T cells favors viral control in chronic HBV infection. *J Hepatol*. (2020) 72:420–30. doi: 10.1016/j.jhep.2019.09.031

41. Vuitton DA. The ambiguous role of immunity in echinococcosis: protection of the host or of the parasite? *Acta Trop*. (2003) 85:119–32. doi: 10.1016/s0001-706x(02)00230-9

42. Vuitton DA, Zhang SL, Yang Y, Godot V, Beurton I, Mantion G, et al. Survival strategy of *Echinococcus multilocularis* in the human host. *Parasitol Int*. (2006) 55 Suppl:S51–5. doi: 10.1016/j.parint.2005.11.007

43. Mabire M, Hegde P, Hammoutene A, Wan J, Caër C, Sayegh RA, et al. MAIT cell inhibition promotes liver fibrosis regression *via* macrophage phenotype reprogramming. *Nat Commun*. (2023) 14:1830. doi: 10.1038/s41467-023-37453-5

44. Böttcher K, Rombouts K, Saffioti F, Roccarina D, Rosselli M, Hall A, et al. MAIT cells are chronically activated in patients with autoimmune liver disease and promote profibrogenic hepatic stellate cell activation. *Hepatology*. (2018) 68:172–86. doi: 10.1002/hep.29782

45. Wang H, Chen Z, McCluskey J and Corbett AJ. Mouse models illuminate MAIT cell biology. *Mol Immunol*. (2021) 130:55–63. doi: 10.1016/j.molimm.2020.12.007

46. Le Bourhis L, Martin E, Péguillet I, Guihot A, Froux N, Coré M, et al. Antimicrobial activity of mucosal-associated invariant T cells. *Nat Immunol*. (2010) 11:701–8. doi: 10.1038/ni.1890

47. Chua WJ, Truscott SM, Eickhoff CS, Blazevic A, Hoft DF and Hansen TH. Polyclonal mucosa-associated invariant T cells have unique innate functions in bacterial infection. *Infection Immunity*. (2012) 80:3256–67. doi: 10.1128/iai.00279-12

48. Grimaldi D, Le Bourhis L, Sauneuf B, Dechartres A, Rousseau C, Ouaaz F, et al. Specific MAIT cell behaviour among innate-like T lymphocytes in critically ill patients with severe infections. *Intensive Care Med*. (2014) 40:192–201. doi: 10.1007/s00134-013-3163-x

49. Meermeier EW, Laugel BF, Sewell AK, Corbett AJ, Rossjohn J, McCluskey J, et al. Human TRAV1-2-negative MR1-restricted T cells detect S. pyogenes and alternatives to MAIT riboflavin-based antigens. *Nat Commun*. (2016) 7:12506. doi: 10.1038/ncomms12506

50. Lepore M, Kalinichenko A, Calogero S, Kumar P, Paleja B, Schmaler M, et al. Functionally diverse human T cells recognize non-microbial antigens presented by MR1. *Elife*. (2017) 6:e24476. doi: 10.7554/eLife.24476

51. Wong EB, Ndung'u T and Kasprowicz VO. The role of mucosal-associated invariant T cells in infectious diseases. *Immunology*. (2017) 150:45–54. doi: 10.1111/imm.12673

52. van Wilgenburg B, Scherwitzl I, Hutchinson EC, Leng T, Kurioka A, Kulicke C, et al. MAIT cells are activated during human viral infections. *Nat Commun*. (2016) 7:11653. doi: 10.1038/ncomms11653

53. Moreira ML, Borges-Fernandes LO, Pascoal-Xavier MA, Ribeiro ÁL, Pereira VHS, Pediongco T, et al. The role of mucosal-associated invariant T cells in visceral leishmaniasis. *Front Immunol*. (2022) 13:926446. doi: 10.3389/fimmu.2022.926446

54. Valot B, Rognon B, Prenel A, Baraquin A, Knapp J, Anelli M, et al. Screening of antigenic vesicular fluid proteins of *Echinococcus multilocularis* as potential viability biomarkers to monitor drug response in alveolar echinococcosis patients. *Proteomics Clin Appl*. (2017) 11:11–12. doi: 10.1002/prca.201700010

Frontiers in Immunology

Explores novel approaches and diagnoses to treat immune disorders.

The official journal of the International Union of Immunological Societies (IUIS) and the most cited in its field, leading the way for research across basic, translational and clinical immunology.

Discover the latest Research Topics

See more →

Frontiers

Avenue du Tribunal-Fédéral 34
1005 Lausanne, Switzerland
frontiersin.org

Contact us

+41 (0)21 510 17 00
frontiersin.org/about/contact